IMPACT OF COVID-19 LOCKDOWNS ON THE REGIONAL AND GLOBAL OCEANS AND COASTS

EDITED BY: D. Swain, Deepak R. Mishra, Stefano Vignudelli, Christine M. Lee and Domenico D'Alelio

PUBLISHED IN: Frontiers in Marine Science

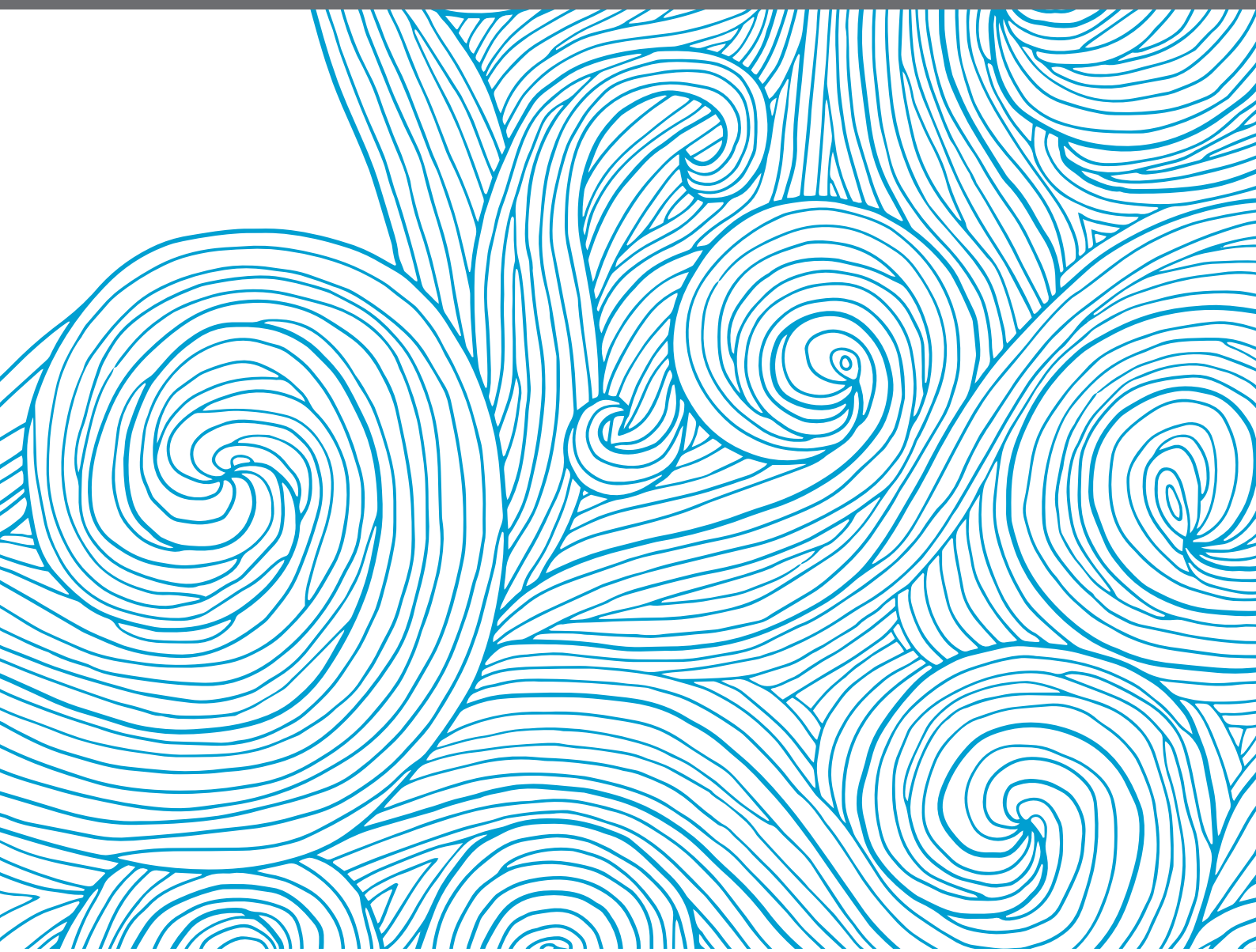

frontiers Research Topics

frontiers

ISSN 1664-8714
ISBN 978-2-88974-924-9
DOI 10.3389/978-2-88974-924-9

About Frontiers

Frontiers is more than just an open-access publisher of scholarly articles: it is a pioneering approach to the world of academia, radically improving the way scholarly research is managed. The grand vision of Frontiers is a world where all people have an equal opportunity to seek, share and generate knowledge. Frontiers provides immediate and permanent online open access to all its publications, but this alone is not enough to realize our grand goals.

Frontiers Journal Series

The Frontiers Journal Series is a multi-tier and interdisciplinary set of open-access, online journals, promising a paradigm shift from the current review, selection and dissemination processes in academic publishing. All Frontiers journals are driven by researchers for researchers; therefore, they constitute a service to the scholarly community. At the same time, the Frontiers Journal Series operates on a revolutionary invention, the tiered publishing system, initially addressing specific communities of scholars, and gradually climbing up to broader public understanding, thus serving the interests of the lay society, too.

Dedication to Quality

Each Frontiers article is a landmark of the highest quality, thanks to genuinely collaborative interactions between authors and review editors, who include some of the world's best academicians. Research must be certified by peers before entering a stream of knowledge that may eventually reach the public - and shape society; therefore, Frontiers only applies the most rigorous and unbiased reviews.
Frontiers revolutionizes research publishing by freely delivering the most outstanding research, evaluated with no bias from both the academic and social point of view. By applying the most advanced information technologies, Frontiers is catapulting scholarly publishing into a new generation.

What are Frontiers Research Topics?

Frontiers Research Topics are very popular trademarks of the Frontiers Journals Series: they are collections of at least ten articles, all centered on a particular subject. With their unique mix of varied contributions from Original Research to Review Articles, Frontiers Research Topics unify the most influential researchers, the latest key findings and historical advances in a hot research area! Find out more on how to host your own Frontiers Research Topic or contribute to one as an author by contacting the Frontiers Editorial Office: frontiersin.org/about/contact

IMPACT OF COVID-19 LOCKDOWNS ON THE REGIONAL AND GLOBAL OCEANS AND COASTS

Topic Editors:
D. Swain, Indian Institute of Technology Bhubaneswar, India
Deepak R. Mishra, University of Georgia, United States
Stefano Vignudelli, National Research Council (CNR), Italy
Christine M. Lee, NASA Jet Propulsion Laboratory (JPL), United States
Domenico D'Alelio, University of Naples Federico II, Italy

Citation: Swain, D., Mishra, D. R., Vignudelli, S., Lee, C. M., D'Alelio, D., eds. (2022). Impact of COVID-19 Lockdowns on the Regional and Global Oceans and Coasts. Lausanne: Frontiers Media SA. doi: 10.3389/978-2-88974-924-9

Table of Contents

05 ***Did the Coronavirus Disease 2019 Lockdown Phase Influence Coastal Water Quality Parameters off Major Indian Cities and River Basins?***
Aneesh Anandrao Lotliker, Sanjiba Kumar Baliarsingh, R. Venkat Shesu, Alakes Samanta, R. Chandrasekhar Naik and T. M. Balakrishnan Nair

16 ***Assessment of Water Quality Along the Southeast Coast of India During COVID-19 Lockdown***
K. Vijay Prakash, Ch. S. Geetha Vimala, T. Preethi Latha, Chiranjivi Jayaram, P. V. Nagamani and Ch. N. V. Laxmi

29 ***Effect of COVID-19 Anthropause on Water Clarity in the Belize Coastal Lagoon***
Ileana A. Callejas, Christine M. Lee, Deepak R. Mishra, Stacey L. Felgate, Claire Evans, Abel Carrias, Andria Rosado, Robert Griffin, Emil A. Cherrington, Mariam Ayad, Megha Rudresh, Benjamin P. Page and Jennifer A. Jay

40 ***Corrigendum: Effect of COVID-19 Anthropause on Water Clarity in the Belize Coastal Lagoon***
Ileana A. Callejas, Christine M. Lee, Deepak R. Mishra, Stacey L. Felgate, Claire Evans, Abel Carrias, Andria Rosado, Robert Griffin, Emil A. Cherrington, Mariam Ayad, Megha Rudresh, Benjamin P. Page and Jennifer A. Jay

41 ***Anomalous Reduction of the Total Suspended Matter During the COVID-19 Lockdown in the Hooghly Estuarine System***
Chiranjivi Jayaram, Rajdeep Roy, Neethu Chacko, Debadatta Swain, Ramunaidu Punnana, S. Bandyopadhyay, S. B. Choudhury and Dibyendu Dutta

52 ***Variations of Colored Dissolved Organic Matter in the Mandovi Estuary, Goa, During Spring Inter-Monsoon: A Comparison With COVID-19 Outbreak Imposed Lockdown Period***
Albertina Dias, Siby Kurian, Suresh Thayapurath and Anil K. Pratihary

62 ***COVID-19 Impacts on Beaches and Coastal Water Pollution at Selected Sites in Ecuador, and Management Proposals Post-pandemic***
Franklin I. Ormaza-González, Divar Castro-Rodas and Peter J. Statham

78 ***Aerosol Induced Changes in Sea Surface Temperature Over the Bay of Bengal Due to COVID-19 Lockdown***
T. S. Sarin, V. Vinoj, D. Swain, K. Landu and E. Suhas

87 ***Measuring the Impact of the COVID-19 Shutdown on Great Lakes Water Quality Using Remote Sensing***
Karl R. Bosse, Michael J. Sayers, Robert A. Shuchman, John Lekki and Roger Tokars

103 ***Long-Term Trends and Impact of SARS-CoV-2 COVID-19 Lockdown on the Primary Productivity of the North Indian Ocean***
N. Sunanda, J. Kuttippurath, R. Peter, Kunal Chakraborty and A. Chakraborty

116 ***Sustenance of Indian Moored Buoy Network During COVID-19 Pandemic – A Saga of Perseverance***

R. Venkatesan, K. Jossia Joseph, C. Anoopa Prasad, M. Kalyani, M. Arul Muthiah, S. Ramasundaram, P. Murugesh, K. Thirumurugan, R. Sundar, B. Kesavakumar, G. Vengatesan, K. Ramesh, M. V. Martin, K. N. Navaneeth, P. Senthilkumar, Biswajit Haldar, Abhishek Tandon, R. Sridharan, S. Sundar Jesuraj, C. Muthukumar, N. Sundaravadivelu and M. Saravanan

129 ***An Evaluation of the Impact of Pandemic Driven Lockdown on the Phytoplankton Biomass Over the North Indian Ocean Using Observations and Model***

Vivek Seelanki and Vimlesh Pant

frontiers in Marine Science

ORIGINAL RESEARCH
published: 01 April 2021
doi: 10.3389/fmars.2021.648166

Did the Coronavirus Disease 2019 Lockdown Phase Influence Coastal Water Quality Parameters off Major Indian Cities and River Basins?

Aneesh Anandrao Lotliker, Sanjiba Kumar Baliarsingh, R. Venkat Shesu, Alakes Samanta, R. Chandrasekhar Naik and T. M. Balakrishnan Nair*

Indian National Centre for Ocean Information Services, Ministry of Earth Sciences, Government of India, Hyderabad, India

The end of the current decade experienced an outbreak of a new strain of coronavirus classified as severe acute respiratory syndrome coronavirus 2 (SARS-CoV2) [coronavirus disease 2019 (COVID-19)] that spread across the globe within a short span of time and was declared as a global pandemic by the World Health Organization. In order to contain the spread of COVID-19, the Indian Government imposed lockdown in various phases, namely, the strict lockdown period (SLP) and relaxed lockdown period (RLP). The present study addresses changes in the magnitude of satellite-derived water quality parameters in the coastal waters off major Indian cities (Mumbai and Chennai) and river basins (Narmada, Mandovi-Zuari, Netravathi, Periyar, Kaveri, Krishna-Godavari, Mahanadi, and Hooghly) along the eastern Arabian Sea (EAS) and western Bay of Bengal (WBoB) during SLP and RLP. The daily climatology (2003–2019) and anomaly (2020) of different water quality parameters, *viz*., chlorophyll-*a* (chl-*a*), downwelling diffused attenuation coefficient (k_d490), and particulate organic carbon (POC) were used in the present study to eliminate seasonal biases and to unravel the signature of lockdown-induced changes in the magnitude of the above water quality parameters. During the total lockdown period, the magnitude of the above parameters reduced significantly in the coastal waters of both the EAS and the WBoB. However, this reduction was more significant in the coastal waters of the WBoB, attributed to a reduction in the supply of anthropogenic nutrients. Among different studied locations, the magnitude of water quality parameters significantly decreased off Chennai and Hooghly, during SLP, which subsequently increased during RLP probably due to reduction in anthropogenic material influx during SLP and increase during RLP. During RLP, the coastal waters off Mahanadi showed a maximum decrease in the magnitude of water quality parameters followed by Mandovi-Zuari, irrespective of these regions' quantum of anthropogenic material input, possibly due to the higher response time of the ecosystem to reflect the reduction in anthropogenic perturbations. The satellite-retrieved water quality parameters have provided valuable insight to efficiently describe the changes in the health of the Indian coastal environment in terms of phytoplankton biomass and water clarity.

Keywords: satellite, anthropogenic discharge, chlorophyll-*a*, POC, K_d490, Bay of Bengal, Arabian Sea, COVID-19

OPEN ACCESS

Edited by:
Deepak R. Mishra, University of Georgia, United States

Reviewed by:
Haimanti Biswas, Council of Scientific and Industrial Research (CSIR), India
Abhishek Kumar, University of Georgia, United States

****Correspondence:***
Aneesh Anandrao Lotliker
aneesh@incois.gov.in

Specialty section:
This article was submitted to Global Change and the Future Ocean, a section of the journal Frontiers in Marine Science

Received: *31 December 2020*
Accepted: *08 March 2021*
Published: *01 April 2021*

Citation:
Lotliker AA, Baliarsingh SK, Shesu RV, Samanta A, Naik RC and Balakrishnan Nair TM (2021) Did the Coronavirus Disease 2019 Lockdown Phase Influence Coastal Water Quality Parameters off Major Indian Cities and River Basins? Front. Mar. Sci. 8:648166. doi: 10.3389/fmars.2021.648166

INTRODUCTION

The outbreak of a new strain of coronavirus classified as severe acute respiratory syndrome coronavirus 2 (SARS-CoV2) shook the entire world in 2020. The virus was first reported in Wuhan, China, on December 31, 2019, and spread across the globe within a short span of time. The World Health Organization (WHO) named this widespread outbreak as coronavirus disease 2019 (COVID-19) (Cascella et al., 2020). Subsequently, based on the rapid transmission, repeated emergence, and higher causality rate, WHO declared COVID-19 as a pandemic in March 2020. As of November 2020, more than 63.6 million COVID-19 cases have been confirmed in over 220 countries (Worldometers.info, 2020). In order to contain the spread of COVID-19, several countries have imposed a lockdown to maintain physical distancing. The government of India also implemented lockdown in four phases from March 25 to May 31, 2020. The first phase of the lockdown was during March 25 to April 14, 2020. These 21 days of strict lockdown imposed restrictions on physical gathering, industrial operations, and agriculture activities except for emergency services. The restrictions on industrial and agricultural activities were lifted during subsequent phases of lockdown (**Figure 1**)[1].

The industrial and social activities were significantly reduced during various lockdown phases, resulting in the reduction in air and water pollution in different parts of the world, including India (Garg et al., 2020; Lokhandwala and Gautam, 2020; Muhammad et al., 2020; Patel et al., 2020). In general, anthropogenic activities are the source of atmospheric and aquatic pollution. The Indian subcontinent houses many major river estuaries and large cities along the west and east coasts. The coastal waters of India in the vicinity of major cities and river basins are strongly influenced by the anthropogenic discharge (Zingde and Govindan, 2000; Verlecar et al., 2006; Gopal et al., 2018).

The coastal ecosystems around the world cover ∼10% of the total ocean surface area. However, these active land–ocean interaction zones play a pivotal role in the oceanic carbon cycle (Gattuso et al., 1998). In addition, the coastal ocean also acts as a filter for anthropogenic materials before they are transported into the deep sea. On the other hand, the continuous influx of anthropogenic materials also exerts a significant impact on the coastal environments (Hader et al., 2020). In the present century, the coastal waters of several countries are receiving high loads of anthropogenic pollutants that significantly influence the aquatic ecology, sometimes leading to eutrophication (Diaz and Rosenberg, 2008; Seitzinger et al., 2010). Therefore, natural as well as anthropogenic perturbations in the ambient water quality need regular monitoring. In the recent era, satellite-retrieved environmental parameters such as chlorophyll-*a* (chl-*a*; proxy of phytoplankton biomass), particulate organic carbon (POC; indicator of the supply and spreading of the particulate organic matter), and diffused light attenuation coefficient (k_d490; index of water clarity/turbidity) can be efficiently utilized in water quality monitoring (Kratzer et al., 2003; Mishonov et al., 2003; Ni et al., 2008; Kim et al., 2017). Many previous studies have suggested and shown that human-induced material influx is the key cause of pollution in the coastal environment. During the pandemic-induced global lockdown, industrial operations, fishing activities, tourism, agriculture, and aquaculture activities are restricted

[1]https://www.mha.gov.in

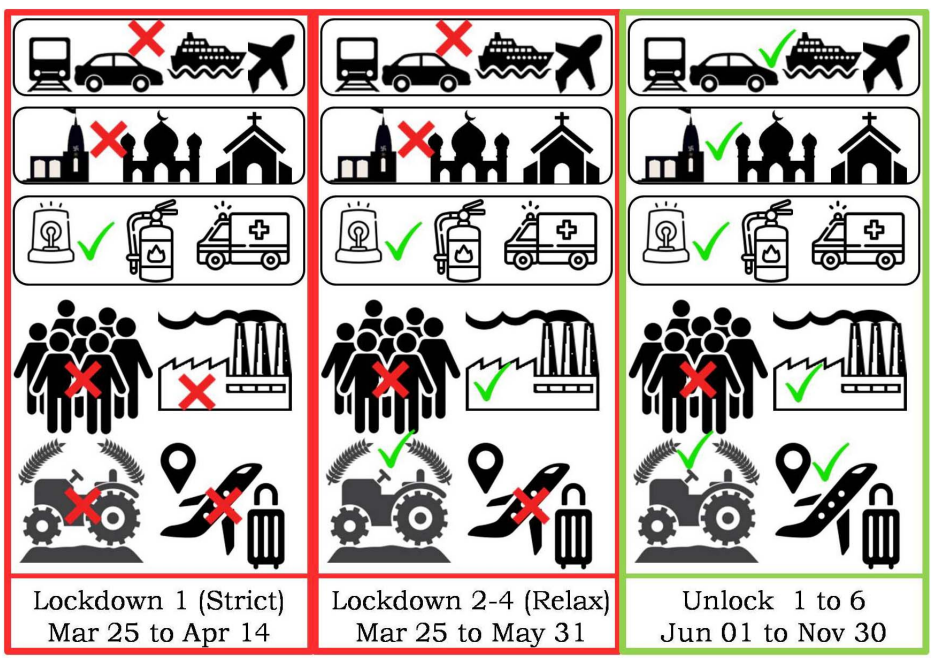

FIGURE 1 | Schematic showing various stages of lockdown and unlock in India during the coronavirus disease 2019 (COVID-19) pandemic.

for specific periods. As anticipated, the level of anthropogenic material input to the coastal waters has dropped significantly and exerted an impact on the coastal water quality of several regions of the world ocean such as the Gulf of Mannar (India), Tangier (Morocco), and Jakarta (Indonesia) (Adwibowo, 2020; Cherif et al., 2020; Yunus et al., 2020; Edward et al., 2021).

India has a long coastline of ∼7,500 km; and the coastal waters of both the west coast [eastern Arabian Sea (EAS)] and east coast [western Bay of Bengal (WBoB)] cater a large variety of ecosystem services. However, the Indian coastal waters are experiencing water quality deterioration due to the increasing influx of anthropogenic materials (Verlecar et al., 2006; Mishra et al., 2015). In the situation of the COVID-19 pandemic, India was under nationwide lockdown for over 2 months. This could have probably altered the anthropogenic inputs to the coastal waters off major Indian cities and river basins. A recent study in the Indian coastal waters has demonstrated an overall reduction in satellite-derived pre-monsoon chl-*a* in the offshore regions of urban centers during the peak of the lockdown in April 2020. This decline was linked to the reduction in anthropogenic nutrient supply to the coastal milieu (Mishra et al., 2020). In this regard, the COVID-19 pandemic-induced lockdown has given an opportunity to understand and quantify the effect of anthropogenic material influx on coastal water ecology on a synoptic scale using satellite remote sensing. The present study demonstrates changes in the magnitude of satellite-derived water quality parameters (chl-*a*, POC, and k_d490), during lockdown phases of COVID-19, in the Indian coastal waters. It is important to mention here that the Indian coastal waters experience strong seasonality in the variation of water quality parameters attributed to a multitude of environmental forcing including the effect of tropical cyclones (Banse, 1987; Kone et al., 2009; Vinayachandran, 2009). Therefore, daily climatology and anomaly-based assessment are very important to eliminate the biases of seasonal and extreme events. The present study has an advantage in this regard through the adoption of such criteria.

MATERIALS AND METHODS

Study Area

The present study was carried out at 10 strategic locations of the Indian coastal waters bordering the west (EAS) and east coasts (WBoB) (**Figure 2**). The locations in the coastal

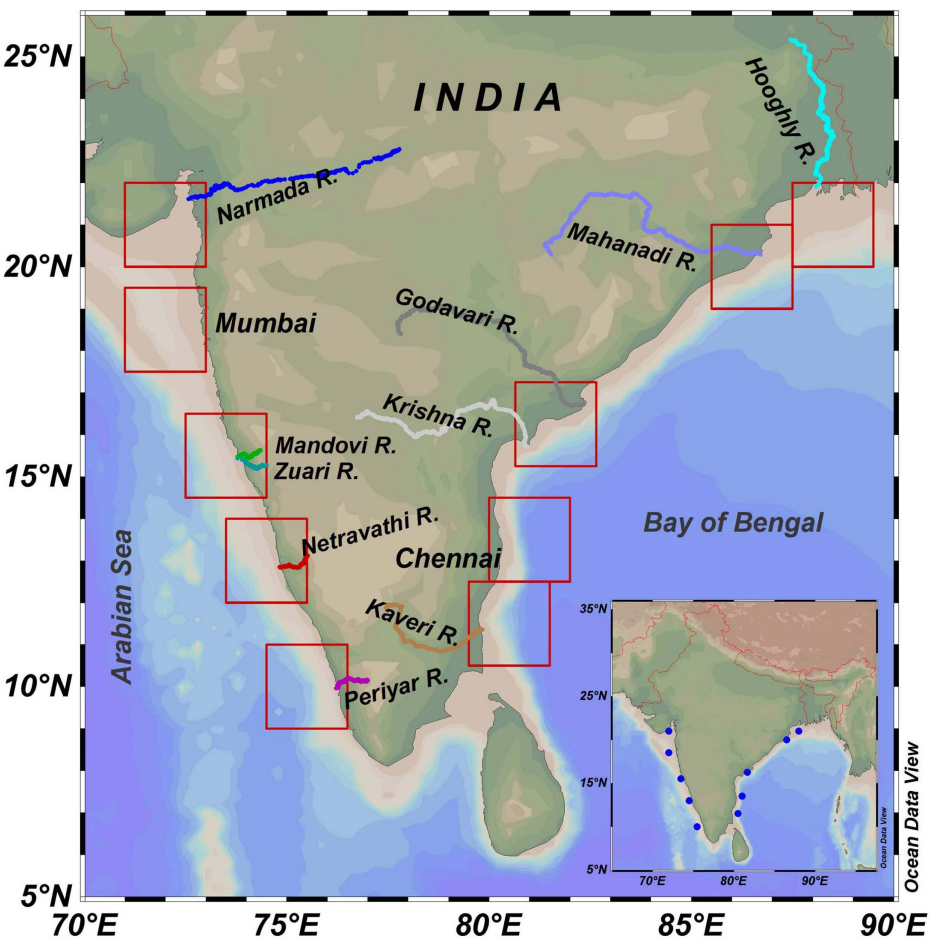

FIGURE 2 | Map showing study regions (2° × 2° square boxes) in the Indian coastal waters. The details of geographic domains are provided in **Table 1**.

TABLE 1 | Geographic positions and environmental attributes of the study regions.

Sl	Area	Latitude (N)	Longitude (E)	Remarks
1.	Narmada	20.00–22.00	71.00–73.00	Under the influence of industrial city, Surat
2.	Mumbai	17.50–19.50	71.00–73.00	Major metropolis
3.	Mandovi-Zuari	14.50–16.50	72.50–74.50	Tourism and major port
4.	Netravathi	12.00–14.00	73.50–75.50	Mangalore city and port
5.	Periyar	09.00–11.00	74.50–76.50	Kochi city and port
6.	Kaveri	10.50–12.50	79.50–81.50	—
7.	Chennai	12.50–14.50	80.00–82.00	Major metropolis
8.	Krishna-Godavari	15.25–17.25	80.65–82.65	Major port
9.	Mahanadi	19.00–21.00	85.50–87.50	Paradeep city and port
10.	Hooghly	20.00–22.00	87.50–89.50	Major metropolis, Kolkata

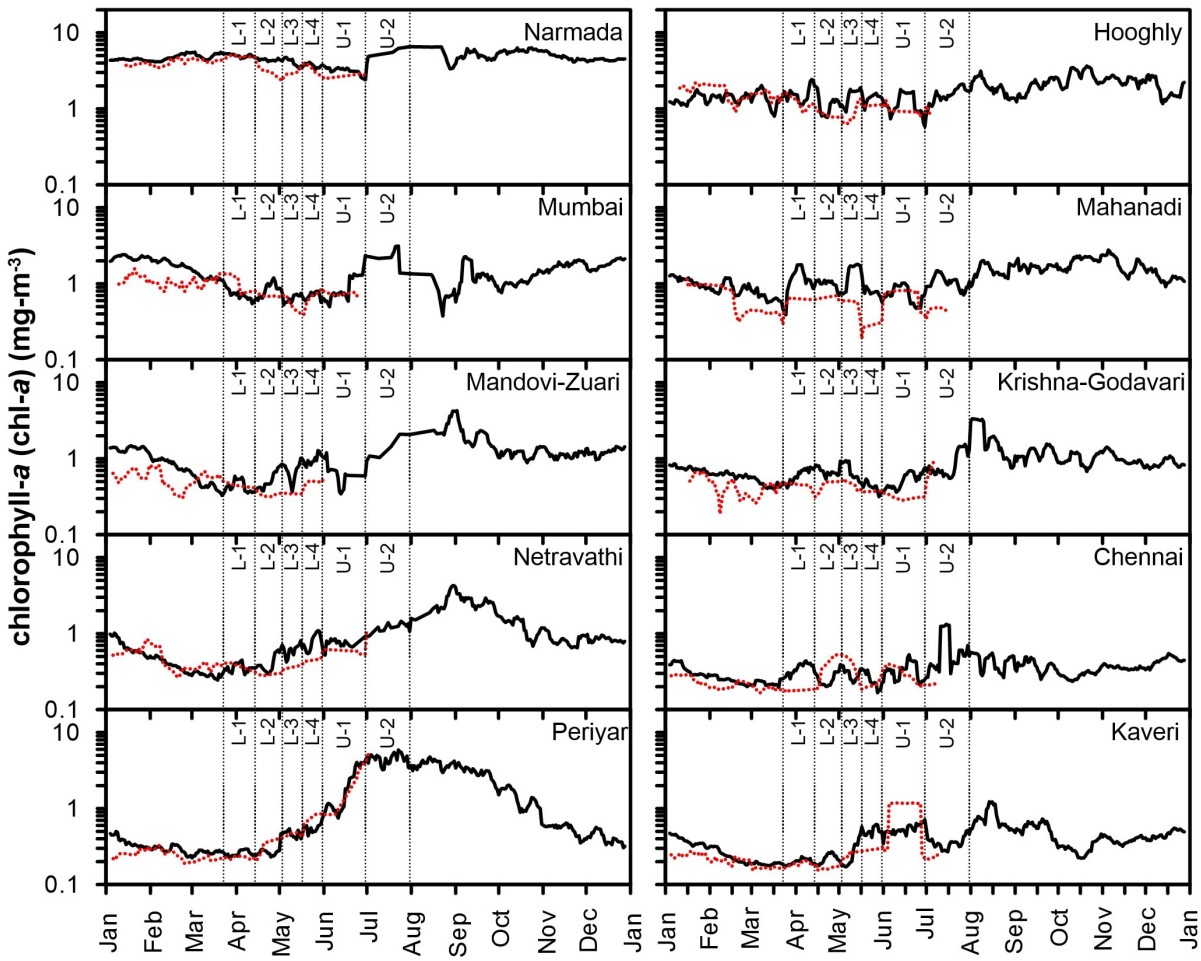

FIGURE 3 | Mean time-series variability in chl-*a* climatology (solid black line) and for the year 2020 (dotted red line) off major Indian cities and river basins.

waters are selected within the vicinity of major Indian cities (Mumbai and Chennai) and river basins (Narmada, Mandovi-Zuari, Netravathi, Periyar, Kaveri, Krishna-Godavari, Mahanadi, and Hooghly). The Indian coastal waters are under the influence of reversing monsoon circulation and coastal currents. Several physical processes such as upwelling, currents, and surface winds play pivotal roles in sustaining the food web initiated by phytoplankton in the coastal waters of the WBoB and the EAS. Apart from the natural oceanographic forcing, the coastal waters of both the basins receive a huge amount of river influx and anthropogenic discharge from different urban, agricultural, and industrial centers that influence the coastal water quality and phytoplankton ecology (Gomes et al., 2000; Kumar et al., 2007, 2018; Thomas et al., 2013).

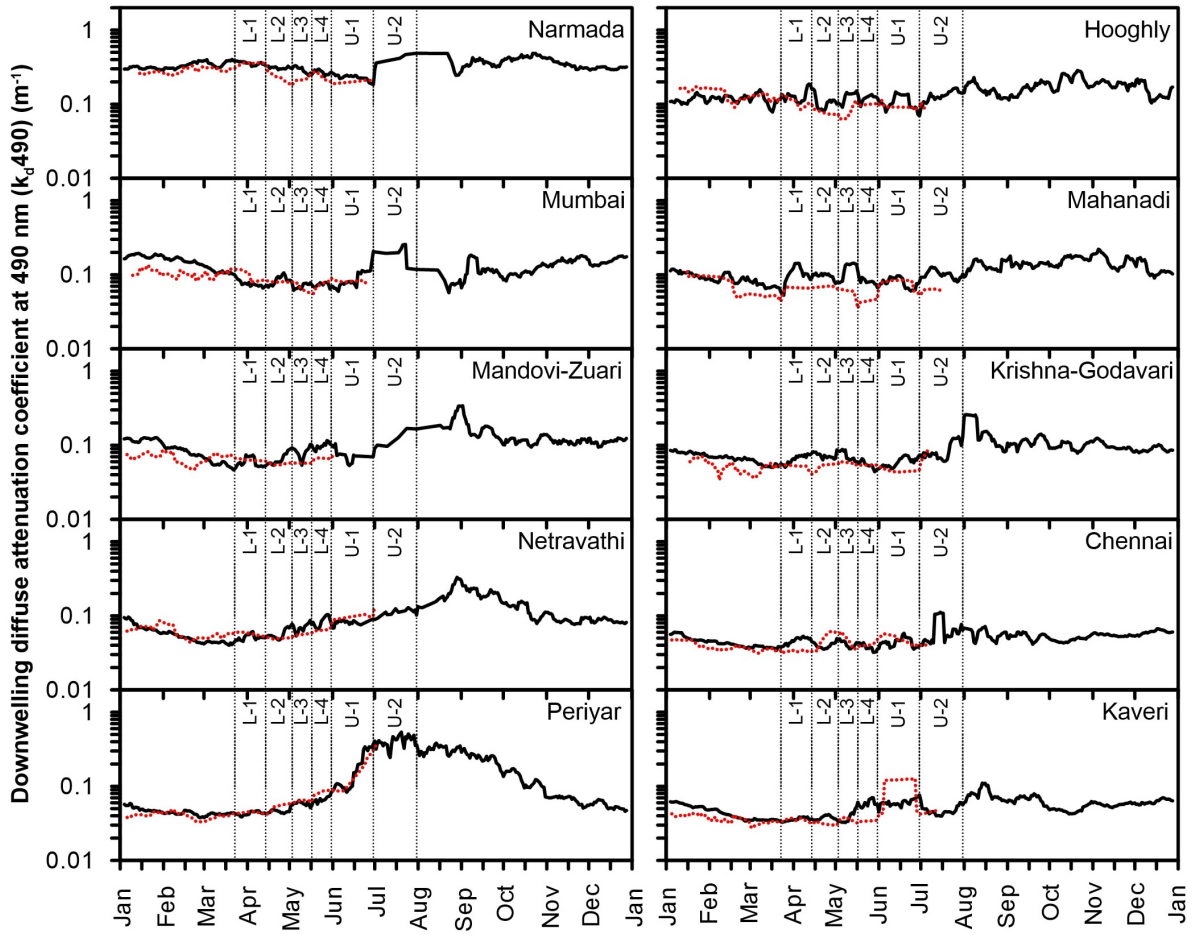

FIGURE 4 | Mean time-series variability in k_d490 climatology (solid black line) and for the year 2020 (dotted red line) off major Indian cities and river basins.

Satellite Data and Processing

The Moderate Resolution Imaging Spectroradiometer onboard Aqua satellite (MODISA) level 3 daily data of different water quality parameters (chl-*a*, k_d490, POC) was taken from OceanColor Web[2], which are processed (levels 0–3) by Ocean Biology Processing Group (OBPG) of the National Aeronautics and Space Administration (NASA). The level 3 standard mapped data products with 4-km spatial resolution, for each variable, were retrieved from January 1, 2003, to July 31, 2020, and processed using RStudio software. The level 3 standard data products of MODISA use sensor-default bio-optical algorithms for retrieval of chl-*a* (O'Reilly et al., 1998, 2000a; Hu et al., 2012), POC (Stramski et al., 2008), and k_d490 (O'Reilly et al., 2000b; Lee et al., 2005). A detailed description of the genesis of algorithms, sensitivity, and performance validation is in the cited literature (in the parentheses of each parameter). A recent study by Scott and Werdell (2019) have demonstrated a similar L2 and L3 satellite-to-*in situ* performance for MODISA chl-*a*. In addition, L3 data are available with a regular Earth-grid frame of reference, which makes the data processing easier without losing the data quality and accuracy. It is also important to mention here that OBPG applies 17 quality flags while processing the data in order to produce the best quality output. In addition, OBPG datasets was checked for acceptable range limits while computing the mean values.

The retrieval accuracy of ocean color satellite products is limited in the coastal waters as compared with open ocean. However, recent studies have demonstrated reasonably well performance of ocean color bio-optical algorithms in retrieving chl-*a* with errors less than 30% for the full range of variability over a large area in the coastal waters (Tilstone et al., 2013; Kahru et al., 2014). Tilstone et al. (2013) have demonstrated a good match [unbiased percentage difference (UPD) < 7.5%] between remote reflectance (R_{rs}) retrieved from MODISA and *in situ* in the Indian coastal waters, which justified the use of satellite data for studying the variability of environmental parameters. The high degree of correlation between *in situ* and MODISA R_{rs} also provides confidence to use these products for studying the trend of environmental parameters in the Indian coastal waters. The data from January 1, 2003, to December 31, 2019, were used for the preparation of climatology $[\overline{X}]$; and the data from January 1, 2020, to July 31, 2020 $[X]$ along

[2]https://oceancolor.gsfc.nasa.gov/

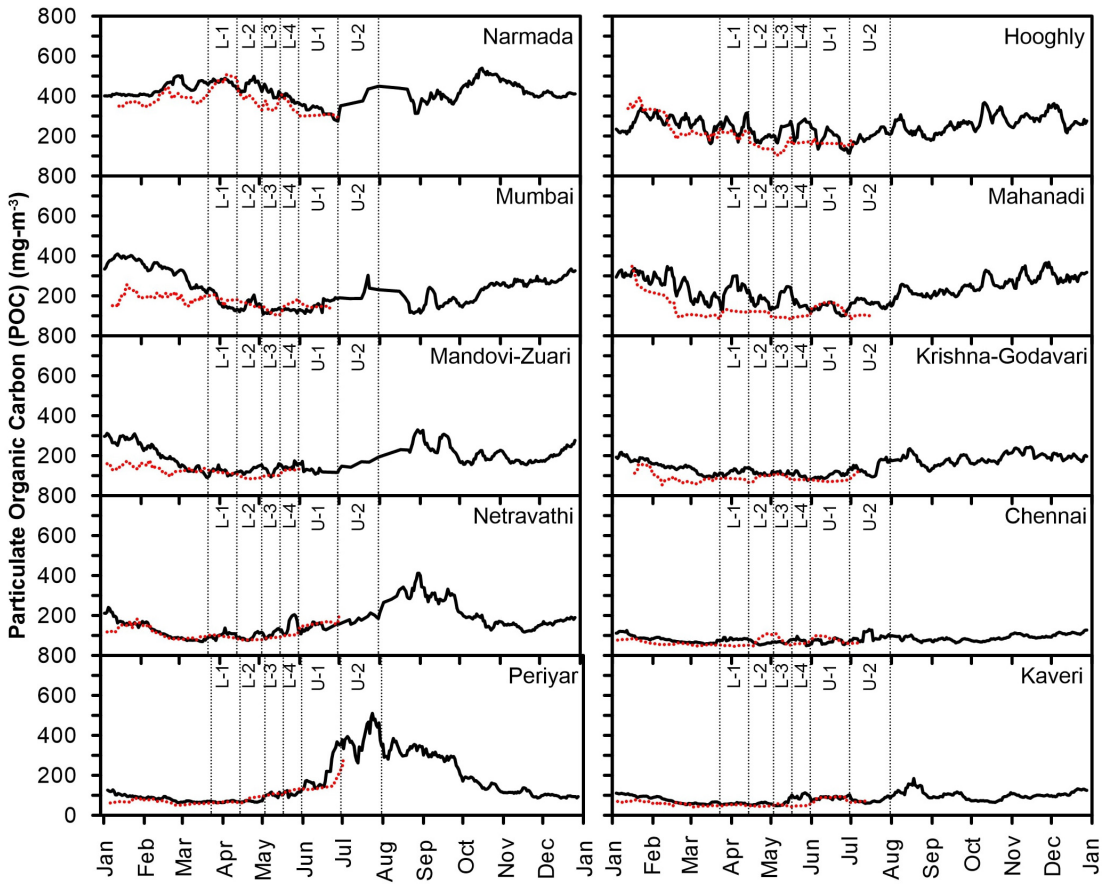

FIGURE 5 | Mean time-series variability in POC climatology (solid black line) and for the year 2020 (dotted red line) off major Indian cities and river basins.

with the aforementioned climatology were used to calculate the anomaly $\left[X - \overline{X}\right]$. Subsequently, the climatology and anomaly were averaged over 2° × 2° box within the region of interest (**Table 1**). Further, the satellite-retrieved parameters were averaged into two categories to understand the variability during the strict lockdown period (SLP; March 25 to April 14, 2020) and relaxed lockdown period (RLP; April 15 to May 31, 2020). All the illustrations and graphics were prepared using Ocean Data View (ODV) (Schlitzer, 2002) and Grapher and SeaWiFS Data Analysis System (SeaDAS) software packages.

RESULTS AND DISCUSSION

The variability in the magnitude of MODISA-retrieved water quality parameters (chl-*a*, POC, and k_d490) was analyzed for various lockdown and unlock phases of COVID-19 in the offshore of major Indian cities (Mumbai and Chennai) and river basins (Narmada, Mandovi-Zuari, Netravathi, Periyar, Kaveri, Krishna-Godavari, Mahanadi, and Hooghly). The daily climatology (2003–2019) and anomaly (2020) of the above parameters were generated from MODISA, describing changes in the magnitude of chl-*a*, k_d490, and POC.

The North Indian Ocean exhibits a strong seasonal variability in water quality parameters as evident from the climatology (**Figures 3–5**). Therefore, in the present analysis, the anomaly was used to eliminate seasonality. The spatial distribution of chl-*a*, k_d490, and POC anomaly during April and May 2020 is illustrated in **Figure 6**. The overall result showed a negative anomaly indicating a reduction in the magnitude of water quality parameters in the coastal waters of both the EAS and the WBoB during the total lockdown period (SLP and RLP). However, the reduction in magnitude was more significant in the WBoB as compared with the EAS.

The river discharge carrying industrial, agricultural, and urban effluents could have played an important role behind the contrasting scenarios in the variability of the environmental parameters in the Indian coastal waters. In general, the coastal waters of the WBoB receive a large volume of river discharge through the major Indian rivers such as Ganga, Brahmaputra, Mahanadi, Godavari, Krishna, and Kaveri (Shetye et al., 1996; Howden and Murtugudde, 2001). In addition to the oceanic processes, river discharge acts as a major source of phytoplankton growth-promoting inorganic nutrients and suspended sediments to the WBoB and plays an important in sustaining the food web (Bharathi et al., 2018). However, the river discharges infused

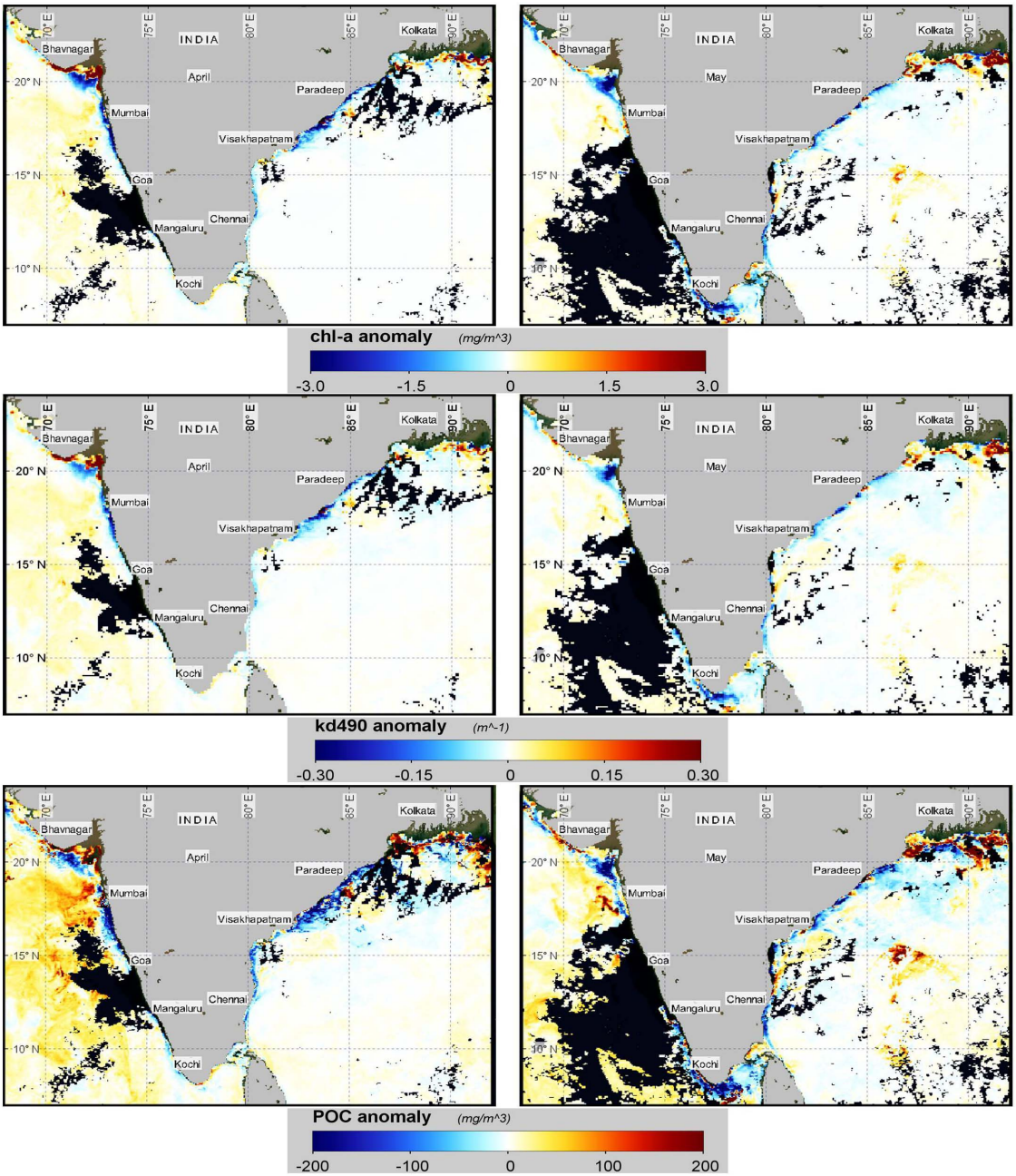

FIGURE 6 | Spatial distribution of chl-*a*, k_d490, and POC anomaly for April and May 2020 derived using MODISA data.

with higher concentration of land-derived nutrients sometimes lead to over-enrichment and result in eutrophication affecting the coastal water quality of the WBoB (Sattar et al., 2014; Sarma et al., 2020). On the other hand, the coastal waters of the EAS receive a lower quantum of freshwater discharge in comparison with the WBoB. Therefore, the possible reduction in the supply of anthropogenic nutrients especially from agriculture practices, industrial effluents, and urban wastes through terrigenous/river discharge could have resulted in lower productivity and improved water clarity during the lockdown period. A recent study has reported a significant reduction in turbidity levels in the upstream of Ganga River during the lockdown period, which signified the reduction in anthropogenic pollutant level (Garg et al., 2020). It is also important to mention here that apart from land-derived inputs, the lower atmospheric fallouts also play an important role in modulating the coastal food chain. Concomitantly, Mishra et al. (2020) have hypothesized the decrease in the concentration of chl-*a* in the Indian coastal waters due to the reduction in the atmospheric nutrient deposition in the coastal waters as well as watershed fluxes due to the lockdown.

In order to quantify the changes in the magnitude of water quality parameters, during the COVID-19 lockdown period, the percent change in anomaly with respect to climatology was computed. The mean anomaly in the magnitude of water quality parameters, during SLP and RLP, off major Indian cities and river basins in the coastal waters of the WBoB and the EAS are illustrated in **Figure 7**. During SLP, the coastal waters of the WBoB showed a significant negative anomaly in water quality parameters (chl-*a*, 10–51%; k_d490, 4–27%; POC, 12–37%). On the other hand, in the coastal waters of EAS, the positive anomaly was observed off Mumbai, Mandovi-Zuari, and Netravathi (chl-*a*, 14%; k_d490, 19%). However, the anomaly was not significant off Mumbai and Mandovi-Zuari. The overall variability in the magnitude of water quality parameters, in the Indian coastal waters, discerned maximum negative anomaly off Chennai (chl-*a*, 51%; k_d490, 27%; POC, 37%) followed by off Hooghly (chl-*a*, 31%; k_d490, 26%; POC, 20%).

During RLP, the WBoB showed negative anomaly at all the locations (chl-*a*, 17–61%; k_d490, 18–49%; POC, 16–53%) except off Chennai, where chl-*a* (12%) and k_d490 (11%) showed positive anomaly. The coastal waters of EAS showed negative anomaly at all the locations (chl-*a*, 15–56%; k_d490, 4–33%; POC, 12–32%) except off Periyar, where the magnitude of all water quality parameters showed positive anomaly (chl-*a*, 22%; k_d490, 17%; POC, 11%). As per a recent report, the Periyar River had continued to receive anthropogenic discharge even during the lockdown period and thereby possibly resulted in a higher magnitude of the studied parameters (Satheesh, 2020). Among different studied locations in the coastal waters of the WBoB, the magnitude of all water quality parameters significantly decreased off Chennai during SLP, which subsequently increased during RLP.

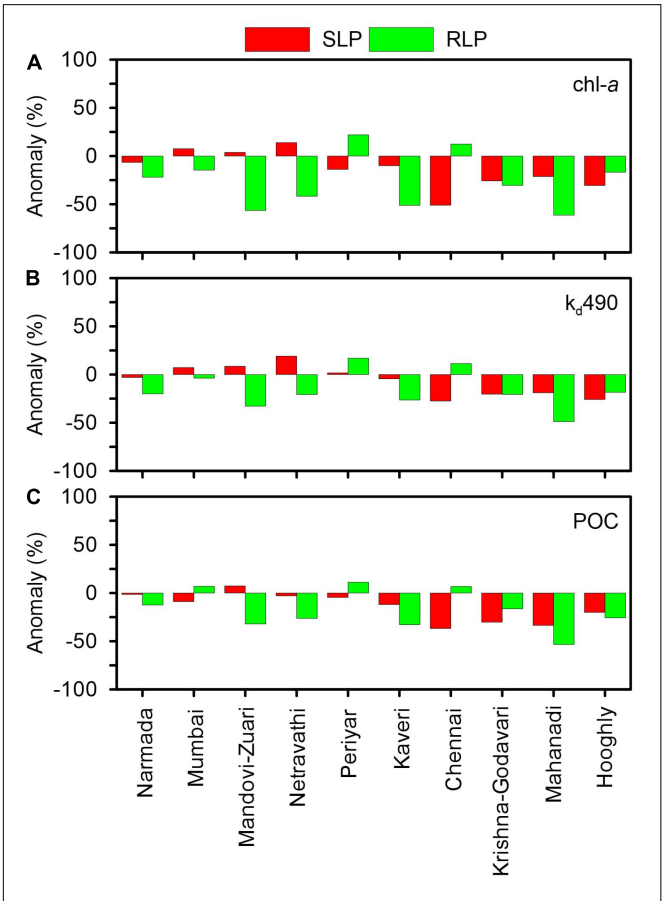

FIGURE 7 | Mean anomaly of **(A)** chl-*a*, **(B)** k_d490, and **(C)** POC during strict (March 25 to April 14, 2020) and relaxed lockdown (April 15 to May 31, 2020) off major Indian cities and river basins.

The metropolis of Chennai generates a high volume of anthropogenic pollutants. The coastal waters of Chennai experience episodes of eutrophication and toxic algal blooms due to the city pollutants brought by the Adyar and Cooum Rivers (Shanmugam et al., 2007; Mishra et al., 2015). Therefore, it can be hypothesized that the higher load of anthropogenic pollutants could have not allowed phytoplankton to flourish. However, during RLP, an increase in chl-*a* anomaly was probably attributed to the relative reduction in pollution stress. Analogous to Chennai, the coastal waters off Hooghly also receive a significant load of anthropogenic pollutants. The Hooghly River is one of the major distributaries of Ganga River. After traveling a considerable distance from the upstream, the river passes through the urbanized metropolitan city of Kolkata and carries all the anthropogenic materials into the coastal waters of the WBoB. The recent reports showed a significant increase of the water transparency in the upper reaches of Ganga River during the lockdown period, signifying a reduction in anthropogenic influx (Garg et al., 2020). Concomitantly, the subsequent reduction in the pollution stress restored phytoplankton growth in the downstream (Hooghly estuary), which has been also reported during the lockdown period (Pal et al., 2020; Sengupta et al., 2020). In general, the estuaries act as a filter for the anthropogenic material before passing into the adjoining sea. Therefore, the reduction in excess anthropogenic materials restored the phytoplankton growth by optimally utilizing the nutrients. Therefore, these coastal waters also showed an increase in the magnitude of chl-*a* from SLP to RLP.

During RLP, the maximum percentage decrease in concentration was observed off Mahanadi (chl-*a*, 61%; k_d490, 49%; POC, 53%). Although the coastal waters off Mandovi-Zuari estuary receive lesser anthropogenic inputs than the coastal waters off Mahanadi, they also followed a decreasing pattern in the studied parameters (chl-*a*, 56%; k_d490, 33%; POC, 32%) with a higher percentage next to off Mahanadi. The response times of these ecosystems to reflect the variability in biogeochemical parameters could have played an important role behind the decreased magnitude of water quality parameters during RLP (Drupp et al., 2011). It can be hypothesized that the coastal water productivity was sustained using the available nutrients in the ecosystem during SLP. Subsequently, after the reduction in the anthropogenically sourced nutrients during SLP, the decrease in the magnitude of chl-*a* and POC was reflected in the lag phase during RLP. A recent study has reported a similar instance off Mahanadi showing a decrease in the magnitude of chl-*a* attributed to anthropogenic nitrate reduction during SLP (Mishra et al., 2020).

CONCLUSION

In recent decades, anthropogenic activities in the coastal regions have risen at an unprecedented pace, which poses a significant threat to coastal water habitats. The stochastic anthropogenic nutrient supplies to the coastal areas result in recurrent events of eutrophication, algal blooms (sometimes toxic), phytoplankton community shift, and depletion in aquatic oxygen concentration. As urbanization and population growth are rising, several research programs and monitoring plans are undergoing to address this global concern and to understand the root causes as well as long-term impact.

The COVID-19 pandemic-induced lockdown pave the way to an opportunity to understand and quantify the effect of anthropogenic material influx on coastal water ecology. In this regard, the present study has addressed the temporal variation in the magnitude of satellite-retrieved water quality parameters (chl-*a*, k_d490, and POC), in the Indian coastal waters, during different phases of lockdown. The satellite (MODISA)-retrieved magnitudes of water quality parameters have provided valuable insight to efficiently describe the changes in response to the lockdown. As the North Indian Ocean exhibits seasonality in the spatio-temporal variation of water quality parameters, an anomaly-based assessment was adopted in this study to eliminate the seasonal biases. The overall results discerned a decrease in the magnitude of water quality parameters in the coastal waters of both the EAS and the WBoB during the total lockdown period (SLP and RLP). However, the reduction was more significant in the WBoB as compared with the EAS. The larger decrease in the magnitude of water quality parameters in WBoB was attributed to the reduction in the supply of anthropogenic nutrients. During SLP, the coastal waters of the WBoB showed a significant negative anomaly in the magnitude of water quality parameters, which was not the case for the EAS due to the lesser dependence on the river-borne anthropogenic material. Among different studied locations in the coastal waters of the WBoB, the magnitude of all water quality parameters significantly reduced off Chennai and Hooghly, during SLP, which subsequently increased during RLP. The coastal waters off Chennai and Hooghly showed the clear signature of lockdown attributed to the reduction in anthropogenic pollutant influx during SLP and subsequent increase during RLP. Among all the studied locations during RLP, the maximum decrease in the magnitude of water quality parameters was observed off Mahanadi followed by Mandovi-Zuari, possibly due to the higher response time of these ecosystems to reflect the reduction in anthropogenic perturbations. In general, the significant reduction in anthropogenic fluxes of nutrients, during the first phase of lockdown, could have led to the decrease in the surfeit primary production and organic matter, thus increasing the water clarity and improvement in the health of the coastal environment.

DATA AVAILABILITY STATEMENT

The datasets presented in this study can be found in online repositories. The names of the repository/repositories and accession number(s) can be found below: https://oceandata.sci.gsfc.nasa.gov/MODIS-Aqua/Mapped/Daily/4km/.

AUTHOR CONTRIBUTIONS

TMBN provided motivation to conceptualize the study. AAL conceived and conceptualized the study. AAL, RVS, and RCN downloaded and processed satellite data. AAL and AS prepared the graphical illustrations with substantial input from SKB. AAL, SKB, and AS interpreted the data. AAL and SKB prepared the first draft of the manuscript with the critical input of AS. TMBN and RVS reviewed and edited the manuscript. All authors contributed to the article and approved the submitted version.

FUNDING

This study has been undertaken as a part of the project entitled "Coastal Monitoring" under the umbrella of "Ocean Services, Modelling, Application, Resources and Technology (O-SMART)" scheme, sanctioned by the Indian Ministry of Earth Sciences (MoES) vide Administrative Order no. MoES/36/OOIS/CM/2019 dated May 7, 2019.

ACKNOWLEDGMENTS

We are thankful to the Director, Indian National Centre for Ocean Information Services (INCOIS), Ministry of Earth Sciences, Hyderabad, India, for the encouragement. We wish to acknowledge the NASA-GSFC for providing satellite data of MODIS and the development team of SeADAS. We also acknowledge RStudio for processing satellite data. This is INCOIS contribution no. 406.

REFERENCES

Adwibowo, A. (2020). Does social distancing have an effect on water quality? An evidence from Chlorophyll-a level in the water of populated Southeast Asian coasts. *Preprints*. doi: 10.20944/preprints202005.0091.v1

Banse, K. (1987). Seasonality of phytoplankton chlorophyll in the central and northern Arabian Sea. *Deep Sea Res. Part A Oceanogr. Res. Pap.* 34, 713–723. doi: 10.1016/0198-0149(87)90032-x

Bharathi, M. D., Sarma, V. V. S. S., Ramaneswari, K., and Venkataramana, V. (2018). Influence of river discharge on abundance and composition of phytoplankton in the western coastal Bay of Bengal during peak discharge period. *Mar. Pollut. Bull.* 133, 671–683. doi: 10.1016/j.marpolbul.2018.06.032

Cascella, M., Rajnik, M., Cuomo, A., Dulebohn, S. C., and Di Napoli, R. (2020). *Features, Evaluation and Treatment Coronavirus (COVID-19). In Statpearls [internet]*. Treasure Island, FL: StatPearls Publishing.

Cherif, E. K., Vodopivec, M., Mejjad, N., Esteves da Silva, J. C., Simonoviè, S., and Boulaassal, H. (2020). COVID-19 pandemic consequences on coastal water quality using WST Sentinel-3 Data: case of Tangier. *Morocco. Water* 12:2638. doi: 10.3390/w12092638

Diaz, R. J., and Rosenberg, R. (2008). Spreading dead zones and consequences for marine ecosystems. *Science* 321, 926–929. doi: 10.1126/science.1156401

Drupp, P., De Carlo, E. H., Mackenzie, F. T., Bienfang, P., and Sabine, C. L. (2011). Nutrient inputs, phytoplankton response, and CO_2 variations in a semi-enclosed subtropical embayment, Kaneohe Bay, Hawaii. *Aquat. Geochem.* 17, 473–498. doi: 10.1007/s10498-010-9115-y

Edward, J. P., Jayanthi, M., Malleshappa, H., Jeyasanta, K. I., Laju, R. L., Patterson, J., et al. (2021). COVID-19 lockdown improved the health of coastal environment and enhanced the population of reef-fish. *Mar. Pollut. Bull.* 165:112124. doi: 10.1016/j.marpolbul.2021.112124

Garg, V., Aggarwal, S. P., and Chauhan, P. (2020). Changes in turbidity along Ganga River using Sentinel-2 satellite data during lockdown associated with COVID-19. *Geomatics Nat. Hazards Risk* 11, 1175–1195. doi: 10.1080/19475705.2020.1782482

Gattuso, J. P., Frankignoulle, M., and Wollast, R. (1998). Carbon and carbonate metabolism in coastal aquatic ecosystems. *Annu. Rev. Ecol. Systemat.* 29, 405–434. doi: 10.1146/annurev.ecolsys.29.1.405

Gomes, H. R., Goes, J. I., and Saino, T. (2000). Influence of physical processes and freshwater discharge on the seasonality of phytoplankton regime in the Bay of Bengal. *Cont. Shelf Res.* 20, 313–330. doi: 10.1016/s0278-4343(99)00072-2

Gopal, V., Shanmugasundaram, A., Nithya, B., Magesh, N. S., and Jayaprakash, M. (2018). Water quality of the Uppanar estuary, Southern India: implications on the level of dissolved nutrients and trace elements. *Mar. Pollut. Bull.* 130, 279–286. doi: 10.1016/j.marpolbul.2018.03.046

Hader, D. P., Banaszak, A. T., Villafañe, V. E., Narvarte, M. A., González, R. A., and Helbling, E. W. (2020). Anthropogenic pollution of aquatic ecosystems: emerging problems with global implications. *Sci. Tot. Environ.* 713:136586. doi: 10.1016/j.scitotenv.2020.136586

Howden, S. D., and Murtugudde, R. (2001). Effects of river inputs into the Bay of Bengal. *J. Geophys. Res. Oceans* 106, 19825–19843. doi: 10.1029/2000jc000656

Hu, C., Lee, Z., and Franz, B. (2012). Chlorophyll-*a* algorithms for oligotrophic oceans: a novel approach based on three-band reflectance difference. *J. Geophys. Res.* 117:C01011. doi: 10.1029/2011jc007395

Kahru, M., Kudela, R. M., Anderson, C. R., Manzano-Sarabia, M., and Mitchell, B. G. (2014). Evaluation of satellite retrievals of ocean chlorophyll-a in the California Current. *Rem. Sens.* 6, 8524–8540. doi: 10.3390/rs6098524

Kim, H. C., Son, S., Kim, Y. H., Khim, J. S., Nam, J., Chang, W. K., et al. (2017). Remote sensing and water quality indicators in the Korean West coast: Spatio-temporal structures of MODIS-derived chlorophyll-*a* and total suspended solids. *Mar. Pollut. Bull.* 121, 425–434. doi: 10.1016/j.marpolbul.2017.05.026

Kone, V., Aumont, O., Lévy, M., and Resplandy, L. (2009). Physical and biogeochemical controls of the phytoplankton seasonal cycle in the Indian Ocean: a modeling study. Indian ocean biogeochemical processes and ecological variability. *Geophys. Monogr. Ser.* 185:350.

Kratzer, S., Hakansson, B., and Sahlin, C. (2003). Assessing Secchi and photic zone depth in the Baltic Sea from satellite data. *Ambio* 32, 577–585. doi: 10.1579/0044-7447-32.8.577

Kumar, P. S., Kumaraswami, M., Rao, G. D., Ezhilarasan, P., Sivasankar, R., Rao, V. R., et al. (2018). Influence of nutrient fluxes on phytoplankton community and harmful algal blooms along the coastal waters of southeastern Arabian Sea. *Cont. Shelf Res.* 161, 20–28. doi: 10.1016/j.csr.2018.04.012

Kumar, S. P., Nuncio, M., Ramaiah, N., Sardesai, S., Narvekar, J., Fernandes, V., et al. (2007). Eddy-mediated biological productivity in The Bay Of Bengal during fall and spring intermonsoons. *Deep Sea Res. Part I Oceanogr. Res. Pap.* 54, 1619–1640. doi: 10.1016/j.dsr.2007.06.002

Lee, Z. P., Du, K. P., and Arnone, R. (2005). A model for the diffuse attenuation coefficient of downwelling irradiance. *J. Geophys. Res. Oceans* 110:C02016. doi: 10.1029/2004JC002275

Lokhandwala, S., and Gautam, P. (2020). Indirect impact of COVID-19 on environment: A brief study in Indian context. *Environ. Res.* 188:109807. doi: 10.1016/j.envres.2020.109807

Mishonov, A. V., Gardner, W. D., and Richardson, M. J. (2003). Remote sensing and surface POC concentration in the South Atlantic. *Deep Sea Res. Part II Top. Stud. Oceanogr.* 50, 2997–3015. doi: 10.1016/j.dsr2.2003.07.007

Mishra, D. R., Kumar, A., Muduli, P. R., Equeenuddin, S., Rastogi, G., Acharyya, T., et al. (2020). Decline in phytoplankton biomass along Indian Coastal waters due to COVID-19 Lockdown. *Remote Sens.* 12:2584. doi: 10.3390/rs12162584

Mishra, P., Panda, U. S., Pradhan, U., Kumar, C. S., Naik, S., Begum, M., et al. (2015). Coastal water quality monitoring and modelling off Chennai city. *Proc. Eng.* 116, 955–962. doi: 10.1016/j.proeng.2015.08.386

Muhammad, S., Long, X., and Salman, M. (2020). COVID-19 pandemic and environmental pollution: a blessing in disguise? *Sci. Total Environ.* 728:138820. doi: 10.1016/j.scitotenv.2020.138820

Ni, H. G., Lu, F. H., Luo, X. L., Tian, H. Y., and Zeng, E. Y. (2008). Riverine inputs of total organic carbon and suspended particulate matter from the Pearl River Delta to the coastal ocean off South China. *Mar. Pollut. Bull.* 56, 1150–1157. doi: 10.1016/j.marpolbul.2008.02.030

O'Reilly, J. E., Maritorena, S., Mitchell, B. G., Siegel, D. A., Carder, K. L., Garver, S. A., et al. (1998). Ocean color chlorophyll algorithms for SeaWiFS. *J. Geophys. Res.* 103, 24937–24953. doi: 10.1029/98jc02160

O'Reilly, J. E., Maritorena, S., O'Brien, M. C., Siegel, D. A., Toole, D., Menzies, D., et al. (2000a). *SeaWiFS Postlaunch Calibration and Validation Analyses, Part 3. NASA Tech. Memo. 2000-206892*, Vol. 11, eds S. B. Hooker and E. R. Firestone (Maryland: NASA Goddard Space Flight Center), 49.

O'Reilly, J. E., Maritorena, S., Siegel, D. A., O'Brien, M. C., Toole, D., Mitchell, B. G., et al. (2000b). *Ocean Color Chlorophyll a Algorithms for SeaWiFS, OC2, and OC4: Version 4. SeaWiFS Postlaunch Calibration and Validation Analyses, Part, 3*. Greenbelt, MD: NASA Goddard Space Flight Center, 9–23.

Pal, N., Barman, P., Das, S., Zaman, S., and Mitra, A. (2020). Status of brackish water phytoplankton during COVID-19 lockdown phase. *NUJS J. Regulatory Stud.* 75–78.

Patel, P. P., Mondal, S., and Ghosh, K. G. (2020). Some respite for India's dirtiest river? Examining the Yamuna's water quality at Delhi during the COVID-19 lockdown period. *Sci. Total Environ.* 744:140851. doi: 10.1016/j.scitotenv.2020.140851

Sarma, V. V. S. S., Krishna, M. S., and Srinivas, T. N. R. (2020). Sources of organic matter and tracing of nutrient pollution in the coastal Bay of Bengal. *Mar. Pollut. Bull.* 159:111477. doi: 10.1016/j.marpolbul.2020.111477

Satheesh, S. (2020). The pandemic does not stop the pollution in River Periyar. *Interface J. Soc. Mov.* 12, 250–257.

Sattar, M. A., Kroeze, C., and Strokal, M. (2014). The increasing impact of food production on nutrient export by rivers to the Bay of Bengal 1970–2050. *Mar. Pollut. Bull.* 80, 168–178. doi: 10.1016/j.marpolbul.2014.01.017

Schlitzer, R. (2002). *Ocean Data View*. Available online at: https://odv.awi.de/ (accessed December 2, 2020).

Scott, J. P., and Werdell, P. J. (2019). Comparing level-2 and level-3 satellite ocean color retrieval validation methodologies. *Opt. Express* 27, 30140–30157. doi: 10.1364/oe.27.030140

Seitzinger, S. P., Mayorga, E., Bouwman, A. F., Kroeze, C., Beusen, A. H. W., Billen, G., et al. (2010). Global river nutrient export: a scenario analysis of past and future trends. *Global Biogeochem. Cy* 24:GB0A08. doi: 10.1029/2009GB003587

Sengupta, T., Pramanick, P., and Mitra, A. (2020). Nutrient load in the River Ganges during the COVID-19 lockdown phase: a ground zero observation. *NUJS J. Regulatory Stud.* 79–83.

Shanmugam, P., Neelamani, S., Ahn, Y. H., Philip, L., and Hong, G. H. (2007). Assessment of the levels of coastal marine pollution of Chennai city, Southern India. *Water Resour. Manag.* 21, 1187–1206. doi: 10.1007/s11269-006-9075-6

Shetye, S. R., Gouveia, A. D., Shankar, D., Shenoi, S. S. C., Vinayachandran, P. N., Sundar, D., et al. (1996). Hydrography and circulation in the western Bay of Bengal during the northeast monsoon. *J. Geophys. Res. Oceans* 101, 14011–14025. doi: 10.1029/95jc03307

Stramski, D., Reynolds, R. A., Babin, M., Kaczmarek, S., Lewis, M. R., Röttgers, R., et al. (2008). Relationships between the surface concentration of particulate organic carbon and optical properties in the eastern South Pacific and eastern Atlantic Oceans. *Biogeoscinces* 5, 171–201. doi: 10.5194/bg-5-171-2008

Thomas, L. C., Padmakumar, K. B., Smitha, B. R., Devi, C. A., Nandan, S. B., and Sanjeevan, V. N. (2013). Spatio-temporal variation of microphytoplankton in the upwelling system of the south-eastern Arabian Sea during the summer monsoon of 2009. *Oceanologia* 55, 185–204. doi: 10.5697/oc.55-1.185

Tilstone, G. H., Lotliker, A. A., Miller, P. I., Ashraf, P. M., Kumar, T. S., Suresh, T., et al. (2013). Assessment of MODIS-Aqua chlorophyll-a algorithms in coastal

and shelf waters of the eastern Arabian Sea. *Cont. Shelf Res.* 65, 14–26. doi: 10.1016/j.csr.2013.06.003

Verlecar, X. N., Desai, S. R., Sarkar, A., and Dalal, S. G. (2006). Biological indicators in relation to coastal pollution along Karnataka coast, India. *Water Res.* 40, 3304–3312. doi: 10.1016/j.watres.2006.06.022

Vinayachandran, P. N. (2009). Impact of physical processes on chlorophyll distribution in the Bay of Bengal. Indian Ocean Biogeochemical Processes and Ecological Variability. *Geophys. Monogr. Ser.* 185, 71–86. doi: 10.1029/2008gm000705

Worldometers.info (2020). *Worldometers.info. Coronavirus Updates.* Available online at: https://www.worldometers.info/ (accessed December 10, 2020).

Yunus, A. P., Masago, Y., and Hijioka, Y. (2020). COVID-19 and surface water quality: Improved lake water quality during the lockdown. *Sci. Tot. Environ.* 731:139012. doi: 10.1016/j.scitotenv.2020.139012

Zingde, M. D., and Govindan, K. (2000). "Health status of the coastal waters of Mumbai and regions around," in *Environmental Problems of Coastal Areas in India*, ed. V. K. Sharma (New Delhi: Bookwell Publishers), 119–132.

Conflict of Interest: The authors declare that the research was conducted in the absence of any commercial or financial relationships that could be construed as a potential conflict of interest.

frontiers in Marine Science

ORIGINAL RESEARCH
published: 13 April 2021
doi: 10.3389/fmars.2021.659686

Assessment of Water Quality Along the Southeast Coast of India During COVID-19 Lockdown

K. Vijay Prakash[1], Ch. S. Geetha Vimala[2], T. Preethi Latha[3], Chiranjivi Jayaram[4], P. V. Nagamani[5] and Ch. N. V. Laxmi[2]*

[1] Department of Ocean Engineering, Indian Institute of Technology Madras, Chennai, India, [2] School of Spatial Information Technology, Jawaharlal Nehru Technological University, Kakinada, India, [3] Amaravathi Metropolitan Region Development Authority, Vijayawada, India, [4] Regional Remote Sensing Centre-East, National Remote Sensing Centre, Kolkata, India, [5] National Remote Sensing Centre, Hyderabad, India

The COVID-19 pandemic has affected the entire world and has had a devastating impact on both lives and livelihoods in India. The only way to defeat the rapid spread of COVID-19, is to shut down socio-economic activities and to maintain minimal human interaction with the implementation of a lockdown. Such lockdowns have manifested in a pollution curtailment in almost all spheres of the planet, including in marine pollution. Quantifying this decrease in pollution levels enables the scientific community to assess the contribution of anthropogenic (especially non-essential) activities to global/regional pollution levels. This paper aims to study the impact of the stringent lockdown period (phase 1 and 2) on coastal water quality along the Chennai coast of India, by analyzing suspended matter concentration (SPM), a key element of water quality and diffuse attenuation coefficient, $K_d(490)$, using LANDSAT-8 Operational Land Imager (OLI) data. LANDSAT-8/OLI, L1TP scenes were subjected to radiometric calibration and atmospheric correction to derive surface reflectance values from raw digital numbers using ACOLITE software and a brief insight has been given for the Dark Spectrum Fitting algorithm used in ACOLITE. SPM concentration decreased by 15.48 and 37.50% in the Chennai and Ennore ports, respectively, due to minimal vessel movement and cargo handling. The stringent lockdown led to the operation of fewer thermal plant units, thus less fly ash was emanated, resulting in a 28.05% reduction in SPM levels over Ennore creek. As industrial and commercial activities subsided, the city's water bodies became clearer than they were just a fortnight prior to the lockdown, with a reduction of 22.26% of SPM in Adyar and 33.97% in Cooum riverine estuaries. Decrease in $K_d(490)$ showed a positive relationship with SPM and thus improved coastal water quality because of the reduction of SPM during this period. The variations in PM2.5 and PM10 concentrations were studied using National Air Quality Monitoring Programme (NAMP) data and reduced levels in particulate matter concentration (PM2.5 and PM10) for the Adyar residential area (24.38 and 28.43%) and for the Nungampakkam commercial area (36.09 and 67.18%) were observed. A significant reduction in PM2.5 concentration (45.63%) was observed in the Ennore-Manali Industrial region.

Keywords: COVID-19 lockdown, water quality, Chennai coastal waters, suspended particulate matter, diffuse attenuation coefficient, ACOLITE

OPEN ACCESS

Edited by:
Deepak R. Mishra, University of Georgia, United States

Reviewed by:
Chandrasekar Nainarpandian, Manonmaniam Sundaranar University, India
Matthew Lewis, Bangor University, United Kingdom

****Correspondence:***
P. V. Nagamani
pvnagamani@gmail.com

Specialty section:
This article was submitted to Coastal Ocean Processes, a section of the journal Frontiers in Marine Science

Received: *28 January 2021*
Accepted: *16 March 2021*
Published: *13 April 2021*

Citation:
Vijay Prakash K, Geetha Vimala ChS, Preethi Latha T, Jayaram C, Nagamani PV and Laxmi ChNV (2021) Assessment of Water Quality Along the Southeast Coast of India During COVID-19 Lockdown. Front. Mar. Sci. 8:659686. doi: 10.3389/fmars.2021.659686

INTRODUCTION

COVID-19 has had an impact the entire world, and India has also felt this impact. The spread of COVID-19 has been so vast that the World Health Organization (WHO) declared it a pandemic and has designated it as medical emergency. To overcome the rapid and far-reaching spread of the disease, in the absence of proven medications, social distancing measures were put in place as the only way to minimize the human interaction. Inevitably, the country was put under lockdown. In this regard, the Indian Government took a strong stand against social life around the entire country starting in mid-March 2020. The prevalence of the pandemic, caused by the severe acute respiratory syndrome coronavirus 2 (SARS-CoV-2) named by International Committee on Taxonomy of Viruses (ICTV), continued to spread around the world and by mid-June 2020, around 213 countries has been affected. To date, more than 10 million cases of the virus infection have been reported worldwide, with the majority of fatalities being reported in the USA, Spain, and Italy (Worldometers.info, 2020).

Lockdown has substantially restricted public life in almost all sectors. There has been a cessation of aviation services, railways, including sub-urban electric trains and metro trains, buses, cars, and taxis with the exception of essential cargos. Other than services falling in the essential category, most industrial activities were suspended. The entertainment and hospitality industry, educational institutions, private and government offices, as well as religious and social gatherings were all placed under total lockdown.

Power generation in India decreased by as much as 26.5% during the country-wide lockdown, including a 33% decrease in coal-based power generation (Saraswat and Saraswat, 2020). The Scripps Institute of Oceanography estimated that fossil fuel consumption around the world will decline by about 10% due to COVID-19 (SCRIPPS, 2020). Since the activities of citizens and industries were shut down for weeks, the Air Quality Index (AQI) across major cities improved, particularly due to the reduction in NO_2, PM10, and PM2.5 caused by vehicles and industry (Central Pollution Control Board-India, 2020; Laxmipriya and Narayanan, 2020; Navinya et al., 2020; Sharma et al., 2020). These environmental benefits are a result of the halting of industrial and economic activity and not because of proactive action to control pollution or to mitigate climate change. The lockdown also brought a unique opportunity to assess the effect of anthropogenic activities on air, water quality, and atmospheric greenhouse gas concentrations and its influence on global temperatures. Quantifying the pollution status in various spheres during the lockdown period is an important activity for researchers to understand the short and long-term effects the spread of COVID-19 might have on the climate.

Coastal regions are dynamic in nature because of river discharges, industrial effluents, ship traffic, dredging, waste dumping, and sewage disposal etc. Population growth, climate change and variability, and changing land use practices all contribute to the stress of coastal water quality. The anthropogenic activities along the coastal regions are major contributors to marine water pollution. Due to the shutdown of anthropogenic activities, improvements in coastal water quality (decrease in Suspended matter concentration) were observed along the west coast of India (Yunus et al., 2020) and in the Hooghly estuarine region in the northern Bay of Bengal (Jayaram et al., unpublished data). An attempt has been made to study the water pollution in the Chennai coastal waters during the COVID-19 lockdown period, through the water quality parameters. Ocean color remote sensing techniques are useful and adapted to perform spatio-temporal studies on coastal water quality. Water quality can be measured in terms of biological, physical, and chemical indicators such as turbidity, chlorophyll-a, algae (harmful and non-harmful), pollution-sediment, temperature, metals, dissolved oxygen, nutrients (primarily phosphorus and nitrogen), and many other contaminants.

This study mainly focused on the Suspended Particulate Matter (SPM) concentration derived from satellite remote sensing measurements. The term "suspended matter" does not apply to a single type of material, but to a whole family of materials with their own individual characteristics (Sathyendranath, 2000). These particulates include anything drifting or floating in the water, from sediment, silt, and sand to plankton and algae (Fondriest Environmental Inc, 2014). SPM concentration levels are largely governed by the pollution load from anthropogenic origin, especially in connection with coastal waters situated within reach of metropolitan/industrial cities. SPM has therefore been considered to assess the variation in pollution levels, i.e., water quality in Chennai coastal waters. In addition to SPM, diffuse attenuation coefficient $K_d(490)$, an apparent optical property, also defines optical water quality (Kirk, 1988). It shows how strongly light intensity at a specified wavelength (490 nm) is attenuated within the water column and also indicates turbidity of the water column. It is directly related to the presence of scattering particles in the water column, either organic or inorganic, and is therefore an indication of water clarity. To assess the anticipated atmospheric fallout, reduction in particulate matter concentrations of PM2.5 and PM10 were also reported on during this lockdown period.

STUDY AREA

Chennai ("The Detroit of India"), the metropolis of the Indian state of Tamil Nadu, is located on the Coromandel Coast off the Bay of Bengal (BoB), and has two major ports (Chennai and Ennore) and numerous coastal Industries. The study area is situated in between 80.25°E–80.50°E and 13°N–13.35°N, as shown in **Figure 1**. Littoral regions are of great concern, due to the fact that they are not only the most productive areas but also hot spots of pollution. Massive populations and the congregation of industries in Chennai are impairing the rivers of Kosasthalaiyar, Cooum, and Adyar by ceaseless depositing of treated/untreated sewage. These rivers ultimately discharge into BoB. Dumping of dredged material is a major threat to Ennore Creek (EC), which further leads to the blockage of water flow. This creek receives wastewater, which includes treated effluents and untreated wastewater from industrial sources in Ennore-Manali areas. The two power plants in Chennai (Kalpakkam

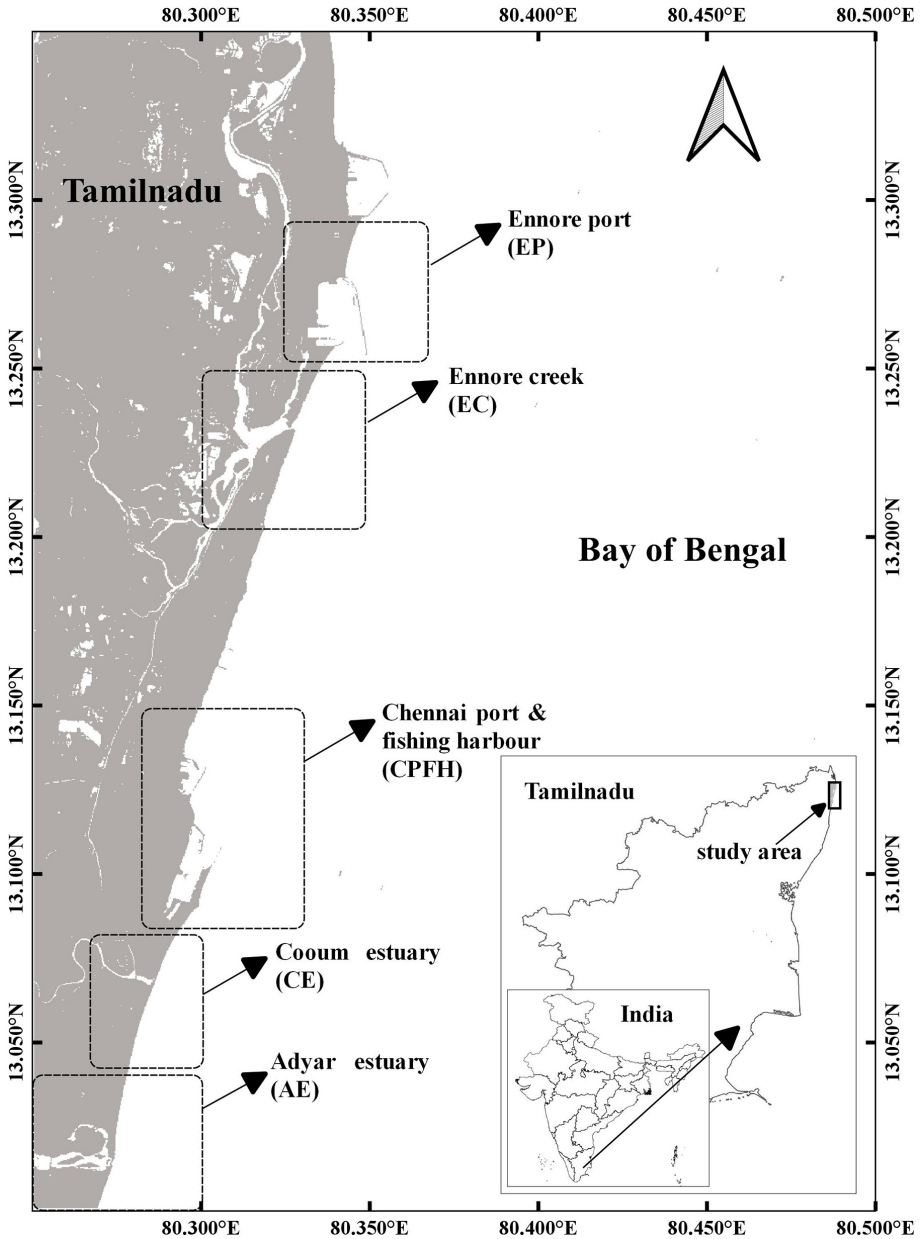

FIGURE 1 | Study area and prominent regions prone to marine pollution along the Chennai coast.

and Ennore) emanate thermal effluents into the sea, which leads to a rise in temperature levels over several square kilometers. In addition to this, direct dumping of waste as well as harbor activities such as dredging, cargo handling, ship traffic, oil spillages etc., also accompany the marine pollution. All of this waste discharge results in ecological changes including a marginal decrease in dissolved oxygen, pH, and primary productivity (Ramesh et al., 2008). The sites that are prone to marine pollution, such as the ports of Chennai and Ennore, the river mouths of Kosasthalaiyar (Ennore creek), Cooum, and Adyar were therefore considered in this study (Gowri and Ramachandran, 2001; Shanmugam et al., 2007).

The Chennai coast is characterized by a semi-diurnal tide with a maximum ∼1.2 m tidal range (Mishra et al., 2015). The mixing and sediment transport phenomena are highly dependent on tidal ebbing and flooding conditions (Kalaivani and Krishnaveni, 2015). Sediment transport is northerly from April to October and southerly from November to March. The sediment transport rate is high throughout the year, with a maximum of about 2×10^5 m^3 per month in June and a minimum of about 0.7×10^5 m^3 per month in March (Chandramohan et al., 1990). Mishra et al. (2015) conducted field campaigns along the Chennai coast (January 2013–December 2014) and reported SPM concentration ranges in between 11 and

160.5 g m^{-3} with a mean value of 34.8 g m^{-3} in the dry season (January–June).

DATA AND METHODOLOGY

Data

Landsat-8/OLI has spectral bands with central wavelengths close to that of dedicated ocean color sensors. The resolution of current ocean color sensors is one of the key limiting factors for water quality applications in near-shore regions, as they are unable to accurately resolve coastal ocean characteristics (Mouw et al., 2015). Optical sensor OLI has native spatial resolution of 30 m and is therefore better suited to resolve detailed features of SPM in the near-shore region compared to conventional ocean color sensors. Additionally, improved sensor signal-to-noise ratio and radiometric resolution of OLI, permits the application of this land-designed sensor for marine applications (Trinh et al., 2017). It provides the capability to optically map active components of the upper water column in inland and coastal waters with minimized coastal contamination. These characteristics indicate that Landsat-8/OLI images are suitable and were found to provide appropriate data for retrieval, estimation, and monitoring of water quality parameters on a regional scale (Lim and Choi, 2015; Vanhellemont and Ruddick, 2015; Wei et al., 2018). However, Landsat-8/OLI data may not be advisable when studying extremely dynamic and large-scale features due to its low temporal resolution and synoptic coverage compared to MODIS, AVHRR, VIIRS etc. To study the impact different phases of lockdown (**Supplementary Table 1**) had on water quality along the Chennai coast, April (stringent lockdown period) was chosen and Landsat-8/OLI instrument L1TP (Level 1 and Terrain Precision) scenes of path/row-142/051 were downloaded from NASA's USGS Earth-Explorer website for the period of 2013–2020.

Pre-processing

Landsat-8/OLI, L1TP scenes were subjected to radiometric calibration and atmospheric correction to derive surface reflectance values from raw digital numbers using the ACOLITE package, developed by the Royal Belgian Institute of Natural Sciences (Vanhellemont and Ruddick, 2018). It is an image-based Atmospheric Correction algorithm that estimates radiance by correcting for molecular and aerosol scattering in the atmosphere using the Gordon and Wang (1994) approach. Molecular reflectance correction, based on viewing and illumination geometries, is performed with a 6SV-based look-up table.

ACOLITE employs the Dark Spectrum Fitting (DSF) algorithm (Vanhellemont and Ruddick, 2018; Vanhellemont, 2019) for atmospheric correction. The DSF algorithm considers the atmosphere as homogenous and estimates atmospheric path reflectance by assuming approximate zero water-leaving radiance for the pixels, in at least one of the sensor bands of the scene. **Figure 2** provides a brief insight into DSF aerosol correction. The aerosol model and best fitting band combination, which gives the lowest RMSD between observed dark spectrum (ρ_{dark}) and estimated atmospheric path reflectance (ρ_{path}), is selected for the atmospheric correction. ACOLITE performs glint correction to obtain glint-free surface reflectance by estimating sun glint reflectance from the SWIR bands, significantly improving the data availability for this nadir viewing sensor (Harmel et al., 2018; Vanhellemont, 2019).

SPM Retrieval

SPM plays a vital role in Primary production, pollutant transport, and other biogeochemical processes in coastal marine environments (Kravchishina et al., 2018). Curran et al. (1987) and Novo et al. (1989) investigated the form of the relationship between SPM and water-leaving reflectance in coastal waters and showed that single band algorithms may be adopted where SPM increases with increasing reflectance. Ahn et al. (2001) pointed out that single bands at longer wavelengths in visible portions are highly useful for deriving SPM concentrations in turbid waters. After performing the atmospheric correction for the scenes, to retrieve the suspended particulate matter (SPM), a generic multi-sensor SPM algorithm for turbid waters developed by Nechad et al. (2010) was adapted for this study. The algorithm is based on a reflectance model (Gordon et al., 1988) and is calibrated using *in-situ* reflectance and SPM measurements made over the southern North Sea area from 2001 to 2006. Nechad et al. (2010) proposed an algorithm based on Inherent Optical Properties (IOP) for turbid waters (case 2 waters). SPM is related to the ratio of total backscattering (b_b) to total absorption (a). Assumptions made in this algorithm derivation are that particulate backscattering (b_{bp}) and particulate absorption are proportional to the SPM concentration, that spatio-temporal variability of non-particulate absorption (a_{np}) is negligible, and that non-particulate back-scattering is zero.

$$TSM\left[gm^{-3}\right] = \frac{A^{\rho} \times \rho_w}{1 - \frac{\rho_w}{C^{\rho}}} \tag{1}$$

ρ_w is the water-leaving reflectance which can be derived from the remote sensing reflectance (R_{rs}), $\rho_w = \pi R_{rs}$. A^{ρ} is obtained from a non-linear regression analysis using *in-situ* reflectance and SPM data and C^{ρ} is calibrated using standard IOP data (Mobley, 1994; Babin et al., 2003a,b; Lubac and Loisel, 2007). For Ladsat-8 data, R_{rs} at red band (central wavelength = 655nm) is used for SPM retrieval. Generic coefficients (corresponding to 655nm) were taken from Table 1 and Table 4 of Nechad et al. (2010), A^{ρ} = 289.29 and C^{ρ} = 0.1686. Mathematical formulations for these calibration coefficients are given below,

$$A^{\rho}\left[gm^{-3}\right] = \frac{A}{\gamma}; A\left[gm^{-3}\right] = \frac{a_{np}}{b^*_{bp}} \tag{2}$$

$$C^{\rho}\left[dimensionless\right] = \frac{\gamma C}{1+C}; C\left[dimensionless\right] = \frac{b^*_{bp}}{a^*_p}$$

$$\gamma = \pi R \frac{f'}{Q} \cong 0.216$$

Where A and C are calibration parameters, and b^*_{bp} and a^*_p are SPM specific particulate backscattering and absorption, respectively. R is the constant and represents

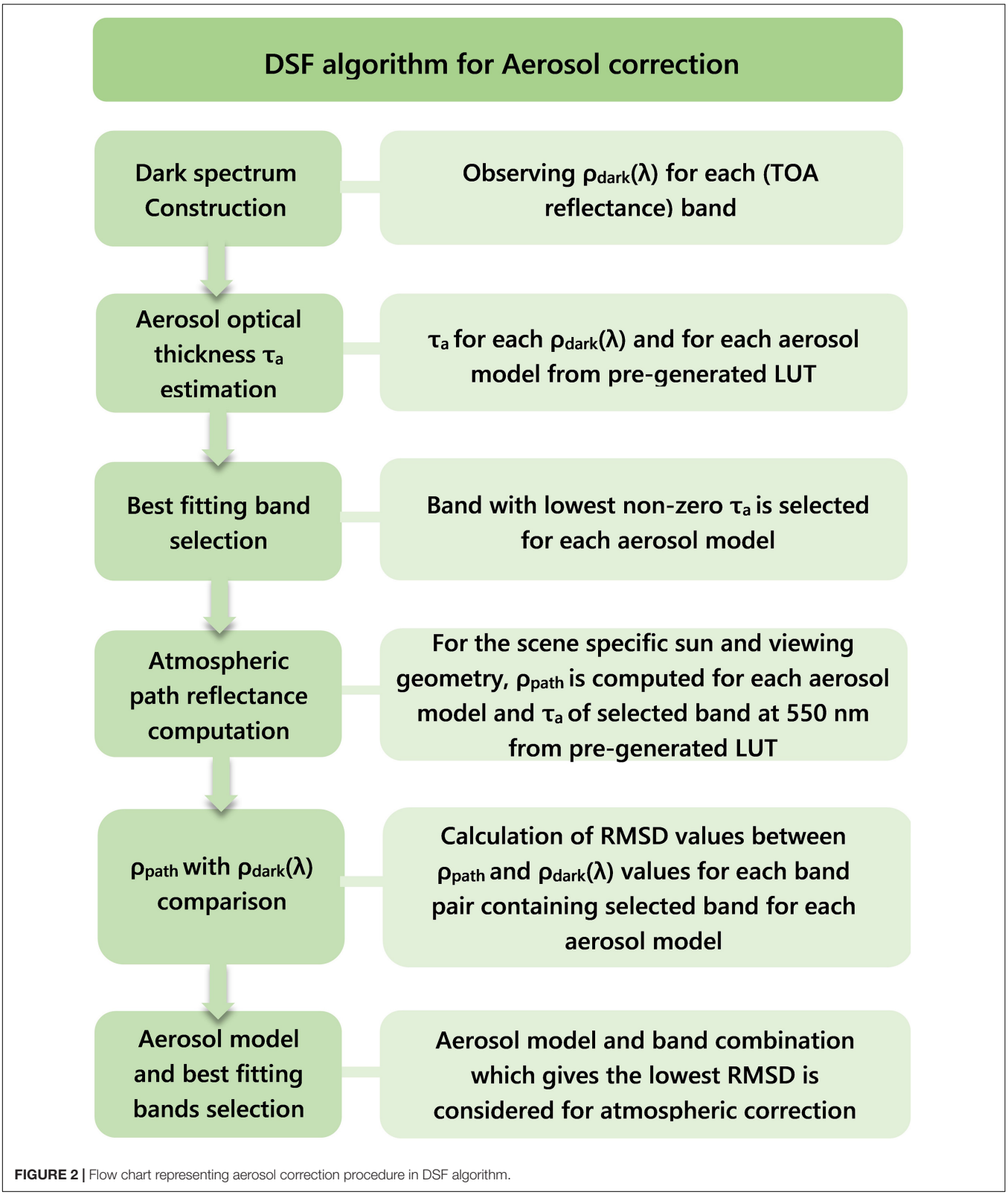

FIGURE 2 | Flow chart representing aerosol correction procedure in DSF algorithm.

reflection and refraction effects at the sea surface = 0.529 (Morel and Gentili, 1996), f' is a varying dimensionless factor (Morel and Gentili, 1991) and Q is the ratio of subsurface upwelling irradiance to the subsurface upwelling radiance. f'/Q = 0.13 for sediment-dominated waters (Loisel and Morel, 2001).

TABLE 1 | Statistical parameters of SPM for all prominent regions in the study area.

Region	April mean SPM (g m^{-3})				
	Long-term	During stringent lockdown	Observed reduction	Percentage reduction (%)	Negative Anomaly RMSD
CPFH	8.91	7.53	1.38	15.48	2.21
EP	13.41	8.38	5.03	37.50	4.85
EC	13.30	9.57	3.73	28.05	3.59
CE	13.16	10.23	2.93	22.26	2.46
AE	12.48	8.24	4.24	33.97	3.70

K_d(490) Retrieval

Diffuse attenuation coefficient (K_d) has strong relationship with IOPs such as absorption coefficient (a) (Smith and Baker, 1981; Lee et al., 2002; Lee et al., 2005; Lee et al., 2015) and back scattering coefficient (b_b) (Gordon et al., 1988; Lee et al., 2002; Sun et al., 2014). A semi analytical approach developed by Lee et al. (2002), and a Quasi Analytical Algorithm (QAA) has been adapted to redeem K_d(490) for this study. K_d(490) retrieval involves calculation of a(490) and b_b(490) by analytically inverting remote sensing reflectance (Lee et al., 2005). These IOPs are further used to calculate K_d(490) from the Eq. 3.

$$K_d = m_0 a + m_1 (1 - m_2 a - m_3 a) b_b \quad (3)$$

Where $m_0 = 1 + 0.005\theta_a$, θ_a is the solar zenith angle in air. The values for model constants m_1, m_2, and m_3 are 4.18, 0.52, and 10.8, respectively (Lee et al., 2005). These values remain constant for different waters and different wavelengths and it is to be noted that a and b_b changes with water mass and wavelength, as well as with solar zenith angle.

RESULTS AND DISCUSSION

The long-term mean was calculated using L8 scenes of April (2013–20) and April-2020 (2^{nd} & 18^{th}, April-2020) scenes were used to compute mean values for the stringent lockdown period. Negative anomalies were observed in the majority of locations/pixels in all prominent regions of the study area. Mean, percentage, and root mean square differences (RMSD) were computed. The entire region was considered while computing mean differences and their percentages, whereas pixels with negative anomalies were isolated and computed RMSDs for those pixels.

Variation in Suspended Particulate Matter

The potential variances in SPM concentration, are either due to anthropogenic activities or biogeochemical processes taking place in the system (Kuppusamy and Giridhar, 2006). The seasonal and biogeochemical processes remained the same whereas anthropogenic activities were shut down (exemption was given to essential services) during the COVID-19 lockdown. Delineating the contribution of anthropogenic activities to SPM levels has therefore been assessed in this study. An anticipated decrease of SPM concentration is clearly observed in all prominent regions of the study area and their corresponding statistical inferences are presented in **Table 1**.

The statistics revealed by the Chennai port (Chennai Port—Tamil Nadu, 2020) says that, there was a 40% decrease in cargo handled and a 36% decrease in vessel traffic during April 2020 (**Supplementary Figure 1**). Fishing activities were completely paused due to the absence of ice and because of the workforce being in lockdown (ThePrint, 2020). It was observed that SPM concentration at the CPFH region decreased about 15.48% (refer **Table 1**). The Ennore port handled 3228 kilotons of cargo, which is much less compared to Chennai port during the months of April and May 2020. Due to this, SPM concentration during the stringent lockdown period at EP drastically reduced by 37.5% (refer to **Table 1**). It was noticed that the pause in port and fishing activities contrived the coastal water quality (refer to **Figure 3**).

The Tamil Nadu State's peak electricity demand plummeted with the shutdown of commercial and industrial units and led to a drastic drop (about 30%) in power demand. All of these factors led to a reduction in SPM of around 28.05% over EC (refer to **Table 1** and **Figure 3**). As industrial and commercial activities subsided during the lockdown period, the city's water bodies became clearer than they were just a fort-night prior to the lockdown, with no industrial effluents flowing in from closed factories. The Adyar river now carries 70 cusecs of relatively clean water and no froth has been noticed anywhere along the river due to the absence of chemicals. The flow of 60 cusecs of gray water from the units has now come down to 10 cusecs (The Times of India, 2020) and SPM concentrations were decreased by 22.26 and 33.97% at CE and AE, respectively (**Table 1**); corresponding maps are presented in **Figure 3**.

Variation in Diffuse Attenuation Coefficient

The impact the COVID-19 lockdown had on K_d(490) was also studied along with SPM, and the observed results for the five prominent units selected in the Chennai coastal waters are outlined in **Table 2**. Comparable variability was observed in K_d(490) concentrations due to a decline of suspended and dissolved solids contributed from respective sources.

A decrease of cargo and vessel movement in the Chennai port, and also in relation to the decrease of SPM up to 15.48%, K_d(490) shows high transparency levels at the fishing harbor and port (**Figure 4**) with an 8.62% decrease in the light attenuation varying from ∼0.45 to ∼0.7 m^{-1} leading to water clarity. This observation shows the impact of

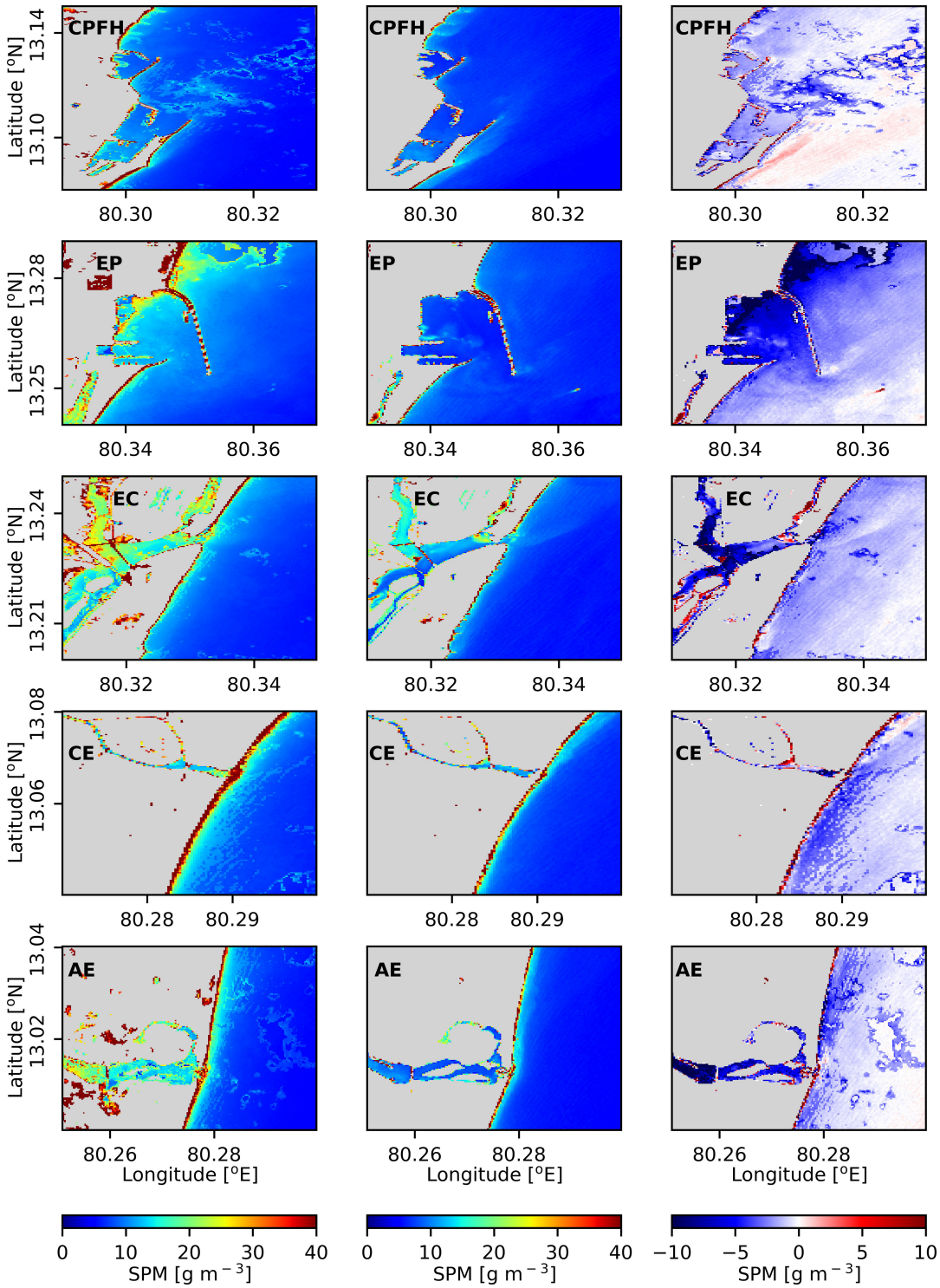

FIGURE 3 | Long-term (left), April 2020 (middle), and April 2020 anomaly (right) mean distributions of SPM over prominent regions in the study area.

lockdown with a pause in port and fishing activities. The EP showed a 11.69% decrease in the light attenuation, resulting in high transparency during the lockdown period, as shown in **Figure 4**. The $K_d(490)$ varies from ∼0.45 to ∼0.7 m^{-1} as observed in the CPFH region. This indicates that port regions of EP and CPFH had a maximum decrease in both SPM distribution and $K_d(490)$ light attenuation, showing the impact lockdown had.

TABLE 2 | Statistical parameters of $K_d(490)$ for all prominent regions in the study area.

Region	April mean $K_d(490)$ (m^{-1})				
	Long-term	During stringent lockdown	Observed reduction	Percentage reduction (%)	Negative Anomaly RMSD
CPFH	0.5837	0.5290	0.05	8.62	0.0665
EP	0.6956	0.5780	0.12	17.14	0.1255
EC	0.7732	0.6757	0.11688	11.69	0.07958
CE	0.7552	0.6305	0.13	17.10	0.1001
AE	0.725	0.559	0.17	23.28	0.1217

SPM distribution over EC showed a maximum 28.05% decrease during the lockdown period which was also observed with a 17.14% decrease in the light attenuation from $K_d(490)$, showing clear waters along the coast compared to the long-term mean. This can be attributed to the shutdown of industrial and dredging activities which resulted in reduced pollution and thus increasing coastal water quality in the EC.

The AE region located south of the Chennai port, indicates a maximum decrease of 23.28% difference compared to the long-term mean, which is also correlated to the maximum 33.97% decrease of SPM. The $K_d(490)$ varies $<1\ m^{-1}$ showing reasonable transparency compared to the long-term distribution of $K_d(490)$. Whereas in the CE region, located in between the CPFH and AE, $K_d(490)$ distribution is observed with a 17.10% decrease along the coast. These estuarine regions are more susceptible to marine pollution, revealing the impact of lockdown in the reduced SPM concentrations and $K_d(490)$ distribution in the coastal waters.

PM2.5 and PM10 Concentrations

The major sources for PM2.5 and PM10 concentrations in atmosphere are industries, dust and vehicular emissions. The variations in PM2.5 and PM10 concentrations in the Chennai local atmosphere were studied for this lockdown period by considering three National Air Quality Monitoring Programme (NAMP) stations at different LULC zones. The PM2.5 and PM10 data of Adyar (residential), Nungampakkam (commercial), and Manali (industrial) stations have been acquired from the pollution control boards of the State and Central governments for the period of 2018–2020. PM10 data is not available for Manali station and in the case of Adyar and Nungampakkam stations, the 2018 PM2.5 data is not available. The trend of specified air quality parameters has been assessed by analyzing pre- and during lockdown levels. As vehicles stayed off the road, construction was put on hold, and factories stopped production, the levels of microscopic particulate matter (PM2.5) started to drop (EcoWatch, 2020). It was observed that there was a profound decrease in particulate matter concentrations and the corresponding results are presented in following sections.

While measuring particulate matter concentrations in Adyar station, the results indicated a decrease in PM2.5 and PM10 over a period (February to May) in 2020 when compared with long-term mean values (**Figures 5**, **6**). The percentage reduction during the stringent lockdown period (24.38% and 28.43%) was marginal because of the persistent contribution of domestic pollutants in residential zones (**Table 3**). The main sources of particulate matter in commercial areas are vehicular emissions. A significant drop in PM2.5 and PM10 (**Figures 5**, **6**) levels were observed (36.09 and 67.18%) in Nungampakkam during the stringent lockdown period (**Table 3**) due to extensive restrictions implemented for public transport and vehicle movement. Other than the essential category units, most industries were shut during the COVID-19 lockdown. A profound improvement in air quality was observed in Manali due to reduced industrial emissions (**Table 3** and **Figures 5**, **6**).

Discussion

Decreased SPM levels in response to the COVID-19 lockdown indicated a reduced influx of contaminants (size $\geq$0.45 microns) into coastal waters. Unlike SPM concentration, the $K_d(490)$ parameter reveals the combined effect of suspended and dissolved matter (majorly Color Dissolved Organic Matter) on light attenuation (Kirk, 1994; Gallegos and Moore, 2000). Decrease in K_d (490) values resulted in improved water quality and the same was observed in all the prominent regions of study during the lockdown period. This decrease in K_d (490) can be related to three possibilities:

i. Both suspended and dissolved matters were decreased
ii. Suspended matter decreased whereas dissolved matter remained the same
iii. Dissolved matter decreased whereas suspended matter remained the same

Though the impact lockdown had on dissolved matter is not quantified in the present study, a decrease in dissolved matter levels could be expected due to the shutdown of anthropogenic activities. The first two cases show an in-phase relationship with the SPM results of this study, but the third case exhibited contradictory behavior. As the inorganic suspended matter shows dominance in the turbid coastal waters, the absence of their respective sources will certainly have an impact on their abundance and there is no possibility of occurrence for the third case during COVID-19 lockdown. A decrease in $K_d(490)$ therefore shows an in-phase/positive relationship with SPM (**Figure 7**) and substantiates improved coastal water quality through the reduction of SPM during the stringent lockdown period.

In general, spatio-temporal variability of SPM concentration levels in coastal waters mainly depends on domestic and industrial sewage, atmospheric fallout, runoff, tides, and re-suspension of sediments. Among these, the components

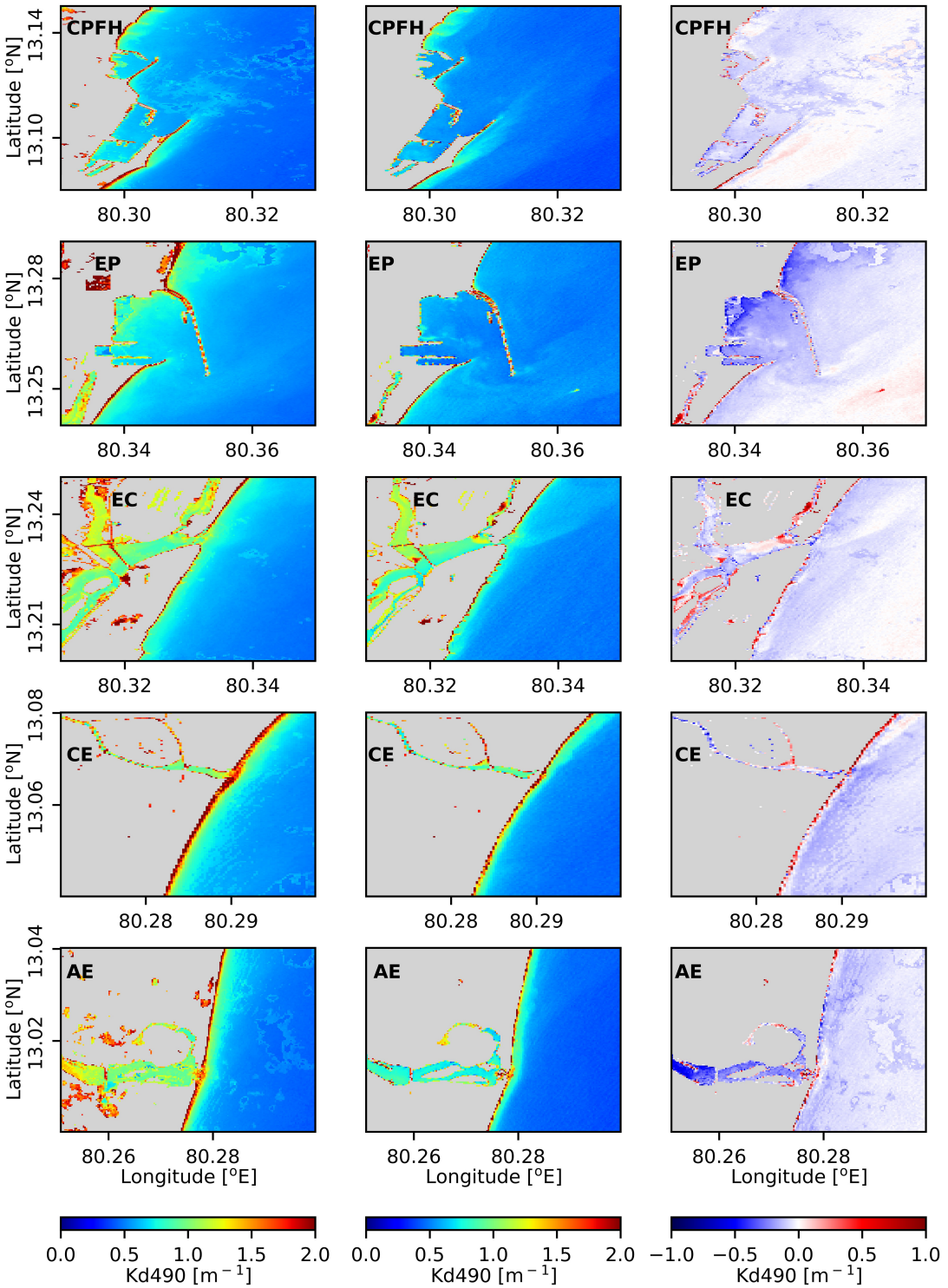

FIGURE 4 | Long-term (left), April 2020 (middle), and April 2020 anomaly (right) mean distributions of $K_d(490)$ over prominent regions in the study area.

associated with anthropogenic activities are: sewage that originates from domestic sources and industrial outlets; atmospheric particulate matter that releases from vehicular emissions, and industries. A direct increase or decrease in the aforementioned components will certainly have an impact on SPM levels. Apart from the anthropogenic contribution, the rest can be attributed to natural variability. Landsat-8 scenes of 2 and 18 April 2020 were considered, while computing

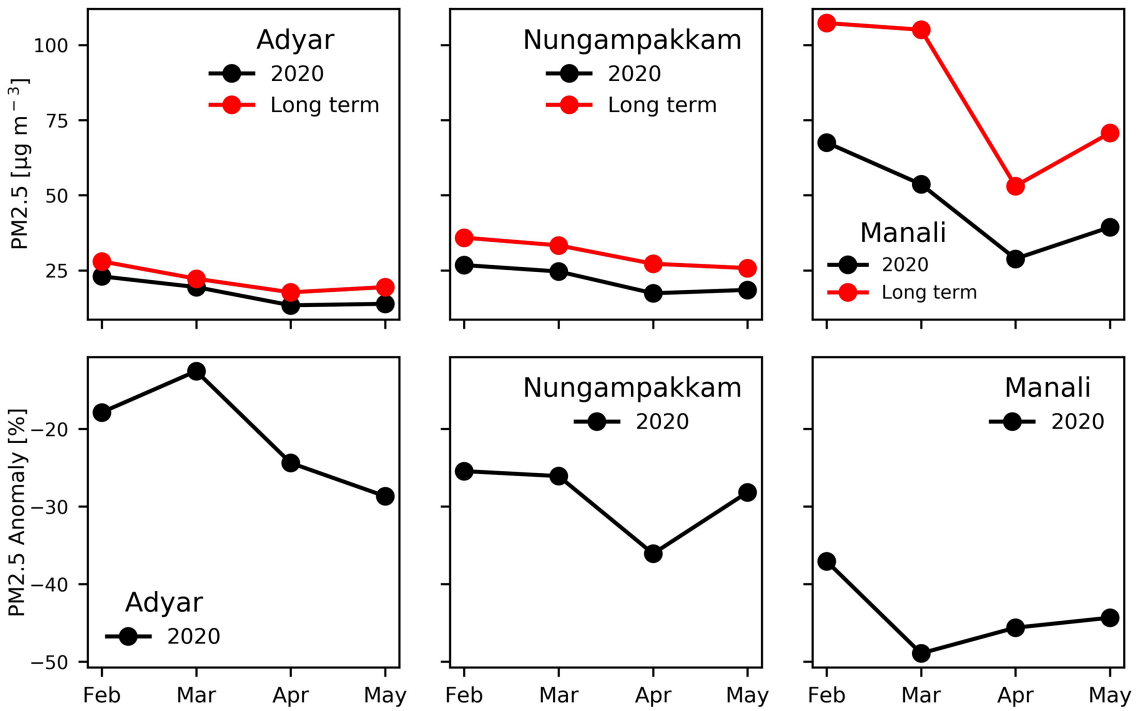

FIGURE 5 | Plots representing variations in monthly means and their percentage anomalies with long-term data of PM2.5 data at residential (Adyar), commercial (Nungampakkam), and industrial (Manali) zones.

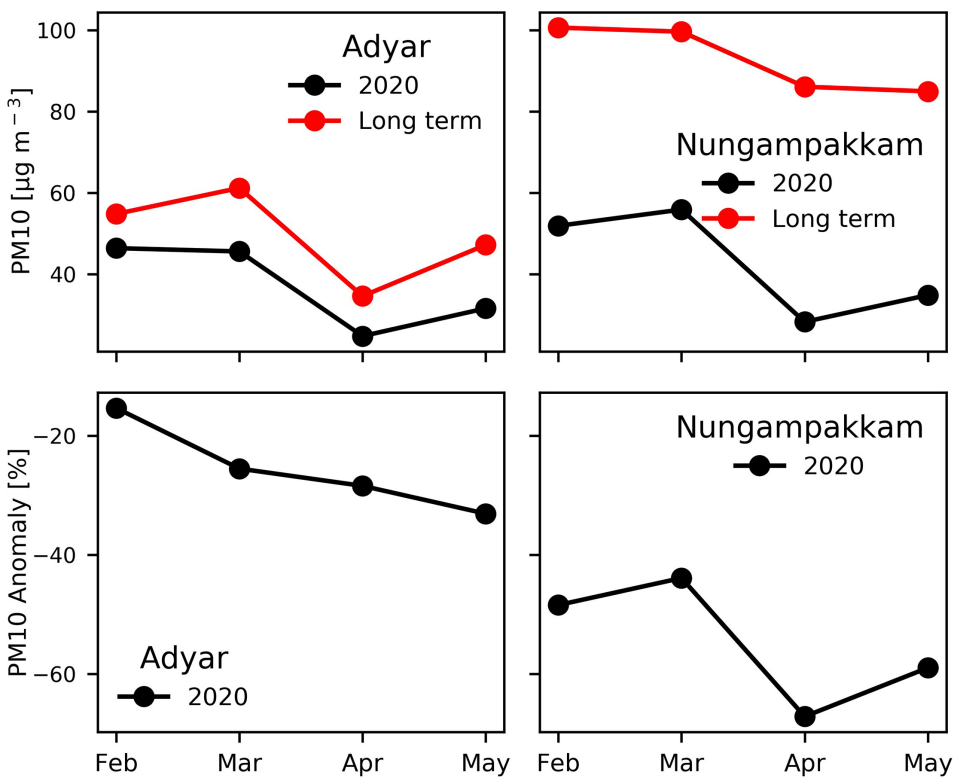

FIGURE 6 | Plots representing variations in monthly means and their percentage anomalies with long-term data of PM10 data at residential (Adyar), commercial (Nungampakkam), and industrial (Manali) zones.

TABLE 3 | Statistical analysis of monthly particulate matter mean data.

Month	Long-term ($\mu g\ m^{-3}$)		2020 Year ($\mu g\ m^{-3}$)		Observed reduction ($\mu g\ m^{-3}$)		Percentage reduction (%)	
	PM2.5	PM10	PM2.5	PM10	PM2.5	PM10	PM2.5	PM10
Adyar (residential zone)								
February	28	54.79	23	46.38	5	8.41	17.86	15.35
March	22.21	61.19	19.43	45.57	2.78	15.62	12.54	25.53
April	17.69	34.58	13.38	24.75	4.31	9.8	**24.38**	**28.43**
May	19.43	47.19	13.86	31.57	5.57	15.62	28.68	33.1
Nungampakkam (commercial zone)								
February	35.87	100.63	26.75	51.88	9.13	48.75	25.44	48.45
March	33.31	99.63	24.63	55.88	8.69	43.75	26.08	43.91
April	27.19	86.08	17.38	28.25	9.81	57.83	**36.09**	**67.18**
May	25.75	84.94	18.50	34.83	7.25	50.11	28.16	58.99
Manali (industrial zone)								
February	107.28	N/A	67.54	N/A	39.74	N/A	37.05	N/A
March	105.06		53.64		51.42		48.94	
April	53.07		28.86		24.28		**45.63**	
May	70.78		39.36		31.36		44.34	

Bold values represent data for April 2020, which is the month considered for analysis.

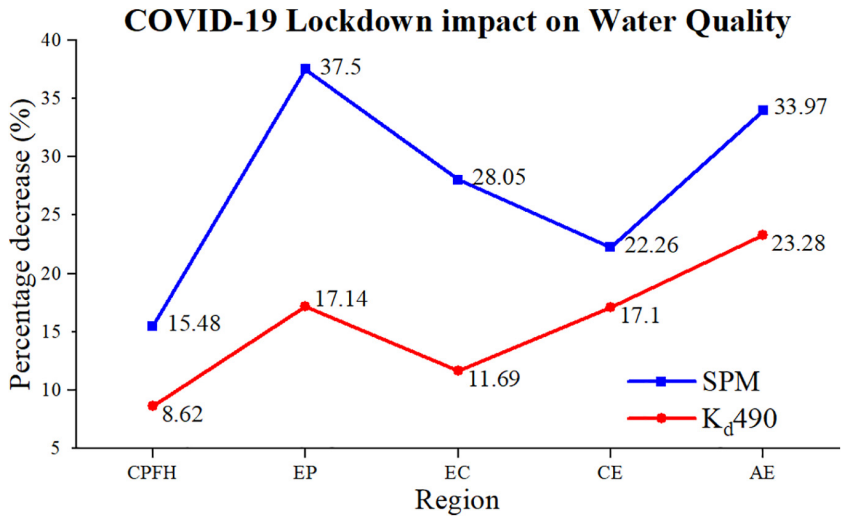

FIGURE 7 | Plot representing positive relationship between SPM and K_d490.

mean SPM values for the stringent lockdown period, observed reduction in SPM levels. In view of checking natural SPM variability, the authors verified any deviation from the prevailing or natural/climatic conditions in the study region. The Northeast monsoon (October–December) is a major source of rainfall in Tamil Nadu and the state is entirely dependent on rains for recharging its water resources. From a CPC global unified gauge-based analysis of daily precipitation data, it was observed that there is no rainfall during the times of Landsat-8 coverage. It was observed that Landsat-8 overpassed the Chennai coast during low-tide, on both days. So, the natural variability of SPM associated with runoff and tidal currents could be eliminated. The observed reduction in SPM levels can therefore be solely attributed to the stringent lockdown period.

CONCLUSION

The impact of the COVID-19 lockdown on coastal water quality across the Chennai region was studied by analyzing the suspended particulate matter concentration (SPM). Anthropogenic activities' contribution to SPM levels was assessed for all five prominent regions in the study area. A decrease in SPM concentration (15.48, 37.50%) was clearly observed due to minimal vessel movement and cargo handling at the Chennai and Ennore ports. SPM levels over Ennore creek/estuary were reduced by 28.05%, and can be attributed to limited industrial activities in Ennore-Manali area and the decreased fly ash emissions from thermal power plants. As industrial and commercial activities subsided during the

lockdown period, the city's water bodies, Adyar and Cooum, were clearer than the pre-lockdown period, with no industrial effluents flowing in from closed factories. The suspended matter over these estuaries was reduced by 22.26 and 33.97%. A decrease in $K_d(490)$ showed an in-phase/positive relationship with SPM and substantiated the improved coastal water quality through the reduction of SPM during the lockdown period. The variations in PM2.5 and PM10 concentrations in the Chennai local atmosphere were studied for this stringent lockdown period considering three NAMP stations at different LULC zones. The extensive restrictions imposed on public transport and vehicular movement reduced the particulate matter concentration (PM2.5 and PM10) for the Adyar residential area (24.38 and 28.43%) and for the Nungampakkam commercial area (36.09 and 67.18%). A significant reduction in PM2.5 concentration (45.63%) was observed for the Manali industrial region. Peters et al., 2012 reported rapid growth in pollution levels (CO_2) after the global financial crisis occurred in 2008 to 2009. Once the situation stabilizes, and returns to normality as seen during the pre-lockdown period, a rebound of pollution levels in all spheres of earth can be expected within a short time span. This study propounds the necessity of sustainable development to maintain a balanced environment, otherwise the COVID-19 lockdown scenario will simply replicate the rise in pollution seen after the 2008 to 2009 global financial crisis.

DATA AVAILABILITY STATEMENT

Publicly available datasets were analyzed in this study. This data can be found here: https://earthexplorer.usgs.gov/; https://app.cpcbccr.com/; https://tnpcb.gov.in/air-quality.php.

AUTHOR CONTRIBUTIONS

KV, CG, and TP were research scholars working under the guidance of PN (Head and Scientist-F, Biological Oceanography Division, National Remote Sensing Centre-ISRO, Hyderabad). CJ (Scientist-E, RRSC East, NRSC-ISRO, Kolkata) and CL (Asst. Professor, JNTU, Kakinada) are co-guides for this research work. KV, CG, and TP were involved in literature survey, data downloading, outputs preparation and basic drafting. PN, CJ, and CL have supervised and guided the whole work and finalized manuscript drafting. All authors contributed to the article and approved the submitted version.

ACKNOWLEDGMENTS

We thank and acknowledge USGS for distributing Landsat-8 data freely. The pollution control boards of Tamil Nadu state (TNPCB, Chennai) and the Central Government (CPCB, New Delhi) are thanked for providing PM2.5 and PM10 data. We thank and acknowledge NOAA/OAR/ESRL PSL for distributing CPC Global Unified Precipitation data. We thank the National Remote Sensing Centre, Hyderabad (ISRO) for providing the infrastructure to carry out this work.

SUPPLEMENTARY MATERIAL

The Supplementary Material for this article can be found online at: https://www.frontiersin.org/articles/10.3389/fmars.2021.659686/full#supplementary-material

REFERENCES

Ahn, Y. H., Moon, J. E., and Gallegos, S. (2001). Development of suspended particulate matter algorithms for ocean color remote sensing. *Korea. J. Remote Sens.* 17, 285–295.

Babin, M., Morel, A., Fournier-Sicre, V., Fell, F., and Stramski, D. (2003a). Light scattering properties of marine particles in coastal and open ocean waters as related to the particle mass concentration. *Limnol. Oceanogr.* 48, 843–859. doi: 10.4319/lo.2003.48.2.0843

Babin, M., Stramski, D., Ferrari, G. M., Claustre, H., Bricaud, A., Obolensky, G., et al. (2003b). Variations in the light absorption coefficients of phytoplankton, non-algal particles and dissolved organic matter in coastal waters around Europe. *J. Geophys. Res.* 108:3211. doi: 10.1029/2001JC000882

Central Pollution Control Board-India (2020). *Impact of Lockdown (25th March to 15th April) on Air Quality*. Available online at: https://cpcb.nic.in/openpdffile.php?id=TGF0ZXN0RmlsZS9fMTU4ODE1NjM0OF9tZWRpYXBob3RvMjEyNDEucGRm (accessed June 25, 2020).

Chandramohan, P., Nayak, B. U., and Raju, V. S. (1990). Long-shore transport model for south Indian and Sri Lankan coasts. *J. Waterw. Port C ASCE* 116, 408–424. doi: 10.1061/(ASCE)0733-950X1990116:4(408)

Chennai Port - Tamil Nadu (2020). *Port Statistics*. Available online at: https://www.chennaiport.gov.in/content/cargo-wise-traffic-handled (accessed June 25, 2020).

Curran, P. J., Hansom, J. D., Plummer, S. E., and Pedley, M. I. (1987). Multispectral remote sensing of nearshore suspended sediments: a pilot study. *Int. J. Remote Sens.* 8, 103–112. doi: 10.1080/01431168708948618

EcoWatch (2020). *India's Air Pollution Plummets in COVID-19 Lockdown*. Available online at: https://www.ecowatch.com/india-air-pollution-coronavirus (accessed June 25, 2020).

Fondriest Environmental Inc (2014). *Turbidity, Total Suspended Solids and Water Clarity-Fundamentals of Environmental Measurements*. Available online at: https://www.fondriest.com/environmental-measurements/parameters/water-quality/turbidity-total-suspended-solids-water-clarity (accessed June 20, 2020).

Gallegos, C. L., and Moore, K. A. (2000). "Factors contributing to water-column light attenuation," in *Chesapeake Bay Submerged Aquatic Vegetation Water Quality and Habitat-Based Requirements and Restoration Targets: A Second Technical Synthesis*, ed. R. A. Batiuk (Annapolis, MD: EPA Chesapeake Bay Program), 35–54.

Gordon, H. R., Brown, O. B., Evans, R. H., Brown, J. W., Smith, R. C., Baker, K. S., et al. (1988). A semianalytical radiance model of ocean color. *J. Geophys. Res.* 93, 10909–10924. doi: 10.1029/JD093iD09p10909

Gordon, H. R., and Wang, M. (1994). Retrieval of water-leaving radiance and aerosol optical thickness over the oceans with SeaWiFS: a preliminary algorithm. *Appl. Opt.* 33, 443–452. doi: 10.1364/AO.33.000443

Gowri, V. S., and Ramachandran, S. (2001). "Coastal pollution of Chennai city, Coastal geomorphology of India," in *Institute of Ocean Management*, ed. S. Ramachandran, (Chennai: Anna University), 1187–1206.

Harmel, T., Chami, M., Tormos, T., Reynaud, N., and Danis, P.-A. (2018). Sunglint correction of the Multi-Spectral Instrument (MSI)-SENTINEL-2 imagery over inland and sea waters from SWIR bands. *Remote Sens. Environ.* 204, 308–321. doi: 10.1016/j.rse.2017.10.022

Kalaivani, K., and Krishnaveni, M. (2015). Multivariate statistical analysis of pollutants in Ennore creek, south-east coast of India. *Glob. Nest J.* 17, 618–627. doi: 10.30955/gnj.001669

Kirk, J. T. O. (1988). Optical water quality-What does it mean and how should we measure it? *J. Water Pollut. Control Fed.* 60, 194–197.

Kirk, J. T. O. (1994). *Light and Photosynthesis in Aquatic Ecosystems*. Cambridge: Cambridge University Press.

Kravchishina, M. D., Klyuvitkin, A. A., Lukashin, V. N., Politova, N. V., Novigatsky, A. N., and Lisitsyn, A. P. (2018). Distribution of suspended particulate matter in the Caspian Sea. *Russ. Meteorol. Hydrol.* 43, 697–705. doi: 10.3103/S1068373918100096

Kuppusamy, M. R., and Giridhar, V. V. (2006). Factor analysis of water quality characteristics including trace metal speciation in the coastal environmental system of Chennai Ennore. *Environ. Int.* 32, 174–179. doi: 10.1016/j.envint.2005.08.008

Laxmipriya, S., and Narayanan, R. M. (2020). Seasonal variation in atmospheric particulate matter pollution-a comparative study in part of greater Chennai, India during and before SARS-Cov-2 pandemic in India. *J. Xidian Univ.* 14, 5957–5964. doi: 10.37896/jxu14.5/645

Lee, Z. P., Carder, K. L., and Arnone, R. (2002). Deriving inherent optical properties from water colour: a multi-band quasi-analytical algorithm for optically deep waters. *Appl. Opt.* 41, 5755–5772. doi: 10.1364/AO.41.005755

Lee, Z. P., Du, K. P., and Arnone, R. (2005). A model for the diffuse attenuation coefficient of downwelling irradiance. *J. Geophys. Res.* 2005:C02016. doi: 10.1029/2004JC002275

Lee, Z. P., Shang, S., Hu, C., Du, K., Weidemann, A., Hou, W., et al. (2015). Secchi disk depth: a new theory and mechanistic model for underwater visibility. *Remote Sens. Environ.* 169, 139–149. doi: 10.1016/j.rse.2015.08.002

Lim, J., and Choi, M. (2015). Assessment of water quality based on Landsat 8 operational land imager associated with human activities in Korea. *Environ Monit Assess* 187, 384. doi: 10.1007/s10661-015-4616-1

Loisel, H., and Morel, A. (2001). Non-isotropy of the upward radiance field in typical coastal (Case 2) waters. *Int. J. Remote Sens.* 22, 275–295. doi: 10.1080/014311601449934

Lubac, B., and Loisel, H. (2007). Variability and classification of remote sensing reflectance spectra in the eastern English Channel and southern North Sea. *Remote Sens. Environ.* 110, 45–58. doi: 10.1016/j.rse.2007.02.012

Mishra, P., Panda, U. S., Pradhan, U., Kumar, C. S., Naik, S., Begum, M., et al. (2015). Coastal water quality monitoring and modelling off Chennai city. *Proced. Eng.* 116, 955–962. doi: 10.1016/j.proeng.2015.08.386

Mobley, C. D. (1994). *Light and Water*. London: Academic Press.

Morel, A., and Gentili, B. (1991). Diffuse reflectance of oceanic waters: its dependence on Sun angle as influenced by the molecular scattering contribution. *Appl. Opt.* 30, 4427–4438. doi: 10.1364/AO.30.004427

Morel, A., and Gentili, B. (1996). Diffuse reflectance of oceanic waters. III. Implication of bidirectionality for the remote-sensing problem. *Appl. Opt.* 35, 4850–4862. doi: 10.1364/AO.35.004850

Mouw, C. B., Greb, S., Aurin, D., DiGiacomo, P. M., Lee, Z., Twardowski, M., et al. (2015). Aquatic color radiometry remote sensing of coastal and inland waters: challenges and recommendations for future satellite missions. *Remote Sens. Environ.* 160, 15–30. doi: 10.1016/j.rse.2015.02.001

Navinya, C., Patidar, G., and Phuleria, H. C. (2020). Examining effects of the COVID-19 national lockdown on ambient air quality across Urban India. *Aerosol. Air Qual. Res.* 20, 256. doi: 10.4209/aaqr.2020.05.0256

Nechad, B., Ruddick, K. G., and Park, Y. (2010). Calibration and validation of a generic multisensor algorithm for mapping of total suspended matter in turbid waters. *Remote Sens. Environ.* 114, 854–866. doi: 10.1016/j.rse.2009.11.022

Novo, E. M. M., Hansom, J. D., and Curran, P. J. (1989). The effect of viewing geometry and wavelength on the relationship between reflectance and suspended sediment concentration. *Int. J. Remote Sens.* 10, 1357–1372. doi: 10.1080/01431168908903973

Peters, G. P., Marland, G., Le Quéré, C., Boden, T., Canadell, J. G., and Raupach, M. R. (2012). Rapid growth in CO_2 emissions after the 2008–2009 global financial crisis. *Nat. Clim. Chang.* 2, 2–4. doi: 10.1038/nclimate1332

Ramesh, R., Nammalwar, P., and Gowri, V. S. (2008). *Database on Coastal Information of Tamilnadu*. Report submitted to Environmental Information System (ENVIS), Chennai: Institute for Ocean Management, Anna University.

Saraswat, R., and Saraswat, D. A. (2020). Research opportunities in pandemic lockdown. *Science* 368, 594–595. doi: 10.1126/science.abc3372

Sathyendranath, S. (2000). *Remote Sensing of Ocean Colour in Coastal, and Other Optically-Complex Waters*. San Ysidro, CA: IOCCG.

SCRIPPS (2020). *Research in the Time of COVID-19*. Available online at: https://scripps.ucsd.edu/news/research-time-covid-19 (accessed April 17, 2020).

Shanmugam, P. S. N., Ahn, Y.-H., Philip, L., and Hong, G.-H. (2007). Assessment of the levels of coastal marine pollution of Chennai city, Southern India. *Water Resour. Manag.* 21, 1187–1206. doi: 10.1007/s11269-006-9075-6

Sharma, S., Zhang, M., Gao, J., Zhang, H., and Kota, S. H. (2020). Effect of restricted emissions during COVID-19 on air quality in India. *Sci. Total Environ.* 728:138878. doi: 10.1016/j.scitotenv.2020.138878

Smith, R. C., and Baker, K. S. (1981). Optical properties of the clearest natural waters (200-800 nm). *Appl. Opt.* 20, 177–184. doi: 10.1364/AO.20.000177

Sun, D. Y., Qiu, Z. F., Li, Y. M., Shi, K., Huang, C. C., and Gong, S. Q. (2014). New strategy to improve estimation of diffuse attenuation coefficient for highly turbid inland waters. *Int. J. Remote Sens.* 35, 3350–3371. doi: 10.1080/01431161.2014.904972

ThePrint (2020). Fishing industry suffers another blow as workers are stranded on boats, debt is piling up. Available online at: https://theprint.in/india/fishing-industry-suffers-another-blow-as-workers-are-stranded-on-boats-debt-is-piling-up (accessed June 25, 2020).

The Times of India (2020). *Pollutants Down, Chennai's Rivers Cleaner*. Available online at: https://timesofindia.indiatimes.com/city/chennai/pollutants-down-citys-rivers-cleaner (accessed June 25, 2020).

Trinh, R. C., Fichot, C. G., Gierach, M. M., Holt, B., Malakar, N. K., Hulley, G., et al. (2017). Application of Landsat 8 for monitoring impacts of wastewater discharge on coastal water quality. *Front. Mar. Sci.* 4:329. doi: 10.3389/fmars.2017.00329

Vanhellemont, Q. (2019). Adaptation of the dark spectrum fitting atmospheric correction for aquatic applications of the Landsat and Sentinel-2 archives. *Remote Sens. Environ.* 225, 175–192. doi: 10.1016/j.rse.2019.03.010

Vanhellemont, Q., and Ruddick, K. (2015). Advantages of high quality SWIR bands for ocean colour processing: examples from Landsat-8. *Remote Sens. Environ.* 161, 89–106. doi: 10.1016/j.rse.2015.02.007

Vanhellemont, Q., and Ruddick, K. (2018). Atmospheric correction of metre-scale optical satellite data for inland and coastal water applications. *Remote Sens. Environ.* 216, 586–597. doi: 10.1016/j.rse.2018.07.015

Wei, J., Lee, Z., Garcia, R., Zoffoli, L., Armstrong, R. A., Shang, Z., et al. (2018). An assessment of Landsat-8 atmospheric correction schemes and remote sensing reflectance products in coral reefs and coastal turbid waters. *Remote Sens. Environ.* 215, 18–32. doi: 10.1016/j.rse.2018.05.033

Worldometers.info (2020). *Coronavirus Updates*. Available online at: https://www.worldometers.info/coronavirus (accessed June 26, 2020).

Yunus, A. P., Masago, Y., and Hijioka, Y. (2020). COVID-19 and surface water quality: improved lake water quality during the lockdown. *Sci. Total Environ.* 731:139012. doi: 10.1016/j.scitotenv.2020.139012

Conflict of Interest: The authors declare that the research was conducted in the absence of any commercial or financial relationships that could be construed as a potential conflict of interest.

frontiers in Marine Science

BRIEF RESEARCH REPORT
published: 05 May 2021
doi: 10.3389/fmars.2021.648522

Effect of COVID-19 Anthropause on Water Clarity in the Belize Coastal Lagoon

Ileana A. Callejas[1], Christine M. Lee[2], Deepak R. Mishra[3], Stacey L. Felgate[4,5], Claire Evans[4], Abel Carrias[6], Andria Rosado[7], Robert Griffin[8], Emil A. Cherrington[9], Mariam Ayad[10], Megha Rudresh[3], Benjamin P. Page[11] and Jennifer A. Jay[1]*

[1] Department of Civil and Environmental Engineering, University of California, Los Angeles, Los Angeles, CA, United States, [2] Jet Propulsion Laboratory, California Institute of Technology, Pasadena, CA, United States, [3] Department of Geography, University of Georgia, Athens, GA, United States, [4] Ocean Biogeosciences, National Oceanography Centre, Southampton, United Kingdom, [5] Ocean and Earth Sciences, University of Southampton, Southampton, United Kingdom, [6] Faculty of Science & Technology, University of Belize, Belmopan, Belize, [7] Coastal & Marine Data Centre, Coastal Zone Management Authority & Institute, Belize City, Belize, [8] Department of Atmospheric and Earth Science, University of Alabama in Huntsville, Huntsville, AL, United States, [9] Earth System Science Center, University of Alabama in Huntsville, Huntsville, AL, United States, [10] Department of Ocean Sciences, University of California, Santa Cruz, Santa Cruz, CA, United States, [11] Water Resources Center, University of Minnesota, St. Paul, MN, United States

OPEN ACCESS

Edited by:
Christopher Edward Cornwall, Victoria University of Wellington, New Zealand

Reviewed by:
Rutger De Wit, UMR 9190 Centre Pour la Biodiversité Marine, l'exploitation et la Conservation, France
Eberhard Gischler, Goethe University Frankfurt, Germany

***Correspondence:**
Christine M. Lee
christine.m.lee@jpl.nasa.gov

Specialty section:
This article was submitted to Global Change and the Future Ocean, a section of the journal Frontiers in Marine Science

Received: *31 December 2020*
Accepted: *12 April 2021*
Published: *05 May 2021*

Citation:
Callejas IA, Lee CM, Mishra DR, Felgate SL, Evans C, Carrias A, Rosado A, Griffin R, Cherrington EA, Ayad M, Rudresh M, Page BP and Jay JA (2021) Effect of COVID-19 Anthropause on Water Clarity in the Belize Coastal Lagoon. Front. Mar. Sci. 8:648522. doi: 10.3389/fmars.2021.648522

The Coronavirus disease 2019 (COVID-19) pandemic halted human activities globally in multiple sectors including tourism. As a result, nations with heavy tourism, such as Belize, experienced improvements in water quality. Remote sensing technologies can detect impacts of "anthropauses" on coastal water quality. In this study, moderate resolution imaging spectroradiometer (MODIS) satellite data were employed along the Belizean coast to investigate impacts of the COVID-19 shutdown on water quality. The attenuation coefficient at 490 nm, $K_d(490)$, was used as an indicator of water quality, with a lower $K_d(490)$ indicating increased water clarity. Four Coastal Management Zones were characterized by marine traffic as high traffic areas (HTAs) and two as low traffic areas (LTAs). Monthly composites for two periods, 2002–2019 (baseline) and 2020 were examined for $K_d(490)$. For months prior to the COVID-19 shutdown in Belize, there was generally no significant difference in $K_d(490)$ ($p > 0.05$) between 2020 and baseline period in HTAs and LTAs. Through the shutdown, K_d was lower in 2020 at HTAs, but not for LTAs. At the LTAs, the $K_d(490)$s observed in 2020 were similar to previous years through October. In November, an unusually active hurricane season in 2020 was associated with decreased water clarity along the entire coast of Belize. This study provides proof of concept that satellite-based monitoring of water quality can complement *in situ* data and provide evidence of significant water quality improvements due to the COVID-19 shutdown, likely due to reduced marine traffic. However, these improvements were no longer observed following an active hurricane season.

Keywords: diffuse attenuation coefficient, moderate resolution imaging spectroradiometer, remote sensing, water quality, marine traffic, Belize Barrier Reef Reserve System, water clarity

INTRODUCTION

The Central American nation of Belize is home to the Belize Barrier Reef Reserve System, the largest barrier reef system in the northern hemisphere and a World Heritage Site (UNESCO, 1996; Cherrington et al., 2010, 2020). Belize's reef system is approximately 250 km in length, 963 km^2 in area, and is located 0.5-80 km offshore between Mexico and Guatemala's borders (Gischler and Hudson, 2004; Baumann et al., 2019; Claudino-Sales, 2019). This reef system contains hundreds of reef patches which developed during the Holocene (Gischler and Hudson, 2004; Eckert et al., 2019). Belize's coral reefs support high levels of biodiversity (Young, 2008), and provide essential ecosystem services such as coastal protection and fisheries (Hoegh-Guldberg et al., 2007), and important economic revenue as tourism is a primary contributor to the economy (Murray, 2020). Since 1998, the main use for Belize's reefs has been identified as tourism and thus the nation must continuously monitor tourism impacts in order to prevent the degradation of the reefs and preserve Belize's competitiveness in ecotourism markets (Gibson et al., 1998; Diedrich, 2007).

The Coronavirus disease 2019 (COVID-19) pandemic caused shifts in the environment and climate due to global lockdowns resulting in a reduction of social and economic activities (Bar, 2020; Rume and Islam, 2020). On March 23, 2020, a mandatory quarantine was placed on Ambergris Caye within Belize followed by a countrywide state of emergency (SoE) declared on March 30, 2020 (Government of Belize Press Office, 2020b; United Nations, 2020a). To limit the spread of COVID-19, Belize closed their borders to international travelers by closing land borders and its international airport (Government of Belize Press Office, 2020a). On October 1, 2020, the reopening phase of Belize's international airport began while expecting 140 travelers on its first day (Government of Belize Press Office, 2020c).

Tourism has declined on a global scale, which can have devastating impacts on local and regional economies. Other observed impacts include a reduction of anthropogenic footprint on natural ecosystems (Bar, 2020). Remote sensing datasets are especially well-positioned to assess these changes by providing a mechanism to observe larger scale responses to these declines in human activity, often referred to as the "anthropause" (Rutz et al., 2020). This is especially important in data-scare regions such as Belize. For example, Landsat-8, Sentinel-2, Sentinel-3, and moderate resolution imaging spectroradiometer (MODIS) have been used to evaluate changes in air quality emissions (Wang and Christopher, 2003; Gupta et al., 2006; Mishra et al., 2021), water clarity (Barnes et al., 2013; Zheng et al., 2016; Kuhn et al., 2019), and coastal/ocean productivity (Ho et al., 2017; Astuti et al., 2018; Caballero et al., 2020). A variety of satellites have been used for impact assessment such as Landsat-8 (Nanda et al., 2020; Patel et al., 2020; Yunus et al., 2020), PlanetScope (Niroumand-Jadidi et al., 2020), Sentinel-2 (Braga et al., 2020; Garg et al., 2020), Sentinel-3 (Cherif et al., 2020; Mishra et al., 2020), and MODIS (Gaiser et al., under revision). Multiple studies report reductions in air, water, and noise pollution due to global lockdown orders. Within the hydrosphere, rivers (Dutta et al., 2020; Garg et al., 2020; Patel et al., 2020), lakes (Yunus et al., 2020), lagoons (Braga et al., 2020; Niroumand-Jadidi et al., 2020), and coastal regions (Cherif et al., 2020; Mishra et al., 2020) experienced improvements in water quality with decreases in turbidity, pollution, and pathogens. Improvements in water quality were attributed to reductions in industrial discharges, boat traffic, and public interactions in general. These anthropogenic activities tend to increase water column turbidity and sediment resuspension in the near-shore environments and diminish water quality in the lagoon. Here, we hypothesize that the COVID-19 lockdowns and the subsequent decline in tourism and marine traffic will improve the water clarity in the Belizean coast, namely near major ports and tourist regions.

To test the hypothesis, we used satellite datasets, model produced runoff and precipitation outputs, and marine traffic data conjunctively to investigate the impacts of the COVID-19 pandemic on coastal water quality in Belize. Using the vertical diffuse attenuation coefficient [$K_d(490)$] as the primary indicator of water quality, we compared the monthly variations in water clarity in 2020 to that observed from 2002 to 2019.

METHODS

Study Area and High and Low Marine Traffic Areas

Belize is located between Mexico and Guatemala with approximately 280 km of coastline. The climate is tropical with high humidity occurring from June to October. Belize is also on the western side of "Hurricane Alley" with tropical storms and hurricanes appearing from June to November (Morales-Vela et al., 2000). Most of Belize's major cities, towns, tourist centers, and residential properties are located along the coast. The Belizean coastal lagoon is classified as a Case-1 waters like other Caribbean coastal waters (Alvain et al., 2005; Mishra et al., 2005b, 2007; Shi and Wang, 2010) as well as being oligotrophic in nature (Gómez, 2014; Mélin and Vantrepotte, 2015). In addition, multiple studies operate under the knowledge and understanding of these water being oligotrophic (Mendoza et al., 2009; Contreras-Silva et al., 2020; Correa-Ramirez et al., 2020; Guimarais et al., 2021) which is necessary for the development and flourishing of corals (Warne et al., 2005; Guimarais et al., 2021). The Belizean coast hosts multiple diverse ecosystems including coral reefs, mangroves, and seagrasses (Cherrington et al., 2010; Baumann et al., 2016; Verutes et al., 2017; Sweetman et al., 2019; Helmuth et al., 2020) which not only attract tourists but also play an integral role in mitigating coastal erosion and impacts from tropical storms (Cooper et al., 2009). Though these ecosystems contribute millions of United States dollars to Belize's economy (Cooper et al., 2009), industries such as tourism, fisheries, real estate, and agriculture stand to threaten the very ecosystems that allow them to operate (Verutes et al., 2017). Tourism season in Belize takes place during in dry, winter months from November to April (Renaud, 2020).

Belize's Integrated Coastal Zone Management Plan (ICZMP) divides its coast into nine regions based on biological, geographical, economic, and administrative characteristics

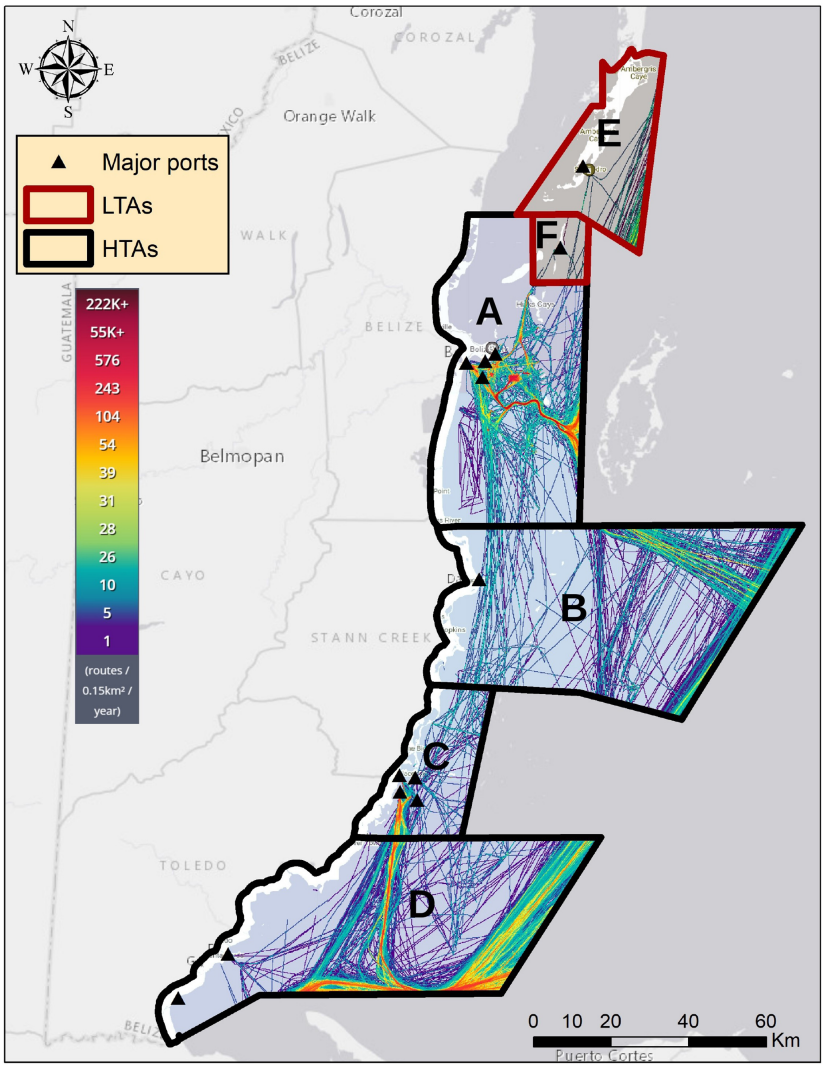

FIGURE 1 | Belize Coastal Zones, Major Ports, and Marine Traffic Density. Six coastal areas were used in this study: **(A)** Central Region, **(B)** South Northern Region, **(C)** South Central Region, **(D)** Southern Region, **(E)** Ambergris Caye, and **(F)** Caye Caulker. Areas **(A–D)** are denoted as high traffic areas (HTAs) and E & F as low traffic areas (LTAs). Each zone is filled with 2019 marine traffic density maps where the color of each line corresponds to the number of routes/0.15 km^2/year.

(Coastal Zone Management Authority and Institute [CZMAI], 2016). Six of these nine regions were characterized as high and low traffic areas (HTAs and LTAs, respectively) based on a 2019 marine traffic density map assumed to depict typical traffic patterns prior to COVID-related lockdowns (**Figure 1**). The four HTAs comprise the Central Region which includes Belize City (A), South Northern Region which includes Dangriga (B), part of South Central Region containing Placenia, Big Creek, and Harvest Caye (C), and the Southern Region containing Punta Gorda and Barranco (D). The two LTAs are to the north, at Ambergris Caye (E), and Caye Caulker (F).

High Traffic Areas

Belize City is the largest city within the Belize District (17.5046° N, 88.1962° W) and is home to the nation's principal port (Belize City Council, 2020). The Port of Belize Limited is located on the south side of Belize City and is responsible for containerized and break bulk cargo (Belize Port Authority, 2020b). Other major port facilities in Belize City include Puma Energy Bahamas SA for bulk fuel import, Fort Street Tourism Village, a water taxi terminal operated by the Belize Border Management Agency (BMA), Radisson Fort George, and Old Belize port.

Dangriga is a town in southern Belize and the capital of Stann Creek District (16.9696° N, 88.2315° W). Though the Commerce Bight port 1.5 miles south of Dangriga is currently not operational (Belize Port Authority, 2020a), Dangriga is known as "the cultural capital of Belize" and is a popular tourist location (Belize.com, 2020).

Placencia is located on the Placencia Peninsula (16.5212° N, 88.3713° W) on the southeast coast of Belize within

the Stann Creek District and is rapidly growing in tourism (Wells et al., 2014; Renaud, 2020). Just south of the Stann Creek District in the Toledo District is the Port of Big Creek, the nation's second major port (7 News Belize, 2020), responsible for banana exports, crude oil tank farming, and sugar storage (Port of Big Creek, 2020). South of both Big Creek and Placencia and a mile off the coast is Harvest Caye, a private island developed for tourism by a Miami-based Norwegian Cruise Line (Renaud, 2020). Belize City and Placencia are two major coastal cities which have experienced coral growth declines (Baumann et al., 2019) and mangrove clearings (Cherrington et al., 2010).

Punta Gorda (16.0989° N, 88.8095° W) and Barranco (16.0011° N, 88.9186° W) are both towns located in the southernmost region of Belize located in the Toledo District. Punta Gorda is the capital of the Toledo District and is home to the Punta Gorda Port (Belize Port Authority, 2020c). The Port of Barranco is a very small port in the town of Barranco (FleetMon, 2020).

Low Traffic Areas

San Pedro is a town in the southern part of Ambergris Caye in the Belize District in northern Belize (17.9214° N, 87.9611° W). There is a water taxi terminal with six berths located in San Pedro under the Belize BMA (Belize Port Authority, 2020d).

Caye Caulker is a small island off the coast of Belize (17.7612° N, 88.0277° W) accessible by water taxis and small planes (CayeCaulker.org, 2020).

Satellite Images

The average vertical diffuse attenuation coefficient for downwelling irradiance at 490 nm, $K_d(490)$, was calculated in Google Earth Engine (GEE) from images collected from MODIS onboard the Aqua satellite. The images processed in GEE started from June 4, 2002 to July 31, 2020. The rest of the images for 2020 were downloaded from https://oceancolor.gsfc.nasa.gov/and ingested into GEE. All images were Level-3 daily images with a spatial resolution of 4 km and $K_d(490)$ was calculated using the NASA operational algorithm (Werdell and Bailey, 2005). The algorithm is a fourth-order polynomial between blue and green remote sensing reflectances (Rrs) and $K_d(490)$. The algorithm is based on two high quality bio-optical global datasets, the SeaWiFS Bio-Optical Archive and Storage System (SeaBASS) and the NASA bio-Optical Marine Algorithm Data (NOMAD) archives. Though the datasets encompass a broad range of water types and locations, certain oceanic regions remain underrepresented.

The NASA operational algorithm is as follows for the MODIS sensor:

$$K_d(490) = 10^{(-0.8813-2.0584x+2.5878x^2-3.4885x^3-1.5061x^4)} + 0.0166$$

where $x = \log_{10}\frac{Rrs(488)}{Rrs(547)}$. Beside numerous open ocean applications, MODIS-derived $K_d(490)$ products have also been used in turbid coastal water (Tomlinson et al., 2019), for coastal river plume characterization during high flow (López et al., 2013), and turbidity impacts on coral health (Freitas et al., 2019; Martínez-Castillo et al., 2020). Caribbean coastal waters are generally considered as Case-1 waters because thriving seagrass and reef habitats help reduce water column turbidity (Mishra et al., 2005a, 2007). The NASA operational algorithm for $K_d(490)$ has also been used specifically in coastal Caribbean regions (López et al., 2013; García-Sais et al., 2017; Vega Sequeda et al., 2017). A function was created to calculate $K_d(490)$ for each image and the newly calculated band was appended to the image collection. Monthly averages for $K_d(490)$ were calculated for the coast of Belize using a mean reducer for LTAs and HTAs and compared between 2020 and the baseline period. The number of pixels included in each monthly calculation was obtained through the count reducer which computes the number of non-null inputs. Percent difference maps of $K_d(490)$ were also created in GEE by filtering the images for each respective month of the year, taking the average for the years of 2002–2019 and 2020, and mapping the percent difference between the two time frames. A decrease in $K_d(490)$ indicates a decline in water clarity, generally associated with degradation in water quality, whereas an increase in $K_d(490)$ indicates an increase in water clarity, associated with an improvement.

Marine Traffic Data

Marine traffic data were obtained from the company MarineTraffic[1] for ports and anchorages in Belize from January 2020 to November 2020 (**Figure 2**). The data uses both Automated Identification System (AIS) data and data from satellite receivers. The data includes arrival and departure data for ports in Belize City, Belize City anchorage, Old Belize, Radisson Fort George, Placencia, Big Creek, Big Creek anchorage, Harvest Caye, San Pedro, and Caye Caulker. The company also detects port calls from Dangriga, Punta Gorda, and Barranco ports, but in 2020 there were no port calls detected through AIS or satellite data for these ports.

Runoff and Precipitation Models

Monthly time-averaged precipitation and runoff were calculated over Belize using NASA's Modern-Era Retrospective analysis for Research and Applications, Version 2 (MERRA-2) model from June 2002 to October 2020. MERRA-2 is a global atmospheric reanalysis produced by NASA's Global Modeling and Assimilation Office (NASA Global Modeling and Assimilation Office, 2020). For precipitation, the "total surface precipitation" variable was used (M2TMNXFLX v5.12.4) and for runoff, the "overland runoff including throughflow" variable was used (M2TMNXLND v5.12.4). The model outputs were extracted from NASA Giovanni[2].

Statistical Analysis

For each month of the year where data were available, data for each location for years 2002–2019 and for the year 2020 were grouped and tested for normality using histograms created in R (R Core Team, 2020). In no cases were both the previous years and 2020 found to be normal, so the Wilcoxon unpaired test was used to test the null hypothesis that there was no difference

[1] marinetraffic.com

[2] https://giovanni.gsfc.nasa.gov/giovanni/

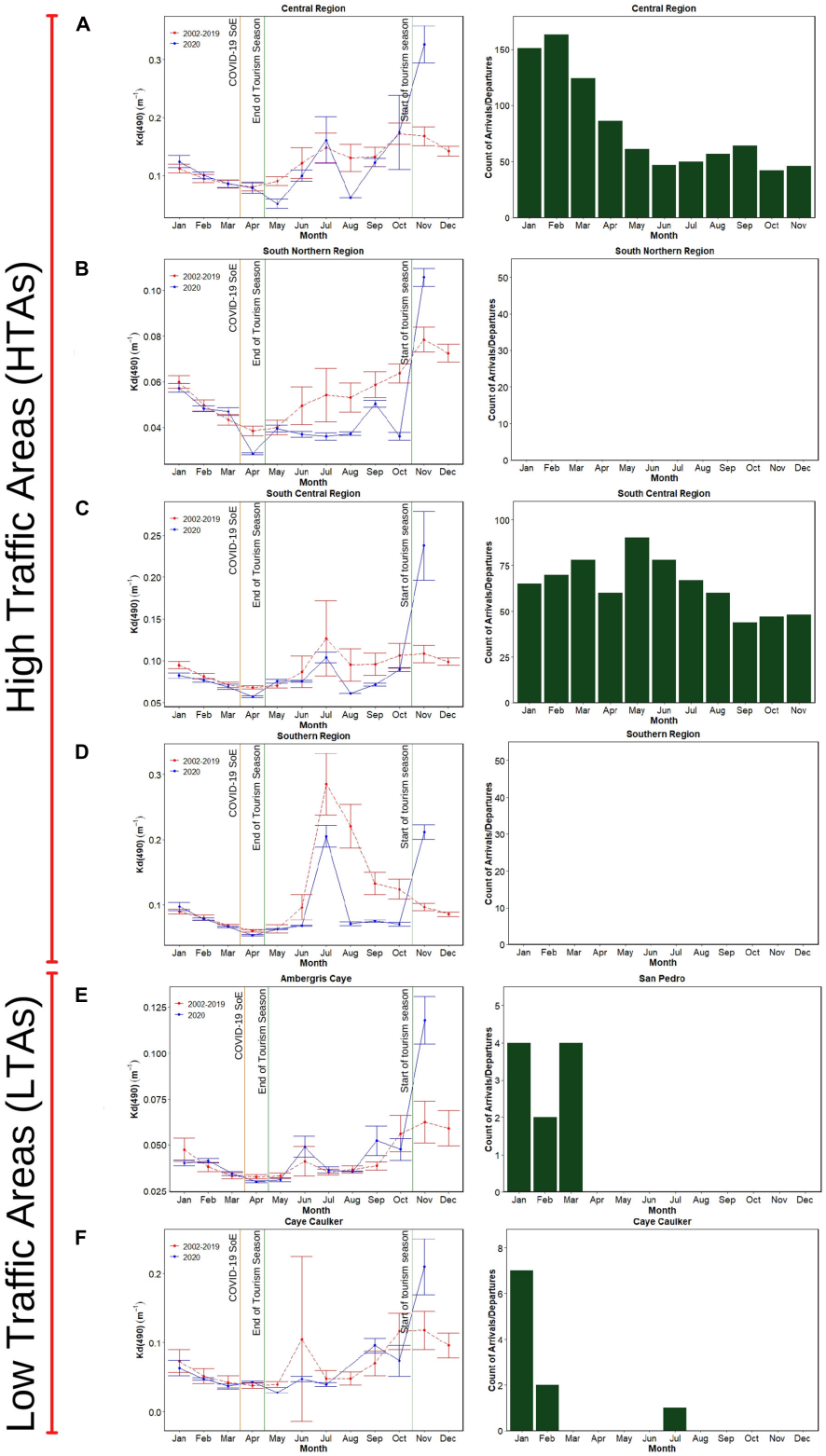

FIGURE 2 | $K_d(490)$ Time Series Plots and 2020 Total Port Counts. The first vertical column of figures are plots of monthly $K_d(490)$ values and standard deviations for the 2020 and 2002–2019 time periods. The orange vertical line marks the time of the COVID-19 SoE in Belize. The green lines represent the beginning and end of the tourist season in Belize. The second column of figures are total port counts for each month for 2020. Some ports did not have any port calls in 2020 through AIS or satellite data. Each lettered row of plots corresponds to the areas in **Figure 1**. **(A)** Central Region, **(B)** South Northern Region, **(C)** South Central Region, **(D)** Southern Region, **(E)** Ambergris Caye, and **(F)** Caye Caulker.

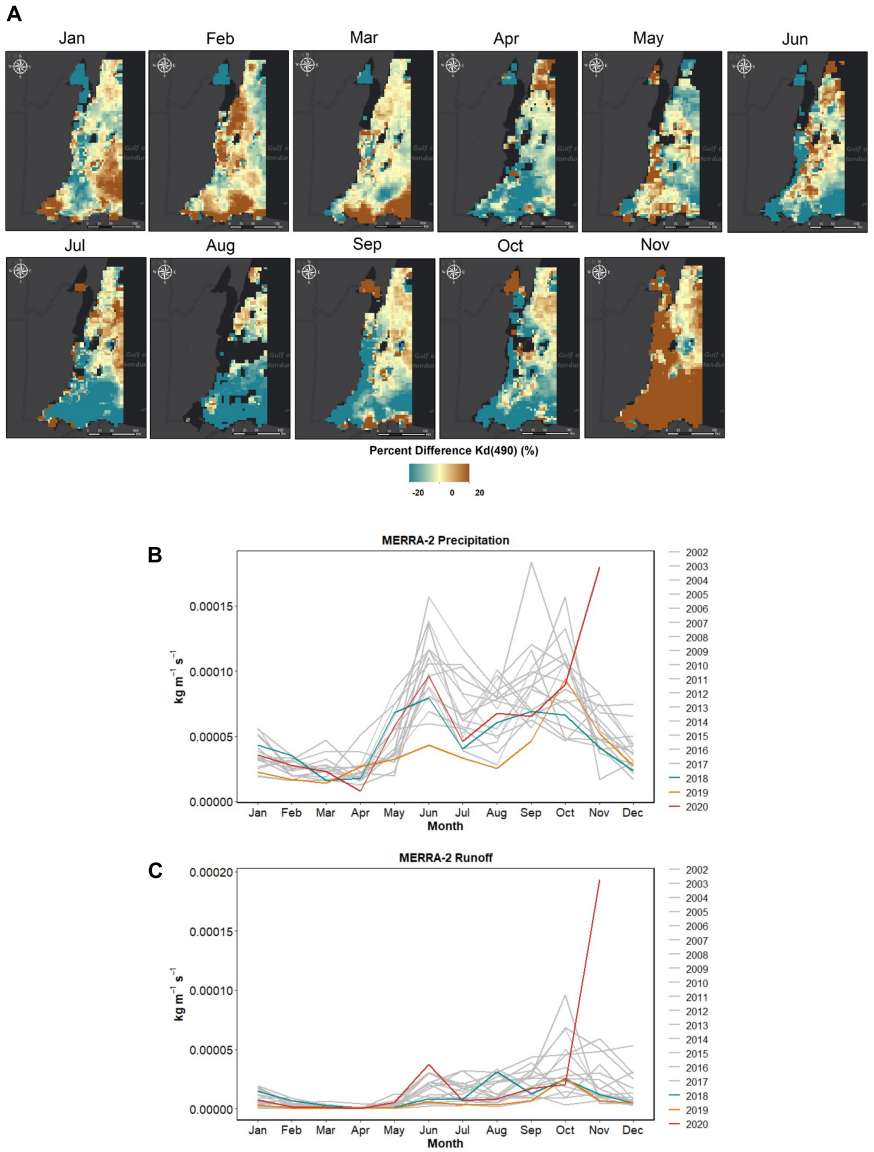

FIGURE 3 | Percent Difference K_d(490) Maps and MERRA-2 Model Outputs. **(A)** Monthly percent difference maps comparing 2020 K_d(490) values against those of the 2002–2019 (baseline) time period. **(B)** MERRA-2 precipitation output for the country of Belize from 2002 to 2020 in kg m^{-1} s^{-1}. **(C)** MERRA-2 runoff output for Belize from 2002 to 2020 in kg m^{-1} s^{-1}.

between 2020 and previous years. We computed means and standard deviation for both time periods.

RESULTS

At the start of 2020 prior to the Belize SoE COVID shutdown, the K_d(490) was consistently similar to that observed for previous years, with no significant differences observed for any location (**Figure 2**). However, the monthly K_d(490) maps show notable decreases in K_d(490) along the Belizean coast at HTAs following the initial lockdown orders in place on March 23, 2020 compared to the 2002-2019 average (**Figure 3A**). Following the SOE in April, 2020 data showed a lower K_d (indicating increased water clarity) compared to previous years in (most) HTAs, but not the LTAs. For example, for HTA-D, which includes Placencia, the average K_d(490) from 2002 to 2019 for the month of April was 0.068 m^{-1} (SD 0.002), while for 2020 the value was 0.057 m^{-1} (SD 0.001). In May of 2020, HTA-A, which includes Belize's most popular port, shows a K_d of 0.051 m^{-1} (SD 0.008) in 2020, compared to 0.090 m^{-1} (SD 0.008) for the years 2002–2019. See **Table 1** for the *p*-values for hypothesis testing for the difference between 2020 and previous years. While LTAs showed some differences in means, these tended to be smaller, and statistically significant differences were only observed at HTAs. For both HTAs and LTAs for the months of June and July, none of the

TABLE 1 | Wilcoxon test *p*-values for each month between $K_d(490)$ values in 2020 versus 2002–2019 baseline for all regions.

Site	Coastal region	HTA/LTA	Wilcoxon test *p*-values										
			January	February	March	April	May	June	July	August	September	October	November
A	Central region	HTA	0.679	0.374	0.987	0.705	0.029*	0.895	0.651	0.269	0.982	0.067	0.006*
B	South Northern region	HTA	0.806	0.866	0.164	0.018*	0.429	0.988	0.479	0.250	0.83	0.006*	0.033*
C	South Central region	HTA	0.082	0.250	0.230	0.046*	0.165	0.359	-	0.113	0.004*	0.496	< 0.001*
D	Southern region	HTA	0.600	0.968	0.423	0.483	0.063	0.403	0.852	0.044*	0.009*	0.003*	< 0.001*
E	Ambergris Caye	LTA	0.131	0.021*	0.504	0.313	0.382	-	0.590	0.787	0.591	0.419	0.002*
F	Caye Caulker	LTA	0.567	0.353	0.481	–	–	–	–	–	0.162	0.178	0.009*

An asterisk is used to denote p-values less than 0.05. Orange highlighting indicates the $K_d(490)$ in 2020 was lower than that in previous years. Green highlighting shows where $K_d(490)$ was higher in 2020 than in previous years.

observed differences in means were significant, possibly due to the tourism season ending so no major differences in marine traffic would be expected.

Figure 3A shows the percent difference of $K_d(490)$ between 2020 and previous years. A greater fraction of the coastal waters shows a decrease (blue) compared to previous years for the months of April through October. In November 2020, $K_d(490)$ increases (brown) drastically across the entire coast. This increase coincides with a record-breaking hurricane season where Belize experienced impacts of Hurricanes Nana, Eta, Iota, and Tropical Storm Cristobal (Amandala Newspaper, 2020). **Figures 3B,C** show the precipitation and runoff for 2002 through 2020 of Belize. While month to month 2020 was not an atypical year for precipitation through the month of October, both precipitation and runoff were dramatically elevated for the month of November (**Figures 3B,C**).

Because $K_d(490)$ incorporates both inorganic and organic components within the water column, we tested for correlations between *in situ* chlorophyll-a and MODIS-derived $K_d(490)$. Using a dataset from 2018 and 2019, we saw no significant correlation between chlorophyll-a and $K_d(490)$ after calculating the Spearman's rank order correlation coefficient following tests for normality using Q–Q plots and histograms (Spearman's rho = 0.34) (see **Supplementary Material**).

DISCUSSION

This preliminary study shows that MODIS $K_d(490)$ data can be used to better understand spatiotemporal changes in water quality impacts associated with environmental disturbances. This is particularly important in locations where *in situ* data are limited and healthy ecosystems are essential to the local economy. Belize relies on robust tourist traffic to support the economy, and water clarity is critical for coral reef health (De'ath and Fabricius, 2010). Marine traffic due to both commerce and tourism have the potential to result in decreased water clarity through an increase in suspended solids. In addition, marine traffic is also shown to increase nutrient depositions which spurs phytoplankton growth (Zhang et al., 2021). For this site, chlorophyll-a and $K_d(490)$ were not significantly associated, suggesting that $K_d(490)$ is mainly attributed to sediment resuspension rather than algal particles. Nonetheless, the possible contribution of chlorophyll-a to MODIS $K_d(490)$ at the study site needs further investigation, and future data collection should attempt to deconvolute their signals.

The COVID-19 shutdown in 2020, along with the availability of satellite data with an extended recorded (2002–2019), presented an opportunity to understand the impacts of tourism on water quality and subsequent effects on coral reef health in a data-scarce region. As shown in this work, the COVID-19 shutdown resulted in increased water clarity in areas along the Belizean coast with typically high marine traffic, while water clarity was similar in areas with typically low marine traffic during the tourism season. This finding, along with knowledge of the relationships between water clarity and reef health, provides insight on the role of commerce and tourism on the long-term sustainability of the northern hemisphere's largest barrier reef system. Additionally, this finding is similar to other studies that investigated COVID-19 impacts on turbidity, suspended particulate matter (SPM), and total suspended matter (TSM). Studies in India show a 15.9% decrease in SPM in a lake (Yunus et al., 2020), a significant reduction in the usual pre-monsoon phytoplankton content in coastal waters (Mishra et al., 2020), water quality index increase of 37% in the Yamuna River (Patel et al., 2020), and reductions in turbidity in the Ganga River (Garg et al., 2020) all with notable changes in April 2020. A couple of studies of the Venice Lagoon, which has high water traffic, found decreases of TSM (Niroumand-Jadidi et al., 2020) and increases in water clarity (Braga et al., 2020) during their lockdowns in March and April 2020.

One expected outcome of this study is a further collaboration with colleagues at the Coastal Zone Management Authority Institute, who is committed to the protection and sustainable management of coastal resources and the ICZMP. The ICZMP is an evidence-based set of policy recommendations that enable an improved understanding of how land management might impact coastal and marine resources (Coastal Zone Management Authority and Institute [CZMAI], 2016).

This work also observes substantial water clarity changes, e.g., anomalous coastal plumes, following the active hurricane season in 2020, an observation enabled by high-frequency, freely available satellite data such as MODIS. Hurricane events in November 2020 coincided with a significant decrease in water clarity compared with November during the baseline period (Aronson et al., 2000; Haines, 2019). Future work should include evaluating the changing climatology of

hurricane events on corresponding plumes into the marine environment. Furthermore, it is critical that future work considers *in situ* datasets that would allow improved tuning of remote sensing based estimates of water quality as well as improved characterization of plume constituents. It has been observed that these Belize coastal plumes can be comprised of a variety of constituents, including sediments, agricultural runoff, and sewage (Maidens and Burke, 2005; Macintyre et al., 2009; Emrich et al., 2017; Wells et al., 2019), with Soto et al. (2009) observing a consistent year-to-year river plume occurrences with coral ecosystems (Soto et al., 2009). Though classified as oligotrophic, river plumes can often cause Caribbean waters to become mesotrophic (Warne et al., 2005; Torregroza-Espinosa et al., 2021). In Belize, New River is known to cause a decline in water quality affecting surrounding corals due to poor farming practices and deforestation (Espinoza-Avalos et al., 2009; Reyes et al., 2019). Corals in particular are highly sensitive to changing conditions and it is expected that agricultural runoff and water temperature increases may contribute to their declines (Baumann et al., 2019).

CONCLUSION

Remote sensing can be used to evaluate these coupled events and their spatial and temporal effects on coastal waters. This study observes an improvement in water clarity during COVID-19 shutdowns in Belize, followed by a decline in water clarity following an atypical, active hurricane season. Use of remote sensing is especially important for coastal waters, as populations rise and population density and development along the coasts continue to increase (Martínez et al., 2007; Glavovic, 2017; Elliott et al., 2019). Remote sensing of water quality holds great promise to improve detection of changes in water quality and ecosystem health in data-scarce locations impacted by development, tourism, or climate change, and may represent an asset for nations and entities seeking to set and advance toward the UN Sustainable Development Goals[3] (United Nations, 2020b). This study in particular is closely linked with SDG 14.1 (life in water). Satellite data can be used to extend ground-based monitoring programs to increase the temporal and spatial density of data. Future research will involve the use of match-ups between *in situ* and satellite data to further investigate long-term relationships between *in situ* water quality parameters such as chlorophyll-a and TSM and isolate any signal related to COVID-19 lockdowns.

[3] https://sdgs.un.org/goals/goal14

DATA AVAILABILITY STATEMENT

The raw data supporting the conclusions of this article will be made available by the authors, without undue reservation.

AUTHOR CONTRIBUTIONS

IC, JJ, DM, and CL wrote the manuscript. IC developed all scripts and performed the data processing and analysis with some guidance from BP. CL, DM, RG, and EC conceived the study. CL, JJ, and DM co-advised the research. CL, RG, and JJ acquired the funding. EC, MA, RG, AR, SF, AC, MR, and CE contributed to the development of the project and manuscript editing. All authors contributed to the article and approved the submitted version.

FUNDING

This work was supported by the NASA RRNES (Grant #80NSSC20K1746) and NASA ROSES A.8 (cooperative agreement number #80NSSC19K0200), UCLA's Center for Diverse Leadership in Science, and the Joan Doren Family Foundation. This work was performed in part at the Jet Propulsion Laboratory, California Institute of Technology, under contract with the National Aeronautics and Space Administration.

ACKNOWLEDGMENTS

We thank Nicole Auil Gomez, Phillips Myles, and Alexander Tewfik (Wildlife Conservation Society, Belize), Clara Wheelock (University of Georgia) for their support during the project.

SUPPLEMENTARY MATERIAL

The Supplementary Material for this article can be found online at: https://www.frontiersin.org/articles/10.3389/fmars.2021.648522/full#supplementary-material

REFERENCES

Alvain, S., Moulin, C., Dandonneau, Y., and Bréon, F. M. (2005). Remote sensing of phytoplankton groups in case 1 waters from global SeaWiFS imagery. *Deep. Res. Part I Oceanogr. Res. Pap.* 52, 1989–2004. doi: 10.1016/j.dsr.2005.06.015

Amandala Newspaper (2020). *Record-Breaking 2020 Hurricane Season Ends Today*. Available online at: https://amandala.com.bz/news/record-breaking-2020-hurricane-season-ends-today/ (accessed December 19, 2020).

Aronson, R. B., Precht, W. F., Macintyre, I. G., and Murdoch, T. J. T. (2000). Coral bleach-out in Belize. *Nature* 405:36. doi: 10.1038/35011132

Astuti, I. S., Mishra, D. R., Mishra, S., and Schaeffer, B. (2018). Spatio-temporal dynamics of inherent optical properties in oligotrophic northern Gulf of Mexico estuaries. *Cont. Shelf Res.* 166, 92–107. doi: 10.1016/j.csr.2018.06.016

Bar, H. (2020). COVID-19 lockdown: animal life, ecosystem and atmospheric environment. *Environ. Dev. Sustain.* doi: 10.1007/s10668-020-01002-7 [Epub ahead of print].

Barnes, B. B., Hu, C., Schaeffer, B. A., Lee, Z., Palandro, D. A., and Lehrter, J. C. (2013). MODIS-derived spatiotemporal water clarity patterns in optically shallow Florida Keys waters: a new approach to remove bottom contamination. *Remote Sens. Environ.* 134, 377–391. doi: 10.1016/j.rse.2013.03.016

Baumann, J. H., Ries, J. B., Rippe, J. P., Courtney, T. A., Aichelman, H. E., Westfield, I., et al. (2019). Nearshore coral growth declining on the Mesoamerican Barrier Reef System. *Glob. Chang. Biol.* 25, 3932–3945. doi: 10.1111/gcb.14784

Baumann, J. H., Townsend, J. E., Courtney, T. A., Aichelman, H. E., Davies, S. W., Lima, F. P., et al. (2016). Temperature regimes impact coral assemblages along environmental gradients on lagoonal reefs in Belize. *PLoS One* 11:e0162098. doi: 10.1371/journal.pone.0162098

Belize City Council (2020). *About Belize City*. Available online at: https://web.archive.org/web/20140723140609/http://belizecitycouncil.org/about-belize-city (accessed December 17, 2020).

Belize.com (2020). *Stann Creek Belize - Home Of Culture Capital Dangriga*. Available online at: https://belize.com/stann-creek/ (accessed December 30, 2020).

Belize Port Authority (2020a). *Commerce Bight*. Available online at: https://www.portauthority.bz/port-facilities/commerce-bight/ (accessed December 30, 2020).

Belize Port Authority (2020b). *Port Facilities*. Available online at: https://www.portauthority.bz/port-facilities/ (accessed December 17, 2020).

Belize Port Authority (2020c). *Punta Gorda Port*. Available online at: https://www.portauthority.bz/port-facilities/punta-gorda-port/ (accessed December 30, 2020).

Belize Port Authority (2020d). *San Pedro Terminal*. Available online at: https://www.portauthority.bz/port-facilities/san-pedro-terminal/ (accessed December 30, 2020).

Braga, F., Scarpa, G. M., Brando, V. E., Manfè, G., and Zaggia, L. (2020). COVID-19 lockdown measures reveal human impact on water transparency in the Venice Lagoon. *Sci. Total Environ.* 736:612. doi: 10.1016/j.scitotenv.2020.139612

Caballero, I., Fernández, R., Escalante, O. M., Mamán, L., and Navarro, G. (2020). New capabilities of Sentinel-2A/B satellites combined with in situ data for monitoring small harmful algal blooms in complex coastal waters. *Sci. Rep.* 10, 1–14. doi: 10.1038/s41598-020-65600-1

CayeCaulker.org (2020). *Belize Travels, Lodging, Diving, Guides, Mayan Tours, Fishing, Hotels and Resorts, Paradise for Scuba, Vacation, Beaches Relaxing, Fishing Tourism, Vacations, Adventures*. Available online at: https://cayecaulker.org/ (accessed December 30, 2020).

Cherif, E. K., Vodopivec, M., Mejjad, N., Esteves, J. C. G., and Simonovi˘, S. (2020). COVID-19 pandemic consequences on coastal water. *Water* 12:2638.

Cherrington, E. A., Griffin, R. E., Anderson, E. R., Hernandez Sandoval, B. E., Flores-Anderson, A. I., Muench, R. E., et al. (2020). Use of public Earth observation data for tracking progress in sustainable management of coastal forest ecosystems in Belize, Central America. *Remote Sens. Environ.* 245:111798. doi: 10.1016/j.rse.2020.111798

Cherrington, E. A., Hernandez, B. E., Trejos, N. A., Smith, O. A., Anderson, E. R., Flores, A. I., et al. (2010). *Identification of Threatened and Resilient Mangroves in the Belize Barrier Reef System*. Panama: CATHALAC.

Claudino-Sales, V. (2019). "Belize barrier reef system, Belize," in *Coastal World Heritage Sites. Coastal Research Library*, Vol. 28, (Dordrecht: Springer). doi: 10.1007/978-94-024-1528-5_66

Coastal Zone Management Authority and Institute [CZMAI] (2016). Belize integrated coastal zone management plan: the vision for our coast (ICZMP). *Minsitry Agric. For. Fish. Environ. Sustain. Dev.* 265, 1–265.

Contreras-Silva, A. I., Tilstra, A., Migani, V., Thiel, A., Pérez-Cervantes, E., Estrada-Saldívar, N., et al. (2020). A meta-analysis to assess long-term spatiotemporal changes of benthic coral and macroalgae cover in the Mexican Caribbean. *Sci. Rep.* 10, 1–12. doi: 10.1038/s41598-020-65801-8

Cooper, E., Burke, L., and Bood, N. (2009). *Coastal Capital: Economic Contribution of Coral Reefs and Mangroves to Belize*. Washington, DC: World Resourse Institute, 53.

Correa-Ramirez, M., Rodriguez-Santana, Á, Ricaurte-Villota, C., and Paramo, J. (2020). The Southern Caribbean upwelling system off Colombia: water masses and mixing processes. *Deep. Res. Part I Oceanogr. Res. Pap.* 155:103145. doi: 10.1016/j.dsr.2019.103145

De'ath, G., and Fabricius, K. (2010). Water quality as a regional driver of coral biodiversity and macroalgae on the Great Barrier Reef. *Ecol. Appl.* 20, 840–850.

Diedrich, A. (2007). The impacts of tourism on coral reef conservation awareness and support in coastal communities in Belize. *Coral Reefs* 26, 985–996. doi: 10.1007/s00338-007-0224-z

Dutta, V., Dubey, D., and Kumar, S. (2020). Cleaning the River Ganga: Impact of lockdown on water quality and future implications on river rejuvenation strategies. *Sci. Total Environ.* 743:140756. doi: 10.1016/j.scitotenv.2020.140756

Eckert, R. J., Studivan, M. S., and Voss, J. D. (2019). Populations of the coral species *Montastraea cavernosa* on the Belize Barrier Reef lack vertical connectivity. *Sci. Rep.* 9, 1–11. doi: 10.1038/s41598-019-43479-x

Elliott, M., Day, J. W., Ramachandran, R., and Wolanski, E. (eds). (2019). "Chapter 1 – A synthesis: what is the future for coasts, estuaries, deltas and other transitional habitats in 2050 and beyond?," in *Coasts and Estuaries* (Amsterdam: Elsevier), 1–28. doi: 10.1016/B978-0-12-814003-1.00001-0

Emrich, K., Martinez-Colon, M., and Alegria, H. (2017). Is untreated sewage impacting coral reefs of Caye Caulker, Belize? *J. Foraminifer. Res.* 47, 20–33. doi: 10.2113/gsjfr.47.1.20

Espinoza-Avalos, J., Islebe, G. A., and Hernandez-Arana, H. A. (2009). "El sistema ecológico de la bahía de Chetumal," in *Corozal: Costa Occidental Del Mar Caribe*, eds H. A. H.-A. J. Espinoza-Avalos and G. A. Islebe (Lerma Campeche: ECOSUR).

FleetMon (2020). *Port of Barranco, Belize - Arrivals, Schedule and Weather Forecast*. Available online at: https://www.fleetmon.com/ports/barranco_bzbar_14265/?language=en (accessed December 30, 2020).

Freitas, L. M., Oliveira, M., de, D. M., Leão, Z. M. A. N., and Kikuchi, R. K. P. (2019). Effects of turbidity and depth on the bioconstruction of the Abrolhos reefs. *Coral Reefs* 38, 241–253. doi: 10.1007/s00338-019-01770-3

García-Sais, J. R., Williams, S. M., and Amirrezvani, A. (2017). Mortality, recovery, and community shifts of scleractinian corals in Puerto Rico one decade after the 2005 regional bleaching event. *PeerJ* 2017:e3611. doi: 10.7717/peerj.3611

Garg, V., Aggarwal, S. P., and Chauhan, P. (2020). Changes in turbidity along Ganga River using Sentinel-2 satellite data during lockdown associated with COVID-19. *Geomat. Nat. Hazards Risk* 11, 1175–1195. doi: 10.1080/19475705.2020.1782482

Gibson, J., McField, M., and Wells, S. (1998). Coral reef management in Belize: an approach through integrated coastal zone management. *Ocean Coast. Manag.* 39, 229–244. doi: 10.1016/S0964-5691(98)00007-6

Gischler, E., and Hudson, J. H. (2004). Holocene development of the Belize Barrier Reef. *Sediment. Geol.* 164, 223–236. doi: 10.1016/j.sedgeo.2003.10.006

Glavovic, B. C. (2017). "Coasts," in *International Encyclopedia of Geography: People, the Earth, Environment and Technology*, eds D. Richardson, N. Castree, M. F. Goodchild, A. Kobayashi, W. Liu, and R. A. Marston. doi: 10.1002/9781118786352.wbieg0817

Gómez, R. A. (2014). Spectral reflectance analysis of the Caribbean Sea. *Geofis. Int.* 53, 385–398. doi: 10.1016/S0016-7169(14)70073-X

Government of Belize Press Office (2020a). *COVID-19 - Alert Regarding Border Closures*. Available online at: https://www.pressoffice.gov.bz/covid-19-alert-regarding-border-closures/ (accessed December 17, 2020).

Government of Belize Press Office (2020b). *State of Emergency Declared for Ambergris Caye*. Belmopan: Government of Belize Press Office. (accessed December 5, 2020).

Government of Belize Press Office (2020c). *The Philip Goldson International Airport Successfully Reopens. 1-2*. Available online at: https://www.pressoffice.gov.bz/the-philip-goldson-international-airport-successfully-reopens/ (accessed December 28, 2020).

Guimarais, M., Zúñiga-Ríos, A., Cruz-Ramírez, C. J., Chávez, V., Odériz, I., van Tussenbroek, B. I., et al. (2021). The conservational state of coastal ecosystems on the mexican caribbean coast: environmental guidelines for their management. *Sustain* 13, 1–25. doi: 10.3390/su13052738

Gupta, P., Christopher, S. A., Wang, J., Gehrig, R., Lee, Y., and Kumar, N. (2006). Satellite remote sensing of particulate matter and air quality assessment over global cities. *Atmos. Environ.* 40, 5880–5892. doi: 10.1016/j.atmosenv.2006.03.016

Haines, S. (2019). Managing expectations: articulating expertise in climate services for agriculture in Belize. *Clim. Change* 157, 43–59. doi: 10.1007/s10584-018-2357-1

Helmuth, B., Leichter, J. J., Rotjan, R. D., Castillo, K. D., Fieseler, C., Jones, S., et al. (2020). High resolution spatiotemporal patterns of seawater temperatures across the Belize Mesoamerican Barrier Reef. *Sci. Data* 7, 1–6. doi: 10.1038/s41597-020-00733-6

Ho, J. C., Stumpf, R. P., Bridgeman, T. B., and Michalak, A. M. (2017). Using landsat to extend the historical record of lacustrine phytoplankton blooms: a Lake Erie case study. *Remote Sens. Environ.* 191, 273–285. doi: 10.1016/j.rse.2016.12.013

Hoegh-Guldberg, O., Mumby, P. J., Hooten, A. J., Steneck, R. S., Greenfield, P., Gomez, E., et al. (2007). Coral reefs under rapid climate change and ocean acidification. *Science* 318, 1737–1742. doi: 10.1126/science.1152509

Kuhn, C., de Matos Valerio, A., Ward, N., Loken, L., Sawakuchi, H. O., Kampel, M., et al. (2019). Performance of Landsat-8 and Sentinel-2 surface reflectance products for river remote sensing retrievals of chlorophyll-a and turbidity. *Remote Sens. Environ.* 224, 104–118. doi: 10.1016/j.rse.2019.01.023

López, R., López, J. M., Morell, J., Corredor, J. E., and Del Castillo, C. E. (2013). Influence of the Orinoco River on the primary production of eastern Caribbean surface waters. *J. Geophys. Res. Ocean.* 118, 4617–4632. doi: 10.1002/jgrc.20342

Macintyre, I. G., Toscano, M. A., Feller, I. C., and Faust, M. A. (2009). Decimating mangrove forests for commercial development in the Pelican cays, Belize: long-term ecological loss for short-term gain? *Smithson. Contrib. Mar. Sci.* 25, 281–290.

Maidens, J., and Burke, L. (2005). *Belize Coastal Threat Atlas*. Washington, DC: World Resourse Institute.

Martínez, M. L., Intralawan, A., Vázquez, G., Pérez-Maqueo, O., Sutton, P., and Landgrave, R. (2007). The coasts of our world: ecological, economic and social importance. *Ecol. Econ.* 63, 254–272. doi: 10.1016/j.ecolecon.2006.10.022

Martínez-Castillo, V., Paola Rodríguez-Troncoso, A., Reyes-Bonilla, H., Aguilar-Cruz, C. A., and Rangel-Dávalos, C. (2020). Reproduction of the endangered endemic saffron coral to the Gulf of California *Porites sverdrupi* (Anthozoa: Scleractinia): implications for its long-term maintenance. *Helgol. Mar. Res.* 74:6. doi: 10.1186/s10152-020-00538-5

Mélin, F., and Vantrepotte, V. (2015). How optically diverse is the coastal ocean? *Remote Sens. Environ.* 160, 235–251. doi: 10.1016/j.rse.2015.01.023

Mendoza, W. G., Zika, R. G., Corredor, J. E., Morrel, J., Ko, D. S., and Mooers, C. N. K. (2009). Developmental strategy for effective sampling to detect possible nutrient fluxes in oligotrophic coastal reef waters in the Caribbean. *J. Oper. Oceanogr.* 2, 35–47. doi: 10.1080/1755876X.2009.11020107

Mishra, D. R., Kumar, A., Muduli, P. R., Equeenuddin, S. M., Rastogi, G., Acharyya, T., et al. (2020). Decline in phytoplankton biomass along indian coastal waters due to COVID-19 lockdown. *Remote Sens.* 12:2584. doi: 10.3390/rs12162584

Mishra, D. R., Narumalani, S., Rundquist, D., and Lawson, M. (2005a). Characterizing the vertical diffuse attenuation coefficient for downwelling irradiance in coastal waters: implications for water penetration by high resolution satellite data. *ISPRS J. Photogramm. Remote Sens.* 60, 48–64. doi: 10.1016/j.isprsjprs.2005.09.003

Mishra, D. R., Narumalani, S., Rundquist, D., and Lawson, M. (2005b). High-resolution ocean color remote sensing of benthic habitats: a case study at the Roatan Island, Honduras. *IEEE Trans. Geosci. Remote Sens.* 43, 1592–1603. doi: 10.1109/TGRS.2005.847790

Mishra, D. R., Narumalani, S., Rundquist, D., Lawson, M., and Perk, R. (2007). Enhancing the detection and classification of coral reef and associated benthic habitats: a hyperspectral remote sensing approach. *J. Geophys. Res.* 112:C08014. doi: 10.1029/2006JC003892

Mishra, R. K., Agarwal, A., and Shukla, A. (2021). Predicting ground level PM $_{2.5}$ concentration over Delhi using Landsat 8 satellite data. *Int. J. Remote Sens.* 42, 827–838. doi: 10.1080/2150704X.2020.1832279

Morales-Vela, B., Olivera-Gómez, D., Reynolds, J. E., and Rathbun, G. B. (2000). Distribution and habitat use by manatees (*Trichechus manatus manatus*) in Belize and Chetumal Bay. *Mexico. Biol. Conserv.* 95, 67–75. doi: 10.1016/S0006-3207(00)00009-4

Murray, R. (2020). A governance analysis of three MPAs in Belize: conservation objectives compromised by tourism development priorities? *Mar. Policy* 2020:104243. doi: 10.1016/j.marpol.2020.104243

Nanda, D., Mishra, D. R., and Swain, D. (2020). COVID-19 lockdowns induced land surface temperature variability in mega urban agglomerations in India. *Environ. Sci. Process. Impacts* 23, 144–159. doi: 10.1039/D0EM00358A

NASA Global Modeling and Assimilation Office (2020). *MERRA-2*. Available online at: https://gmao.gsfc.nasa.gov/reanalysis/MERRA-2/ (accessed December 30, 2020).

News Belize (2020). *Big Business At Big Creek Port*. Available online at: http://www.7newsbelize.com/sstory.php?nid=34664 (accessed December 18, 2020).

Niroumand-Jadidi, M., Bovolo, F., Bruzzone, L., and Gege, P. (2020). Physics-based bathymetry and water quality retrieval using planetscope imagery: impacts of 2020 COVID-19 lockdown and 2019 extreme flood in the Venice lagoon. *Remote Sens.* 12:2381. doi: 10.3390/RS12152381

Patel, P. P., Mondal, S., and Ghosh, K. G. (2020). Some respite for India's dirtiest river? Examining the Yamuna's water quality at Delhi during the COVID-19 lockdown period. *Sci. Total Environ.* 744:140851. doi: 10.1016/j.scitotenv.2020.140851

Port of Big Creek (2020). *Port of Big Creek*. Available online at: http://www.portofbigcreek.com/#smoothscroll-facts-module (accessed December 18, 2020).

R Core Team (2020). *R: A Language and Environment for Statistical Computing*. Vienna: R Core Team.

Renaud, L. (2020). Cruise tourism threatens to drive land speculation and displacement in Belize. *NACLA Rep. Am.* 52, 442–447. doi: 10.1080/10714839.2021.1840177

Reyes, T., Gilchrist, H., Lacasse, O., Peiffer, F., Duffy, H., and Druskat, A. (2019). *Five Years in Bacalar Chico Marine Reserve?: an Evaluation of Reef Health and Reserve Effectiveness Between*, Vol. 44. London: Blue Ventures, 105. Blue Ventures Conservation Report.

Rume, T., and Islam, S. M. D. U. (2020). Environmental effects of COVID-19 pandemic and potential strategies of sustainability. *Heliyon* 6:e04965. doi: 10.1016/j.heliyon.2020.e04965

Rutz, C., Loretto, M. C., Bates, A. E., Davidson, S. C., Duarte, C. M., Jetz, W., et al. (2020). COVID-19 lockdown allows researchers to quantify the effects of human activity on wildlife. *Nat. Ecol. Evol.* 4, 1156–1159. doi: 10.1038/s41559-020-1237-z

Shi, W., and Wang, M. (2010). Characterization of global ocean turbidity from moderate resolution imaging Spectroradiometer ocean color observations. *J. Geophys. Res.* 115:C11022. doi: 10.1029/2010JC006160

Soto, I., Andréfouët, S., Hu, C., Muller-Karger, F. E., Wall, C. C., Sheng, J., et al. (2009). Physical connectivity in the Mesoamerican barrier reef system inferred from 9 years of ocean color observations. *Coral Reefs* 28, 415–425. doi: 10.1007/s00338-009-0465-0

Sweetman, B. M., Foley, J. R., and Steinberg, M. K. (2019). A baseline analysis of coastal water quality of the port Honduras marine reserve, Belize: a critical habitat for sport fisheries. *Environ. Biol. Fish.* 102, 429–442. doi: 10.1007/s10641-018-0811-6

Tomlinson, M. C., Stumpf, R. P., and Vogel, R. L. (2019). Approximation of diffuse attenuation, K_d, for MODIS high-resolution bands. *Remote Sens. Lett.* 10, 178–185. doi: 10.1080/2150704X.2018.1536301

Torregroza-Espinosa, A. C., Restrepo, J. C., Escobar, J., Pierini, J., and Newton, A. (2021). Spatial and temporal variability of temperature, salinity and chlorophyll-a in the Magdalena River mouth, Caribbean Sea. *J. South Am. Earth Sci.* 105:102978. doi: 10.1016/j.jsames.2020.102978

UNESCO (1996). "World heritage committee," in *Proceedings of the 20th Convention concerning the Protection of the World Cultural and Natural Heritage*, Baku.

United Nations (2020a). *Coronavirus Disease - COVID 19 Situation Note No . 4. 1-6*. Available online at: https://reliefweb.int/sites/reliefweb.int/files/resources/COVID 19 Situation Report No 4 BELIZE Final.pdf (accessed December 9, 2020).

United Nations (2020b). *Goal 14 - Conserve and Sustainably Use the Oceans, Seas and Marine Resources for Sustainable Development*. Available online at: https://sdgs.un.org/goals/goal14 (accessed December 30, 2020).

Vega Sequeda, J. C., Zea, S., and Bernal, G. (2017). Efectos de eventos oceánicos extremos en formaciones coralinas de islas del rosario, Caribe Colombiano. *CICIMAR Oceán.* 32:25. doi: 10.37543/oceanides.v32i1.194

Verutes, G. M., Arkema, K. K., Clarke-Samuels, C., Wood, S. A., Rosenthal, A., Rosado, S., et al. (2017). Integrated planning that safeguards ecosystems and balances multiple objectives in coastal Belize. *Int. J. Biodivers. Sci. Ecosyst. Serv. Manag.* 13, 1–17. doi: 10.1080/21513732.2017.1345979

Wang, J., and Christopher, S. A. (2003). Intercomparison between satellite-derived aerosol optical thickness and PM2.5. *Res. Lett* 30:2095. doi: 10.1029/2003GL018174

Warne, A. G., Webb, R. M. T., and Larsen, M. C. (2005). *Water, Sediment, and Nutrient Discharge Characteristics of Rivers in Puerto Rico, and their Potential Influence on Coral Reefs*. Reston: U.S. Geological Survey, 58. U.S. Geological Survey Investigation Report 2005-5206.

Wells, C. E., Alex Webb, W., Prouty, C. M., Zarger, R. K., Trotz, M. A., Whiteford, L. M., et al. (2019). Wastewater technopolitics on the southern coast of Belize. *Econ. Anthropol.* 6, 277–290. doi: 10.1002/sea2.12145

Wells, E. C., Zarger, R. K., Whiteford, L. M., Mihelcic, J. R., Koenig, E. S., and Cairns, M. R. (2014). The impacts of tourism development on perceptions and practices of sustainable wastewater management on the Placencia Peninsula, Belize. *J. Clean. Prod.* 111, 430–441. doi: 10.1016/j.jclepro.2014.08.050

Werdell, P. J., and Bailey, S. W. (2005). An improved in-situ bio-optical data set for ocean color algorithm development and satellite data product validation. *Remote Sens. Environ.* 98, 122–140. doi: 10.1016/j.rse.2005.07.001

Young, C. A. (2008). Belize's Ecosystems: threats and challenges to conservation in Belize. *Trop. Conserv. Sci.* 1, 18–33. doi: 10.1177/194008290800100102

Yunus, A. P., Masago, Y., and Hijioka, Y. (2020). COVID-19 and surface water quality: improved lake water quality during the lockdown. *Sci. Total Environ.* 731:139012. doi: 10.1016/j.scitotenv.2020.139012

Zhang, C., Shi, Z., Zhao, J., Zhang, Y., Yu, Y., Mu, Y., et al. (2021). Impact of air emissions from shipping on marine phytoplankton growth. *Sci. Total Environ.* 769:145488. doi: 10.1016/j.scitotenv.2021.145488

Zheng, Z., Ren, J., Li, Y., Huang, C., Liu, G., Du, C., et al. (2016). Remote sensing of diffuse attenuation coefficient patterns from Landsat 8 OLI imagery of turbid inland waters: a case study of Dongting Lake. *Sci. Total Environ.* 573, 39–54. doi: 10.1016/j.scitotenv.2016.08.019

Conflict of Interest: The authors declare that the research was conducted in the absence of any commercial or financial relationships that could be construed as a potential conflict of interest.

frontiers in Marine Science

CORRECTION
published: 16 June 2021
doi: 10.3389/fmars.2021.711089

Corrigendum: Effect of COVID-19 Anthropause on Water Clarity in the Belize Coastal Lagoon

Ileana A. Callejas[1], Christine M. Lee[2], Deepak R. Mishra[3], Stacey L. Felgate[4,5], Claire Evans[4], Abel Carrias[6], Andria Rosado[7], Robert Griffin[8], Emil A. Cherrington[9], Mariam Ayad[10], Megha Rudresh[3], Benjamin P. Page[11] and Jennifer A. Jay[1]*

[1] Department of Civil and Environmental Engineering, University of California, Los Angeles, Los Angeles, CA, United States, [2] Jet Propulsion Laboratory, California Institute of Technology, Pasadena, CA, United States, [3] Department of Geography, University of Georgia, Athens, GA, United States, [4] Ocean Biogeosciences, National Oceanography Centre, Southampton, United Kingdom, [5] Ocean and Earth Sciences, University of Southampton, Southampton, United Kingdom, [6] Faculty of Science & Technology, University of Belize, Belmopan, Belize, [7] Coastal & Marine Data Centre, Coastal Zone Management Authority & Institute, Belize City, Belize, [8] Department of Atmospheric and Earth Science, University of Alabama in Huntsville, Huntsville, AL, United States, [9] Earth System Science Center, University of Alabama in Huntsville, Huntsville, AL, United States, [10] Department of Ocean Sciences, University of California, Santa Cruz, Santa Cruz, CA, United States, [11] Water Resources Center, University of Minnesota, St. Paul, MN, United States

Keywords: diffuse attenuation coefficient, moderate resolution imaging spectroradiometer, remote sensing, water quality, marine traffic, Belize barrier reef reserve system, water clarity

OPEN ACCESS

Approved by:
Frontiers Editorial Office, Frontiers Media SA, Switzerland

***Correspondence:**
Christine M. Lee
christine.m.lee@jpl.nasa.gov

Specialty section:
This article was submitted to Global Change and the Future Ocean, a section of the journal Frontiers in Marine Science

Received: *17 May 2021*
Accepted: *18 May 2021*
Published: *16 June 2021*

Citation:
Callejas IA, Lee CM, Mishra DR, Felgate SL, Evans C, Carrias A, Rosado A, Griffin R, Cherrington EA, Ayad M, Rudresh M, Page BP and Jay JA (2021) Corrigendum: Effect of COVID-19 Anthropause on Water Clarity in the Belize Coastal Lagoon. Front. Mar. Sci. 8:711089. doi: 10.3389/fmars.2021.711089

A Corrigendum on

Effect of COVID-19 Anthropause on Water Clarity in the Belize Coastal Lagoon
by Callejas, I. A., Lee, C. M., Mishra, D. R., Felgate, S. L., Evans, C., Carrias, A., et al. (2021). Front. Mar. Sci. 8:490. doi: 10.3389/fmars.2021.648522

In the original article, we did not include the full attribution for worked carried out by JPL co-authors. We would like to add that research by JPL co-authors was performed at the Jet Propulsion Laboratory, California Institute of Technology, under contract with the National Aeronautics and Space Administration.

The updated funding statement should read:

"This work was supported by the NASA RRNES (Grant #80NSSC20K1746) and NASA ROSES A.8 (cooperative agreement number #80NSSC19K0200), UCLA's Center for Diverse Leadership in Science, and the Joan Doren Family Foundation. This work was performed in part at the Jet Propulsion Laboratory, California Institute of Technology, under contract with the National Aeronautics and Space Administration."

The authors apologize for this error and state that this does not change the scientific conclusions of the article in any way. The original article has been updated.

frontiers in Marine Science

ORIGINAL RESEARCH
published: 13 May 2021
doi: 10.3389/fmars.2021.633493

Anomalous Reduction of the Total Suspended Matter During the COVID-19 Lockdown in the Hooghly Estuarine System

Chiranjivi Jayaram[1], Rajdeep Roy[2], Neethu Chacko[1], Debadatta Swain[3], Ramunaidu Punnana[4], S. Bandyopadhyay[1], S. B. Choudhury[2] and Dibyendu Dutta[1]*

[1] Regional Remote Sensing Center–East, National Remote Sensing Centre, Indian Space Research Organisation (NRSC/ISRO), Kolkata, India, [2] National Remote Sensing Center, Indian Space Research Organisation (ISRO), Hyderabad, India, [3] School of Earth, Ocean and Climate Sciences, Indian Institute of Technology Bhubaneswar, Bhubaneswar, India, [4] Centre for Studies on Bay of Bengal, Andhra University, Visakhapatnam, India

The impact of the coronavirus disease 2019 (COVID-19) lockdown in the Hooghly estuarine region, India is assessed using the total suspended matter (TSM) concentration. The estimation of TSM is performed using Landsat-8/operational land imager (OLI), and an intercomparison of TSM load during the pre-lockdown and lockdown periods is done. It is observed that during the lockdown period, TSM reduced by 30–50%. This is a significant observation considering the ecological balance of the region and the fact that it is home to the largest mangroves in the world. This change in suspended matter presumably reflects the influence of reduction in anthropogenic activities owing to the COVID-19 lockdowns, such as industries, closure of shipping activities (through less dredging), and brick kilns (through less sediment removal), which are generally the primary contributors in this region. Even though these observed changes are representative of the positive influence of the COVID-19 lockdown, its implications in estuarine biogeochemistry still remain poorly quantified. The decrease in TSM content may increase light penetration, thereby increasing the primary productivity. In addition, low sediment load reaching the Bay of Bengal could influence the carbon export due to reduction in ballasting effect as reported from this region. In summary, the influence of the COVID-19 lockdown on the biogeochemistry of the aquatic ecosystem appears rather complex than thought earlier and may vary regionally based on local hydrodynamics. The analysis elucidates the complex interplay of regional lockdown and its implication in modulation of local biogeochemistry. However, the relative importance of each process in the Hooghly estuary remains to be fully evaluated.

Keywords: COVID-19 lockdown, water quality, Hooghly estuary, total suspended matter concentration, remote sensing

OPEN ACCESS

Edited by:
Raghab Ray,
University of Tokyo, Japan

Reviewed by:
Frida Sidik,
Ministry for Marine Affairs and Fisheries of the Republic of Indonesia, Indonesia
Xiaoguang Ouyang,
The Chinese University of Hong Kong, China

****Correspondence:***
Chiranjivi Jayaram
chvchiranjivi@hotmail.com;
jayaram_cv@nrsc.gov.in

Specialty section:
This article was submitted to Global Change and the Future Ocean, a section of the journal Frontiers in Marine Science

Received: *25 November 2020*
Accepted: *06 April 2021*
Published: *13 May 2021*

Citation:
Jayaram C, Roy R, Chacko N, Swain D, Punnana R, Bandyopadhyay S, Choudhury SB and Dutta D (2021) Anomalous Reduction of the Total Suspended Matter During the COVID-19 Lockdown in the Hooghly Estuarine System. Front. Mar. Sci. 8:633493. doi: 10.3389/fmars.2021.633493

INTRODUCTION

The precise estimation of sediment concentration in the estuaries is imperative to deduce pollution levels, ecological impacts, and erosion in the region. Extensive *in situ* sampling of the region or satellite-based estimation of the sediments is generally used for this. Remote sensing of total suspended matter (TSM) has gained special importance in coastal water quality-related studies due

to the logistical constraints involved in regular *in situ* sampling of the sediments (Nechad et al., 2010). TSM estimation is carried out by using a variety of satellite sensors at different spatial and temporal resolutions (*viz*, SeaWiFS, MODIS, MERIS, and OCM) (McClain et al., 2004; Miller and McKee, 2004; Doerffer and Schiller, 2010; Shanthi et al., 2013). However, the data obtained from these sensors are relatively coarse (250 m^{-1} km) that hampers the estimation of TSM at finer spatial scale in the estuarine areas. Availability of sensors, such as the operational land imager (OLI) onboard Landsat-8, with higher signal to noise ratio, higher radiometric resolution (12-bit), and a spatial resolution of 30 m have provided suitable opportunities for resolving the nearshore sediment and chlorophyll concentration in the recent years (Vanhellemont and Ruddick, 2014; Trinh et al., 2017). These characteristics of Landsat-8 sensor also facilitate the elimination of aerosol contribution and atmospheric correction approach applicable to the global ocean color missions (Franz et al., 2015).

The recent outbreak of the coronavirus disease 2019 (COVID-19) pandemic enforced most countries to adopt lockdown measures to arrest the spread of the outbreak imposing severe restrictions on people's movement, as well as industrial and other anthropogenic activities. The Government of India too implemented stringent lockdowns starting March 24, 2020 and then relaxing it in different phases from June 1, 2020. Most of the earliest impacts of the lockdowns were seen as positive effects on the environment in terms of significant improvement in air and water qualities in many major cities across the world (Dantas et al., 2020; Lian et al., 2020; Mahato et al., 2020; Selvam et al., 2020; Zambrano-Monserrate et al., 2020; Zangari et al., 2020). However, studies reporting the lockdown impact on the coastal water quality were rather limited (Depellegrin et al., 2020; Mishra et al., 2020; Yunus et al., 2020), even though the sudden nationwide lockdowns provided a unique opportunity to look at the sediment load and understand its implication on the biogeochemical dynamics of estuarine systems.

Anthropogenic activities have profound impact on the coastal waters due to increasing population and their needs, widespread industries, shipping, domestic sewage, and agricultural activities. The COVID-19 lockdown has provided an opportunity to assess the anthropogenic activities on the coastal water quality of the region. In the Indian subcontinent, studies by Garg et al. (2020) and Patel et al. (2020) analyzed the water quality of the Ganga and Yamuna rivers, respectively, during the COVID-19-related lockdown period using remote sensing and *in situ* observations. These regions are upstream of the Ganges catchment. They reported the suspended particulate matter and turbidity to have reduced considerably during the lockdown period. The present study aims at analyzing sediment concentration toward the downstream of the Ganges through the Hooghly River estuary during the lockdown period. In this regard, it is hypothesized that the COVID-19-induced lockdown will improve the water quality of the Hooghly estuary. Since it was not possible to carry out field data collection in the Hooghly estuary during the lockdown period, satellite-derived TSM from Landsat-8/OLI was utilized as proxy for water quality to understand the effect of the COVID-19 lockdown on the Hooghly estuarine system and discuss sediment load, its spatial distribution, and the possible implication on regional biogeochemistry as compared with the pre-lockdown conditions. As TSM is widely considered an important water quality parameter, the reduction in TSM in the study area could be inferred as the improvement in the water quality, which also quantifies the anthropogenic impact on the coastal water quality.

The Study Region section presents an overview of the study area. The "Data and Methods" section details the *in situ* data collected during earlier field campaigns and estimation of TSM using Landsat-8/OLI data for the study period. The results of intercomparison between *in situ* and satellite-derived TSM for winter monsoon of 2019 and TSM distribution during the pre-monsoon season (April) for 2016–2020 are presented in the "Results and Discussion" section. The significance of the anomalous reduction of TSM during April 2020 (lockdown) and its implications on the regional biogeochemistry were also discussed. The important conclusions and future scope are elucidated in the "Conclusion" section.

STUDY REGION

Hooghly River estuary in the Indian subcontinent is the western boundary of the largest delta in the world that is formed by the distributaries of the Ganges and the Brahmaputra rivers (**Figure 1**). The lower section of the estuary stretches through the rich mangrove forests known as the Sundarbans and provides the primary shipping channel to the major port (Kolkata port trust) through Kolkata and Haldia docks in the upper and lower sections, respectively. This estuary is shallow, funnel shaped and is considered as a positive estuary that traces its path through the southern region of the state of West Bengal in India (Rakshit et al., 2014). The climate of the region could be categorized into pre-monsoon (March–May), monsoon (June–September), and post-monsoon (October–January). The pre-monsoon period is considered as the dry period with scanty or no rainfall, whereas the monsoon season accounts for the maximum rainfall, and lower precipitation is prevalent during the post-monsoon season (Khan, 1995; Rakshit et al., 2014). The highest river discharge (3,000 $\pm$ 1,000 m^3 s^{-1}) in the Hooghly estuary is observed during the monsoon season that reduces to the minimum (1,000 $\pm$ 80 m^3 s^{-1}) during the pre-monsoon season (Mukhopadhyay et al., 2006; Ray et al., 2015).

Annual sediment load discharged by the Ganges into the Bengal fan is $\sim 324 \times 10^6$ tons that is approximately one-third of the total sediment load discharged by the Ganges–Brahmaputra River system (Ray et al., 2015; Khan et al., 2018). From the studies of Mouyen et al. (2018) on the annual sediment load of major rivers across the world, it was observed that the Ganges–Brahmaputra River system had the highest sediment load with 1,081 Mt $year^{-1}$, followed by the Amazon (778 Mt $year^{-1}$), the Changjiang (477 Mt $year^{-1}$), and the Irrawaddy (333 Mt $year^{-1}$). These values signify the sediment dynamics of the Hooghly estuarine system in the

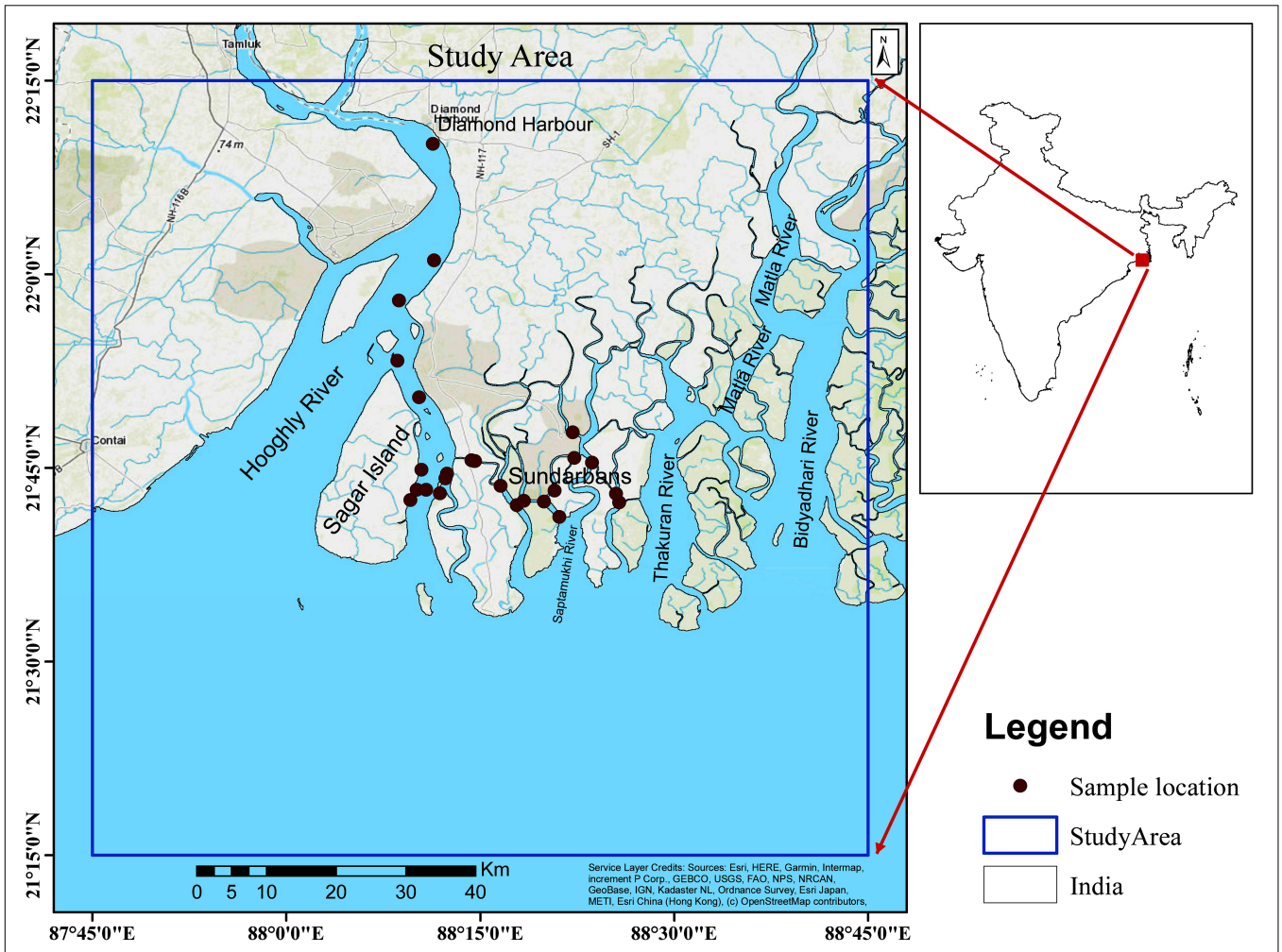

FIGURE 1 | Map showing the location of the study region (inset) in the northern Bay of Bengal. Red dots indicate the locations of the *in situ* total suspended matter (TSM) observations during December 9–11, 2019.

northern Bay of Bengal. Apart from the sediment discharge brought by the river runoff, anthropogenic activities, such as the operational maintenance dredging of the Kolkata port trust, contribute immensely to the sediment concentration apart from the numerous brick kilns and industries dotting on either side of the Hooghly River.

Chacko and Jayaram (2017) have reported the TSM concentrations variations to be highly dynamic, spatial, and temporal in the northern coastal Bay of Bengal comprising the Hooghly estuarine region. They observed the maximum TSM concentration in the summer monsoon season (June–September) and the minimum in the spring season (March–May). These were attributed to the monsoonal discharge through the Ganges–Hooghly River systems. Tremendous amounts of sediments get transported through river discharge and are deposited in the channel with the rest flushed into the Bay of Bengal. Anthropogenic activities, such as dredging the channel, greatly dominate the TSM concentration variability in the estuary. The complex shape of the estuary with activities, such as deepening and lengthening of the channel, resulting in bank erosion was observed to amplify the suspended sediment concentration further. In addition, tides are known to influence the total suspended load in the estuary region. The Hooghly estuary is a macrotidal estuary with tidal amplitudes approximating 6 m. The tides in the region are predominantly semidiurnal in nature with the neap tides during spring ranging from 1.8 to 5.2 m height and a velocity as high as 6 knots (Sadhuram et al., 2005). During peak tidal flows, sand is transported downstream by the tide on the seaward face and is returned to the estuary during ebb flow.

Furthermore, the Hooghly estuary receives approximately 13 m^3/s of industrial effluent and urban wastewater (Sadhuram et al., 2005, and references therein) from densely populated and industrial cities, such as Kolkata and Haldia. All these make the Hooghly estuarine system highly vulnerable to anthropogenic perturbation and, hence, imperative to monitor its water quality regularly. Given the importance of the Hooghly estuary in terms of ecology and economy of the region, it is also an

ideal estuarine system to study the impact of the COVID-19-induced lockdowns that resulted in the suspension of several anthropogenic activities for months.

DATA AND METHODS

Hydrographic Sampling

An observational campaign was carried out in the Hooghly estuary and the adjoining western part of the Sundarbans region from December 9–11, 2019 during which water sampling was carried out at 29 stations (**Figure 1**) representing the pre-COVID-19 phase. As part of the campaign, a factory calibrated SeaBird Electronics (SBE) 9/11+ conductivity–temperature–depth profiler (CTD), optode oxygen electrode, and fluorescence sensors were used at all locations to record the physical and chlorophyll profiles from the surface to fairly close to the bottom depth. From the CTD profiles (**Figure 2**), it was observed that the water temperature at the upper end of the estuary was relatively cooler (by 0.8°C) than that at the lower region. The corresponding salinity values at the upper estuary ranged between 13 and 14 psu gradually increasing to 21 psu at the lower end, thereby suggesting intrusion of the Bay of Bengal coastal waters at these stations. The variability in the stations belonging to the Sundarbans region is not as dynamic as the Hooghly River estuary as the region is more tide dominant and less terrestrial runoff than the Hooghly River.

Several water samples were also simultaneously collected from 1 m below the surface with a Niskin sampler attached to a nylon rope on board fishing trawlers. Samples for dissolved inorganic carbon (DIC) were collected first, followed by pH, nutrients, and TSM. DIC and nutrient samples were poisoned with saturated mercury chloride ($HgCl_2$) as per the standard oceanographic protocol (US JGOFS) (see Knap et al., 1996). The samples were then analyzed at the biological oceanography laboratory at the National Remote Sensing Centre (NRSC), without any pre-filtration and analyzed using a coulometer (model no. CM5015). DIC measurements were accurate to <2 μmol kg^{-1} with precision within 0.1% as relative standard deviation (RSD) based on replicate measurements of certified reference material (CRM) batch number 170 obtained from Dickenson Laboratory, Scripps Institute of Oceanography, San Diego, CA, United States. Furthermore, inorganic nutrients (nitrate and phosphate) were determined by standard spectrophotometric methods (Grasshoff et al., 1999) using the Skalar Autoanalyzer (San++) from Skalar Analytical B.V., Netherlands. The uncertainties determined from multiple measurements of replicate samples for nutrients were $<\pm 0.1$ μmol L^{-1} based on the CRM 170. pH was measured using a Metrohm pH meter at an accuracy of ±0.002 units. Samples for TSM analyses were obtained by filtering <0.3 L of water through pre-combusted pre-weighed Whatman GF/F filters and were kept frozen at −4°C. To quantify TSM, the frozen filters were thawed and dried at 60°C for 72 h in a drying oven and weighed after recovering to room temperature in a desiccator. TSM concentration was determined by subtracting the weight of the filter before filtration from its dry weight after filtration of a known volume of water.

Satellite Data and Processing

Level-1C, Landsat-8/OLI data obtained from the US Geological Survey (USGS[1]) for the study period were used to derive the suspended sediment concentration in the Hooghly estuary. Landsat-8 has 11 bands at different spatial resolutions (8 multi-spectral bands at 30 m, 1 panchromatic band at 15 m, and two thermal bands at 100 m resolution) with a repeat period of 16 days. ACOLITE (Ver. 20190326.0), an image-based package specifically developed for marine, coastal, and inland waters by the Royal Belgian Institute of Natural Sciences (RBINS), was used to process the individual OLI scenes (Vanhellemont, 2019). Dark spectrum fitting (DSF) algorithm, which does not require any prior selection of the "BLACK" band but just an optimal band selection during the processing, was used for the atmospheric correction of the Landsat images (Vanhellemont and Ruddick, 2018; Vanhellemont, 2019). Furthermore, the aerosol model in this approach was selected based on the root mean square difference (RMSD) between the representative dark spectrum (ρ_{dark}) and the estimated path reflectance (ρ_{path}). The RMSD was computed for each spectral band, and the combination with the lowest RMSD was selected for the final atmospheric correction of the corresponding scene/sub-scene (Vanhellemont, 2019). In the present study, the Maritime model (Model2) of the ACOLITE package was utilized as it resulted in the RMSD in the estimation of the "ρ_{path}." This method employs a robust automated band selection process, and aerosol correction accounts for the spatial variability of aerosols (both type and concentration) without affecting the noise level in the output product (Vanhellemont and Ruddick, 2018; Caballero et al., 2020). The glint correction performed for the imagery consists of the bands and pixels with the least estimate of aerosol optical thickness. This method allows the path reflectance that is insensitive to the sun glint (Vanhellemont, 2019).

Total suspended matter was then derived from the processed images by using the algorithm developed by Nechad et al. (2010) from the water leaving reflectance of red band (λ = 655 nm) following the expression:

$$\mathrm{TSW} = \frac{A\rho_w}{1 - \frac{\rho_w}{C}}$$

Where ρ_w is the water leaving reflectance (655 nm), and A = 289.29 and C = 0.1686 are the empirical coefficients. The Nechad et al. (2010) algorithm has been applied successfully across various regions as it is tuned and developed based on the selection of two independent yet homogeneous datasets for calibration and validation (Dogliotti et al., 2015; Ciancia et al., 2020). The model configuration allows for the adjustment to different satellite sensors/bands (Odermatt et al., 2012). The TSM concentrations derived using the satellite observations were compared with *in situ* TSM observations carried out during December 9–11, 2019. The nearest possible OLI image for the study region was available for December 16, 2019, which was then used to derive TSM at the locations where *in situ*

[1]https://earthexplorer.usgs.gov

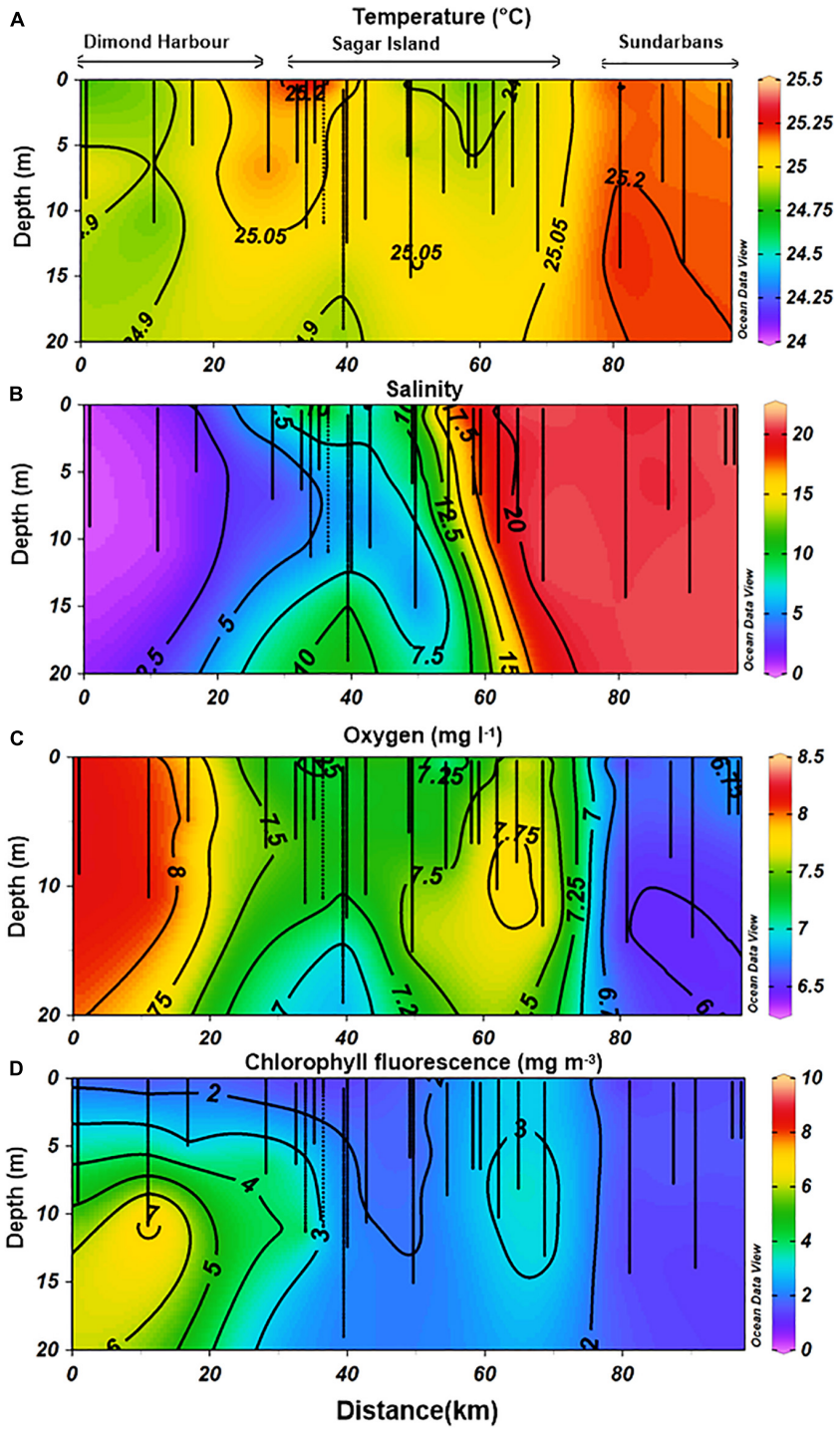

FIGURE 2 | Vertical distribution of **(A)** temperature (°C), **(B)** salinity (psu), **(C)** oxygen (mg L^{-1}), and **(D)** chlorophyll fluorescence (mg m^{-3}) in the upper 20 m as observed at 29 stations of the Hooghly estuary (as shown in **Figure 1**). Depths of the conductivity–temperature–depth (CTD) lowered are indicated by the gray lines within the figures.

observations were carried out. The average of 3 × 3 pixels with *in situ* location as the center was considered as the spatial colocation criteria for intercomparison between *in situ* and satellite-derived TSM.

The 5-years mean (2016–2020) of TSM for the month of April (pre-monsoon) was computed with all the available cloud-free TSM imageries. The details of the Landsat-8/OLI data are provided in **Table 1**. In order to deduce the deviation from the

mean during April of every year, the 5-years mean TSM for April is subtracted from the data for the corresponding year to arrive at TSM anomaly for that year.

RESULTS AND DISCUSSION

In Situ TSM Load and Regional Hydrography Along the Hooghly Estuary

The hydrographic campaign conducted during December 2019 was used to characterize the pre-lockdown conditions of the Hooghly estuary and the western part of the Sundarbans region in terms of biogeochemical parameters. The physical characteristics of the surface waters sampled along with the other biogeochemical parameters are illustrated in **Figure 2** and **Table 2**. *In situ* TSM load showed strong spatial variation from the upper end of the estuary (Diamond Harbor) to the lower end (Sagar Island and the adjoining Sundarbans region) along with a steep salinity gradient. The TSM load was greater than 100 g m^{-3} during December 2019 within the inner estuary. It decreased by ∼10 g m^{-3} within the middle of the estuary, but reaching a load of 60–80 g m^{-3} within the Sundarbans delta. During December 2019, the average value of TSM was 94 g m^{-3} within the Hooghly estuary with the lowest and the highest values ranging between 58 and 127 g m^{-3}, respectively. The high TSM load within the upper estuary also coincides with low pH values (<7.900).

Furthermore, chlorophyll concentration in the middle of the estuary was higher by 1 mg m^{-3} than that in the upper and the lower estuary regions coinciding with increase in dissolved oxygen and decrease in surface turbidity. In general, the oxygen concentrations in the lower estuary decreased by 1 mg L^{-1} compared with the upper estuary. We believe that this decrease in oxygen is presumably due to large organic matter degradation at the lower end of the estuary associated with very shallow depths. Here, the depth ranged between 6 and 10 m, and the water column remained well mixed (**Figure 2**). Among the nutrients, nitrate showed a strong trend opposite to salinity gradient. The highest concentration of nitrate was associated with the upper estuary and decreased gradually toward the lower end (Sundarbans region). Nitrate ranged between <1 and 62 μmol kg^{-1}, whereas phosphate varied between <1 and 1.78 μmol kg^{-1} during winter monsoon in the study domain. Phosphate concentrations in the upper estuary were higher than those in the middle estuary and showed an increasing trend within the Sundarbans region (lower estuary). Occasionally, lower concentrations of phosphate (<1 μmol kg^{-1}) were also observed around the lower estuary. The lowest pH values (∼7.572) and DIC of 2,705 μmol kg^{-1} were observed in the surface waters at the Diamond Harbor. These values decreased further below 1,700 μmol kg^{-1} in the middle of the estuary, but again rising to ∼2,240 μmol kg^{-1} toward the Sundarbans region. The average value of DIC was found to be 2,248 μmol kg^{-1} and had a range between 1,652 and 3,196 μmol kg^{-1}.

TABLE 1 | Details of the Landsat-8 data used in the study.

Sl. no.	Year	Date	Landsat-8/OLI tile
1	2016	Apr-11-2016	LC08_L1TP_138045_20160411_20170326_01_T1
2	2017	Apr-14-2017	LC08_L1TP_138045_20170414_20170501_01_T1
3	2017	Apr-30-2017	LC08_L1TP_138045_20170430_20170515_01_T1
4	2018	Apr-17-2018	LC08_L1TP_138045_20180417_20180501_01_T1
5	2019	Apr-04-2019	LC08_L1TP_138045_20190404_20190421_01_T1
6	2019	Apr-20-2019	LC08_L1TP_138045_20190420_20190507_01_T1
7	2020	Apr-06-2020	LC08_L1TP_138045_20200406_20200410_01_T1
8	2020	Apr-22-2020	LC08_L1TP_138045_20200422_20200508_01_T1

Comparison Between *In Situ* and Satellite-Derived TSM During December 2019

To assess the accuracy of the TSM derived from Landsat-8 observations using the generic single band algorithm proposed by Nechad et al. (2010), *in situ* TSM observations were compared with the satellite-derived TSM for December 2019. The root mean square error (RMSE) between the two datasets (no. of points = 27) is 10.89 g m^{-3}, mean absolute error (MAE) is 30.21 g m^{-3}, and correlation (R) is 0.3. The RMSE value of 10.89 g m^{-3} approximately matches the accuracy limits (±10 g m^{-3}) specified by Nechad et al. (2010), thereby concurring with the *in situ* observations for further analysis. Relatively poor correlation could also result due to the temporal difference between the satellite and *in situ* observations used for intercomparison, but it is an acceptable limitation.

The spatial distribution of TSM in the study region before lockdown corresponding to December 2019 is shown in **Figure 3**. The TSM concentration is high in the Hooghly River and relatively less in the adjoining Indian portion of the Sundarbans Islands (**Figure 3**). This could be attributed to the runoff contributed by the catchment of the Hooghly River, whereas it is absent in the case of the inter-tidal riverine network prevalent in the Sundarbans region. This is evident from the salinity profile (**Figure 2**) where the salinity increased (>20 psu) toward Sagar Island and in the Sundarbans region. The satellite-derived TSM within the lower estuary ranged between 100 and 150 g m^{-3}, almost equivalent to the concentrations of *in situ* TSM in the region.

Total Suspended Matter Distribution for the Month of April (2016–2020)

The mean TSM concentration in the Hooghly estuary for the 5-years period 2016–2020 derived from the Landsat-8/OLI is shown in **Figure 4**. From the figure, the concentration of the mean TSM during April is observed to be relatively very less than that during the post-monsoon season (December 2019, **Figure 3**). The reduction in TSM concentration during April (pre-monsoon period) is attributed to the decrease in the river

TABLE 2 | Biogeochemical properties of surface waters along the salinity gradient of the estuary during December 2019 (north–east monsoon).

	Stn. no.	Date/time	Latitude (°N)	Longitude (°E)	TSM (g m^{-3})	DIC (μmol kg^{-1})	pH	NO_3 (μmol kg^{-1})	PO_4 (μmol kg^{-1})
Diamond harbor	1	09-12-201913.41	22°10.323′	88°11.761′	112	2,705	7.572	61.9	1.78
	2	09-12-2019 14.27	22°00.797′	88°12.557′	89	2,705	7.921	59.6	1.72
	3	09-12-201914.54	21°57.915′	88°09.012′	90	3,196	7.858	59.3	1.77
	4	09-12-201915.41	21°52.850′	88°08.431′	121	2,473	7.807	56.8	1.66
	5	09-12-201916.24	21°50.771′	88°10.978′	114	2,388	7.977	55.0	1.77
	6	09-12-201920.08	21°45.539′	88°14.555′	58	2,902	7.900	49.8	1.44
Sagar island	7	10-12-201906.12	21°45.545′	88°14.548′	79	2,560	7.697	22.9	0.98
	8	10-12-201907.10	21°45.330′	88°14.330′	72	1,793	7.811	16.40	1.06
	9	10-12-201908.40	21°45.711′	88°12.939′	58	2,340	7.811	18.7	1.06
	10	10-12-201909.37	21°44.571′	88°12.427′	87	2,196	7.897	16.9	1.11
	11	10-12-201910.10	21°43.030′	88°11.950′	127	1,852	7.391	21.6	1.28
	12	10-12-201911.00	21°42.596′	88°09.609′	103	2,383	7.888	11.5	1.04
	13	10-12-201911.30	21°43.343′	88°10.101′	134	2,172	7.878	22.8	1.05
	14	10-12-201912.10	21°44.871′	88°10.458′	103	2,172	7.923	23.0	0.87
	15	10-12-201914.00	21°43.336′	88°10.797′	170	2,172	7.923	23.0	0.87
	16	10-12-201915.13	21°43.336′	88°10.797′	112	1,850	7.758	25.5	0.81
	17	10-12-201916.17	21°44.247′	88°12.310′	86	2,738	7.924	32.4	0.89
Sundarbans region	18	11-12-201906.30	21°45.551′	88°14.558′	99	1,803	7.781	23.1	0.83
	19	11-12-201908.32	21°43.627′	88°16.597′	136	1,865	7.885	12.0	1.40
	20	11-12-201909.37	21°42.140′	88°17.802′	77	2,086	7.773	5.4	1.35
	21	11-12-201910.15	21°42.495′	88°18.330′	101	2,514	7.620	0.8	1.33
	22	11-12-201912.09	21°42.477′	88°19.955′	67	1,725	7.639	2.9	1.50
	23	11-12-201912.36	21°41.232′	88°21.136′	94	1,652	7.897	13.3	1.11
	24	11-12-201913.20	21°43.274′	88°20.772′	92	2,144	7.867	10.8	1.46
	25	11-12-201914.22	21°45.807′	88°22.272′	17	2,051	7.905	11.1	1.55
	26	11-12-201915.22	21°42.337′	88°25.754′	95	2,433	7.690	8.5	1.51
	27	11-12-201915.40	21°43.021′	88°25.498′	83	1,731	7.865	9.9	1.80
	28	11-12-201916.44	21°45.421′	88°23.667′	73	2,369	7.863	11.9	1.66
	29	11-12-201918.12	21°47.786′	88°21.953′	92	2,240	7.865	11.6	1.39

runoff and precipitation as expounded by Rudra (2014) and Chacko and Jayaram (2017). Furthermore, the annual cycle of TSM in the Hooghly estuary and the adjoining Sundarbans region showed the least concentration during the March–May period as observed from the studies of Jayaram et al. (2021). The

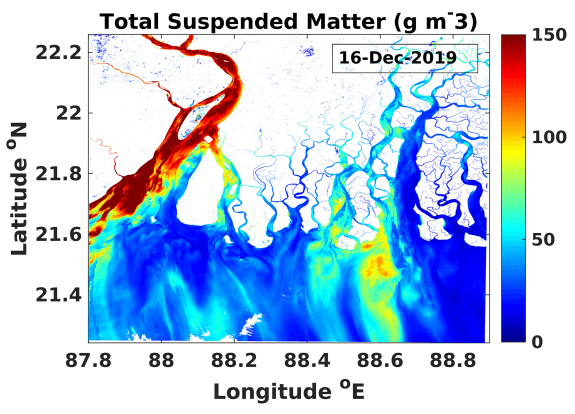

FIGURE 3 | The TSM concentration derived from Landsat-8 data pertaining to December 16, 2019.

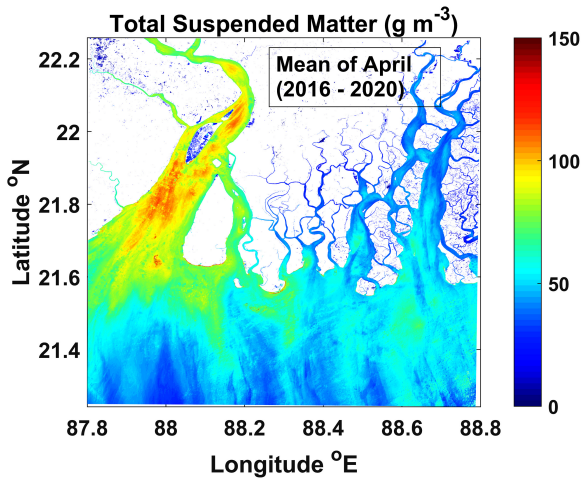

FIGURE 4 | Mean TSM concentration during April for the period 2016–2020 derived from Landsat-8/OLI.

variability of TSM anomaly for the month of April during 2016–2019 is shown in **Figure 5**. The spatial distribution pattern of the TSM anomaly shows that considerable year to year variability

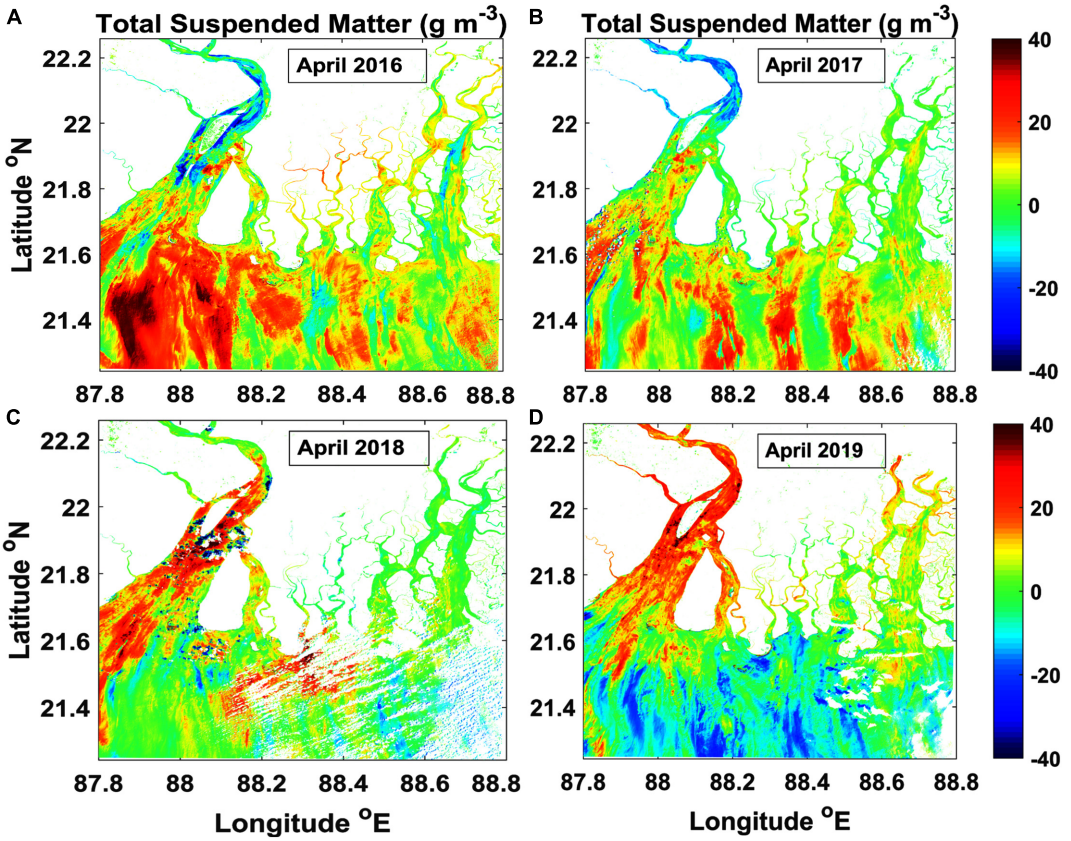

FIGURE 5 | Anomaly of TSM concentration during April **(A)** 2016, **(B)** 2017, **(C)** 2018 and **(D)** 2019.

exists in these 4 years. The highest concentration of TSM occurred during April 2019, and the lowest TSM concentration occurred during April 2016. The TSM concentrations depicted a varied spatial distribution between the lower and upper regions in the Hooghly estuary. The anomaly maps demonstrate that while the major reduction in the TSM levels occurs in the upper estuary, the TSM concentration remained elevated throughout the years in the lower estuary. In the regions offshore, however, reduction in TSM concentration was observed in April 2019.

Total Suspended Matter Distribution During the COVID-19 Lockdown Period (April 2020) and Its Possible Biogeochemical Implications

Total suspended matter anomaly for April 2020 is computed by subtracting the 5-years mean TSM from the April 2020 data as shown in **Figure 6A**. From the figure, large negative anomaly (up to -40 g m^{-3}) values were observed during April 2020 compared with the previous years (2016–2019) (**Figure 5**). The negative anomalies have progressively increased from the upper estuary (Diamond Harbor) (-10 g m^{-3}) toward the lower estuary (Sagar Island) (−40 g m^{-3}) and spread throughout the Sundarbans region. **Figure 6** depicts the consistent increase in the percentage of TSM reduction from the upper to the lower estuary. It is evident that the upper estuary is punctuated by dense human settlements, which may contribute to the relatively lesser TSM reduction than the lower estuary. Since the study period reports TSM variability during the month of April, the impact of river discharge is considered to be negligible on the TSM distribution. This substantial reduction in TSM concentration during April 2020 coincided with the COVID-19 lockdown period. The reduction could be attributed to the suspension of several major anthropogenic activities during the lockdown period, such as closure of numerous brick kilns on either bank of the Hooghly River and closure of all the industrial units all along the river. Only very limited activities pertaining to ship traffic for emergency services, limited commercial fishing, and curtailed dredging activities were in progress during the lockdown period. The contrasts in the TSM values prevalent during the lockdown period as against the normal years could then be attributed to the contribution of sewage drained from the major metropolis of Kolkata and suburban regions, tides, and minimal river discharge.

To further quantify the reduction in TSM concentration during the lockdown period, the percentage reduction of TSM during April 2020 with respect to the 5-years mean TSM for the months of April was computed (**Figure 6B**). The reduction up to 30–50% of TSM compared with the 5-years mean

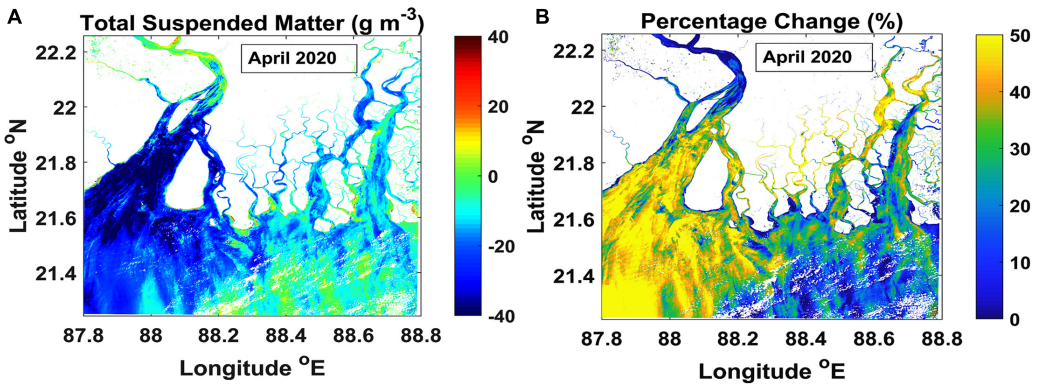

FIGURE 6 | (A) Total suspended matter anomaly during April 2020. **(B)** Percentage decrease of TSM with respect to the 5-years mean.

presumably reflects the approximate contribution of industrial effluent discharge, shipping, and dredging activities on the water quality of the Hooghly estuary. The region is home to the largest mangrove forests and other flora and fauna that are dependent on the estuarine waters. Nutrient dynamics and DIC data highlight the modest reduction between Sagar Island and Sundarbans region during post-monsoon that presumably reflects some recycling within the upper estuary (Diamond Harbor region). Mukhopadhyay et al. (2006) estimated ∼7% loss in DIC and nutrients during estuarine transport to coastal ocean in this study region based on a model. High DIC values observed at the upper estuary near Diamond Harbor are consistent with the earlier reports (Mukhopadhyay et al., 2006; Samanta et al., 2015). Nearly 40–50% of the DIC is generated within the estuary, and annual DIC flux from the Hooghly estuary accounts for ∼1% of the global river DIC flux to the oceans (Samanta et al., 2015). Due to the stringent lockdown measures enforced during the COVID-19 pandemic, a reduction in the anthropogenic activities and sediment load in the estuarine region was imperative as observed in the study region in April 2020. This could lead to lesser DIC concentration during the lockdown period due to less organic load (for example, closing of tannery industries along the Ganges). Furthermore, lithogenic matter and high detritus inputs from the Gangetic Bay of Bengal were found to cause more ballast effect along with a higher share of the organic matter export from the euphotic zone to the deep sea in this region (Ittekot and Laane, 1991; Rao et al., 1994; Meybeck and Ragu, 1997; Gauns et al., 2005; Rixen et al., 2019). The presence of clay minerals/sediments in the Hooghly–Sundarbans region has been known to adsorb the nutrient particles, thus regulating their concentrations in the shallow waters (Lal, 1978; Vaithiyanathan et al., 1993). Although probable decrease in TSM content may increase the light penetration within the estuary, thereby increasing the primary production. However, low suspended sediments may also reduce the ballast effect offshore, thereby reducing the carbon export as reported earlier (Ittekot and Laane, 1991). A reduction in ∼50% load in TSM as observed from satellite data may presumably reduce the partial pressure of carbon dioxide in water (pCO2w) due to reduced turbidity and increase primary production within the surface waters. Furthermore, less sediment load may influence the heterotrophic activity due to availability of less organic matter. All these highlight the complex biogeochemical interaction between the river-derived inputs and carbon cycling as a result of the lockdown in the Hooghly estuarine region. However, to understand the wider implications on the estuarine ecology, further investigation with larger datasets is necessary.

CONCLUSION

Satellite-derived TSM data were analyzed for the Hooghly estuarine system during the COVID-19-induced lockdown period (April 2020) and compared with the previous years (2016–2019). The 5-years average of TSM during April (2016–2020) has shown that the TSM concentration is high in the upstream of the estuary with gradual reduction toward the mouth of the estuary and the adjoining Sundarbans region. The anomaly of TSM computed from the long-term mean for the month of April has shown that the TSM concentration is less by ∼30–40 g m^{-3}, which approximates to 30–50%. This reduction in suspended matter presumably reflects the decrease in industrial contribution on the water quality of this estuary. Furthermore, closure of shipping activities in the shallow channel (through less dredging) and brick kilns (through less sediment removal) may have played a pivotal role. Although the observed changes represent the positive influence of the COVID-19 lockdown, its influence on biogeochemistry appears rather complex than said. We hypothesize that the decrease in TSM content in the estuarine regions may increase the light penetration, thereby increasing the primary productivity and carbon dioxide sequestration. However, less sediment load reaching the Bay of Bengal may have influenced the carbon export due to reduction in ballasting effect, thereby modulating the carbon cycle offshore. The above observations highlight the fact that the influence of the COVID-19 lockdown on the biogeochemistry of the aquatic ecosystem is complicated to delineate and may vary regionally based on local hydrodynamics and circulation pattern. This is significant

in terms of the ecological balance of the study region that is home to the largest mangrove forests and other flora and fauna with a strong dependence on these estuarine waters. The present study emphasizes the role of anthropogenic impact on the fragile coastal ecosystems and advocates for the sustainable management of the coastal water quality for ecology and economy of the region.

DATA AVAILABILITY STATEMENT

The original contributions presented in the study are included in the article/supplementary material, further inquiries can be directed to the corresponding author.

AUTHOR CONTRIBUTIONS

CJ, RR, NC, and DS conceptualization. CJ, RR, RP, and NC data curation. CJ and RR formal analysis. SB, SC, and DD project administration. CJ, RR, and NC roles/writing and prepared the initial draft of the manuscript. All authors have participated in the review of the manuscript and writing – review and editing.

FUNDING

The field data were collected under the project "Ecological studies of Hooghly estuary and its environment using remote sensing, modeling, and *in situ* measurements" (LIC: 606901IW701), funded by the National Remote Sensing Center, Indian Space Research Organization.

ACKNOWLEDGMENTS

The authors thank USGS for making available the Landsat-8/OLI data. We place on record our gratitude to the crew and boat captain of M/s. Sundarban Safari for their support during the field campaign in the Hooghly estuary. The authors are also thankful to the Chief General Manager, RCs, Deputy Director, Earth and Climate Science Area, the Director, NRSC for their keen interest in our work and encouragement provided during our seasonal *in situ* data collection campaigns. The authorities at IIT Bhubaneswar are also acknowledged for facilitating the collaborative participation in the campaign with instrument support. The reviewers and the journal editorial board are acknowledged for their valuable comments and suggestions in improving the manuscript.

REFERENCES

Caballero, I., Fernández, R., Escalante, O. M., Mamán, L., and Navarro, G. (2020). New capabilities of Sentinel – 2A/B satellites combined with *in situ* data for monitoring small harmful algal blooms in complex coastal waters. *Sci. Rep.* 10:8743. doi: 10.1038/s41598-020-65600-1

Chacko, N., and Jayaram, C. (2017). Variability of total suspended matter in the northern coastal Bay of Bengal as observed from satellite data. *J. Indian Soc. Remote Sens.* 45, 1077–1083. doi: 10.1007/s12524-016-0650-x

Ciancia, E., Campanelli, A., Lacava, T., Palombo, A., Pascucci, S., Pergola, N., et al. (2020). Modeling and multi-temporal characterization of total suspended matter by the combined use of Sentinel–2 MSI and Landsat 8–OLI data: the Pertusillo Lake case study (Italy). *Remote Sens.* 12:2147. doi: 10.3390/rs12132147

Dantas, G., Siciliano, B., França, B. B., da Silva, C. M., and Arbilla, G. (2020). The impact of COVID-19 partial lockdown on the air quality of the city of Rio de Janerio, Brazil. *Sci. Total Environ.* 729:139085. doi: 10.1016/j.scitotenv.2020.139085

Depellegrin, D., Bastianini, M., Fadini, A., and Menegon, S. (2020). The effects of COVID-19 induced lockdown measures on maritime settings of a coastal region. *Sci. Total Environ.* 740:140123. doi: 10.1016/j.scitotenv.2020.140123

Doerffer, R., and Schiller, H. (2010). The MERIS case 2 water algorithm. *Int. J. Remote Sens.* 28, 517–535. doi: 10.1080/01431160600821127

Dogliotti, A. I., Ruddick, K., Nechad, B., Doxaran, D., and Knaeps, E. (2015). A single algorithm to retrieve turbidity from remotely-sensed data in all coastal and estuarine waters. *Remote Sens. Environ.* 156, 157–168. doi: 10.1016/j.rse.2014.09.020

Franz, B. A., Bailey, S. W., Kuring, N., and Werdell, J. P. (2015). Ocean color measurements with the operational land imager on landsat-8: implementation and evaluation in SeaDAS. *J. Appl. Remote Sens.* 9:096070. doi: 10.1117/1.JRS.9.096070

Garg, V., Aggarwal, S. P., and Chauhan, P. (2020). Changes in turbidity along Ganga River using Sentinel–2 satellite data during lockdown associated with COVID–19. *Geomatics Nat. Hazards Risk* 11, 1175–1195. doi: 10.1080/19475705.2020.1782482

Gauns, M., Madhupratap, M., Ramaiah, N., Jyothibabu, R., Fernandes, V., Paul, J. T., et al. (2005). Comparative accounts of biological productivity characteristics and estimates of carbon fluxes in the Arabian Sea and the Bay of Bengal. *Deep Sea Res. 2 Top. Stud. Oceanogr.* 52, 2003–2017. doi: 10.1016/j.dsr2.2005.05.009

Grasshoff, K., Kremling, K., and Ehrhardt, M. (1999). *Methods of Seawater Analysis. 3rd Edn*. Weinheim: Wiley-VCH. 632.

Ittekot, V., and Laane, R. (1991). "Fate of riverine organic matter," in *Biogeochemistry of Major World Rivers*, SCOPE 42 Edn, eds E. Degens, S. Kempe, and J. Richy (Hoboken, NJ: John Wiley).

Jayaram, C., Patidar, G., Swain, D., Chowdary, V. M., and Bandyopadhyay, S. (2021). Total suspended matter distribution in the Hooghly river estuary and the Sundarbans: a remote sensing approach. *IEEE J. Sel. Top. Appl. Earth Obs. Remote Sens. (in press)*

Khan, R. A. (1995). "Ecology of the Hugli-Matla estuarine system," in *Hugli-Matla, West Bengal, part 2. Estuarine Ecosystem Series*, ed. A. K. Ghosh (Calcutta: Zoological Survey of India), 417–464.

Khan, S., Sinha, R., Whitehead, P., Sarkar, S., Jin, L., and Futter, M. N. (2018). Flows and sediment dynamics in the Ganga River under present and future climate scenarios. *Hydrol. Sci. J.* 63, 763–782. doi: 10.1080/02626667.2018.1447113

Knap, A. H., Michaels, A., Close, A. R., Ducklow, H., and Dickson, A. G. (1996). *Protocols for the Joint Global Ocean Flux Study (JGOFS) Core Measurements. JGOFS Reprint of the IOC Manuals and Guides No. 29, UNESCO 1994*, Vol. 19. Paris: UNESCO, 210.

Lal, D. (1978). "Transfer of chemical species through estuaries to oceans," in *Proceedings of UNESCO/SCOR Workshop on Biogeochemistry of Estuarine Sediments*, (Melreus, Belgium), 166–170.

Lian, X., Huang, J., Huang, R., Liu, C., Wang, L., and Zhang, T. (2020). Impact of city lockdown on the air quality of COVID-19 hit of Wuhan city. *Sci. Total Environ.* 742:140556. doi: 10.1016/j.scitotenv.2020.140556

Mahato, S., Pal, S., and Ghosh, K. G. (2020). Effect of lockdown amid COVID-19 pandemic on the air quality of the megacity of Delhi. India. *Sci. Total Environ.* 730:139086. doi: 10.1016/j.scitotenv.2020.139086

McClain, C. R., Feldman, G. C., and Hooker, S. B. (2004). An overview of the SeaWiFS project and strategies for producing a climate research quality global ocean bio-optical time series. *Deep Sea Res. 2* 51, 5–42. doi: 10.1016/j.dsr2.2003.11.001

Meybeck, M., and Ragu, A. (1997). *River Discharges to the Oceans: an Assessment of Suspended Solids, Major Ions and Nutrients*, Vol. 245. Nairobi: UNEP.

Miller, R. L., and McKee, B. A. (2004). Using MODIS Terra 250 m imagery to map concentrations of total suspended matter in coastal waters. *Remote Sens. Environ.* 93, 259–266. doi: 10.1016/j.rse.2004.07.012

Mishra, D. R., Kumar, A., Muduli, P. R., Equeenuddin, Sk. Md., Rastogi, G., Acharyya, T., et al. (2020). Decline in Phytoplankton Biomass along Indian coastal waters due to COVID-19 lockdown. *Remote Sens.* 12:2584. doi: 10.3390/rs12162584

Mouyen, M., Longuevergne, L., Steer, P., Crave, A., Lemoine, J. M., Save, H., et al. (2018). Assessing modern river sediment discharge to the ocean using satellite gravimetry. *Nat. Commun.* 9:3384. doi: 10.1038/s41467-018-05921-y

Mukhopadhyay, S. K., Biswas, H., De, T. K., and Jana, T. K. (2006). Fluxes of nutrients from the tropical River Hooghly at the land-ocean boundary of Sundabans, NE Coast of Bay of Bengal, India. *J. Mar. Syst.* 62, 9–21. doi: 10.1016/j.jmarsys.2006.03.004

Nechad, B., Ruddick, K., and Park, Y. (2010). Calibration and validation of a generic multi-sensor algorithm for mapping of total suspended matter in turbid waters. *Remote Sens. Environ.* 114, 854–866. doi: 10.1016/j.rse.2009.11.022

Odermatt, D., Gitelson, A., Brando, V. E., and Schaepman, M. (2012). Review of constituent retrieval of optically deep and complex waters from satellite imagery. *Remote Sens. Environ.* 118, 116–126. doi: 10.1016/j.rse.2011.11.013

Patel, P. P., Mondal, S., and Ghosh, K. G. (2020). Some respite for India's dirtiest river? Examining the Yamuna's water quality at Delhi during the COVID-19 lockdown period. *Sci. Total Environ.* 744:140851. doi: 10.1016/j.scitotenv.2020.140851

Rakshit, D., Biswas, S. N., Sarkar, S. K., Bhattacharya, B. D., Godhantaraman, N., and Satpathy, K. K. (2014). Seasonal variations in species composition, abundance, biomass and production rate of tintinnids (*Ciliata*: Protozoa) along the Hooghly (Ganges) River estuary, India: a multivariate approach. *Environ. Monitor. Assess.* 186, 3063–3078. doi: 10.1007/s10661-013-3601-9

Rao, C. K., Naqvi, S. W. A., Dileep Kumar, M., Varaprasad, S. J. D., Jayakumar, J. A., George, M. D., et al. (1994). Hydrochemistry of the Bay of Bengal: possible reasons for a different water-column cycling of carbon and nitrogen from the Arabian Sea. *Mar. Chem.* 47, 279–290. doi: 10.1016/0304-4203(94)90026-4

Ray, R., Rixen, T., Baum, A., Malik, A., Gleixner, G., and Jana, T. K. (2015). Distribution, sources and biogeochemistry of organic matter in a mangrove dominated estuarine system (Indian Sundarabans) during the pre-monsoon. *Estuar. Coast. Shelf Sci.* 167, 404–413. doi: 10.1016/j.ecss.2015.10.017

Rixen, T., Birgit, G., Kay-Christian, E., and Ramaswamy, V. (2019). The ballast effect of lithogenic matter and its influences on the carbon fluxes in the Indian Ocean. *Biogeosciences* 16, 485–503. doi: 10.5194/bg-16-485-2019

Rudra, K. (2014). Changing river courses in the western part of the Ganga–Brahmaputra delta. *Geomorphology* 227, 87–100. doi: 10.1016/j.geomorph.2014.05.013

Sadhuram, Y., Sarma, V. V., Murthy, T. V. R., and Rao, B. P. (2005). Seasonal variability of physiochemical characteristics of the Haldia channel of Hooghly estuary, India. *J. Earth Syst. Sci.* 114, 37–49. doi: 10.1007/BF02702007

Samanta, S., Dalai, T. K., Pattanaik, J. K., Rai, S. K., and Mazumdar, A. (2015). Dissolved inorganic carbon (DIC) and its δ13C in the Ganga (Hooghly) River estuary, India: evidence of DIC generation via organic carbon degradation and carbonate dissolution. *Geochem. Cosmochim. Acta* 165, 226–248. doi: 10.1016/j.gca.2015.05.040

Selvam, S., Muthukumar, P., Venkatramanan, S., Roy, P. D., Bharath, K. M., and Jesuraja, K. (2020). SARS-CoV-2 pandemic lockdown: effects on air quality in the industrialized Gurjarat state of India. *Sci. Total Environ.* 737:140391. doi: 10.1016/j.scitotenv.2020.140391

Shanthi, R., Poornima, D., Raja, S., Sethubathi, G. V., Thangaradjou, T., Balasubramanian, T., et al. (2013). Validation of OCM-2 sensor performance in retrieving chlorophyll and TSM along the southwest Bay of Bengal coast. *J. Earth Syst. Sci.* 122, 479–489. doi: 10.1007/s12040-013-0286-y

Trinh, R. C., Fichot, C. G., Gierach, M. M., Holt, B., Malakar, N. K., Hulley, G., et al. (2017). Application of Landsat 8 for monitoring impacts of wastewater discharge on coastal water quality. *Front. Mar. Sci.* 4:329. doi: 10.3389/fmars.2017.00329

Vaithiyanathan, P., Jha, P. K., and Subramanian, V. (1993). Phosphorus distribution in the sediments of the Hooghly (Ganges) Estuary, India. *Estuar. Coast. Shelf Sci.* 37, 603–614. doi: 10.1006/ecss.1993.1076

Vanhellemont, Q., and Ruddick, K. (2014). Turbid wakes associated with offshore wind turbines observed with Landsat 8. *Remote Sens. Environ.* 145, 105–115. doi: 10.1016/j.rse.2014.01.009

Vanhellemont, Q. (2019). Adaptation of the dark spectrum fitting atmospheric correction for aquatic applications of the Landsat and Sentinel-2 archives. *Remote Sens. Environ* 225, 175–192. doi: 10.1016/j.rse.2019.03.010

Vanhellemont, Q., and Ruddick, K. (2018). Atmospheric correction of metre-scale optical satellite data for inland and coastal water applications. *Remote Sens. Environ.* 216, 586–597. doi: 10.1016/j.rse.2018.07.015

Yunus, A. P., Masago, Y., and Hijoka, Y. (2020). COVID-19 and surface water quality: improved lake water quality due to the lockdown. *Sci. Total Environ.* 731:13902. doi: 10.1016/j.scitotenv.2020.139012

Zambrano-Monserrate, M. A., Ruano, M. A., and Sanchez-Alcalde, L. (2020). Indirect effects of COVID-19 on the environment. *Sci. Total Environ.* 728:138813. doi: 10.1016/j.scitotenv.2020.138813

Zangari, Z., Hill, D. T., Charette, A. T., and Mirowsky, J. E. (2020). Air quality changes in New York City during the COVID-19 pandemic. *Sci. Total Environ.* 742:140496. doi: 10.1016/j.scitotenv.2020.140496

Conflict of Interest: The authors declare that the research was conducted in the absence of any commercial or financial relationships that could be construed as a potential conflict of interest.

frontiers in Marine Science

ORIGINAL RESEARCH
published: 20 May 2021
doi: 10.3389/fmars.2021.638583

Variations of Colored Dissolved Organic Matter in the Mandovi Estuary, Goa, During Spring Inter-Monsoon: A Comparison With COVID-19 Outbreak Imposed Lockdown Period

Albertina Dias[1,2], Siby Kurian[1], Suresh Thayapurath[1] and Anil K. Pratihary[1]*

[1] CSIR-National Institute of Oceanography, Panaji, India, [2] School of Earth, Ocean, and Atmospheric Sciences, Goa University, Taleigão, India

OPEN ACCESS

Edited by:
D. Swain,
Indian Institute of Technology Bhubaneswar, India

Reviewed by:
Mar Nieto-Cid,
Spanish Institute of Oceanography, Spain
Fernanda Giannini,
Federal University of Rio Grande, Brazil

***Correspondence:**
Siby Kurian
siby@nio.org

Specialty section:
This article was submitted to Marine Biogeochemistry, a section of the journal Frontiers in Marine Science

Received: *07 December 2020*
Accepted: *29 April 2021*
Published: *20 May 2021*

Citation:
Dias A, Kurian S, Thayapurath S and Pratihary AK (2021) Variations of Colored Dissolved Organic Matter in the Mandovi Estuary, Goa, During Spring Inter-Monsoon: A Comparison With COVID-19 Outbreak Imposed Lockdown Period. Front. Mar. Sci. 8:638583. doi: 10.3389/fmars.2021.638583

Colored dissolved organic matter (CDOM) is one of the important fractions of dissolved organic matter (DOM) that controls the availability of light in water and plays a crucial role in the cycling of carbon. High CDOM absorption in the Mandovi Estuary (Goa) during spring inter-monsoon (SIM) is largely driven by both *in-situ* production and anthropogenic activities. Here we have presented the CDOM variation in the estuary during SIM of 2014–2018 and compared it with that of 2020 when the COVID-19 outbreak imposed lockdown was implemented. During 2020, low CDOM absorption was observed at the mid-stream of the estuary as compared to the previous years, which could be attributed to low autochthonous production and less input from anthropogenic activities. On the other hand, high CDOM observed at the mouth during 2020 is linked to autochthonous production, as seen from the high concentrations of chlorophyll *a*. High CDOM in the upstream region could be due to both autochthonous production and terrestrially derived organic matter. Sentinel-2 satellite data was also used to look at the variations of CDOM in the study region which is consistent with *in-situ* observations. Apart from this, the concentration of nutrients (NO_3^-, NH_4^+, and SiO_4^{4-}) in 2020 was also low compared to the previous reports. Hence, our study clearly showed the impact of anthropogenic activities on CDOM build-up and nutrients, as the COVID-19 imposed lockdown drastically controlled such activities in the estuary.

Keywords: CDOM, Mandovi Estuary, COVID-19 lockdown, Sentinel-2, anthropogenic activities

INTRODUCTION

Dissolved organic matter (DOM) is one of the key pools of organic carbon in natural waters (Hedges, 1992), and colored DOM (CDOM) is that fraction of DOM that interacts with light (Blough and Del Vecchio, 2002; Nelson and Siegel, 2002; Nelson et al., 2007). CDOM controls the availability of light in water and plays an important role in regulating the chemical processes in water (Mopper and Kieber, 2002; Coble, 2007). CDOM can be produced *in-situ* by biological

production and microbial mediated remineralization of organic matter (autochthonous) or transported from terrestrial sources (allochthonous) and removed by photochemical degradation and microbial consumption or be influenced by physical processes such as circulation, upwelling, or mixing (Hansell et al., 2002; D'Sa et al., 2006; Coble, 2007; Nelson and Siegel, 2013). Estuaries form an important link in transporting terrestrial organic carbon to the adjoining coastal waters. It is estimated that dissolved organic carbon (DOC) in the oceans is 662 Pg C (Hansell et al., 2009) compared to the terrestrial biota, which contains 600–1,000 Pg C (Falkowski et al., 2000).

The Mandovi and Zuari estuaries form the major riverine channel in the state of Goa. The estuaries of Goa have been studied extensively for various biogeochemical parameters (Shetye et al., 2007; Anand et al., 2014; Shynu et al., 2015; Araujo et al., 2018); however, studies on CDOM in these estuaries are limited (Menon et al., 2011; Dias et al., 2017, 2020a). In recent years, these estuaries have been exploited for various anthropogenic activities (Shynu et al., 2012; Veerasingam et al., 2015), and their influence has also been observed on the CDOM in the estuaries (Dias et al., 2020a). Some of the anthropogenic activities observed along the bank and within the estuaries include the pleasure cruises, floating casinos, shipbuilding/repair yards, sand mining, small and large scale industries, fish processing units, fishing jetties, mine waste rejects, transportation of mineral ores by barges, discharge of treated municipal sewage, domestic waste discharge from the houses and commercial establishments, etc. (Shynu et al., 2015; Dias et al., 2020a).

In late 2019, there was a breakdown of SARS-CoV-2 first reported in China which began to spread over other countries at a high pace by January 2020, and on 11th March 2020 World Health Organization declared it as pandemic[1]. Novel Corona Virus (COVID-19) is considered one of the most virulent diseases in recent times. As a precautionary measure, the Government of India announced a complete lockdown across the country from midnight of 24th March 2020 for 21 days and again thereafter in phases till 8th June 2020[2]. The lockdown was the first-ever opportunity to study the water column characteristics of Mandovi Estuary when most of the anthropogenic activities were either stopped or reduced drastically. There was a halt in transportation activities in the estuary like pleasure cruises, ferry services, ore transportation, etc. Also, the shipbuilding/repair yards at the banks of the estuary, small and large scale industries, sand mining, and commercial establishments were at a standstill during this period.

Other than allochthonous sources, phytoplankton forms an important source of DOM, especially during the non-monsoon season (Dias et al., 2020a), when the terrestrial run-off to the estuary is at the minimum and the residence time of water is greater (Shetye et al., 2007). Nutrients are often a limiting factor for phytoplankton growth. A recent study by Asmala et al. (2018) has shown that nitrogen and phosphorus availability is mainly responsible for phytoplankton extracellular release of DOM and its heterotrophic degradation by bacteria. Given the conditions of lockdown, when anthropogenic activities were at the minimum, *in-situ* production of DOM would be important drivers of DOM variability in the estuary.

To understand the lockdown influence on the CDOM absorption, we carried out sampling in the Mandovi Estuary in early May 2020 during the phased lockdown opening. The objective of this study was to compare the CDOM absorption in the estuary during the spring inter-monsoon (SIM; March–May) of 2014–2018 with that of 2020 when the anthropogenic activities were minimum. To get more insight into the autochthonous production, the variation of nutrients and phytoplankton marker pigments were studied during our observation in 2020.

METHODOLOGY

Field Sampling and Laboratory Measurements

Surface water samples were collected in the Mandovi Estuary at 6 locations during the SIM of 2014–2020 (**Figure 1**). The *in-situ* temperature and salinity were monitored using a thermometer (precision 1°C) and a refractometer($\pm$1–2 psu), respectively, during the recent study (2020). The salinity values of the refractometer were later corrected with reference to Autosal readings. During 2014–2018, the *in-situ* temperature and salinity were measured using the CTD sensor mounted on a profiling radiometer (Satlantic INC) and water samples were collected using a Niskin sampler. In 2020, water samples were collected using a bucket, and sub-sampled in bottles for CDOM, phytoplankton pigments, and nutrients. These samples were transported to the lab in ice and analyzed following standard protocols. For CDOM analysis, water samples were filtered through 0.2 micron nucleopore membrane filters and analyzed using a 10 cm cell on a spectrophotometer, as detailed in Dias et al. (2020a).

Absorption by CDOM $a_g(\lambda)$ m^{-1} is modeled as given in equation 1 (Jerlov, 1976), where λ_0 represents the reference wavelength, and S (nm^{-1}) is the spectral slope over the given spectral range.

$$a_g(\lambda) = a_g(\lambda_0)e^{-S(\lambda-\lambda_0)} \quad (1)$$

We have chosen the reference wavelength as a_g412 (m^{-1}) for the CDOM concentration since a_g412 is employed to determine DOC (Vantrepotte et al., 2015), being the shortest wavelength accessible from the ocean color remote sensing satellites, and also to compare with our previous data from the study area (Dias et al., 2020a). We have used spectral slope in the narrow wavelength range of 275–295 ($S_{275-295}$ nm^{-1}), which provides the nature of DOM, and the Slope ratio, S_R (ratio of slope $S_{275-295}$ to $S_{350-400}$) since it gives information about the molecular weight of DOM and has been widely used to study the impact of photobleaching on DOM (Helms et al., 2008). The spectral slopes are calculated using the linear fit of the log linearized spectrum.

[1]https://www.who.int/news-room/detail/27-04-2020-who-timeline---covid-19

[2]https://www.business-standard.com/article/current-affairs/here-s-a-timeline-of-events-since-lockdown-was-imposed-in-india-120070201413_1.html

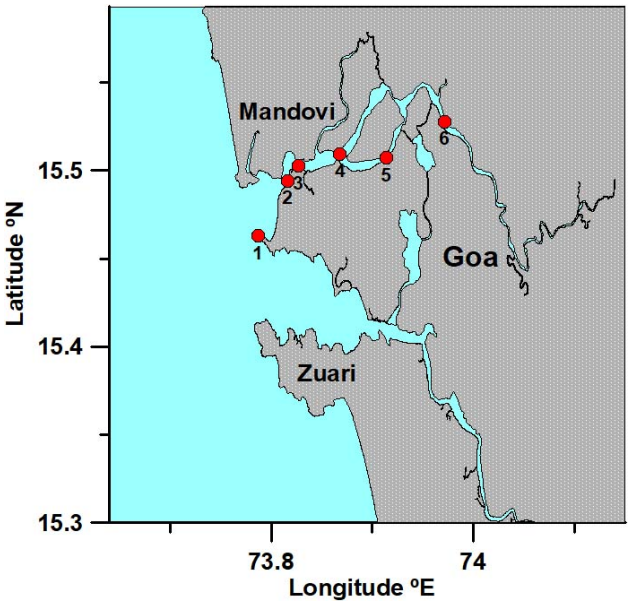

FIGURE 1 | Sampling stations in the Mandovi Estuary. Stations 1 and 2 are the mouth stations (close to Dona Paula Jetty and Kala Academy), Stations 3–5 represents the mid-stream region (close to the Mandovi Bridge, Ribander, and Old Goa Jetty, respectively) and Station 6 represents the upstream region (close to the Amona Bridge).

Fluorescence spectra of CDOM were recorded using a spectrofluorometer (Cary Eclipse, Varian) equipped with a xenon lamp. The samples were scanned with an excitation range of 200–450 nm, and emissions were recorded from 250 to 600 nm with a slit width of 5 nm each. The details of data acquisition and corrections are detailed in Dias et al. (2020b). The corrected fluorescence data was then used to calculate the fluorescence indices. The two fluorescence indices used in this study are the humification index (HIX), which is an indicator of the content of humic substances (Zsolnay et al., 1999), and the biological index (BIX), which is an index of autochthonous contribution. HIX is the ratio of the area between emission wavelengths of 435–480 nm to the area between 300 and 345 nm at an excitation wavelength of 254 nm. In contrast, BIX is the ratio of the fluorescence intensity emitted at 380 nm to that at 430 nm at an excitation wavelength of 310 nm (Huguet et al., 2009).

Phytoplankton pigments were analyzed by filtering 1 L of water onto GF/F filters (0.7 μm) under dark and cold conditions. The samples were extracted in 3 mL methanol and analyzed on a HPLC 1200 series (Agilent Technologies) as detailed in Kurian et al. (2012). Chlorophyll *a* is usually used as a proxy for phytoplankton biomass, while accessory pigments are specific to phytoplankton groups and give information on the community composition (Gieskes et al., 1988; Mackey et al., 1996; Jeffrey et al., 1997; Prézelin et al., 2000). Here we used the pigment-based size classification proposed by Uitz et al. (2006) to get more insight into the phytoplankton size classes [micro- (>20 μm), nano- (20–2 μm), and pico-phytoplankton(<2 μm)]. The fraction of each pigment-based size class with respect to the total phytoplankton biomass is calculated as follows:

$$
\begin{aligned}
f_{micro}\% &= 100 \times (1.41[Fuco] + 1.41[Peri])/wDP \\
f_{nano}\% &= 100 \times (1.27[Hex-fuco] + 0.35[But-fuco] \\
&+ 0.60[Allo])/wDP \\
f_{pico}\% &= 100 \times (1.01[TChlb] + 0.86[Zea])/wDP
\end{aligned}
$$

where wDP is the weighted sum of the concentration of seven diagnostic pigments:

$$
\begin{aligned}
wDP &= 1.41[Fuco] + 1.41[Peri] + 1.27[Hex-fuco] \\
&+ 0.35[But-fuco] + 0.60[Allo] + 1.01[TChlb] + 0.86[Zea]
\end{aligned}
$$

Nutrient samples were frozen after collection and analyzed shortly using Skalar Autoanalyser following the standard colorimetric method (Grasshoff et al., 1999) with precisions ± 0.06, ± 0.01, ± 0.003, ± 0.06 μM for NO_3^-, NH_4^+, PO_4^{3-}, and SiO_4^{4-}, respectively.

Satellite Data Processing

In addition to *in-situ* data, we used the ocean color satellite data from Sentinel-2 (launched by the European space agency in the year 2015) to compare the CDOM in the Mandovi Estuary during the COVID-19 imposed lockdown (May 2020) with that in previous years (2017–2019). This satellite was opted because it gives high spatial resolution (10–60 m) and multiple spectral bands ranging from visible to short wave infrared, having narrow bandwidth suitable for monitoring our estuaries. Sentinel-2, Level-1C cloud-free satellite data closest to the *in-situ* sampling dates were downloaded from the publicly available Sentinel Scientific Data Hub[3]. Sentinel-2 toolbox within the sentinel application platform (SNAP) version 8 was used to process the image from L1C (top-of-atmosphere reflectance) to L2A (bottom-of-atmosphere reflectance). The L1C product was re-sampled to 10 m resolution using band 2 of Sentinel-2. Atmospheric correction was done using the Case 2 Regional Coast Color (C2RCC) processor version 1.1 (Brockmann et al., 2016). The C2RCC processor uses the radiative transfer simulations of water leaving radiances and top-of-atmosphere radiances inverted by a neural network. To ensure data quality we used the default flags in the C2RCC processor for indicating a failure from atmospheric correction (Rtosa_OOS and Rtosa_OOR) and IOP retrieval (Rhow_OOR and IOP_OOR). The C2RCC processor gives CDOM at 443 nm, whereas a_g at 412 nm was used as the absorption coefficient for CDOM in our study; hence a new algorithm was required to derive a_g at 412 nm.

For the development of the CDOM algorithm, we used *in-situ* data of remote sensing reflectance, R_{rs} (Sr^{-1}) from 2014 to 2018 measured from these waters along with the NOMAD dataset (Werdell and Bailey, 2005). Various band ratio algorithms

[3]https://scihub.copernicus.eu/dhus/#/home

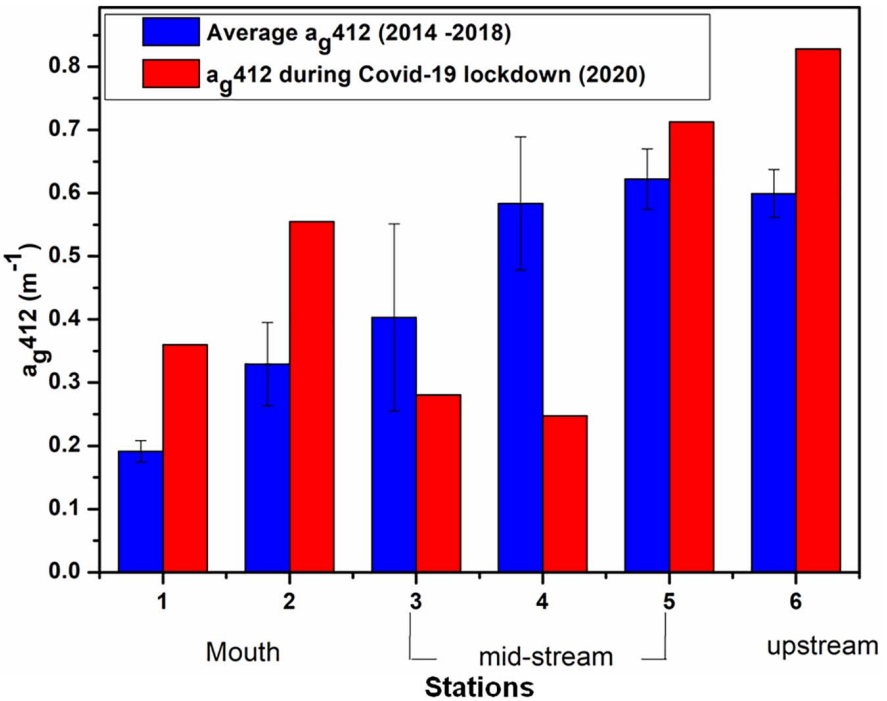

FIGURE 2 | Spatial variations of CDOM absorption a_g412 (m^{-1}) during 2014–2018 (blue) and 2020 (red) along the Mandovi Estuary.

previously used to derive CDOM from Sentinel-2 were evaluated (Toming et al., 2016; Chen et al., 2017, 2020; Ruescas et al., 2018; Xu et al., 2018; Zhao et al., 2018; Al-Kharusi et al., 2020; da Silva et al., 2020; Soomets et al., 2020). The band ratio of remote sensing reflectance (R_{rs}) at 490 and 665 was found to be the optimum combination for our data set (R^2 = 0.85) (*manuscript under preparation*), and the CDOM was derived at 412 nm. The a_g derived from C2RCC and the new algorithm was evaluated in which the new algorithm showed an improved correlation (r = 0.723) over the CDOM from C2RCC (r = 0.558). The error statistics using the measured and the satellite-derived a_g indicate that the new algorithm (RMSE = 0.17; error = −16.6 %) to derive a_g412 perform better than the C2RCC (RMSE = 0.49; error = −49.2%) for our study region (Shanmugam, 2011).

RESULTS AND DISCUSSION

The surface temperature varied within a narrow range (30–31°C), while salinity varied from 22 to 35 at the sampling locations during 2020, and the values were within the range reported by Dias et al. (2020a). The surface temperature increases while salinity decreases toward the upstream of the estuary. CDOM absorption a_g412 (m^{-1}) during the SIM of 2020 was the highest in the upstream region (0.827 m^{-1}) of the Mandovi Estuary, while a decrease in absorption was observed in the mid-stream region [0.263 m^{-1}, except at a station close to Old Goa Jetty (0.713 m^{-1})] followed by an increase toward the mouth (0.455 m^{-1}) (**Figure 2**). On the other hand, CDOM absorption usually decreased from the upstream toward the mouth during the previous years (2014–2018) (Dias et al., 2020a). Statistics of CDOM absorption (a_g412 m^{-1}) along with slope ($S_{275-295}$ nm^{-1}) and

TABLE 1 | Statistics of CDOM absorption (a_g412 m^{-1}), slope ($S_{275-295}$ nm^{-1}) and slope ratio (S_R) during 2014–2018 with a comparison to 2020 data (precision is ± 0.00002 m^{-1}).

Station no.	Parameters	2014–2018				2020
		Min	Max	Average	SD	
1	a_g412	0.17905	0.20314	0.19109	0.01703	0.3602
Mouth	$S_{275-295}$	0.02334	0.02408	0.023668	0.000384	0.02135
	S_R	1.26847	1.48971	1.383101	0.122477	1.326
2	a_g412	0.2722	0.44148	0.32942	0.06595	0.55504
Mouth	$S_{275-295}$	0.01924	0.02336	0.02102	0.001563	0.0202
	S_R	1.18972	1.55941	1.37900	0.155057	1.228
3	a_g412	0.23929	0.56665	0.407868	0.149157	0.28069
Mid-stream	$S_{275-295}$	0.01914	0.02308	0.02125	0.001656	0.0222
	S_R	1.21985	1.42375	1.287512	0.083397	1.194
4	a_g412	0.49788	0.74953	0.628748	0.097134	0.24746
Mid-stream	$S_{275-295}$	0.01908	0.02093	0.02026	0.000619	0.02192
	S_R	1.096551	1.30576	1.205558	0.074799	1.056
5	a_g412	0.55367	0.6653	0.620984	0.051910	0.7125
Mid-stream	$S_{275-295}$	0.01944	0.02202	0.02043	0.00101	0.01582
	S_R	1.10698	1.24580	1.15349	0.05447	0.902
6	a_g412	0.5485	0.64202	0.60764	0.046274	0.82798
Upstream	$S_{275-295}$	0.01993	0.02104	0.020345	0.000557	0.0202
	S_R	1.06246	1.30981	1.176908	0.093584	1.122

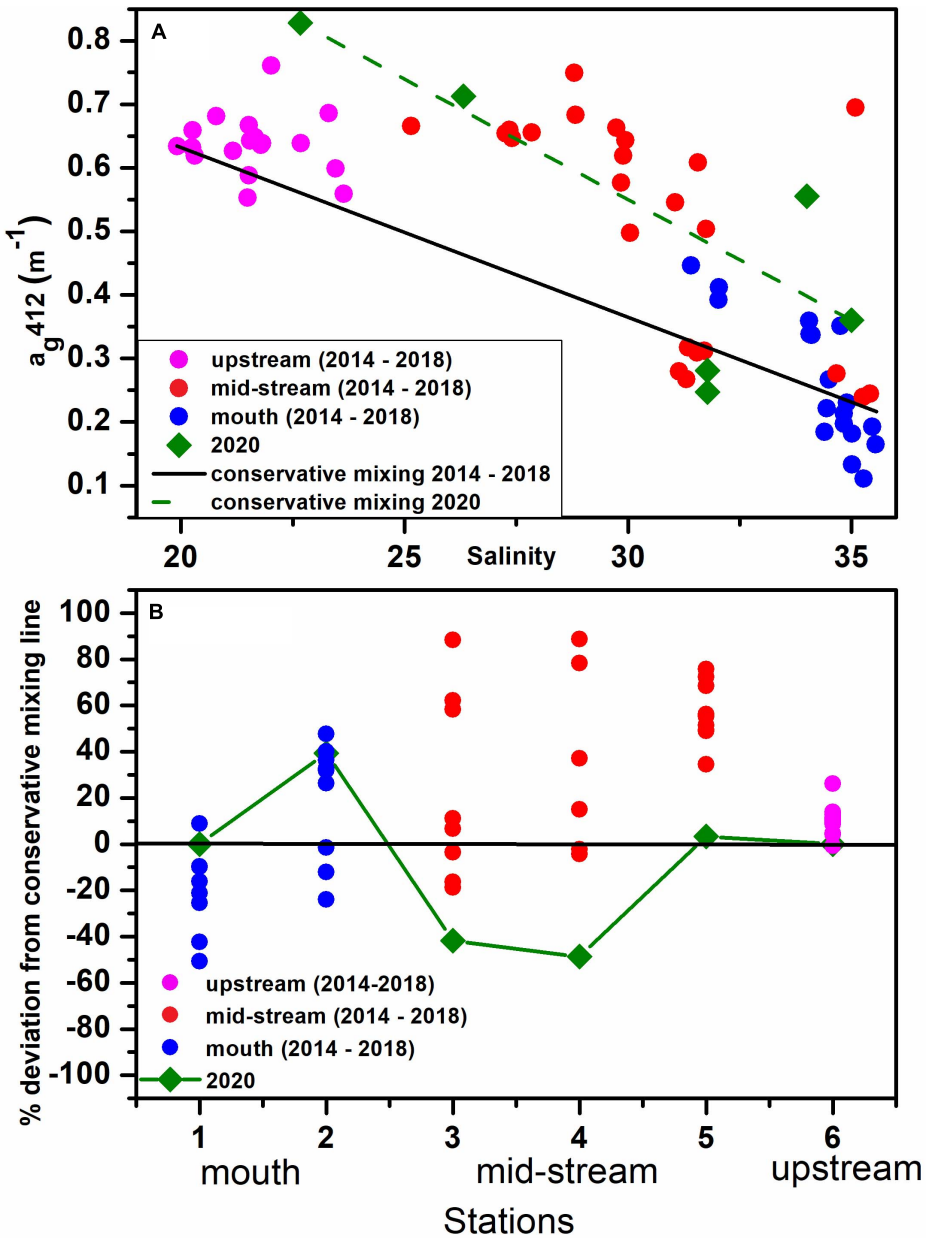

FIGURE 3 | (A) Conservative mixing diagram of CDOM absorption a_g412 (m^{-1}) with salinity during 2014–2018 and 2020. **(B)** Percentage deviation of CDOM absorption ($a_g412\ m^{-1}$) from the conservative mixing line during 2014–2018 and 2020.

slope ratio (S_R) during 2014–2018 and 2020 are provided in **Table 1**.

The upstream region of the Mandovi Estuary showed maximum CDOM absorption during 2020, whereas the spectral slope ($S_{275-295}$ = 0.0202 nm^{-1}) and the slope ratio (S_R = 1.12) are comparable to the previous years. This region of the estuary is mainly under the influence of terrestrial organic matter (Dias et al., 2020a). Apart from this autochthonous production also contribute to the CDOM as seen from the moderate chlorophyll *a* values (**Figure 4A**). However, the HIX (4.45) and BIX (0.67) values at this station were lower than those observed for terrestrial organic matter indicate the photodegraded nature of organic matter. The high solar radiation and longer residence time in the estuary during SIM favors the photodegradation of terrestrial DOM (Dias et al., 2020a).

To study the mixing behavior of CDOM in the estuary a conservative mixing diagram is plotted by joining the high and low salinity end-members (**Figure 3A**). The points falling above the mixing line are attributed to sources, while those below the mixing line are associated with sinks (Stedmon et al., 2003). A prominent non-conservative mixing behavior was observed during the SIM in the study area during the previous years

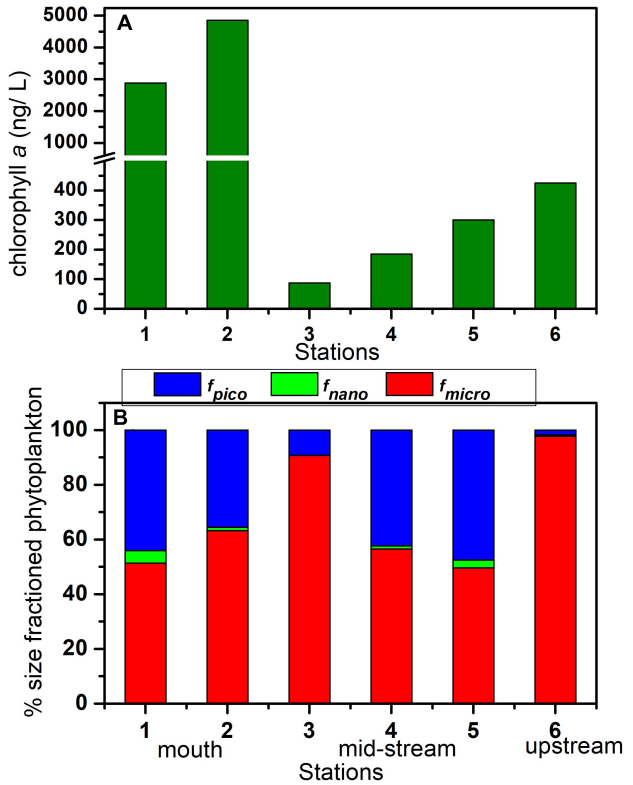

FIGURE 4 | Spatial variation of **(A)** chlorophyll *a* (ng/L) and **(B)** phytoplankton size fractions (%)in the Mandovi Estuary during 2020.

(Dias et al., 2017; 2020a). The maximum deviation from the conservative mixing line (>50% with mostly additions) was observed in the mid-stream region of the estuary during previous years (**Figure 3B**) and was attributed to the anthropogenic activities (Dias et al., 2020a). On the other hand, most of the CDOM values fall very close to the conservative mixing line and show a quasi-conservative mixing behavior in 2020. However, two stations at the mid-stream region (stations 3 and 4) showed very low CDOM absorption with maximum deviation (−40%) from the mixing line (**Figure 3B**). This significant decrease of CDOM (**Figures 2**, **3**) was observed when the COVID-19 outbreak imposed lockdown was implemented. One of the reasons for the decrease in CDOM absorption at the mid-stream region in 2020 (which otherwise showed additions during the previous years; **Figure 3**), could be due to the closure of anthropogenic activities during the lockdown. There was a complete standstill of operating pleasure cruises, water transport systems like barges, shipbuilding activities, and commercial establishments following the government-imposed lockdown, which might have reduced the CDOM. The other reason could be due to the low productivity at the mid-stream region as seen from the lowest chlorophyll *a* concentration (136 ng/L), and hence low input from autochthonous production. The spectral slope $S_{275-295}$ (0.022 nm^{-1}) was highest, and S_R (1.12) was lower during 2020 as compared to the previous years ($S_{275-295}$ = 0.020 nm^{-1} and S_R = 1.27). The BIX was observed to be maximum (>1), and the HIX was observed to be minimum (<4) at these stations. The low CDOM absorption and humification index (low molecular weight DOM) and high spectral slopes, and BIX indicate an autochthonous source of DOM by the microbial reworking of organic matter. This was also observed from the CDOM values (a_g412) falling below the conservative mixing line indicating the removal of organic matter (**Figure 3**). On the other hand, station 5 in the mid-stream region showed an increase in CDOM absorption compared to the previous years. The spectral slope ($S_{275-295}$ = 0.0158 nm^{-1}) and the slope ratio (S_R = 0.90) was lower at this station compared to the previous years ($S_{275-295}$ = 0.020 nm^{-1} and S_R = 1.15) indicating the terrestrial nature of DOM. The BIX (0.54) was the lowest, and HIX (5.22) was the highest at this station compared to the others. The Diwar Island is in close proximity to this station harbored by ample of mangroves, and the terrestrial nature of DOM at this location could be a result of the mangrove leachates.

On the other hand, an increase in the CDOM absorption toward the mouth could be due to high productivity, as seen from high chlorophyll *a* concentrations (3,868 ng/L) near the mouth. Interestingly, the slope of CDOM ($S_{275-295}$) was also found to be lower (0.02077 nm^{-1}) toward the mouth stations in comparison to the previous years (0.0233 nm^{-1}). The slope ratio values were also lower (S_R = 1.27) than those observed during previous years (1.39) as given in **Table 1**. The HIX was also observed to be low (<4), indicating the biological origin of DOM. At the same time, the BIX showed intermediate values (0.6–0.8) at the mouth stations, which point to an autochthonous source of DOM. The high values of slope and slope ratio observed during the previous years were due to efficient photobleaching of DOM during its transport in the estuary (Dias et al., 2020a).

To get more insight into the autochthonous production, we analyzed photosynthetic pigments during recent observation in 2020. The concentration of chlorophyll *a* was very high near the mouth (3,868 ng/L) followed by upstream (362.9 ng/L), whereas its concentration was low (139 ng/L) at the mid-stream region (**Figure 4A**). Hence, high CDOM absorption at the upstream and toward the mouth could be attributed to increased productivity, while low CDOM in the mid-stream region could be due to low autochthonous production along with less input from anthropogenic activities. Phytoplankton size classification based on Uitz et al. (2006) showed dominance (50–90%) of microplankton (f_{micro}) in the estuary followed by the picoplankton (f_{pico}; 1.7–47 %), while the fraction of nanoplankton (f_{nano}) was negligible during 2020 observation (**Figure 4B**). f_{micro}% was maximum (>90%) at the upstream and at station 3 in the mid-stream region, whereas both micro- and pico-plankton contributed to the phytoplankton composition at the other stations. Green *Noctiluca* was visible in the surface waters near the mouth during our sampling. A very good positive correlation (r = 0.95) was found between chlorophyll *a* and CDOM absorption for mouth and mid-stream region, suggesting autochthonous production as the main source of CDOM at these stations (1–4). Whereas, the relationship becomes very poor (r = 0.01) when stations 5 and 6 are included in the correlation, which indicates that apart from autochthonous production other

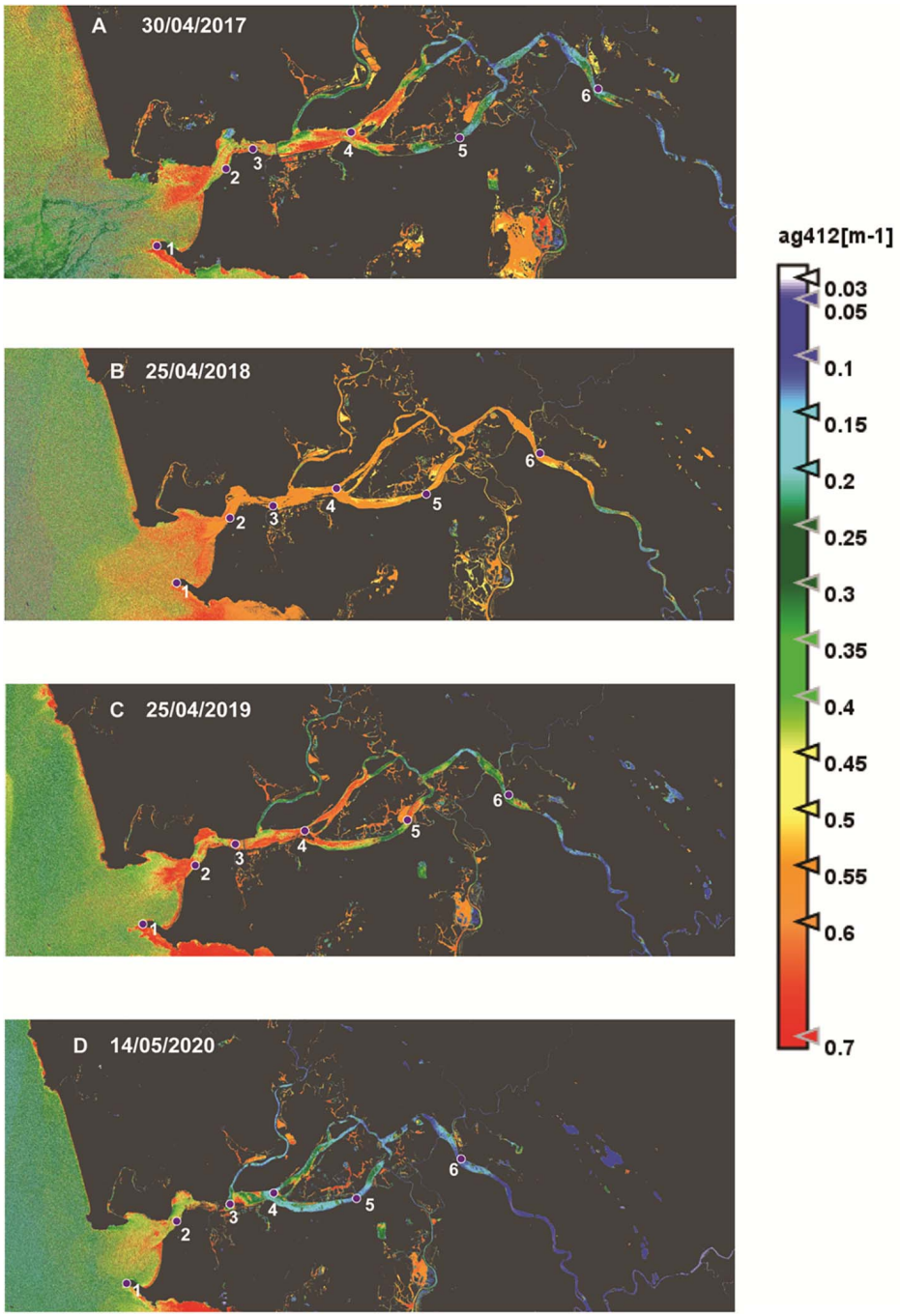

FIGURE 5 | Spatial variation of CDOM ($a_g412\ m^{-1}$) observed from Sentinel-2 during **(A)** 2017, **(B)** 2018, **(C)** 2019, and **(D)** 2020 along the Mandovi Estuary.

sources such as mangrove leachate and terrestrial input might have contributed to the CDOM toward the upstream region.

The CDOM, a_g412 derived from the Sentinel-2 using a new algorithm (**Figure 5**) showed similar spatial and temporal variations as that of *in-situ* data. However, at the upstream (station 6, 28 km from the mouth), the a_g412 from Sentinel-2 was underestimated, probably due to the adjacency effect as the estuary becomes very narrow toward the upstream. CDOM absorption was higher in the mid-stream region during 2017–2019, while low CDOM absorption was observed during the imposed lockdown of 2020 (**Figure 5**). This is consistent with our *in-situ* measurements (**Figure 2**), which suggest the influence of anthropogenic activities on CDOM absorption in the mid-stream region of the Mandovi Estuary, and the effect was observed to be minimal during the lockdown of 2020.

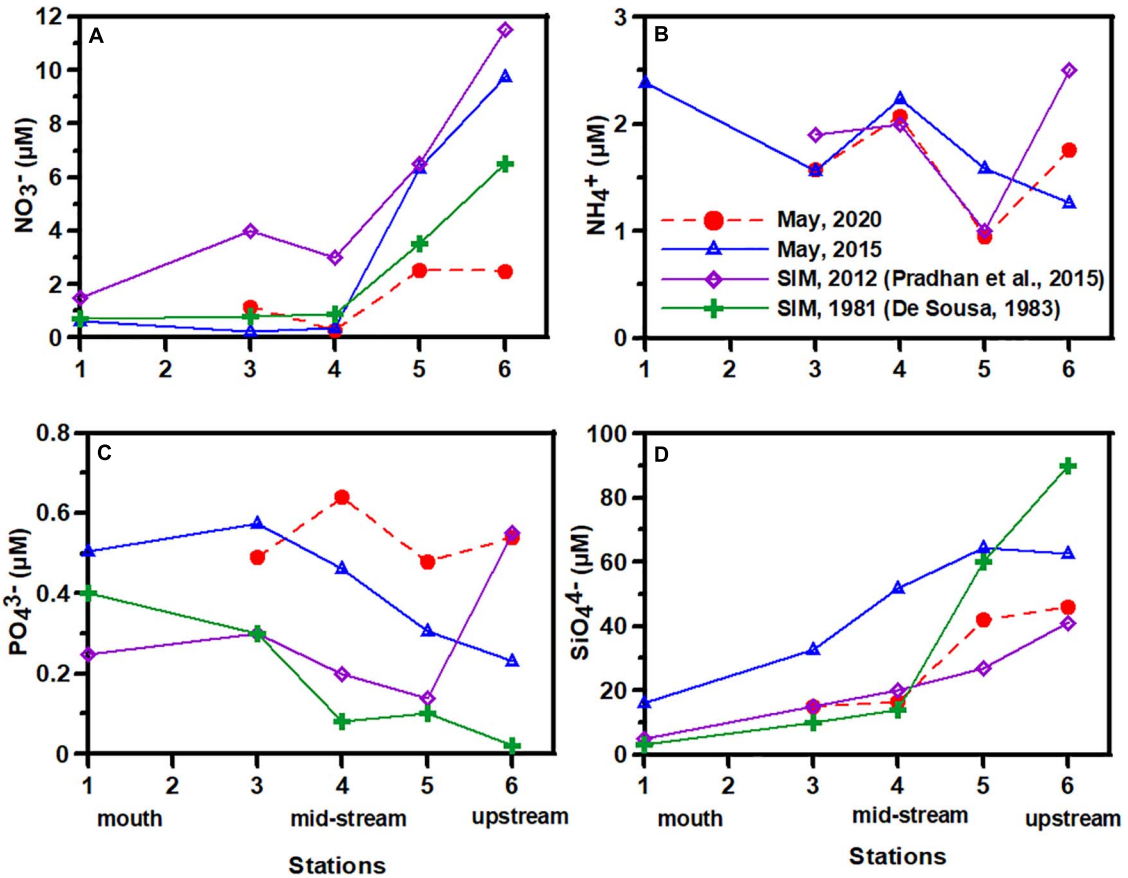

FIGURE 6 | Spatial variation of nutrients **(A)** NO_3^-, **(B)** NH_4^+, **(C)** PO_4^{3-}, and **(D)** SiO_4^{4-} (μM) in the Mandovi Estuary during 2020 with a comparison with the previous measurements during SIM of 2015, 2012 (Pradhan et al., 2015) and 1981 (De Sousa, 1983).

The nutrient concentration in the Mandovi Estuary during May 2020 was compared with earlier measurements (May 2015, De Sousa, 1983; Pradhan et al., 2015, during SIM; **Figure 6**). $NH_4^+$and SiO_4^{4-} didn't show much variation, while PO_4^{3-} values were slightly higher in 2020, whereas NO_3^- concentrations were remarkably lower, especially toward the upstream. During May 2020, the concentrations of NO_3^- and SiO_4^{4-} showed an increasing trend from the mouth toward the upstream, whereas $NH_4^+$and PO_4^{3-} did not show any trend. This increasing trend of NO_3^- and SiO_4^{4-} were similar to our observation in May 2015 and by De Sousa (1983) and Pradhan et al. (2015) during SIM. Although during SIM the variation of PO_4^{3-} and SiO_4^{4-} from mouth to upstream show a regular trend reflecting their conservative mixing behavior (De Sousa, 1983; Upadhyay and Gupta, 1995), the same is not true for NO_3^- which shows a prominent mid-stream maximum reaching up to 6.5–11 μM (De Sousa, 1983; Pradhan et al., 2015; **Figure 6A**). During SIM, NO_3^- increases non-linearly (with salinity) just after station 4, with maximum concentration in the mid-stream-upstream region, and then decreases further upstream (De Sousa, 1983). Such disproportionate NO_3^- increase has been attributed to the run-off from mining industries (De Sousa, 1999) mainly located in the mid-stream-upstream regions of the Mandovi River and to the use of NH_4NO_3 as an explosive. However, unlike NO_3^-, NH_4^+ did not show any mid-stream maximum (**Figure 6B**), which could be due to the high nitrification rate in the estuary (Pratihary et al., unpublished data). The NO_3^- concentration during 2020 (especially toward the upstream, 2.5μM) was lower compared to earlier observations of May 2015, SIM of 2012 (Pradhan et al., 2015), SIM of 1981 (De Sousa, 1983), and this decrease was statistically significant ($p < 0.05$). We attribute this low NO_3^- concentration to the reduced run-off from mining industries during the lockdown period. On the other hand, we observed relatively higher PO_4^{3-} (**Figure 6C**) during May 2020 compared to previous observations, which could be due to relatively lower PO_4^{3-} uptake by phytoplankton owing to lower availability of NO_3^- in the estuarine water, and hence PO_4^{3-} remained in the system. This is supported by the lower chlorophyll *a* values in the mid-stream and upstream region during May 2020 (**Figure 4**) as compared to earlier reports (Krishnakumari et al., 2002; Madondkar et al., 2007). Thus, the observed low CDOM and nutrient concentrations in the estuary during the lockdown period compared to earlier observations could be due to the abrupt cessation of anthropogenic activities in the state of Goa.

CONCLUSION

CDOM showed a spatial variation in the Mandovi Estuary during the SIM of 2020 with high absorption in the upstream region and toward the mouth, and low absorption in the mid-stream region, contrasting with the previous results. A comparison to previous years showed that the low CDOM absorption at the mid-stream is due to low autochthonous production along with less input from anthropogenic activities during the COVID-19 imposed lockdown. Phytoplankton productivity contributed to high CDOM absorption near the mouth, whereas autochthonous production along with terrestrial organic matter contributed to the CDOM in the upstream region. The Sentinel-2 satellite data also showed similar variations of CDOM absorption with low values in the mid-stream region during 2020. The nutrient concentrations were also low during 2020 as compared to the previous reports. This study is the first of its kind to report the impact of imposed lockdown on anthropogenic activities and its influence on CDOM and nutrient concentrations in the Mandovi Estuary. Also, it provided an opportunity to get the CDOM concentrations in the estuary when the anthropogenic activities were at a standstill.

DATA AVAILABILITY STATEMENT

The raw data supporting the conclusions of this article will be made available by the authors, without undue reservation.

AUTHOR CONTRIBUTIONS

AD: sampling, analysis, data processing, and manuscript writing. SK and ST: writing – reviewing and editing. AP: nutrient analysis and editing. All authors contributed to the article and approved the submitted version.

FUNDING

This study was carried out under the institutional project (OLP 2006) of CSIR-National Institute of Oceanography, Goa. The nutrient data of May 2015 was collected under the SIBER-INDIA (GAP-2424) project funded by the Ministry of Earth Sciences, New Delhi.

ACKNOWLEDGMENTS

We are thankful to the Director, CSIR-National Institute of Oceanography, for providing the facilities and support. AD acknowledges CSIR for providing research fellowship. We acknowledge Dr. Hema Uskaikar for providing the nutrient data of May 2015. We are also thankful to the reviewers for their constructive comments which helped to improve the manuscript considerably. We are also grateful to Ms. Aswathi V. K. for her help in nutrient analysis. Mrs. Ramola Antao and Ms. Sushama Sonak are acknowledged for their help in language improvement. This is NIO contribution no. 6728.

REFERENCES

Al-Kharusi, E. S., Tenenbaum, D. E., Abdi, A. M., Kutser, T., Karlsson, J., Bergström, A. K., et al. (2020). Large-scale retrieval of coloured dissolved organic matter in northern lakes using sentinel-2 data. *Remote Sens.* 12:157. doi: 10.3390/rs12010157

Anand, S. S., Anju, K. J., Mathew, D., and Kumar, M. D. (2014). Sub-hourly changes in biogeochemical properties in surface waters of Zuari estuary, Goa. *Environ. Monit. Assess.* 186, 719–724. doi: 10.1007/s10661-013-3410-1

Araujo, J., Naqvi, S. W. A., Naik, H., and Naik, R. (2018). Biogeochemistry of methane in a tropical monsoonal estuarine system along the west coast of India. *Estuar. Coast. Shelf Sci.* 207, 435–443. doi: 10.1016/j.ecss.2017.07.016

Asmala, E., Haraguchi, L., Jakobsen, H. H., Massicotte, P., and Carstensen, J. (2018). Nutrient availability as major driver of phytoplankton-derived dissolved organic matter transformation in coastal environment. *Biogeochemistry* 137, 93–104. doi: 10.1007/s10533-017-0403-0

Blough, N. V., and Del Vecchio, R. (2002). "Chromophoric DOM in the coastal environment," in *Biogeochemistry of Marine Dissolved Organic Matter*, eds D. A. Hansel and C. A. Carlson ((San Diego, CA: Academic Press), 509–546. doi: 10.1016/b978-012323841-2/50012-9

Brockmann, C., Doerffer, R., Peters, M., Kerstin, S., Embacher, S., and Ruescas, A. (2016). Evolution of the C2RCC neural network for Sentinel 2 and 3 for the retrieval of ocean colour products in normal and extreme optically complex waters. *ESASP* 740:54.

Chen, J., Zhu, W., Tian, Y. Q., and Yu, Q. (2020). Monitoring dissolved organic carbon by combining Landsat-8 and Sentinel-2 satellites: case study in Saginaw River estuary, Lake Huron. *Sci. Total Environ.* 718:137374. doi: 10.1016/j.scitotenv.2020.137374

Chen, J., Zhu, W., Tian, Y. Q., Yu, Q., Zheng, Y., and Huang, L. (2017). Remote estimation of colored dissolved organic matter and chlorophyll-a in Lake Huron using Sentinel-2 measurements. *J. Appl. Remote Sens.* 11:036007.

Coble, P. G. (2007). Marine optical biogeochemistry: the chemistry of ocean color. *Chem. Rev.* 107, 402–418. doi: 10.1021/cr050350

da Silva, M. P., Sander de Carvalho, L. A., Novo, E., Jorge, D. S., and Barbosa, C. C. (2020). Use of optical absorption indices to assess seasonal variability of dissolved organic matter in Amazon floodplain lakes. *Biogeosciences* 17, 5355–5364. doi: 10.5194/bg-17-5355-2020

De Sousa, S. N. (1983). Studies on the behaviour of nutrients in the Mandovi estuary during premonsoon. *Estuar. Coast. Shelf Sci.* 16, 299–308. doi: 10.1016/0272-7714(83)90147-6

De Sousa, S. N. (1999). Effect of mining rejects on the nutrient chemistry of Mandovi estuary, Goa. *Indian J. Geo Mar. Sci.* 28, 355–359.

Dias, A., Kurian, S., and Thayapurath, S. (2020b). Optical characteristics of colored dissolved organic matter during blooms of Trichodesmium in the coastal waters off Goa. *Environ. Monit. Assess.* 192, 1–18.

Dias, A., Kurian, S., and Thyapurath, S. (2020a). Influence of environmental parameters on bio-optical characteristics of colored dissolved organic matter in a complex tropical coastal and estuarine region. *Estuar. Coast. Shelf Sci.* 242:106864. doi: 10.1016/j.ecss.2020.106864

Dias, A. B., Thayapurath, S., Sahay, A., and Chauhan, P. (2017). Contrasting characteristics of colored dissolved organic matter of the coastal and estuarine waters of Goa during summer. *Indian J. Geo Mar. Sci.* 46, 860–870.

D'Sa, E. J., Miller, R. L., and Del Castillo, C. (2006). Bio-optical properties and ocean color algorithms for coastal waters influenced by the Mississippi River during a cold front. *Appl. Opt.* 45, 7410–7428. doi: 10.1364/ao.45.007410

Falkowski, P., Scholes, R. J., Boyle, E. E. A., Canadell, J., Canfield, D., Elser, J., et al. (2000). The global carbon cycle: a test of our knowledge of earth as a system. *Science* 290, 291–296. doi: 10.1126/science.290.5490.291

Gieskes, W. W. C., Kraay, G. W., Nontji, A., and Setiapermana, D. (1988). Monsoonal alternation of a mixed and a layered structure in the phytoplankton of the euphotic zone of the Banda Sea (Indonesia): a mathematical analysis of algal pigment fingerprints. *Netherlands J. Sea Res.* 22, 123–137. doi: 10.1016/0077-7579(88)90016-6

Grasshoff, K., Kremling, K., and Ehrhardt, M. (1999). *Methods of Sea-Water Analysis*, 3rd Edn. Weinheim: WILEY-VCH.

Hansell, D. A., Carlson, C. A., Repeta, D. J., and Schlitzer, R. (2009). Dissolved organic matter in the ocean: a controversy stimulates new insights. *Oceanography* 22, 202–211. doi: 10.5670/oceanog.2009.109

Hansell, D. A., Carlson, C. A., and Suzuki, Y. (2002). Dissolved organic carbon export with North Pacific Intermediate Water formation. *Glob. Biogeochem. Cycles* 16, 7–1–7–8. doi: 10.1029/2000gb001361

Hedges, J. I. (1992). Global biogeochemical cycles: progress and problems. *Mar. Chem.* 39, 67–93. doi: 10.1016/0304-4203(92)90096-s

Helms, J. R., Stubbins, A., Ritchie, J. D., Minor, E. C., Kieber, D. J., and Mopper, K. (2008). Absorption spectral slopes and slope ratios as indicators of molecular weight, source, and photobleaching of chromophoric dissolved organic matter. *Limnol. Oceanogr.* 53, 955–969. doi: 10.4319/lo.2008.53.3.0955

Huguet, A., Vacher, L., Relexans, S., Saubusse, S., Froidefond, J. M., and Parlanti, E. (2009). Properties of fluorescent dissolved organic matter in the Gironde Estuary. *Org. Geochem.* 40, 706–719. doi: 10.1016/j.orggeochem.2009.03.002

Jeffrey, S. W., Vesk, M., and Mantoura, R. F. (1997). Phytoplankton pigments: windows into the pastures of the sea. *Nat. Resour.* 33, 14–29.

Jerlov, N. G. (1976). *Marine optics, Elsevier Oceanography Series 14*. Amsterdam: Elsevier Scientific Publishers.

Krishnakumari, L., Bhattathiri, P. M. A., Matondkar, S. G. P., and John, J. (2002). Primary productivity in Mandovi-Zuari estuaries in Goa. *J. Mar. Biol. Assoc. India* 44, 1–13.

Kurian, S., Roy, R., Repeta, D. J., Gauns, M., Shenoy, D. M., Suresh, T., et al. (2012). Seasonal occurrence of anoxygenic photosynthesis in Tillari and Selaulim reservoirs, Western India. *Biogeosciences* 9, 2485–2495. doi: 10.5194/bg-9-2485-2012

Mackey, M. D., Mackey, D. J., Higgins, H. W., and Wright, S. W. (1996). CHEMTAX-a program for estimating class abundances from chemical markers: application to HPLC measurements of phytoplankton. *Mar. Ecol. Prog. Ser.* 144, 265–283. doi: 10.3354/meps144265

Madondkar, S. G. P., Gomes, H., Parab, S. G., Pednekar, S., and Goes, J. I. (2007). "Phytoplankton diversity, biomass, and production," in *The Mandovi and Zuari Estuaries*, eds S. R. Shetye, M. D. Kumar, and D. Shankar (Dona Paula: National Institute of Oceanography), 67–82.

Menon, H. B., Sangekar, N. P., Lotliker, A. A., and Vethamony, P. (2011). Dynamics of chromophoric dissolved organic matter in Mandovi and Zuari estuaries—A study through in situ and satellite data. *ISPRS J. Photogramm. Remote Sens.* 66, 545–552. doi: 10.1016/j.isprsjprs.2011.02.011

Mopper, K., and Kieber, D. J. (2002). "Photochemistry and the cycling of carbon, sulfur, nitrogen and phosphorus," in *Biogeochemistry of Marine Dissolved Organic Matter*, Vol. 455, eds D. A. Hansell and C. A. Carlson (San Diego, CA: Academic Press).

Nelson, N. B., and Siegel, D. A. (2002). "Chromophoric DOM in the open ocean," in *Biogeochemistry of Marine Dissolved Organic Matter*, eds D. A. Hansell and C. A. Carlson (San Diego, CA: Academic Press), 547–578. doi: 10.1016/b978-012323841-2/50013-0

Nelson, N. B., and Siegel, D. A. (2013). The global distribution and dynamics of chromophoric dissolved organic matter. *Annu. Rev. Mar. Sci.* 5, 447–476. doi: 10.1146/annurev-marine-120710-100751

Nelson, N. B., Siegel, D. A., Carlson, C. A., Swan, C., Smethie, W. M. Jr., and Khatiwala, S. (2007). Hydrography of chromophoric dissolved organic matter in the North Atlantic. *Deep Sea Res. Part I Oceanogr. Res. Pap.* 54, 710–731. doi: 10.1016/j.dsr.2007.02.006

Pradhan, U. K., Wu, Y., Shirodkar, P. V., and Zhang, J. (2015). Seasonal nutrient chemistry in mountainous river systems of tropical Western Peninsular India. *Chem. Ecol.* 31, 199–216. doi: 10.1080/02757540.2014.961438

Prézelin, B. B., Hofmann, E. E., Mengelt, C., and Klinck, J. M. (2000). The linkage between Upper Circumpolar Deep Water (UCDW) and phytoplankton assemblages on the west Antarctic Peninsula continental shelf. *J. Mar. Res.* 58, 165–202. doi: 10.1357/002224000321511133

Ruescas, A. B., Hieronymi, M., Mateo-Garcia, G., Koponen, S., Kallio, K., and Camps-Valls, G. (2018). Machine learning regression approaches for colored dissolved organic matter (CDOM) retrieval with S2-MSI and S3-OLCI simulated data. *Remote Sens.* 10:786. doi: 10.3390/rs10050786

Shanmugam, P. (2011). A new bio-optical algorithm for the remote sensing of algal blooms in complex ocean waters. *J. Geophys. Res. Oceans* 116, 1–12. doi: 10.1016/b978-0-12-804644-9.00001-x

Shetye, S. R., DileepKumar, M., and Shankar, D. (2007). *The Mandovi and Zuari Estuaries*. Dona Paula: National Institute of Oceanography.

Shynu, R., Rao, V. P., Kessarkar, P. M., and Rao, T. G. (2012). Temporal and spatial variability of trace metals in suspended matter of the Mandovi estuary, central west coast of India. *Environ. Earth Sci.* 65, 725–739. doi: 10.1007/s12665-011-1119-4

Shynu, R., Rao, V. P., Sarma, V. V. S. S., Kessarkar, P. M., and ManiMurali, R. (2015). Sources and fate of organic matter in suspended and bottom sediments of the Mandovi and Zuari estuaries, western India. *Curr. Sci.* 108, 226–238.

Soomets, T., Uudeberg, K., Jakovels, D., Brauns, A., Zagars, M., and Kutser, T. (2020). Validation and Comparison of Water Quality Products in Baltic Lakes Using Sentinel-2 MSI and Sentinel-3 OLCI Data. *Sensors* 20:742. doi: 10.3390/s20030742

Stedmon, C. A., Markager, S., and Bro, R. (2003). Tracing dissolved organic matter in aquatic environments using a new approach to fluorescence spectroscopy. *Mar. Chem.* 82, 239–254. doi: 10.1016/s0304-4203(03)00072-0

Toming, K., Kutser, T., Laas, A., Sepp, M., Paavel, B., and Nõges, T. (2016). First experiences in mapping lake water quality parameters with Sentinel-2 MSI imagery. *Remote Sens.* 8:640. doi: 10.3390/rs8080640

Uitz, J., Claustre, H., Morel, A., and Hooker, S. B. (2006). Vertical distribution of phytoplankton communities in open ocean: an assessment based on surface chlorophyll. *J. Geophys. Res. Oceans* 111:08005.

Upadhyay, S., and Gupta, R. S. (1995). The behaviour of aluminium in waters of the Mandovi estuary, west coast of India. *Mar. Chem.* 51, 261–276. doi: 10.1016/0304-4203(95)00058-5

Vantrepotte, V., Danhiez, F. P., Loisel, H., Ouillon, S., Mériaux, X., Cauvin, A., et al. (2015). CDOM-DOC relationship in contrasted coastal waters: implication for DOC retrieval from ocean color remote sensing observation. *Opt. Express* 23, 33–54. doi: 10.1364/oe.23.000033

Veerasingam, S., Vethamony, P., ManiMurali, R., and Babu, M. T. (2015). Sources, vertical fluxes and accumulation of petroleum hydrocarbons in sediments from the Mandovi estuary, west coast of India. *Int. J. Environ. Res.* 9, 179–186.

Werdell, P. J., and Bailey, S. W. (2005). An improved in-situ bio-optical data set for ocean color algorithm development and satellite data product validation. *Remote Sens. Environ.* 98, 122–140. doi: 10.1016/j.rse.2005.07.001

Xu, J., Fang, C., Gao, D., Zhang, H., Gao, C., Xu, Z., et al. (2018). Optical models for remote sensing of chromophoric dissolved organic matter (CDOM) absorption in Poyang Lake. *ISPRS J. Photogramm. Remote Sens.* 142, 124–136. doi: 10.1016/j.isprsjprs.2018.06.004

Zhao, J., Cao, W., Xu, Z., Ai, B., Yang, Y., Jin, G., et al. (2018). Estimating CDOM concentration in highly turbid estuarine coastal waters. *J. Geophys. Res. Oceans* 123, 5856–5873. doi: 10.1029/2018jc013756

Zsolnay, A., Baigar, E., Jimenez, M., Steinweg, B., and Saccomandi, F. (1999). Differentiating with fluorescence spectroscopy the sources of dissolved organic matter in soils subjected to drying. *Chemosphere* 38, 45–50. doi: 10.1016/s0045-6535(98)00166-0

Conflict of Interest: The authors declare that the research was conducted in the absence of any commercial or financial relationships that could be construed as a potential conflict of interest.

frontiers in Marine Science

ORIGINAL RESEARCH
published: 01 July 2021
doi: 10.3389/fmars.2021.669374

COVID-19 Impacts on Beaches and Coastal Water Pollution at Selected Sites in Ecuador, and Management Proposals Post-pandemic

Franklin I. Ormaza-González[1], Divar Castro-Rodas[2] and Peter J. Statham[3]*

[1] Escuela Superior Politécnica del Litoral (Faculty of Maritime Engineering and Marine Sciences, FIMMC), ESPOL Polytechnic University, Guayaquil, Ecuador, [2] Centro Nacional de Acuicultura e Investigaciones Marinas, Escuela Superior Politécnica del Litoral, Guayaquil, Ecuador, [3] School of Ocean and Earth Science, University of Southampton, Southampton, United Kingdom

OPEN ACCESS

Edited by:
Christine Lee, NASA Jet Propulsion Laboratory (JPL), United States

Reviewed by:
Annalaura Mancia, University of Ferrara, Italy
Dan Sousa, NASA Jet Propulsion Laboratory (JPL), United States
Emily Ann Smail, University of Maryland, College Park, United States

***Correspondence:**
Franklin I. Ormaza-González
formaza@espol.edu.ec

Specialty section:
This article was submitted to Marine Pollution, a section of the journal Frontiers in Marine Science

Received: *18 February 2021*
Accepted: *20 May 2021*
Published: *01 July 2021*

Citation:
Ormaza-González FI, Castro-Rodas D and Statham PJ (2021) COVID-19 Impacts on Beaches and Coastal Water Pollution at Selected Sites in Ecuador, and Management Proposals Post-pandemic. Front. Mar. Sci. 8:669374. doi: 10.3389/fmars.2021.669374

The COVID-19 pandemic has obliged Governments all around the world to implement confinement and social distancing measures. Leisure and business activities on beaches and in ports have restricted direct and indirect contamination from, for example, plastics, hydrocarbon spillage, microbiological loads, and noise levels. This has led to temporarily improved environmental conditions, and the beaches having conditions closer to Marine Protected Areas. Here we report some impacts that have been studied using local surveys and qualitative observations in Ecuador at the popular beaches and ports of Salinas, Manta, and Galapagos. Satellite data support this information. Online surveys were carried out at critical moments of the pandemic: May (15th) and just after when measures were relaxed a little, but within lockdown in July (21st) 2020. Respondents were asked to compare conditions before and during the pandemic lockdown. Most (97–99%) suggested that beaches had significantly improved from visual observations during confinement. On a scale from 1 (worst) to 5 (best), the beaches of Salinas and Manta respectively were rated 2.2 and 2.8 (less than acceptable) before quarantine, and 4.5 and 4.3 after; results from the second survey (after 18 weeks of restrictions) were much the same. Replies from Galapagos showed a similar trend but with less marked differences. In addition to the beaches having less plastic and garbage, more fish, and large marine organisms, including humpback whales (*Megaptera novaeangliae*), dolphin (bottlenose, *Tursiops truncatus),* and manta ray (*Manta* sp.) were observed near to shore. At Galapagos beaches, turtles, sea lions, and sharks were observed many more times than pre COVID. Quantitative satellite data on Chlorophyl and attenuation coefficient (Kd, 490 nm) support the qualitative survey data that there is an improvement in coastal environment quality. Here we recommend that this unique opportunity resulting from the COVID-19 pandemic is used locally, regionally and globally to construct baseline data sets that include information on physical, chemical, biological, and microbiological factors in coastal zones. These parameters can then help establish

an effective Coastal Zone Management Plan based on beach description and quality (water standards, noise pollution), as well as the human dimension (tourist load, cultural heritage, and economic value indices). This data and information gathering ideally should be done before the beaches become more heavily used again as the pandemic recedes.

Keywords: COVID-19, confinement, beaches, pollution, noise, tourism, ecuador

INTRODUCTION

"As the COVID-19 pandemic sweeps through the world, we must reassess the principles that guide our individual and collective responses and the way we operate in society. In the face of crisis, we must lead with science and humanity," Nat Cancer (2020) (No Author, 2020a) recently asserted. At the end of April 2021, the COVID-19 pandemic globally had 148,894,033 confirmed cases and 3,139,309 deaths (Johns Hopkins Coronavirus Resource Center, 2021), and these figures are only going to increase even though vaccinations have started in many countries. In Ecuador, cases and deaths (both probably underestimated) are respectively 375,329 and 18,389 (28 April 2021[1]), which means 2.2% of its population have been infected and 0.11% has died. Cases are rapidly increasing once more in April 2021, and a further partial lockdown is underway.

National economies have been dramatically hit by the pandemic as a result of (1) air, water, and road transportation very limited or completely prohibited in some places, (2) many public utilities closed such as parks, beaches, and museums, and (3) very low consumer demands for products and services. Bloom et al. (2018) warn that the impacts of the pandemic on economies can be sizable over short and long terms, at both individual and societal levels. Nightmarish economic impacts in 26 countries include a possible drop in sales of 50–75% relative to pre-COVID conditions (De Vito and Gómez, 2020). One of the most affected activities is tourism. According to UNWTO (2020), the economic decline since the arrival of COVID-19 is around 52–78%, with estimated losses just in Q1 2020 of around 80 billion US$, and for the whole year 100 to 120 billion US$. In Ecuador, the tourism sector could lose 540 million US$ in 3 months of standstill (Statista, 2020), with marine and coastal tourism one of the most affected activities. The beach zones of Salinas, Manta, and Galapagos in Ecuador would be expected to be most impacted. It is accepted that tourism exerts strong pressures on natural systems and directly or indirectly contributes to pollution (Navarro, 2019), and excessive demand on coastal benthic and pelagic fisheries (Budzich-Tabor et al., 2014).

Those impacts expected to decrease over the pandemic include plastic (see Li et al., 2016), or any type of debris, and increased microbiological loads due to beach tourism (Natural Resources Defense Council [NRDC], 2014). Another example is noise contamination, which can impact the individual and social behavior of adult fish and mammals as well as metabolism, recruitment, and overall health of marine ecosystems (Peng et al., 2015). Anthropogenic noise has become a real threat to the coastal environment and ecosystem health. Specific examples of impacts include those on turtle behavior and ecology (Samuel et al., 2005), and noise pollution from boat engines disturbing all fish species and particularly marine mammals, sea birds, and turtles (Hazel et al., 2007; Ketten, 2008; Leduc et al., 2021). Artificial light from human activities can also affect multiple trophic levels, by deterring fish (Stocker, 2007; Becker et al., 2013; Bolton et al., 2017) and impacting the hatchling behavior of turtles (Kamrowski et al., 2012; Thums et al., 2016). Noise and illumination (energy contamination, GESAMP, 1991) have been shown to be important even in isolated places like Galapagos, where recently positive impacts of reduced energy pollution have been reported (Jiménez-Uzcátegui, 2020) with populations of seabirds and penguins recovering.

An important aspect of plastic contamination is the exponential increase in the use of bottled water since the outbreak of COVID-19 in countries such as Ecuador, because access to good quality tap water is often restricted as Ogunbode et al. (2021) has reported for developing or underdeveloped countries. The resultant increase in discarded plastic containers will keep growing (Eljarrat, 2020), especially in places with high tourism activity including for Ecuador Galapagos, Salinas and Manta. The use of bottled water is particularly intense on the Galapagos islands, where the potable water is of poor quality (Grube et al., 2020). An additional source of plastic over the COVID-19 pandemic, is masks and gloves that are frequently mandatory. Their random disposal generates a new type of waste that is beyond conventional sanitary disposal management, which is poor and inappropriate for these new plastics (Calma, 2020), and adds to plastic bottle contamination in coastal water zones (Hyde, 2020). Many measures to help disposal of single-use plastic materials have been postponed, so there is potential for increases in plastic pollution during the pandemic (da Costa, 2021).

Despite the above problems, the COVID-19 pandemic measures of confinement and social distancing are producing some positive impacts (at least temporarily) on the environment, such as less atmospheric pollutant gases (CO2, SO2, NO2, etc.). Rosenbloom and Markard (2020) report that air pollution and emissions of greenhouse gases are notably decreasing, while Le Quéré et al. (2020) have reported 17% less daily emissions of CO2 as well as reductions in other gases; see also Ju et al. (2021). Other intrusive pollution types (e.g., noise, waste) in the atmosphere and biosphere (Arora et al., 2020), have also decreased significantly in some populated areas due to reductions in transportation, electricity usage, industrial production (Rosenbloom and Markard, 2020), leisure and fishing activities.

The reduction in contamination on beaches and in coastal water has been seen globally where quarantine measures exist. Beaches in Acapulco (Mexico), Barcelona (Spain), and Salinas

[1]https://www.who.int/countries/ecu/

(Ecuador) now have much more transparent and cleaner waters (Zambrano-Monserrate et al., 2021); the largest lake of India (Vembanad) has around 16% less suspended solids than before the pandemic (Yunus et al., 2020). Also, anecdotal reports in social media talk of marine mammals close to beaches, perhaps in response to the considerable reduction of noise levels. Therefore, in general, environmental conditions have at least temporarily improved (Yunus et al., 2020), and beaches have moved toward the status of temporary Marine Protected Areas. However, there is still very limited information on changes in environmental quality in South American coastal waters that feeds into this more global view.

Whilst there has been an improvement in environmental conditions, perceptions of people who are impacted day by day in places where the economy depends on tourism or fishing activities are not well known. Additionally, we need to have a scientific baseline of data and information that can be combined with public perceptions to articulate a proper tourism, coastal fishing and pollution management plan post the COVID-19 pandemic. The work reported here seeks to provide information and priorities based on environmental qualitative information that is supported by satellite quantitative data at three main Ecuadorian beaches in Salinas, Manta, and Galapagos. We think this is a unique opportunity globally to create a scientific baseline at a time of reduced environmental impact, as beaches and near-shore waters have taken on temporary features of Protected Marine Areas. Such baseline information can help initiate comprehensive management programs (Partelow et al., 2015) for the future, and recommendations stemming from the present study are proposed below.

MATERIALS AND METHODS

At the time of full lockdown and strict restrictions (12th March to 12th September 2020), conventional environmental survey techniques were not possible due to restricted access, lack of staff, and minimal (if any) laboratory facilities in Ecuador. Therefore, online surveys using web-based applications were carried out. Recently, Torrentira (2020) has validated the use of such online interviews under pandemic conditions, and both Abir et al. (2020) and Steele et al. (2021) have successfully used the on-line methodology for surveys under lockdown restrictions.

The main objective of the surveys was to determine if the perceived quality of the beaches and adjacent waters had improved post, relative to pre, COVID-19 lockdown. Three sets of questions were prepared, one for each location, with those from Salinas and Manta being practically the same, except for one question, while the Galapagos questions were slightly different (see **Supplementary Material**). The differences reflected variations between the specific locations. The Galapagos islands are at the core of one of the most important marine reserves in the world, and in general its population is much more aware of environmental conditions and the marine species present. Additionally local people rely almost 100% on sustainable tourism and are therefore well educated in environmental matters.

The data obtained are from the visual observation of beaches and nearshore aquatic wildlife. The first survey was a cross-sectional type (see Setia, 2016) that reported opinions and sightings during May (from 15th) 2020. At this time national lockdown restrictions obliged people to be at home most of the time, beaches were fully closed, no travel between cities was allowed, police, and military guarded the streets and COVID-19 cases and deaths were increasing rapidly. The surveys were carried out over a time window of 76 h, using a form modified from a Google template (Google Forms: Free Online Surveys for Personal Use). The surveys were targeted to have confidence and interval levels of 95 and 5.16% respectively, following the approach of Taherdoost (2017) for example.

The questionnaires (see **Supplementary Material** – SM) were slightly different for each studied site, taking into consideration the main activities at each site and main types of employment. To examine reproducibility, a second round of surveys was carried out over a period of 7 days, 2 months later (from July 21st), using the same form and protocol. During this second survey, some restrictions were eased, for example you could move from city to city at certain times of the day. Observations reported are from respondents living adjacent to the beach zones. Collection of data from face-to face or/and focus group interviews was not possible, because even though the lockdown and restrictions were eased, it was difficult to visit the beaches, and people showed reluctance to talk due to stress from the social confinement and pandemic (see Arnsten, 2020), and because COVID-19 cases were increasing again. This reluctance still exists today (April 2021), as the pandemic situation has worsened.

Both surveys used Instagram, Twitter, Facebook, and WhatsApp to contact a range of individuals living in the named cities close to or in front of the beaches and water's edge, and who also had links to seaside activities including tourism and academic research, as well as normal citizens. The survey form (see **Supplementary Material**) sought information on the individual's observations, knowledge of local beaches and water quality, as well as views on improving environmental quality and tourism. Also, an observer in a quarantined boat in Galapagos reported sightings of turtle, sharks, and other aquatic species from 15 March to 30th April. In two questions (8 and 9) a numerical scale was used to indicate the extent of changes seen going from 1 (no change) to 5 (much change/improvement). Two of the authors live in Salinas and have videos and photographs that give qualitative information about beaches and shore water aquatic species activities (see **Supplementary Material**). The surveys were designed in a very simple way to encourage participation, as they could be completed in less than 5 min.

In order to support the qualitative surveys, quantitative data and information from the NASA satellite instruments Terra (EOS AM-1) and Aqua (EOS PM-1), which are payloads for the "Moderate Resolution Imaging Spectroradiometer – MODIS" (NASA, 2019), were used to measure temporal and spatial

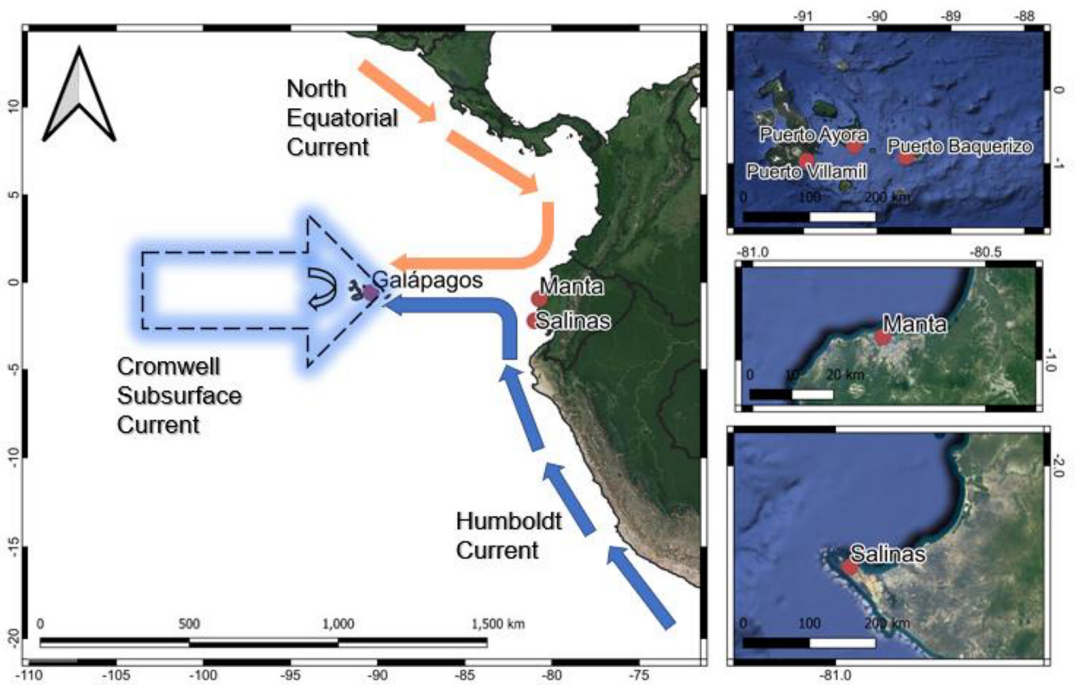

FIGURE 1 | Data collection sites and associated surface current systems.

changes of chlorophyll and the diffuse attenuation coefficient K_d (490 nm), over the timescale of the study.

Study Area

The study sites of Salinas, Manta, and two ports of Galápagos (Puerto Baquerizo Moreno and Puerto Ayora; **Figure 1**) were chosen for local interviews and observations. COVID-19 cases during the first interview period were increasing at all survey sites, deaths were rapidly escalating to dozens per day, and the population was frightened as elsewhere in the world. In Galapagos, even though it is a relatively isolated site, cases were also increasing. Salinas (centered on 2°12′S, 80°56′W) is the most popular and visited beach on the Ecuadorian coast; its economy depends almost completely on tourism, with its diverse beaches ranging from cliffs to fine sand beaches and there are safe swimming areas. However, it has one of the most plastic polluted beaches in Ecuador (Mestanza-Ramón et al., 2019a). Manta (0°57′S, 80°42′W) is the second most important port and the fourth largest economic center in Ecuador. The port takes a variety of large tourist cruisers, industrial vessels, artisanal fishing craft, and cargo ships, and is the most important fishing port in Ecuador (second largest tuna port in the world; Martínez-Ortiz et al., 2015). According to Mestanza-Ramón et al. (2019a) its wide, long beaches are less contaminated by plastic than in Salinas. In the Galapagos Islands Puerto Ayora (0°45′S, 90°18′W) and Puerto Baquerizo Moreno (0°54′S, 89°36′W) are the main harbors, where the economy is solely based on foreign tourism. The islands of Galapagos are a protected Marine Reserve of 133,000 km^2, one of the biggest and most important in the world (Caryl-Sue et al., 2011; Paladines and Chuenpagdee, 2015) and the first World Heritage Site named by UNESCO (Walsh and Mena, 2013) due to its unique ecosystem; Mestanza-Ramón et al. (2019b) have found that the beaches of Galapagos are some of the cleanest in Ecuador. It is noticeable that the three locations above have poor or no domestic water treatment plants. These sites are covered within a recent study (Gaibor et al., 2020) who reported that the southern and central beaches are most affected by the anthropogenic deposition of debris (plastic, paper, cigarette butts, metal, glass, others; plastics represent around 60% of the total debris) that are of local origin. In this study, the clean characteristics of Galapagos beaches are noted as Mestanza-Ramón et al. (2019a) also report.

The study sites provide differing coastal environments where any impacts resulting from COVID-19 measures can be followed. Salinas-Santa Elena (Photo 1, **Supplementary Material**) is one of the most visited beaches in southern Ecuador, and around 400 thousand tourists arrive in the Province between January and June. Half of these come to Salinas, where its baseline population is only around 70 thousand people (Castro-Rodas, 2016; Gad-Salinas, 2020). Manta is a city located on the central coast (**Figure 1**) with 230 thousand inhabitants (Instituto Nacional de Estadística y Censos (INEC), 2010), and is a tourist destination, that is visited by beachgoers from all over Ecuador. As a result of the tuna fishing industry and other activities its inshore waters have different anthropogenic contamination sources to the other sites. The Galapagos Islands (**Figure 1**) have a local population of around 30 thousand people, but it is a popular foreign tourist destination. Thus, in 2019, 271 thousand tourists arrived in the Galapagos protected areas (PNG, 2020), and inefficient planning

TABLE 1 | Results from Salinas and Manta.

Place		Salinas			Manta		
Surveys		Run 1 (*n* = 69)	Run 2 (*n* = 75)	Total (*n* = 144)	Run 1 (*n* = 36)	Run 2 (*n* = 52)	Total (*n* = 88)
Question	Answer	%	%	%	%	%	%
Q1	Yes	98.6	98.7	98.6 (2)	86.1	86.5	86.4 (7)
	No	1.4	1.3	1.4 (2)	13.9	13.5	13.6 (7)
Q2	It is cleaner	44.6	49.6	47.1 (8)	43.8	43.0	43.3 (10)
	There are less plastic	26.8	29.2	28.0 (7)	35.9	34.4	35.0 (10)
	More transparent	28.6	21.2	24.9 (7)	20.3	22.6	21.7 (9)
Q3	Yes	97.1	96.0	96.5 (3)	97.2	96.2	96.6 (4)
	No	2.9	4.0	3.5 (3)	2.8	3.8	3.4 (4)
Q4	Yes	88.4	89.3	88.9 (5)	91.7	92.3	92.0 (6)
	No	11.6	10.7	11.1 (5)	8.3	7.7	8.0 (6)
Q5	Fish in general	62.5	61.8	62.1 (8)	52.9	60.3	57.1 (10)
	Sharks	1.3	2.2	1.8 (2)	0.0	0.0	0.0
	Manta-ray	5.0	4.5	4.7 (3)	3.9	2.9	3.4 (4)
	Dolphins	20.0	19.1	19.5 (6)	29.4	23.5	26.1 (9)
	Whales	6.3	7.9	7.1 (4)	11.8	11.8	11.8 (7)
	Others	5.0	4.5	4.7 (3)	2.0	1.5	1.7 (3)
Q6	Contamination, garbage, new cases of COVID-19 (Salinas)/Garbage, insalubrity, new cases of COVID-19 (Manta)						
Q7	Yes	92.8	90.7	91.7 (4)	91.7	90.4	90.9 (6)
	No	7.2	9.3	8.3 (4)	8.3	9.6	9.1 (6)
Q8	Average	2.2	2.2	2.2	2.8	3.0	2.91
Q9	Average	4.5	4.4	4.5	4.3	4.3	4.29
Q10	Yes	23.2	–	23.2 (7)	61.1	–	61.1 (10)
	No	76.8	–	76.8 (7)	38.9	–	38.9 (10)
Q11	Academic	31.9	32.0	31.9 (8)	0.0	3.8	2.3 (4)
	Research	2.9	4.0	3.5 (3)	2.8	1.9	2.3 (4)
	Tourism	11.6	10.7	11.1 (5)	8.3	11.5	10.2 (6)
	General citizen	53.6	53.3	53.5 (8)	88.9	82.7	85.2 (7)

Run 1 (15th May) and Run 2 (21st July), 2020. Numbers in brackets are confidence interval (±).

and management of the local marine environment have been reported (Walsh and Mena, 2016; Mestanza-Ramón et al., 2019b), which in turn is exerting high pressure on marine resources and leading to contamination (Pecot and Ricaurte-Quijano, 2019; Ricaurte-Quijano et al., 2019), including micro plastics. Given the high volume of visitors under normal conditions, these environments should provide good examples of the impact of reduced human pressures caused by the COVID pandemic.

RESULTS

The first survey was kept online for up to 72 h; and the average times it took participants to complete them were 4.7, 3.5, 3, and 1.9 min for Salinas, Manta, and Galapagos (San Cristobal Y Santa Cruz islands) respectively. The number of respondents from the total population of these sites (roughly 330,000 people) of the study sites was 280. Thus, at a 95% confidence level, the confidence interval is around ± 5.8% according to Taherdoost (2017). The confidence interval for the whole sample per answer varied between ±2 and ±5.8 with 95% confidence. The confidence interval averages for Manta, Salinas, and Galapagos were ±5, ±7, and ±10% respectively. In the first surveys for Salinas, Manta (**Table 1**) and Galapagos (**Table 2**, Puerto Ayora and San Cristobal), 69, 36, and 15 people respectively responded to the survey, with >90% being returned within 24 h. In the second run, there were similar average form completion times with 75, 88, and 32 forms returned respectively, and so total responses for each of the beaches in turn were 144, 89, and 47. Response times in Galapagos were slower in both runs, perhaps due to the internet services that are sometimes poor (Walsh and Mena, 2013).

Responses to the question (see **Supplementary Material**) "has the beach and water visually changed" for Salinas, Manta and Galapagos respectively during and after the lockdowns, were 99, 86, and 73% "Yes," and 1, 14, and 27% "No"; while in the second run they were >99, 87, and 75% "yes," and for "no" 1, 13, and 25% respectively. The respondents said this positive change was because the beaches were free of people over a period of approximately 5 months. In Salinas, 47% said that beaches and water are now cleaner (see **Supplementary Material**

TABLE 2 | Results from Galápagos.

Place	Galápagos						
Surveys		Run 1 (*n* = 15)	Run 2 (*n* = 32)	Total (*n* = 47)	Run 1 (*n* = 15)	Run 2 (*n* = 32)	Total (*n* = 47)
Questions	Answer	Amount	Amount	Amount	%	%	%
Q1	Yes	11	24	35	73.3	75.0	74.5 (12)
	No	4	8	12	26.7	25.0	25.5 (12)
Q2	Average	4.05	3.55	3.8			
Q3	Yes	7	13	20	46.7	40.6	42.6 (14)
	No	8	19	27	53.3	59.4	57.4 (14)
Q4	Average	3.94	3.28	3.61			
Q5	Yes	9	22	31	60.0	68.8	66.0 (12)
	No	6	10	16	40.0	31.3	34.0 (12)
Q6	Yes	10	19	29	66.7	59.4	61.7 (12)
	No	5	13	18	33.3	40.6	38.3 (12)
Q7	Average	4.1	3.24	3.67			
Q8	Yes	11	19	30	73.3	59.4	63.8 (14)
	No	4	13	17	26.7	40.6	36.2 (14)
Q9	Yes	1	19	20	6.7	59.4	42.6 (14)
	No	1	29	30	6.7	90.6	63.8 (14)
Q10	Yes						
	No	1	29	30	6.7	90.6	63.8 (14)
Q11	Tourism	12	20	32	80.0	62.5	68.1 (13)
	Academy	0	4	4	0.0	12.5	8.5 (8)
	Merchant	3	5	8	20.0	15.6	17.0 (11)
	Fishery	0	3	3	0.0	9.4	6.4 (7)

Run 1 (15th May) and Run 2 (21st July), 2020. Numbers in brackets are confidence interval (±).

Photos), 28% said there was less plastic, and 25% that the water was more transparent (**Figure 2**). For Manta beach the answers (**Figure 3**) were 43, 35, and 22% in the same order. In July, the answers were very close to the earlier survey in both places (see **Tables 2**, **3**). In Galapagos, 47% (Puerto Ayora) and 41% (Puerto Baquerizo Moreno) of respondents deem there is less plastic on beaches and 60 and 69% think the water is much clearer than before the pandemic (**Figure 4**), for the first and second survey rounds, respectively. Quantification of plastic volume or weight was not possible, because access to beaches was not allowed during the strict lockdown. The obvious plastic garbage on Salinas beaches (macroplastics: >5 mm) has been monitored by Ormaza-González and Vera-Mosquera (2021) since June 2019 every fortnight at least, and report mass of plastic for a specific area of 100 m^2 (see **Supplementary Material** Photos 2, 3). Macroplastics typically represented 80–100% of total debris, and weighed 500–600 g, for an accumulation period of 7–14 days at station D (2°12′S, 80°59.9′ W). These types of plastic are reported to be of local origin (Gaibor et al., 2020) and are largely from fishing, beach and coastal tourism activities and untreated wastewater. The chemistry of the plastics has not been studied in detail, but visual inspection indicates: polyethylene terephthalate (PET, carbonated drink bottles, jars, microwavable packaging etc.), polyethylene (PE, wide range of uses including bags, plastic bottles), High-density polyethylene (HDPE, detergent bottles, milk jugs, etc.), polypropylene (PP, bottle caps, drinking straws, etc.), polyester (PES, fibers, cord, fishing nets, etc.). Natural materials including, wood, charcoal and seeds, are also found.

Over 96% of surveyed people in both surveys and all places believed that there had been no noise pollution during confinement, which is beneficial to the marine ecosystem, as well as residents. Most surveyed people during the first run (88 and 92% respectively for Salinas and Manta) had seen increased marine organism activity during the quarantine period. After 5 months, similar percentages (89 and 94%) were recorded. These increases most probably reflect the lower impact of humans and there is no noise on the beach or at the seashore. In Galapagos, the observer reported this is particularly true for turtles and sharks, which have been observed frequently during this period. In Salinas, in May 62 and 20% (**Figure 2**) of surveyed people had seen more fish (sardines, mackerel, etc.) and dolphins respectively, close to the beach; in July, the percentages were 62 and 19% in the same order. While in Manta (**Figure 3**), in May 53 and 30%, in July 60 and 23%, of people saw the same change, but also between 18 and 16% of respondents (in both places during May and July) saw whales (humpback and whale-sharks), turtles, manta rays, and other large species. These marine species generally do not get close to the beach, whilst many videos on the web and social media have shown the usual whale-sharks and orcas offshore along the Ecuadorian coast (Zambrano-Alvarado, 2020; see **Supplementary Material**). In Galapagos (**Figure 4**), where sea lions, turtles and shark are observed quite commonly, between 73 and 59% of respondents over both surveys reported an important increase in sightings, scoring between 3 and 4 on a scale from 1 (no change) to 5 (a lot of sightings).

Respondents gave an overall rating for the quality of Salinas beach before and after the 10 weeks of quarantine, as 2.23 and 4.48 respectively on a scale from 1 (worst) to 5 (best). The perceived improvement is clear to see. In Manta, the categorization was similar, 2.83 before and 4.33 after. In July, 18 weeks later, survey results were practically the same in both places (2.24 and 4.44; 2.98 and 4.25). Respondents deemed overall that the beaches had improved their quality in every sense, even in Galapagos where beaches are generally in very good condition, 41–47% of respondents indicated a noticeable quality improvement.

Galapagos, Salinas, and Manta residents in both surveys were afraid that if beaches were suddenly opened, garbage, and noise contamination would increase, and these conditions may contribute to a new pandemic outbreak. At the same time, 95, 90, and 94% respectively of all surveyed people agreed that tourism should be reactivated carefully to revive the local economy, while avoiding a new pandemic outbreak. People in Galapagos agreed with taking scientific data and information to manage tourism properly. A large fraction of all respondents in Salinas and Galapagos (77 and 66%) were unaware of the existence or not of wastewater treatment plants in the area, while in Manta nearly half assumed their presence. Finally, most of the people surveyed in Salinas (**Figure 2**) were general citizens (54–53%), followed by 22–32% with an academic background, and the rest researchers and people

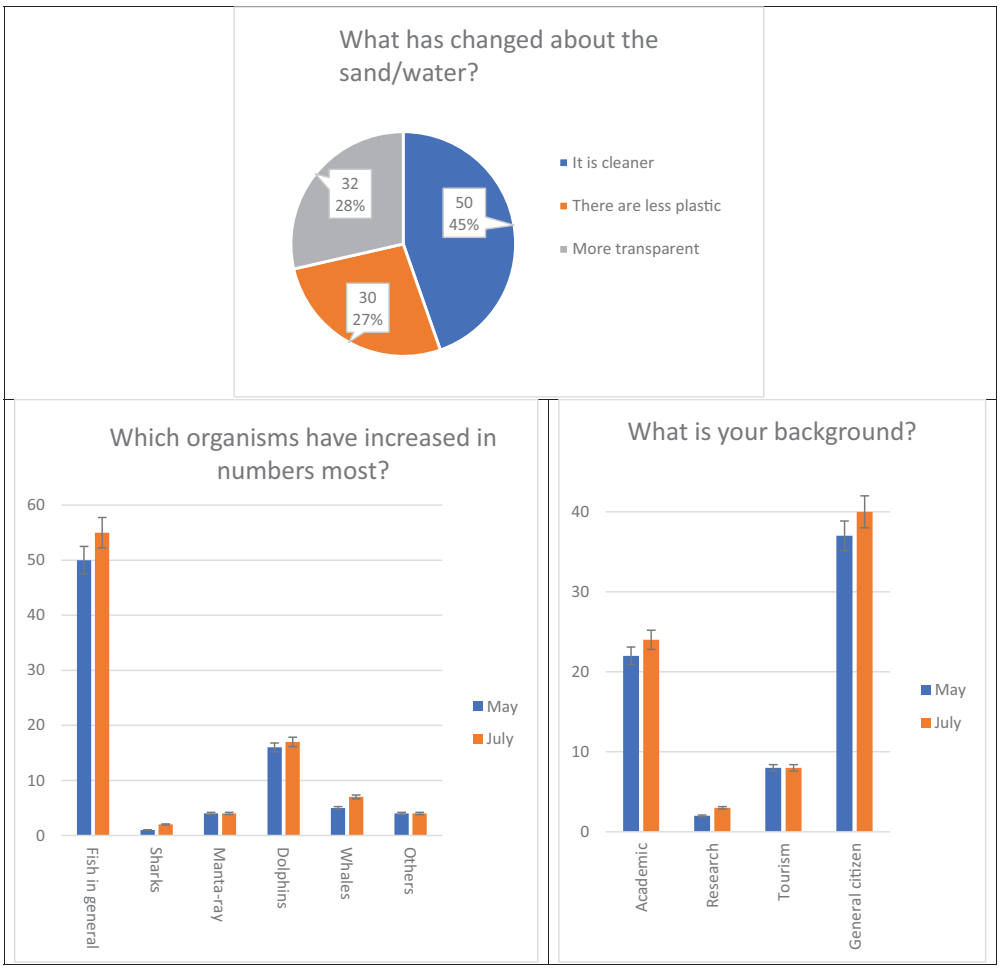

FIGURE 2 | Results from Salinas.

involved with tourism, whilst in Manta 89–83% (**Figure 3**) regarded themselves as common citizens, and 8–12% and 3–4% were involved with tourism and academies, respectively. In Galapagos (**Figure 4**), results were 80–63% tourism and 20–35% fish-traders.

Quantitative satellite information about chlorophyll (**Figure 5**) and diffuse attenuation coefficients (**Figure 6**) along the Ecuadorian coast supports the survey perceptions of improvements in water quality over the lockdown period. The difference between concentrations of Chl in 2019 relative to 2020 (i.e., 2020 minus 2019) changed over the period March (-22 mg.m^{-3}) to April to May (-0.6 mg.m^{-3}) in a progressive manner, indicating a general drop in the difference of Chl. Chlorophyll concentrations from close to Salinas and Manta over these periods were higher in 2019 than 2020, except in May 2020 (Manta). The diffuse attenuation coefficient (Kd), which is an indicator of turbidity of the water column, was used quantitatively to measure water transparency. These data (**Figure 6**) show that over the same period as chlorophyll changes, the water column in 2020 was clearer than in 2019, except where there were coastal phytoplankton blooms. For the Salinas zone in 2019 the Kd values were 0.21, 0.97, 0.14 and in 2020; 0.11, 0.12, and 0.18 m^{-1} for the same months respectively, while near Manta the equivalent data were: 0.24, 1.19, 0.78; and 0.15, 0.34, and 0.01 m^{-1} respectively. The lower Kd in 2020 showed generally less suspended particulate matter in the water column, thus the photic layer increased, and clarity improved.

DISCUSSION

The COVID-19 pandemic has put populations under emotional, economic, and health stresses, and therefore to conduct face to face or online surveys under these circumstances is difficult (Labott et al., 2013; Arnsten, 2020; Steele et al., 2021), and recently Lardone et al. (2021) have reported how these circumstances could affect cognitive processes. Both face-to-face and focus group approaches were tried in the second survey, but people were not prepared to respond, and thus it was executed in the same way as the first. The surveys were designed to be the simplest possible, to ensure responses, because under the stressful and unique pandemic conditions, concentration,

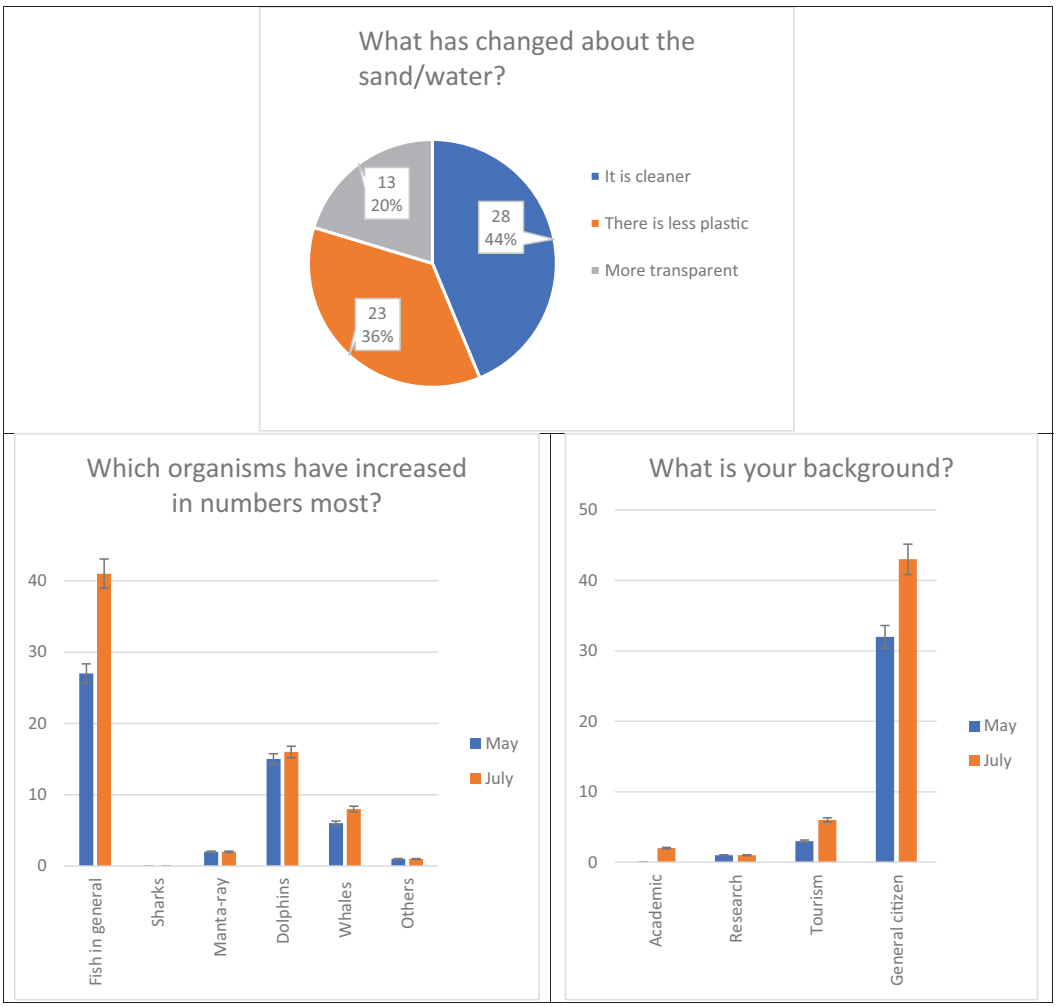

FIGURE 3 | Results from Manta.

reasoning, empathy, patient, and control of emotions as well as thoughts and actions could be compromised (Arnsten, 2020; Lardone et al., 2021). Studies using social media (Google forms) are increasingly accepted and web-based surveys have become one of the most common methods to collect data for research (e.g., Vasantha and Harinarayana, 2016). Steele et al. (2021) reported a full study on cross-sectional surveys on people activity directly affected for the lockdowns, one of the characteristics are the short and unambiguous questions and replies to them; yes, or not for example; like the surveys presented here. Even though the results of second interview confirmed the first one, it must be clear that interview data is based on the perception of interviewed. Biases during on line questionaries during COVID-19 pandemic restrictions have been studied by Schaurer and Weiß (2020), and should to be considered in survey interpretations

The questionnaires (see **Supplementary Material**) were quite simple with just 11 straightforward questions that took respondents between 2 and 5 min to complete: id est, Salinas, 4.73; Manta, 3.48; Puerto Baquerizo Moreno, 2.96; and Puerto Ayora 1.9 min. The quicker answer time from Galapagos could be due to people of these islands being aware of environmental matters given the importance of the marine reserve. The surveys from Salinas and Manta were mostly responded to within 24 h, but from Galapagos it took longer, and fewer people responded, compared to Salinas and Manta. Fortunately, there was one marine biologist quarantined from March to April (6 weeks) on a boat in Puerto Ayora who reported turtle and shark activity as well as water quality on a regular basis.

There is almost a unanimous view that beach zones (sand and coastal water) have notably improved during confinement, at least from a visual point of view (see **Supplementary Material** Photos and Video). The beaches have less garbage in general and plastic in particular, even though there has been an increase in plastic and face mask production and disposal around the world (Calma, 2020; Eljarrat, 2020). Tourists tend to litter beaches, as they seem to lose good behavior regarding the management of their garbage (Oigman-Pszczol and Creed, 2007), Williams et al.

TABLE 3 | Parameters to be measured to create a data baseline for coastal zone management.

Type of parameters	Land	Water
Physical	Geologic studies, textural, petrological, and geochemical variation, types of beaches, sand (granulometry, minerals), gradient of beaches, dunes, erosion rates, macro-micro plastics, Surf zone, sand column	Tides (height and frequency), Waves (swell, fetch), optics (color, transparency, Suspended total Particulate Matter), odor Salinity, Temperature, Currents (littoral and tides) Detailed bathymetry
Chemical	Heavy metal, crystal composition, organic matter, redox equilibria, N, S, Mn. Interstitial water chemistry, Natural and anthropogenic hydrocarbons	pH, dissolved Oxygen, Redox equilibria, dissolved inorganic nutrients (Nitrogen, Phosphorus, Silicate, Mn, Fe, Mg), Dissolved and particulate organic matter, Chlorophyll, Carbonates, Total Dissolved metals (Cr, Pb, Hg, Cd, etc.). alkalinity, total hardness, calcium BOD and COD
Biological	Sand and dune vegetation. Beach species (lizards, crabs) Coastal- Marine birds Identification, population. Genera, species, Bacterial load, parasites, fungi, viruses Fecal index organisms, total coliforms, thermotolerant coliforms, *E. coli* and intestinal enterococci, *Staphylococcus* spp., *Pseudomonas aeruginosa*. *Vibrio parahaemolyticus*, *Candida* spp., Limits: Those recommended by World Health Organization (WHO)/United Nations Environment Programme (UNEP) (1994)	*Escherichia coli*, total coliforms, thermotolerant coliforms, *E. coli* and intestinal enterococci, *Staphylococcus* spp., *Pseudomonas aeruginosa*. *Vibrio parahaemolyticus*, *Candida spp*, adenoviruses, polyomavirus, hepatitis A virus, and noroviruses. Phytoplankton and zooplankton communities. Marine species from level 3–5 of trophic chain.

For details see Eagle (1983), World Health Organization (WHO)/United Nations Environment Programme (UNEP) (1994), Moresco et al. (2012); Patil et al. (2012), and Soto-Varela et al. (2021).

(2016) and Mestanza-Ramón et al. (2019b) have reported cases of littering of popular beaches at Rio de Janeiro, the north Caribbean coast, and Ecuador (including Galápagos). More recently, Gaibor et al., 2020 have found that anthropogenic debris (plastic, paper, cigarette butts, metal, glass, others; plastics, 60%) is mainly of local origin. Thus, if there is limited local anthropogenic activity, the presence of debris tends to reduce. They also reported that the highest concentration of debris was found in the south (Salinas) and central (Manta) coasts. Furthermore, Ormaza-González and Vera-Mosquera (2021), under a Citizen Science remit, have one observation site (so called Station D [2°12″ S and 80°59″ W]) in Salinas, which has been visited almost every fortnight since June 2019. Plastics have been collected from a specific area of around 100 $m^{2,}$ and after weighing, identification and classification, its possible origin is established. Initial results have not been published formally, but they are reported via twitter immediately after measurements; see photos (**Supplementary Material**). Generally, a range of 300–600 g of plastics per week is washed ashore and collected at the study site. Just a few days before the lockdown, on March 7, 2020, 250 g were collected, but by September there was almost no plastic found (**Supplementary Material** Photo 1, lower panel). The impact of plastics on marine ecosystems is clearly recognized, e.g., (Santander-Rodriguez, 2017); Amelia et al. (2021) have reviewed the impact of microplastic on marine ecosystems organism (food web). The range of plastics found is given in the results. Beach tourism has also been reported to Increase microbiological load (Natural Resources Defense Council, 2014), although it was not possible to follow this in the current study. The observed reduction in litter and contamination reported here seems to directly correspond to less use of beaches during the lockdown.

There is a direct relationship between fish demand and tourism (Budzich-Tabor et al., 2014), and as tourism activities stopped, the fishery markets of both cities were partially closed, resulting in less artisanal fishing impact. Different species in the three locations, including small pelagic fish and marine mammals (dolphins, orcas, whales, sea lions) as well as sharks and turtles have been reported in the survey, as well as on social networks (Zambrano-Alvarado, 2020). A marine biologist from Galapagos reported seeing turtles close to the bay (I. San Cristobal) between 10 and 15 times a day; before the confinement, turtles were seen rarely in that area. In a recent press release by the Charles Darwin Foundation (CDF, 2020), Galapagos penguins (*Spheniscus mendiculus*) and flightless cormorant (*Phalacrocorax harrisi*) which have been tracked for the last 30 years are showing increased numbers of individuals, 1,940 and 2,290 respectively, which is a record for these species. The most plausible reason for this is the decrease in noise during pandemic restrictions (Spennemann and Parker, 2020), as it has been shown to affect the behavior of dolphins, sea turtles, sea birds, and other species (Samuel et al., 2005; Hazel et al., 2007; Ketten, 2008), also the event la Niña event 2020–2021 is playing role on this growing number (Lerma et al., 2020). Nonetheless, specific research must be conducted to investigate these possible reasons.

Improvements in the color of coastal water, which is now clearer and bluish-turquoise, has been reported by news (Ramos, 2020; Zambrano-Alvarado, 2020), papers (Zambrano-Monserrate et al., 2020) social networks, and in public and authors videos (see Supplementary Information). This improvement reflects less suspended particulate matter and/or phytoplankton in the water. There is natural flushing of mainland coastal waters by the North Equatorial current, and the Humboldt currents, as well as the residues of the Cromwell current (**Figure 1**). The Cromwell (Knauss, 1963) is a sub-surface current that upwells to the west of Galapagos and can be detected further east (Pak and Zaneveld, 1973) at around 84W and thus closer to the coastline of Ecuador. The Humboldt (Montecino and Lange, 2009) is a coastal current from the Antarctic that reaches Chilean, Peruvian, and Ecuadorian coasts

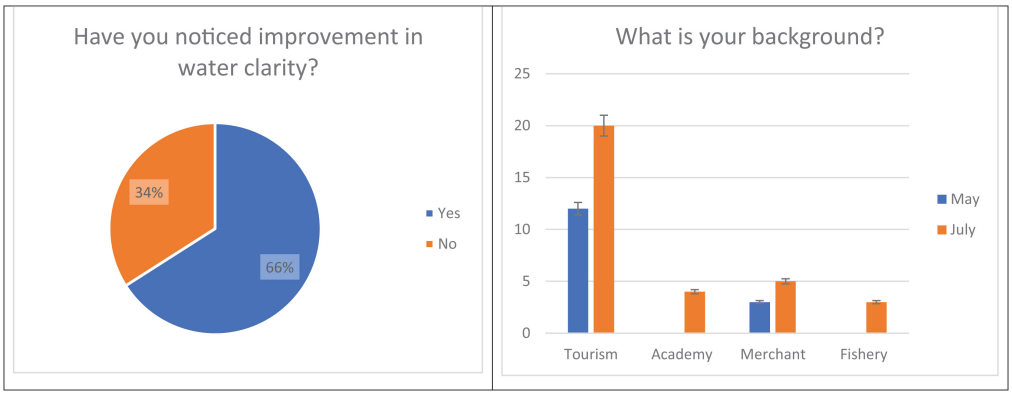

FIGURE 4 | Results from Galapagos.

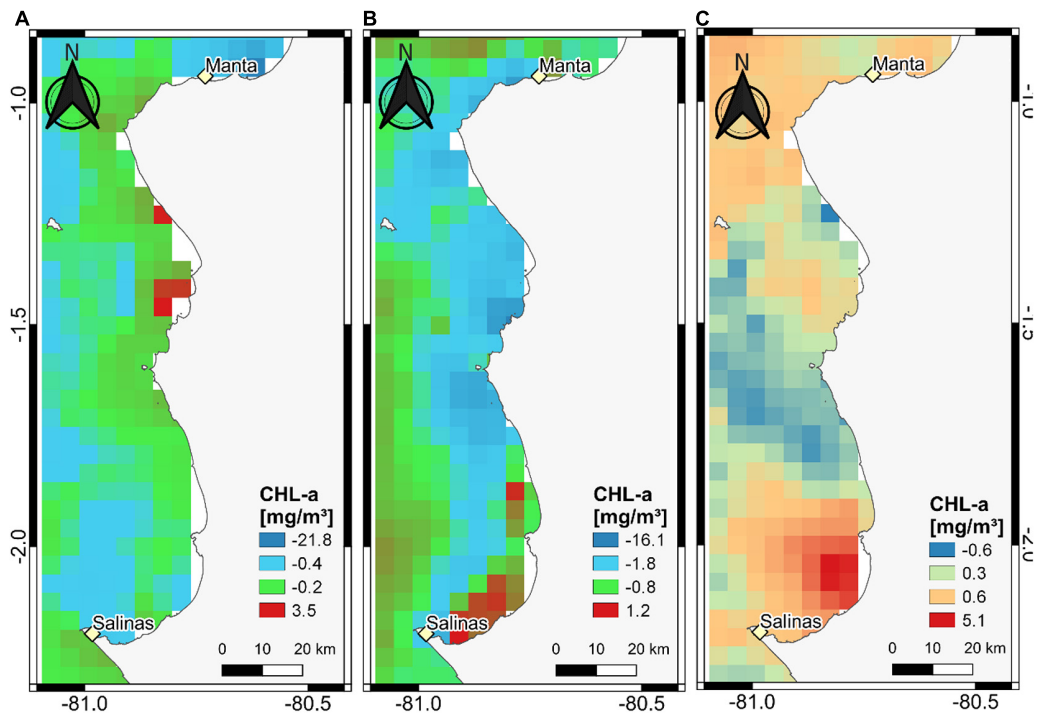

FIGURE 5 | (A-C) Satellite Chlorophyll.

(May-December). Additionally, the north equatorial current (0.2–1.3 m/s)[2] flows toward Ecuadorian coasts and north Galapagos during Jan-April. The Cromwell and Humboldt alone provide flows of 39 and 12 Sverdrup, and these can renew coastal surface waters down to about 100 m. On a global scale there are other coastal systems, in addition to Ecuador, where strong surface oceanic currents replenish nearshore waters and diminish pollutant concentrations (Dalbosco et al., 2020). The replenishment of coastal waters with cleaner offshore water, combined with reduced pollutant inputs during the lockdown, will be expected to transform these zones into an improved environment for biota. These changes have been perceived by people responding to the survey and have also been seen in other beaches and coastal zones around the world (Zambrano-Monserrate et al., 2021), lakes (Yunus et al., 2020), and rivers (Arora et al., 2020).

The data from satellite, which shows that nearshore Chlorophyl concentration and the attenuation coefficient Kd (490 nm) were less in 2020 than 2019, support overall the observations from local people that water was clearer and looked much cleaner in 2020 lockdown than in 2019 over a similar period. The water bodies were less polluted because there was less untreated or partially treated wastewater being introduced, with an improvement in conditions. With less nutrients (N

[2]https://www.windy.com/-Currents

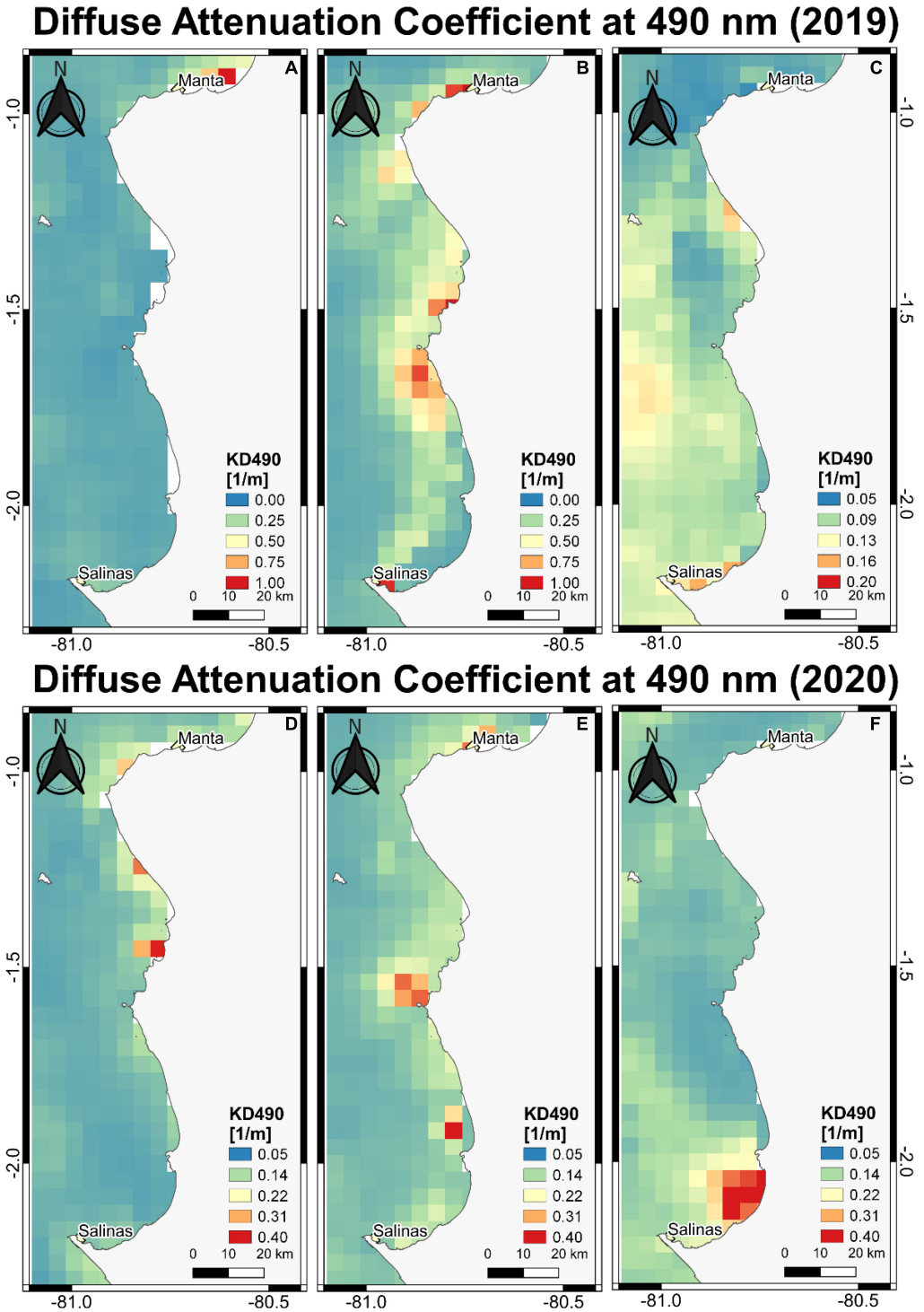

FIGURE 6 | Satellite Atenuation coefficient.

and P) and photosynthetic activity, Chl decreased despite the thicker photic layer. Castro-Rodas (2016) showed that in Salinas coastal waters the concentration of Chlorophyll was associated with discharges of untreated or partially treated waste water. Yunus et al. (2020) has also reported that the largest lake of India (Vembanad) has around 16% less suspended solids than before the pandemic. Also, survey respondents indicated that the water was much clearer. Recently, Cherif et al. (2020) have

also reported an improvement in coastal water quality from Tangier (Morocco) using satellite tools (WST Sentinel-3). As the water quality improves (less contamination, and suspended particulate matter), the photic layer thickness will increase and so photosynthesis may be enhanced if there are adequate nutrients. Thus, satellite data from March, April, and May for 2019 and 2020, before and during pandemic periods, were examined (**Figures 5**, **6**).

For the first occasion in modern times, most of the coastline studied has developed features of marine protected areas. Recent reports from the southeast coast of India (Prakash et al., 2021) and in Brazil (Pereira et al., 2021) contain similar findings to those here.

Most people in the survey responded that they did not know if there were local wastewater plants. Ecuador has a deficit of wastewater treatment plants, with only 29.3% (Instituto Nacional de Estadística y Censos (INEC), 2016) of the wastewater produced being treated. Salinas sewage works serve only 30% of the local population (Castro-Rodas, 2016), and so only a small part of the sewage has primary treatment with the rest being discharged directly to the sea or indirectly through badly constructed latrines. Walsh and Mena (2016) also reported contamination from domestic non-treated sewage in Galapagos. These facts indicate that additional wastewater produced by tourists would generate more health risks. Recently, Quilliam et al. (2020) and Randazzo et al. (2020) have reported the COVID-19 virus in feces and domestic residual waters, and thus Larsen and Wigginton (2020), and Medema et al. (2020) have proposed to correlate the presence of SARS-Coronavirus-2 RNA in Sewage with reported COVID-19. The impact from untreated wastewater on the marine environment and the whole trophic chain (Karen, 2019; Amelia et al., 2021) is a well-known fact.

The absence of tourism has greatly reduced the pressure on the few already overloaded sewage treatment plants in Salinas, Manta, and Galapagos, and therefore eutrophication, plastic and fecal contamination have dramatically decreased; Castro-Rodas (2016) found a direct relationship between phytoplankton growth and dissolved P present in residual untreated waters in Salinas. However, as most surveyed people do not know about the lack of wastewater treatment plants, they are unlikely to be aware of the problems associated with the untreated sewage water. The reduced tourism, whilst economically damaging, has produced less wastewater pollution, and coupled with background renewal of the coastal waters due to oceanic currents have led to cleaner sandy beaches as well as nearshore waters.

The COVID-19 pandemic would ideally merge into a neat, organized, and sustainable return of tourism, industry, and fishing activities in spite of the economic constraints expected immediately post-pandemic. As Pearson et al. (2020) have suggested, COVID-19 with its social, economic, health and economic consequences gives an opportunity to reshape near, medium, and long-term management plans, especially for environments such as beaches and their associated marine resources.

A recommended way ahead is adoption of Integrated Coastal Zone Management (ICZM) processes (Mestanza-Ramón et al., 2019a) that are recognized by the UN (Chapter 17 of Agenda 21, Rio de Janeiro, 1992). This holistic approach provides a framework for planning sustainable tourism and coastal fisheries (Mestanza-Ramón et al., 2019a; Cantasano et al., 2021). It is important to realize that technical approaches alone (including improved wastewater treatment, controlling pollutant sources) are not adequate to provide a solution. An improvement in cultural awareness of environmental quality is needed, as provided through education via schools, colleges, public engagement activities, and media. A different approach to beach tourism should be promoted, organized, and incentivized, in order not only to protect environmental quality, but to stimulate a cultural local heritage (Cantasano et al., 2021). It is suggested that low noise sea-side activities be encouraged in order to reduce acoustic impacts on marine species (Leduc et al., 2021). These and related activities all require active involvement of government decision-makers and managers at local and national levels. Management measures would include assessing tourist load with risk analysis (Silva et al., 2007) as well as regular checking of water and beach quality indexes as described by Lucrezi et al. (2015, 2016).

The ICZM approach requires baseline data and information against which changes caused by reactivation of industry, tourism, fishing, and other activities with an impact on marine nearshore systems, can be measured. Setting of this baseline before changes to the present improved environmental quality occur is an urgent recommendation. Parameters (**Table 3**) must at least include, coastal hydrodynamic (surface, littoral, tidal currents), beach and inshore flora and fauna biodiversity, anthropogenic microbiological load (intestinal and fecal bacteria load), chemical characterization of water bodies (Patil et al., 2012) and beaches, quality indices (Anfuso et al., 2014; da Costa Cristiano et al., 2020), and noise.

CONCLUSION

All three sites examined are under an aggressive and generally poorly organized tourism-driven economy and, as Stumpf et al. (2013) warned, this has produced littered beaches and polluted waters under normal conditions. The COVID-19 pandemic has led to changing conditions, and the public seems to appreciate an improved environmental quality as they value and depend on the natural resources of their surroundings. The populations residing in Salinas, Manta, and Galapagos have clearly noticed a positive change in the quality of beaches due to the absence of tourists caused by COVID-19 (Zielinski and Botero, 2020). The return of marine species and reduction in levels of noise and environmental pollution are the highlights of the survey results, and they corroborate the general perceptions found in social media. These survey observations are consistent with quantitative satellite data on Chl and the diffuse attenuation coefficient for the areas studied. The environmental improvement during the pandemic provides an unparalleled opportunity to construct a baseline dataset for these almost pristine beaches and coastal waters, and to consider future viable management options based on such datasets, as discussed here.

In the future as awareness of the environment grows in the population, and new easier to use technologies become available, there will be an increasing role for collection of data through "citizen science." Examples of improving technologies include: (1) on-line surveys; (2) the development of more sophisticated cell phone applications for measurement of environmental parameters such as water clarity (Sechi disk depth[3]). Initiating Citizen Science could therefore help to develop a science educated society that will respond more positively to better environmental management. However, there are diverse and important concerns about such "citizen- based" data collection and subsequent interpretation (Baker et al., 2021), and care must be taken with evaluating such data.

The COVID-19 pandemic is causing enormous and unpredictable changes in society that will affect lives for generations to come (Nat Ecol Evol, 2020) (No Author, 2020b). Adoption of the recommendations above are needed to limit coastal impacts on these future generations.

DATA AVAILABILITY STATEMENT

The raw data supporting the conclusions of this article will be made available by the authors, without undue reservation.

AUTHOR CONTRIBUTIONS

PFO-G designed the idea of the research and survey, analyzed, and wrote part of the manuscript. DC-R carried out the survey, organized and worked on survey results, downloaded and worked on satellite data. PS contributed to analysis of information and helped write and edit the whole manuscript. All authors contributed to the article and approved the submitted version.

[3] https://www.eyeonwater.org/

ACKNOWLEDGMENTS

FO-G to Daphne Vera my wife, who has been closely linked to the writing of the manuscript; her valuable conversations during the quarantine have been useful. Marine biologist Xavier Romero is greatly appreciated for his Galápagos observations. Perhaps the most important acknowledgment goes to the people (close to three hundred that took time to respond to our survey). We are grateful to three anonymous reviewers for their constructive and insightful comments. Luigi Benincasa, Freddy Pachay, and Gustavo Nuñez in Manta; Daniel Massuh and Isabel Timpe in Galapagos helped with surveys. José D. Castro-Rodas helped with the graphical abstract and edited the Supplementary Videos. Preprint: Ormaza-González and Castro-Rodas (2020).

SUPPLEMENTARY MATERIAL

The Supplementary Material for this article can be found online at: https://www.frontiersin.org/articles/10.3389/fmars.2021.669374/full#supplementary-material

REFERENCES

Abir, T., Kalimullah, N. A., Osuagwu, U. L., Yazdani, D. M., Mamun, A. A., Husain, T., et al. (2020). Factors associated with the perception of risk and knowledge of contracting the SARS-Cov-2 among adults in Bangladesh: analysis of online surveys. *Int. J. Environ. Res. Public Health* 17:5252. doi: 10.3390/ijerph17145252

Amelia, T. S., Khalik, W. M., Ong, M. C., Shao, Y. T., Pan, H. J., and Bhubalan, K. (2021). Marine microplastics as vectors of major ocean pollutants and its hazards to the marine ecosystem and humans. *Progr. Earth Planetary Sci.* 8, 1–26. doi: 10.1186/s40645-020-00405-4

Anfuso, G., Williams, A. T., Hernández, J. C., and Pranzini, E. (2014). Coastal scenic assessment and tourism management in western Cuba. *Tourism Manag.* 42, 307–320.

Arnsten, A. (2020). *The Brain's Response to Stress – How Our Brains May Be Altered During the COVID-19 Pandemic*. Available online at: YouTube: TheBrain'sResponsetoStress-HowOurBrainsMayBeAlteredDuringtheCOVID-19Pandemic-YouTube. (accessed April 20, 2021).

Arora, S., Bhaukhandi, K. D., and Mishra, P. K. (2020). Coronavirus lockdown helped the environment to bounce back. *Sci. Total Environ.* 742:140573. doi: 10.1016/j.scitotenv.2020.140573

Baker, E., Drury, J., Judge, J., Roy, D., Smith, G. C., and Stephens, P. A. (2021). The verification of ecological citizen science data: current approaches and future possibilities. *Citizen Sci.: Theory Practice* 6:12. doi: 10.5334/cstp.351

Becker, A., Whitfield, A. K., Cowley, P. D., Järnegren, J., and Næsje, T. F. (2013). Potential effects of artificial light associated with anthropogenic infrastructure on the abundance and foraging behaviour of estuary-associated fishes. *J. Appl. Ecol.* 50, 43–50. doi: 10.1111/1365-2664.12024

Bloom, D. E., Cadarette, D., and Sevilla, J. P. (2018). Epidemics and the economy: new and recurring infectious diseases can have broad economic repercussions. *Finance Dev.: Q. Publ. Int. Monetary Fund World Bank* 55, 46–49.

Bolton, D., Mayer-Pinto, M., Clark, G. F., Dafforn, K. A., Brassil, W. A., Becker, A., et al. (2017). Coastal urban lighting has ecological consequences for multiple trophic levels under the sea. *Sci. Total Environ.* 576, 1–9. doi: 10.1016/j.scitotenv.2016.10.037

Budzich-Tabor, U., Burch, M., and da Silva, S. G. (2014). *Fisheries and Tourism. European Commission, Directorate-General for Maritime Affairs and Fisheries, Director-General*. Avaialble online at: https://doi.org/10.2771/7410 (accessed March 15, 2021).

Calma, J. (2020). *The COVID-19 Pandemic is Generating Tons of Medical Waste. The Verge*. Available online at: https://www.theverge.com/2020/3/26/21194647/the-covid-19-pandemic-is-generating-tons-of-medical-waste (accessed May 5, 2020).

Cantasano, N., Caloiero, T., Pellicone, G., Aristodemo, F., De Marco, A., and Tagarelli, G. (2021). Can ICZM contribute to the mitigation of erosion and of human activities threatening the natural and cultural heritage of the coastal landscape of Calabria? *Sustainability* 13:1122. doi: 10.3390/su13031122

Caryl-Sue, M., Crooks, M., and Johnson, C. (2011). *Case Study: Galápagos Marine Reserve. National Geography Article*. Avilable online at: https://www.nationalgeographic.org/article/case-study-galapagos-marine-reserve/ (accessed date May 20, 2020).

Castro-Rodas, D. (2016). *Climatología Costera y su Influencia en Las Descargas Residuales en la Península de Santa*. Bachelor's thesis. Guayaquil: ESPOL, 39. Avaliable online at: http://www.dspace.espol.edu.ec/xmlui/handle/123456789/45931

Cherif, E. K., Vodopivec, M., Mejjad, N., Esteves da Silva, J. C., Simonovič, S., and Boulaassal, H. (2020). COVID-19 pandemic consequences on coastal water

quality using WST Sentinel-3 Data: case of Tangier, Morocco. *Water* 12:2638. doi: 10.3390/w12092638

CDF (2020). *Population Records for the Galapagos Penguin and the Flightless Cormorant*. Charles Darwin Foundation: Press. Available online at: https://www.darwinfoundation.org/en/blog-articles/640-population-records-for-the-galapagos-penguin-and-the-flightless-cormorant (accessed October 23, 2020).

da Costa, J. P. (2021). The 2019 Global pandemic and plastic pollution prevention measures: playing catch-up. *Sci. Total Environ.* 774:145806. doi: 10.1016/j.scitotenv.2021.145806

da Costa Cristiano, S., Rockett, G. C., Portz, L. C., and de Souza Filho, J. R. (2020). Beach landscape management as a sustainable tourism resource in Fernando de Noronha Island (Brazil). *Mar. Pollut. Bull.* 150:110621. doi: 10.1016/j.marpolbul.2019.110621

Dalbosco, A. L. P., Franco, D., Barletta, R. D. C., and Trevisan, A. B. (2020). Analysis of currents on the continental shelf off the Santa Catarina Island through measured data. *RBRH* 25, 1–15. doi: 10.1590/2318-0331.252020180175

De Vito, A., and Gómez, J. P. (2020). Estimating the COVID-19 cash crunch: global evidence and policy. *J. Account. Public Policy* 39:106741. doi: 10.1016/j.jaccpubpol.2020.106741

Eljarrat, E. (2020). "El resurgir del plástico por culpa del coronavirus", *National Geographic*. Available online at: https://www.nationalgeographic.com.es/naturaleza/resurgir-plastico-por-culpa-coronavirus_15488 (accessed may 22, 2020).

Eagle, G. A. (1983). "The chemistry of sandy beach ecosystems — a review," in *Sandy Beaches as Ecosystems. Developments in Hydrobiology*, eds A. McLachlan and T. Erasmus (Dordrecht: Springer), 19.

GESAMP (1991). *Food and Agriculture Organization (FAO). Reports and Studies No.47*. Joint Group of Experts on the Scientific Aspects of Marine Pollution (GESAMP). Available online at: http://www.fao.org/3/u3100e/U3100e00.htm (accessed January 18, 2021).

Gad-Salinas (2020). *Demografía*. Available online at: https://www.salinas.gob.ec/index.php/salinas/demografia/106-salinas (accessed May 24, 2020).

Gaibor, N., Condo-Espinel, V., Cornejo-Rodríguez, M. H., Darquea, J. J., Pernia, B., Domínguez, G. A., et al. (2020). Composition, abundance and sources of anthropogenic marine debris on the beaches from Ecuador–a volunteer-supported study. *Mar. Pollut. Bull.* 154:111068. doi: 10.1016/j.marpolbul.2020.111068

Grube, A. M., Stewart, J. R., and Ochoa-Herrera, V. (2020). The challenge of achieving safely managed drinking water supply on San Cristobal island, Galápagos. *Int. J. Hygiene Environ. Health* 228:113547. doi: 10.1016/j.ijheh.2020.113547

Hazel, J., Lawler, I. R., Marsh, H., and Robson, S. (2007). Vessel speed increases collision risk for the green turtle Chelonia mydas. *Endang Species Res.* 3, 105–113.

Hyde, K. (2020). *Residential Water Quality and the Spread of COVID-19 in the United States (April 9, 2020)*. Available online at: https://ssrn.com/abstract=3572341 or http://dx.doi.org/10.2139/ssrn.3572341 (accessed date April 9, 2020).

Instituto Nacional de Estadística y Censos (INEC) (2010). *Población y Demografía. Instituto Nacional de Estadística y Censos*. Available online at: https://www.ecuadorencifras.gob.ec/censo-de-poblacion-y-vivienda/ (accessed May 24, 2020).

Instituto Nacional de Estadística y Censos (INEC) (2016). *Documento Técnico "Estadística Ambiental Económica en Gobiernos Autónomos Descentralizados Municipales" Gestión de Agua Potable y Alcantarillado 2016. Instituto Nacional de Estadística y Censos*. Available online at: https://www.ecuadorencifras.gob.ec/institucional/home/ (accessed May 24, 2020).

Jiménez-Uzcátegui, G. (2020). *Population Records for the Galapagos Penguin and the Flightless Cormorant. Charles Darwin Fundation*. Available online at: https://www.darwinfoundation.org/en/blog-articles/640-population-records-for-the-galapagos-penguin-and-the-flightless-cormorant

Johns Hopkins Coronavirus Resource Center (2021). *COVID-19 Map*. Available online at: https://coronavirus.jhu.edu/map.html (accessed May 24, 2020).

Ju, M. J., Oh, J., and Choi, Y. H. (2021). Changes in air pollution levels after COVID-19 outbreak in Korea. *Sci. Total Environ.* 750:141521. doi: 10.1016/j.scitotenv.2020.141521

Kamrowski, R. L., Limpus, C., Moloney, J., and Hamann, M. (2012). Coastal light pollution and marine turtles: assessing the magnitude of the problem. *Endangered Species Res.* 19, 85–98.

Karen, B. G. (2019). *The Effects of Sewage on Aquatic Ecosystems. Sciencing*. Available online at: https://sciencing.com/effects-sewage-aquatic-ecosystems-21773.html (accessed February 15, 2021).

Ketten, D. R. (2008). Underwater ears and the physiology of impacts: comparative liability for hearing loss in sea turtles, birds, and mammals. *Bioacoustics* 17, 312–315.

Knauss, J. A. (1963). Measurements of the cromwell current. *Deep Sea Res.* 6, 265–274. doi: 10.1016/0146-6313(59)90086-3

Labott, S. M., Johnson, T. P., Fendrich, M., and Feeny, N. C. (2013). Emotional risks to respondents in survey research. *J. Empirical Res. Hum. Res. Ethics: JERHRE* 8, 53–66. doi: 10.1525/jer.2013.8.4.53

Lardone, A., Turriziani, P., Sorrentino, P., Gigliotta, O., Chirico, A., Lucidi, F., et al. (2021). Behavioral restriction determines left attentional bias: preliminary evidence from COVID-19 lockdown. *Front. Psychol.* 12:650715. doi: 10.3389/fpsyg.2021.650715

Larsen, D. A., and Wigginton, K. R. (2020). Tracking COVID-19 with wastewater. *Nat. Biotechnol.* 38, 1151–1153. doi: 10.1038/s41587-020-0690-1

Le Quéré, C., Jackson, R. B., Jones, M. W., Smith, A. J., Abernethy, S., Andrew, R. M., et al. (2020). Temporary reduction in daily global CO 2 emissions during the COVID-19 forced confinement. *Nat. Climate Change* 10, 647–653. doi: 10.1038/s41558-020-0797-x

Leduc, A. O., Nunes, J. A., de Araújo, C. B., Quadros, A. L., Barros, F., Oliveira, H. H., et al. (2021). Land-based noise pollution impairs reef fish behavior: a case study with a Brazilian carnival. *Biol. Conserv.* 253:108910. doi: 10.1016/j.biocon.2020.108910

Lerma, M., Castillo-Guerrero, J. A., Hernández-Vázquez, S. A., and Garthe, S. (2020). Foraging ecology of a marine top predator in the Eastern Tropical Pacifc over 3 years with different ENSO phases. *Mar. Biol.* 167:88. doi: 10.1007/s00227-020-03699-6

Li, W. C., Tse, H. F., and Fok, L. (2016). Plastic waste in the marine environment: a review of sources, occurrence and effects. *Sci. Total Environ.* 56, 333–349. doi: 10.1016/j.scitotenv.2016.05.084

Lucrezi, S., Saayman, M., and Van der Merwe, P. (2015). Managing beaches and beachgoers: lessons from and for the Blue Flag award. *Tourism Manag.* 48, 211–230. doi: 10.1016/j.tourman.2014.11.010

Lucrezi, S., Saayman, M., and Van der Merwe, P. (2016). An assessment tool for sandy beaches: a case study for integrating beach description, human dimension, and economic factors to identify priority management issues. *Ocean Coastal Manag.* 121, 1–22. doi: 10.1016/j.ocecoaman.2015.12.003

Martínez-Ortiz, J., Aires-da-Silva, A. M., Lennert-Cody, C. E., and Maunder, M. N. (2015). The ecuadorian artisanal fishery for large pelagics: species composition and spatio-temporal dynamics. *PLoS One* 10:e0135136.

Medema, G., Heijnen, L., Elsinga, G., Italiaander, R., and Brouwer, A. (2020). Presence of SARS-Coronavirus-2 RNA in sewage and correlation with reported COVID-19 prevalence in the early stage of the epidemic in the Netherlands. *Environ. Sci. Technol. Lett.* 7, 511–516. doi: 10.1021/acs.estlett.0c00357

Mestanza-Ramón, C., Boteroc, C. M., Anfusoa, G., Chica-Ruiza, J. A., Pranzinid, E., and Moosera, A. (2019a). Beach litter in Ecuador and the Galapagos islands: a baseline to enhance environmental conservation and sustainable beach tourism. *Mar. Pollut. Bull.* 140, 573–578. doi: 10.1016/j.marpolbul.2019.02.003

Mestanza-Ramón, C., Sanchez-Capa, M., Figueroa-Saavedra, H., and Rojas-Paredes, J. (2019b). Integrated coastal zone management in continental ecuador and galapagos Islands: challenges and opportunities in a changing tourism and economic context. *Sustainability* 11:6386. doi: 10.3390/su11226386

Montecino, V. C., and Lange, B. (2009). The humboldt current system: ecosystem components and processes, fisheries, and sediment studies. *Progr. Oceanogr.* 83, 65–79. doi: 10.1016/j.pocean.2009.07.041

Moresco, V., Viancelli, A., Nascimento, M. A., Souza, D. S. M., Ramos, A. P. D., Garcia, L. A. T., et al. (2012). Microbiological and physicochemical analysis of the coastal waters of southern Brazil. *Mar. Pollut. Bull.* 64, 40–48. doi: 10.1016/j.marpolbul.2011.10.026

NASA (2019). *MYD17A3HGF MODIS/Aqua Net Primary Production Gap-Filled Yearly L4 Global 500m SIN Grid V006. NASA EOSDIS Land Processes*

DAAC. Available online at: https://doi.org/10.5067/MODIS/MYD17A3HGF.006 (accessed February 15, 2021).

Natural Resources Defense Council (n.d.) (2014). *The Impacts of Beach Pollution. Natural Resources Defense Council*. Available online at: https://www.nrdc.org/sites/default/files/ttw2014_Impacts_of_Beach_Pollution.pdf (accessed date May 16, 2020).

Navarro, N. (2019). Community perceptions of tourism impacts on coastal protected areas. *J. Mar. Sci. Eng.* 7:274.

No Author. (2020a). On being human in the face of a pandemic. *Nat Cancer* doi: 10.1038/s43018-020-0062-2 Online ahead of print

No Author. (2020b). Science in the time of corona. *Nat. Ecol. Evol.* 4:665. doi: 10.1038/s41559-020-1205-7

Ogunbode, T. O., Nejo, Y. T., and Kehinde, O. J. (2021). COVID-19 Pandemic/Lockdown and its impact on sustainable access to safe water in the developing world: a case study. *Eur. J. Basic Med. Sci.* 11, 8–17.

Oigman-Pszczol, S. S., and Creed, J. C. (2007). Quantification and classification of marine litter on beaches along Armação dos Búzios, Rio de Janeiro, Brazil. *J. Coastal Res.* 23, 421–428.

Ormaza-González, F., and Castro-Rodas, D. (2020). COVID-19 impacts on beaches and coastal water pollution: management proposals post-pandemic. *Preprints* 2020:2020060186.

Ormaza-González, F. I., and Vera-Mosquera, D. E. (2021). *Station D, Citizen Science Coastal and Oceanographic Research*. Available online at: https://twitter.com/FranklinOrmaza1 (accessed March 15, 2021).

Pak, H., and Zaneveld, J. G. R. (1973). The cromwell current on the east side of the galapagos Islands. *J. Geophys. Res.* 78, 7845–7859.

Paladines, M. J. B., and Chuenpagdee, R. (2015). Governability assessment of the Galapagos marine reserve. *Maritime Stud.* 14, 1–21. doi: 10.1186/s40152-015-0031-z

Partelow, S., Wehrden, H., and Horn, O. (2015). Pollution exposure on marine protected areas: a global assessment. *Mar. Pollut. Bull.* 100, 352–358. doi: 10.1016/j.marpolbul.2015.08.026

Patil, P. N., Sawant, D. V., and Deshmukh, R. N. (2012). Physico-chemical parameters for testing of water – A review. *Int. J. Environ. Sci.* 3, 1194–1207. doi: 10.6088/ijes.2012030133028

Pearson, R. M., Sievers, M., McClure, E. C., Turschwell, M. P., and Connolly, R. M. (2020). COVID-19 recovery can benefit biodiversity. *Science* 368, 838–839. doi: 10.1126/science.abc1430

Pecot, M., and Ricaurte-Quijano, C. (2019). "Todos a Galápagos?' Overtourism in wilderness areas of the Global South," in *Overtourism: Excesses, Discontents and Measures in Travel and Tourism*, eds C. Milano, J. M. Cheer, and M. Novelli 70–85.

Peng, C., Zhao, X., and Liu, G. (2015). Noise in the Sea and its impacts on marine organisms. *Int. J. Environ. Res. Public Health* 12, 12304–12323. doi: 10.3390/ijerph121012304

Pereira, L. C. C., de Sousa, F., Días, R. C., Pessoa, A. B. B., da Silva, B. R. P., da Costa Baldez, C. A., et al. (2021). Beachgoer perceptions on health regulations of COVID-19 in two popular beaches on the Brazilian Amazon. *Ocean Coastal Manag.* 206:105576. doi: 10.1016/j.ocecoaman.2021.105576

PNG (2020). *Informe Anual de Visitantes a Las Áreas Protegidas de Galápagos 2019. Dirección del Parque Nacional Galápagos. Galápagos - Ecuador*. Available online at: http://www.galapagos.gob.ec/wp-content/uploads/2020/01/INFORME-ANUAL-DE-VISITANTES-2019.pdf (accessed Agust 21, 2020).

Prakash, V. K., Geetha, C. S., Preethi, T., Jayaram, C., Nagamani, P. V., and Laxmi, C. N. V. (2021). Assessment of water quality along the southeast coast of India during COVID-19 lockdown. *Front. Mar. Sci.* 8:338. doi: 10.3389/fmars.2021.659686

Quilliam, R. S., Weidmann, M., Moresco, V., Purshouse, H., O'Hara, Z., and Oliver, D. M. (2020). COVID-19: the environmental implications of shedding SARS-CoV-2 in human faeces. *Environ. Int.* 140:105790. doi: 10.1016/J.ENVINT.2020.105790

Ramos, X. (2020). *Las Luces Blancas de Poblados Costeros y el Ruido Afectan la Anidación de Tortugas y la Eclosión de Los Huevos en Las Playas del ECUADOR. Diario El Universo*. Available online at: https://www.eluniverso.com/noticias/2020/06/14/nota/7871262/tortugas-marinas-ecuador-playas-anidacion (accessed date August 21, 2020).

Randazzo, W., Truchado, P., Cuevas-Ferrando, E., Simón, P., Allende, A., and Sánchez, G. (2020). SARS-CoV-2 RNA titers in wastewater anticipated COVID-19 occurrence in a low prevalence are. *medRxiv[preprint]* 2020.04.22.20075200. doi: 10.1101/2020.04.22.20075200

Ricaurte-Quijano, C., Nacipucha, D., Gavilanes, J., Manner, F., Calles, A., and Cervantes, E. (2019). Beach uses and users in four beaches of the ecuadorian coast: the importance of physical and socioeconomic conditions for recreational beach use assessment in Latin American contexts. *Tourism Mar. Environ.* 14, 163–177. doi: 10.3727/154427319X15634413181250

Rosenbloom, D., and Markard, J. (2020). A COVID-19 recovery for climate. *Science* 368:447. doi: 10.1126/science.abc4887

Samuel, Y., Morreale, S. J., Clark, C. W., Greene, C. H., and Richmond, M. E. (2005). Underwater, low-frequency noise in a coastal sea turtle habitat. *J. Acoust. Soc. Am.* 117:1465. doi: 10.1121/1.1847993

Santander-Rodriguez, V. P. (2017). *Plastic Debris Effect by Zooplanktonic Community in the Galapagos Islands-Santa Cruz and San Cristobal Cases.* Bachelor's thesis. Guayaquil: ESPOL, 13. Avaliable online at: http://www.dspace.espol.edu.ec/xmlui/handle/123456789/41477

Schaurer, I., and Weiß, B. (2020). Investigating selection bias of online surveys on coronavirus-related behavioral outcomes. *Survey Res. Methods* 14, 103–108. doi: 10.18148/srm/2020.v14i2.7751

Setia, M. S. (2016). Methodology series module 3: cross-sectional studies. *Indian J. Dermatol.* 61, 261–264. doi: 10.4103/0019-5154.182410

Silva, C., Alves, F., and Rocha, R. (2007). The management of beach carrying capacity: the case of northern Portugal. *J. Coastal Res.* 135–139. Available online at: https://www.jstor.org/stable/26481571.

Soto-Varela, Z. E., Rosado-Porto, D., Bolívar-Anillo, H. J., Pichón González, C., Granados Pantoja, B., Estrada, D., et al. (2021). Preliminary microbiological coastal water quality determination along the department of atlántico (Colombia): relationships with beach characteristics. *J. Mar. Sci. Eng.* 9:122.

Spennemann, D., and Parker, M. (2020). Hitting the 'pause' button: what does COVID-19 tell us about the future of heritage sounds? *Noise Mapp.* 7, 265–275. doi: 10.1515/noise-2020-0022

Statista. (2020). *Economic Impact of Coronavirus (COVID-19) on the Tourism Sector in Ecuador in 2020, by Scenario*. Available online at: https://www.statista.com/statistics/1106008/coronavirus-economic-impact-tourism-scenario-ecuador/ (accessed date May 24, 2020).

Steele, J., Androulakis-Korakakis, P., Carlson, L., Williams, D., Phillips, S., Smith, D., et al. (2021). The impact of coronavirus (COVID-19) related public-health measures on training behaviours of individuals previously participating in resistance training: a cross-sectional survey study. *Sports Med. [online ahead of print]* 1–20. doi: 10.1007/s40279-021-01438-5

Steele, J., Androulakis-Korakakis, P., Carlson, L., Williams, D., Phillips, S., Smith, D., et al. (2021). The impact of coronavirus (COVID-19) related public-health measures on training behaviours of individuals previously participating in resistance training: a cross-sectional survey study. *Sports Med.* 1–20. doi: 10.1007/s40279-021-01438-5 [online ahead of print].

Stocker, M. (2007). Ocean bioacoustics, human-generated noise and ocean policy. *J. Int. Wildlife Law Policy* 10, 255–272. doi: 10.1080/13880290701769338

Stumpf, C. H., Gonzalez, R., and Noble, R. T. (2013). "Investigating the coastal water quality of the galapagos Islands, ecuador," in *Science and Conservation in the Galapagos Islands: 173 Frameworks & Perspectives, Social and Ecological Interactions in the Galapagos Islands*, eds S. J. Walsh and C. F. Mena (Berlin: Springer), 1.

Taherdoost, H. (2017). Determining sample size; how to calculate survey sample size. *Int. J. Economics Manag. Syst.* 2:2017.

Thums, M., Whiting, S. D., Reisser, J., Pendoley, K. L., Pattiaratchi, C. B., Proietti, M., et al. (2016). Artificial light on water attracts turtle hatchlings during their near shore transit. *R. Soc. Open Sci.* 3:160142. 10.1098/rsos.160142

Torrentira, M. C. (2020). Online Data Collection as adaptation in conducting quantitative and qualitative research during the COVID-19 pandemic. *Eur. J. Educ. Stud.* 7, 78–87. doi: 10.46827/ejes.v7i11.3336

UNWTO (2020). *International Tourism and covid-19*. Available online at: https://www.unwto.org/international-tourism-and-covid-19 (accessed May 24, 2020).

Vasantha, R. N., and Harinarayana, N. S. (2016). *Online Survey Tools: A Case Study of Google Forms*. Paper presented at the National Conference on "Scientific,

Computational & Information Research Trends in Engineering. Mysore: GSSS-IETW. .

Walsh, S., and Mena, C. F. (2013). *Science and Conservation in the Galapagos Islands: Frameworks & Perspectives*. Berlin: Springer.

Walsh, S., and Mena, C. F. (2016). Coupled human–natural systems in the Galapagos. *Proc. Natl. Acad. Sci. U.S.A.* 113, 14536–14543. doi: 10.1073/pnas.1604990113

Williams, A. T., Rangel-Buitrago, N. G., Anfuso, G., Cervantes, O., and Botero, C. M. (2016). Litter impacts on scenery and tourism on the Colombian north Caribbean coast. *Tourism Manag.* 55, 209–224. doi: 10.1016/j.tourman.2016.02.008

World Health Organization (WHO)/United Nations Environment Programme (UNEP) (1994). *Microbiological Quality of Coastal Recreational Waters. Mediterranean Marine Pollution Monitoring and Research Programme (MED POL) Phase II. Annex 1. Copenhagen, WHO Regional Office for Europe*. Geneva: World Health Organization, 5.

Yunus, A. P., Masago, Y., and Hijioka, Y. (2020). COVID-19 and surface water quality: improved lake water quality during the lockdown. *Sci. Total Environ.* 731:139012. doi: 10.1016/j.scitotenv.2020.139012

Zambrano-Alvarado, J. (2020). *Ballenas y Delfines Vuelven a la Costa de Ecuador*. Available online at: https://www.eltelegrafo.com.ec/noticias/sociedad/6/ballenas-delfines-costa-ecuador

Zambrano-Monserrate, M. A., Ruano, M. A., and Sanchez-Alcalde, L. (2021). Indirect effects of COVID-19 on the environment. *Sci. Total Environ.* 728:138813. doi: 10.1016/j.scitotenv.2020.138813

Zielinski, S., and Botero, C. M. (2020). Beach tourism in times of COVID-19 pandemic: critical issues, knowledge gaps and research opportunities. *Int. J. Environ. Res. Public Health* 17:7288. doi: 10.3390/ijerph17197288

Zambrano-Monserrate, M. A., Ruano, M. A., and Sanchez-Alcalde, L. (2020). Indirect effects of COVID-19 on the environment. *Sci. Total Environ.* 728:138813. doi: 10.1016/j.scitotenv.2020

Conflict of Interest: The authors declare that the research was conducted in the absence of any commercial or financial relationships that could be construed as a potential conflict of interest.

frontiers in Marine Science

ORIGINAL RESEARCH
published: 10 August 2021
doi: 10.3389/fmars.2021.648566

Aerosol Induced Changes in Sea Surface Temperature Over the Bay of Bengal Due to COVID-19 Lockdown

T. S. Sarin[1,2], V. Vinoj[1], D. Swain[1], K. Landu[1] and E. Suhas[2]*

[1] School of Earth, Ocean and Climate Sciences, Indian Institute of Technology Bhubaneswar, Arugul, India, [2] Department of Earth and Climate Science, Indian Institute of Science Education and Research, Pune, India

The role of COVID-19 pandemic lockdown in improving air quality was reported extensively for land regions globally. However, limited studies have explored these over oceanic areas close to high anthropogenic activities and emissions. The Bay of Bengal (BoB) basin is one such region adjacent to the highly populated South Asian region. We find that Aerosol Optical Depth (AOD) over the BoB declined by as much as 0.1 or 30% during the peak lockdown of April 2020 compared to long-term climatology during 2003–2019. Simultaneously, the sea surface temperature (SST) rose by 0.5–1.5°C over the central and north-western parts of the BoB with an average increase of 0.83°C. We show that up to 30% of this observed warming is attributable to reduced atmospheric aerosols. The study highlights the importance of anthropogenic emissions reduction due to COVID lockdown on short-term changes to SST over ocean basins with implications to regional weather.

Keywords: atmospheric aerosols, sea surface temperature, COVID-19 lockdown, Bay of Bengal, anthropogenic contribution

OPEN ACCESS

Edited by:
Xi Xiao,
Zhejiang University, China

Reviewed by:
Junyu He,
Zhejiang University, China
Jing Ma,
Nanjing University of Information Science and Technology, China

****Correspondence:***
V. Vinoj
vinoj@iitbbs.ac.in

Specialty section:
This article was submitted to Global Change and the Future Ocean, a section of the journal Frontiers in Marine Science

Received: *31 December 2020*
Accepted: *16 July 2021*
Published: *10 August 2021*

Citation:
Sarin TS, Vinoj V, Swain D, Landu K and Suhas E (2021) Aerosol Induced Changes in Sea Surface Temperature Over the Bay of Bengal Due to COVID-19 Lockdown. Front. Mar. Sci. 8:648566. doi: 10.3389/fmars.2021.648566

INTRODUCTION

COVID-19 was declared a pandemic by the World Health Organization (WHO) in March 2020, which subsequently spread to most countries globally, significantly changing their socio-economic landscapes (Buheji et al., 2020; Martin et al., 2020). Nations across the globe have taken various measures like social distancing, travel restrictions, and complete lockdowns of different durations to slow its spread. Numerous studies have documented multiple impacts of these lockdowns and the associated decrease in anthropogenic emissions in improving the air quality (e.g., Baldasano, 2020; Bauwens et al., 2020; Collivignarelli et al., 2020; Kanniah et al., 2020; Li et al., 2020; Mahato et al., 2020; Muhammad et al., 2020; Otmani et al., 2020; Pandey and Vinoj, 2020; Stratoulias and Nuthammachot, 2020). It is well known that atmospheric aerosols directly affect the surface radiation budget by absorbing and scattering the incoming solar radiation. They also modify the cloud microphysical properties (by acting as cloud condensation nuclei and ice nuclei, changing the size of cloud droplets and hence its albedo) (Twomey, 1977; Yu et al., 2006; Andreae and Rosenfeld, 2008; Boucher et al., 2013). In addition, the absorbing aerosols also change the atmosphere by altering the vertical temperature structure (Johnson et al., 2004; Koch and Del Genio, 2010), thereby affecting the atmospheric convection, droplet evaporation, and the overall cloud cover (called the semi-direct effect, Hansen et al., 1997). All these processes modulate the surface reaching solar radiation (Satheesh et al., 2006; Vinoj et al., 2010) and potentially modulate the surface temperature (Rajeev et al., 2008; Dave et al., 2020).

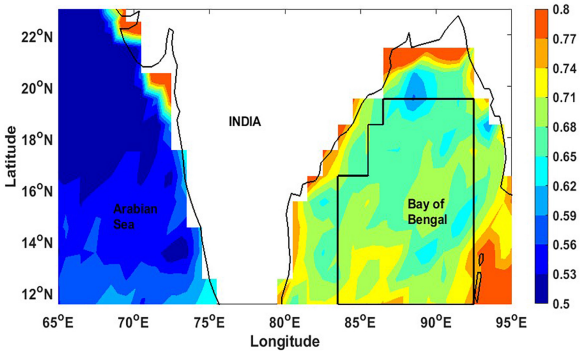

FIGURE 1 | The monthly mean Angstrom Exponent (AE) climatology over the oceanic regions around India during the period 2003–2018 for April.

The Indian Ocean rim countries (especially in South Asia) have undergone significant economic growth in recent times with increased emissions and thus atmospheric aerosol loading (Moorthy et al., 2013). The continental outflow, especially from the heavily aerosol laden Indo-Gangetic Plains (IGP), dominates the aerosol loading over the BoB region (Satheesh et al., 2001, 2006; Vinoj et al., 2004, 2010; Moorthy et al., 2009; Nair et al., 2014; Tiwari et al., 2016) during pre-monsoon (March to May) and the winter (December to February) season. Thus BoB is heavily affected by fine anthropogenic particulates as indicated by the high Angstrom Exponent (AE) (see **Figure 1**) compared to the Arabian Sea (Vinoj and Satheesh, 2003). A study done by Kedia and Ramachandran (2008) found that the anthropogenic contribution to AOD over the Bay of Bengal could be as high as 68–75%. The peak lockdown due to the pandemic occurred during April, coinciding with the period of high aerosol loading over the Indo-Gangetic Plains and hence the BoB (Satheesh et al., 2006; Vinoj and Pandey, 2016).

The sea surface temperature (SST) is an essential parameter for weather and plays a crucial role in regulating the Earth's climate. Previous studies using *in situ* and satellite-based measurements show that the BoB aerosols exert a radiative forcing of −20 to −30 W m^{-2} at the ocean surface (Satheesh, 2002; Dey et al., 2004; Vinoj et al., 2004; Satheesh et al., 2010). An observational study carried out over the Equatorial Indian Ocean showed that aerosols due to Indonesian forest fire exert a surface radiative forcing of −46 W $m^{-2,}$ thereby cooling the ocean surface by 1°C (Rajeev et al., 2008). Similar effects due to aerosol loading and SST were also documented by other studies (Cheng et al., 2005; Dwyer et al., 2010; Patil et al., 2019; Diao et al., 2021; Luo et al., 2021). However, most of these are based on model simulations and hence lack observational constraints.

The COVID-19 lockdown halted activities across large sections of the society by confining the population to their homes resulting in a significant decline in atmospheric anthropogenic aerosol loading (Pandey et al., 2016; Kanniah et al., 2020; Ranjan et al., 2020) as much as 40–60% over the South Asian region. The reduction in emissions and their influence extended far beyond their sources, affecting the air quality over places afar, including oceanic regions downwind such as the Bay of Bengal (BoB) (Pandey and Vinoj, 2020). Despite a good understanding of large-scale, long-range transport of aerosols to BoB from landmass around it (Vinoj et al., 2004; Kumar et al., 2008; Kulshrestha and Kumar, 2014), no study has attempted to understand the effect of aerosols on the SST over this region. Similar areas affected by long-range transport also exist over the South China Sea, north-west Pacific, equatorial Eastern, and the North Atlantic Ocean (Prospero, 1990; Lin et al., 2007; Zhu et al., 2020). Several reasons make such studies unviable. One primary reason is the lack of high-quality aerosol and SST observations from satellites. However, the availability of high-quality datasets since 2000 has made it possible to explore such cases in detail. In addition, the highly dynamic nature and the role of multiple factors affecting SSTs make it difficult to explore these relationships, if any.

Some of the factors affecting SSTs are solar insolation, warm/cold water advection, and other marine processes, namely ocean currents, upwelling/downwelling phenomena, and eddies (Leeuwenburgh and Stammer, 2001; Shinoda, 2005; Krishna, 2008; Mandal et al., 2019; Buckley et al., 2020). In addition, the BoB also receives a sizable freshwater influx from the rivers and undergoes near-surface ocean-atmosphere interactions, which alters the upper ocean processes (Parampil et al., 2010). Past studies have revealed that the circulation in the BoB is primarily wind and buoyancy-driven (Schott and McCreary, 2001; Schott et al., 2002; Liu and Alexander, 2007), which also modulates the surface and subsurface properties in the BoB. These multiple influences induce large variability in SST, with a monotonic decrease toward the South (Srivastava et al., 2018), coinciding with the spatial variability of aerosol loading (Satheesh et al., 2010), indicating a potential relationship.

The lockdown presented a unique opportunity to explore the effect of an unprecedented and substantial decline in aerosols over this region since the start of satellite measurements. This article quantifies the change to SST due to changes in aerosol loading over the Bay of Bengal during the peak pandemic lockdown period of April 2020 using long-term satellite datasets.

DATA AND METHODS

The aerosol optical depth (AOD) data used in this study is obtained from the NASA satellite datasets archived at https://giovanni.gsfc.nasa.gov/giovanni/ for April from 2003 to 2020. All the variables are at a spatial resolution of 1° × 1°. Several investigators have used aerosol optical depth (AOD), a column-averaged measure, to study atmospheric particulate matter load (Pandey and Vinoj, 2020; Ranjan et al., 2020). The Moderate Resolution Imaging Spectroradiometer (MODIS) Terra/Aqua aerosol products are of high quality and validated by multiple studies over India's land and oceanic regions (e.g., Vinoj et al., 2004, 2010; Jethva et al., 2007; Mhawish et al., 2017). The retrieval algorithms are updated periodically (Remer et al., 2005) to improve their accuracy. The latest version of combined MODIS Terra (MOD08_D3) and Aqua (MYD08_D3) collection 6 (Levy et al., 2013) level 3 products is used. The MODIS AOD is estimated in the following wavelengths:

0.47, 0.55, and 0.65 μm with an error of ±0.05 ± 15%τ (Kaufman and Tanré, 1998). In this study, AOD at 0.55 μm is used. The Angstrom Exponent (AE) product used in this study is estimated using 412 nm and 470 nm as the reference wavelengths. The latest collection (collection 6) (Platnick et al., 2017) product significantly reduces uncertainty. Unlike land, the ocean surface is spatially homogeneous, allowing coarser-resolution datasets for the analysis. In addition, level 3 datasets are used for research involving large spatial scales, thereby avoiding small scale heterogeneities, which is not of interest in this study. Observations from MODIS is widely utilized for aerosol and air quality research (Gupta et al., 2006, 2013; Pandey et al., 2016, 2017; Vinoj and Pandey, 2016; Mhawish et al., 2017; Jethva et al., 2018; Mukherjee et al., 2018; Rupakheti et al., 2019) over this region and also globally.

The sea surface temperature (SST), cloud fraction (CFR), and total column water vapor (TWV) is obtained from Atmospheric Infrared Sounder (AIRS) onboard NASA's Aqua satellite. The AIRS is a hyperspectral atmospheric sounder with 2378 infrared channels and four visible/near-infrared channels providing daily long-term global observations (Chahine et al., 2006; Pagano et al., 2006). This study uses the level 3 daily products (AIRSX3STD V007) from the latest version of the datasets (Tian et al., 2020). Past studies have shown good agreement between AIRS and radiosonde data within mission-specific accuracy bounds (Kahn et al., 2008; Prasad and Singh., 2009; Milstein and Blackwell, 2016).

Quality Check and Screening

The MODIS aerosol retrievals ensure high fidelity in their products. They are considered the best available for long-term scientific studies due to their stringent quality control and cloud screening measures. In addition to their regular quality checks, we also carried out a few data reduction strategies for additional confidence. Sometimes, the satellites may report slightly higher aerosol optical depth due to sub-grid cloud contamination even though a significant portion of the grids may be cloud-free. This may lead to a slight increase in the AOD.

Similarly, bright clouds close to clear pixels may lead to stray additional light leaking into nearby pixels leading to reduced AOD. Therefore, all datasets are screened for outliers using percentile-based criteria (top and bottom 5th percentile datasets are removed) though errors are remote. Considering the high quality of MODIS products, this data reduction is not an essential requirement and does not impact the overall results. However, this is done for better confidence in the quantifications made in this study. Also, there is no specific reason for using the 5th percentile for data reduction.

In addition, most meteorological parameters have a distinct seasonality over this region. Therefore, to avoid correlations induced due to these seasonality's, the anomalies/residuals are calculated by subtracting the weekly running mean (calculated using a 7-day window centered on the time point). This allowed the removal of seasonality (within the month) and long-term trend-induced co-variability between AOD and SST. This is an essential requirement as BoB has strong seasonality in both aerosol and sea surface temperature distribution, which can alter the relationship between the two.

Analysis Method

The changes in SSTs due to change in AOD were estimated using two different methods. (1) Using the raw SST and AOD using simple linear regression analysis, but only for clear sky conditions by including only data with CFR < 5% and the total column water vapor below the 20th percentile for each grid point. This is an additional check to avoid any effect due to clouds and water vapor. A linear regression analysis was done using data from all grid points over the whole BoB. The regression coefficients thus obtained provide an estimate of the change in SST as a function of AOD. (2) Using multiple linear regression analysis by using residuals of SST, AOD, TWC, and CFR. Here a regression model is developed at each grid point and is applied to estimate the change in SST only due to change in AOD at that specific grid. The statistical significance of the regression is calculated using the *t*-test.

Additional care was taken to use only grids (see **Figure 1**) at least 1° away from the coast (especially Northern Bay). This was essential to remove any effect of current-induced SST changes close to the coast and avoid any false relationships that may arise due to coastal processes such as upwelling and freshwater flux that may change SSTs (Krishna, 2008). In addition, aerosol retrieval errors are significantly high closer to the coast due to the land-ocean boundary (different algorithms used for the AOD retrievals) and the potential effects of sediment concentrations on the overall surface-atmosphere reflectance errors in aerosol retrievals from satellite sensors (Anderson et al., 2013).

RESULTS AND DISCUSSION

Climatological SST and AOD Over the BoB

The climatological mean AOD and SST for April are shown in **Figures 2A,D**, respectively. These are the climatological spatial patterns expected over this region. The AOD shows a spatial gradient that declines from the North to the South. The high AOD is observed over the Northern BoB with values as high as 0.6–0.8. They become lower as one moves south by more than 50% (0.2–0.3) within a small distance. This is because the head Bay is affected more by the advection of aerosols from North India (especially the Indo-Gangetic Plains) and the coastal regions of India, Bangladesh, and Myanmar (Sumanth et al., 2004; Vinoj et al., 2004; Nair et al., 2009). The high population density and numerous industries over the region mean that emissions over these source regions are relatively high. Northwesterly winds during the period further act as conduits transporting these aerosols to the BoB (Lakshmi et al., 2017). Southern BoB is affected by the surrounding coastal regions and aerosols from the Arabian Sea, which is less affected by anthropogenic activities leading to lower AOD (Nair et al., 2009). One can also see a decrease in loading as we move further away from the coasts. Even in a climatological sense, the high AOD to the North matches with the lower SST below indicating

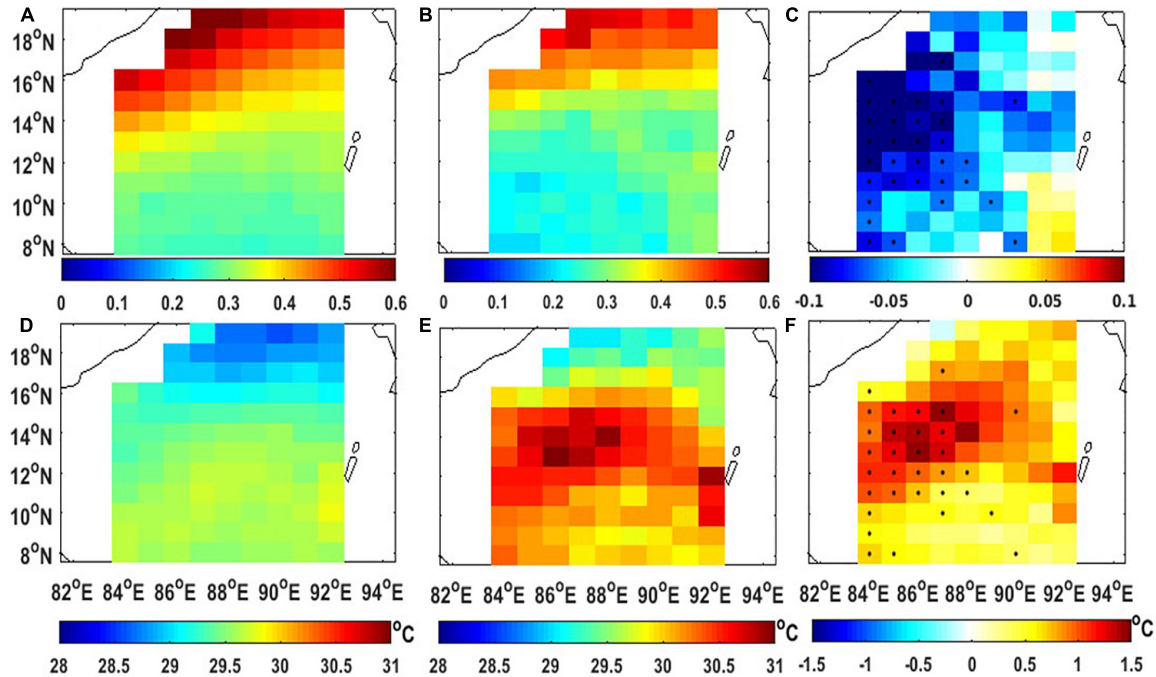

FIGURE 2 | (A) Climatological aerosol loading during April 2003–2019. **(B)** Aerosol loading during April 2020. **(C)** AOD anomaly (dots signify regions where AOD change is more than 20%). **(D)** Climatological SST during April 2003–2019. **(E)** SST during April 2020. **(F)** SST anomaly (dots signify regions where AOD change is more than 20%).

an inverse relationship between AOD and SST. However, due to the possibility of cool freshwater influx from the rivers such as the Ganges and Brahmaputra during this period, it is impossible to argue that this reduced SST is solely caused by the atmospheric aerosols.

Figure 2C shows the anomalies in AOD for the period (April 2020 climatology). It is clear that AOD decreased during this period coinciding with the world's most extensive lockdown affecting more than a billion people in the sub-continent. The AOD decreased by 0.05–0.15 (30–60%) over the Northwest part of BoB. The area average decline was about 0.1 over the whole domain (**Figures 2B,C**). This decline is substantial, knowing that AOD changes even over developed countries were lower than this (Acharya et al., 2020; Sanap, 2021). Even considering the high aerosol-laden IGP, these numbers are substantial (greater than 20–30% for this period). The high decline in percentages corresponds to regions in the south Bay of Bengal due to their ordinarily low loading conditions. During the same period over land, the AOD decreased by 0.4 (Pandey and Vinoj, 2020; Soni et al., 2021). The IGB (major source region for aerosols over BoB) showed the maximum change in AOD.

As already mentioned, the SST is lower over N. BoB and increases toward the South (**Figure 2D**). The spatial distribution and gradients for aerosol and SST are opposite over BoB. In April 2020 (**Figure 2E**), the SST has increased throughout the basin, but more so over North-Western parts during the lockdown period. The **Figures 2C,F** shows the difference between climatology and 2020 for AOD and SST, respectively. It is found that the decline in AOD spatially matches the pattern of increase in SST (**Figure 2F**). The spatial pattern of change in SST and AOD points to the possibility of aerosol decline leading to a substantial increase in SST. The negative relationship in the spatial pattern of AOD and SST (high AOD corresponding to low SST and vice versa) in a climatological sense and the similar and consistent spatial pattern of change during April 2020 points to a possibility of physical causation. Thus both in climatological sense and anomalies (and their exact match in the spatial pattern) during April 2020, the AOD and SST indicate a strong negative relationship.

Earlier studies have established that winds and freshwater forcing are the dominating factors affecting the temporal variability of SST in the BoB (Duncan and Han, 2009; Seo et al., 2009; Akhil et al., 2014; Jana et al., 2015; Srivastava et al., 2018). The buoyancy flux plays a significant role in changing the region's SST (and MLD) during the winter monsoon (January and February). Similarly, wind stress forcing modulates the SST during the summer monsoon period. Investigating the intraseasonal variability of SST in the Indian Ocean during boreal summer using Hybrid Coordinate Ocean Model (HYCOM), Duncan and Han (2009) found that wind plays a much more significant role in altering SSTs than either shortwave fluxes or precipitation. Low wind speed conditions over BoB characterize April; hence insolation is the dominant contributor to the variability in SST. This indicates that aerosol-induced changes to solar insolation may significantly impact the SST variability during this period. The SST variability decreases from North to South, with the northern BoB showing higher SST variability

compared to the southern portion (Srivastava et al., 2018). This is similar to the variability in aerosol loading as well.

Thus, SST's over the BoB is influenced by aerosols. This is not surprising as studies have shown in the past that aerosols lead to the large top of the atmosphere cooling of the order of -1 to -2 W m^{-2} (Andreae et al., 2005). These are expected to be substantially larger in highly polluted regions with extensive aerosol loading such as BoB with top of the atmosphere (surface) forcing being of the order of -6 to -10 W m^{-2} (-30 to -35 W m^{-2}) (Vinoj et al., 2004; Ramachandran, 2005).

Quantifying the SST Change Due to Aerosols

An attempt is made to estimate the change in SST as a function of AOD using daily raw AOD and SST datasets during April 2003–2019 (510 days of data over a large spatial scale with 101 grid points). These datasets have undergone the initial quality checks mentioned in the section "Data and Methods" and correspond to method 1. **Figure 3** shows the contour density plot to establish the relationship between SST and AOD. The SST decreases with an increase in AOD. The value of the slope implies that an increase in unit AOD leads to a roughly 1.64°C decrease in temperature. Therefore, this simple estimate reveals that, on average, a 0.1 difference in AOD may cause SST to change by 0.16°C.

The above assessment is made using raw AOD and SST after the initial screening for outliers and avoiding coastal grids and clouds but may be influenced by seasonality, trends, and other atmospheric parameters. Also, this estimate is valid only for this region for this period. If one has to find the SST change elsewhere, these numbers may vary. This is mainly due to differences in aerosol properties and the specific processes that influence SST over different regions. For example, a stagnant ocean region may show a more significant sensitivity of SST to change in atmospheric constituents and solar insolation than a more dynamic ocean surface. This is also an average estimate for the whole study region. Rajeev et al. (2008) showed that a change in aerosol loading of 0.8 led to a cooling of ∼1°C over the Equatorial Indian Ocean due to the Indonesian forest fire-induced aerosols during September/October 1997. This sensitivity (∼1.25°C for a unit change in AOD) is slightly lower than our estimate of 1.64°C. This may be due to the change in season and differing oceanic processes relevant for that particular region. The SST's are also much warmer during April than September/October. In addition, other marine processes such as eddies may strengthen or dampen the sensitivity of SST to changes in aerosols.

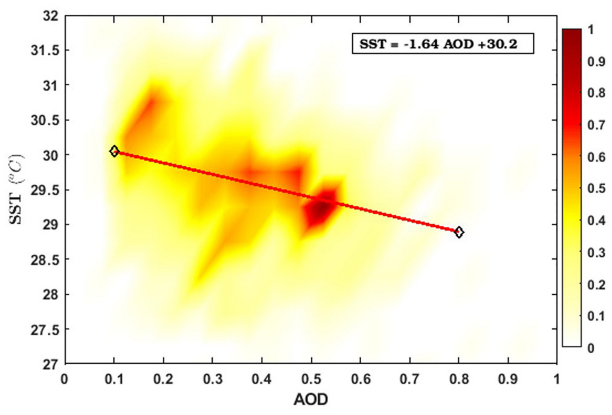

FIGURE 3 | The scatter plot showing the relationship between SST and AOD for April 2003–2019. The color bar represents the number density at each pixel normalized by the maximum over the whole SST-AOD space.

Quantifying the SST Change Due to Aerosols Without Clouds and Water Vapor

A multi-linear regression analysis was carried out (method 2) incorporating AOD, TWV, and CFR in place of simple linear regression to remove the effects induced by other parameters such as CFR and TWV if any. The sensitivity of SST to AOD is calculated by setting the regression coefficients corresponding to all other parameters to zero at each grid point over the BoB.

The total change in SST observed during April 2020 (**Figure 4A**) and that owing to aerosols is shown in **Figure 4B** (method 1) and **Figure 4C** (method 2), respectively. The only difference between **Figures 4B,C** is that one corresponds to change in SST estimated using a single regression coefficient applied to all grid points over BoB and the other where regression coefficients are calculated separately at each grid point. That is the reason for the similarity in the spatial pattern of **Figures 4B**, **Figure 2C**. Both these estimates are based on regression coefficients developed using long-term datasets covering 2003–2019 and applying them to change in AOD observed during 2020. The SST change due to aerosols is seen to be statistically significant at most pixels, where the change in SST is high (**Figure 4C**). The aerosols have a higher effect on SST closer to the coasts (North West) (see **Figure 2C**), as expected. These regions most affected by emissions from the surrounding landmass coincided with a significant decline in AOD during April 2020. Large spatial variability is observed in the warming attributable to aerosols, with the most considerable warming exceeding 1.5°C. Such differences may be possible due to various reasons, including variations in aerosols loading, aerosol type, sea surface properties such as salinity, the thickness of the mixed layer, barrier layer, etc.

Detailed analysis of all these factors is beyond the scope of this work and hence is not attempted. However, most grids show warming close to or greater than 0.2°C (**Figures 4B,C**, shown as yellow contours). These numbers are comparable to those obtained earlier in method 1 (an average of 0.16°C corresponding to a 0.1 change in AOD). This spatial pattern (**Figure 4B**) for April 2020 coinciding with the high-temperature anomaly (**Figure 4A**) provides confidence that AOD decline led to the observed warming. Thus, it may be said that the SST change is in part modulated by a significant decline in aerosol loading due to COVID-19 lockdown over the BoB.

Overall, the whole BoB region shows an average observed warming of 0.83°C during April 2020 (see **Figure 5**), while the

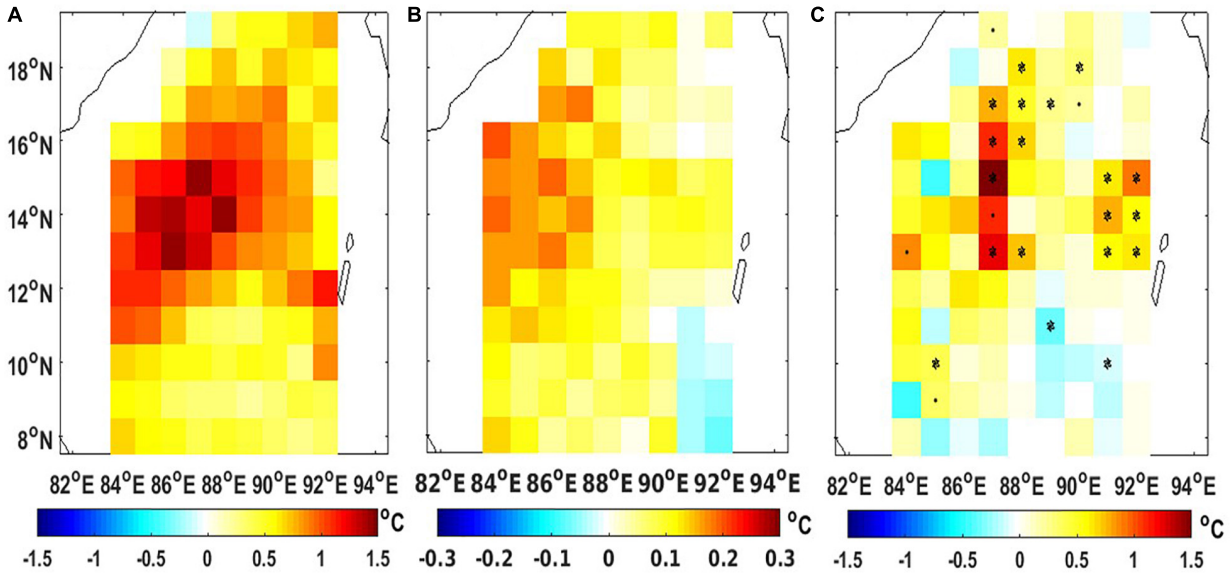

FIGURE 4 | (A) The observed spatial pattern of change in SST. **(B)** Change in SST calculated using method 1. **(C)** Change in SST estimated using method 2 (dots and stars represent statistical significance at 90 and 95% levels, respectively).

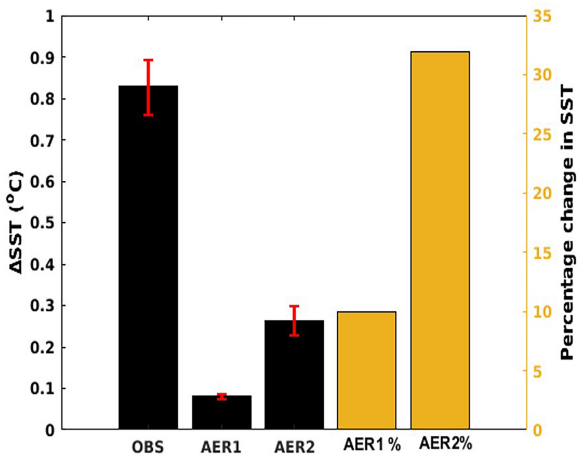

FIGURE 5 | The total warming observed during April 2020 and that attributed to aerosols (AER1 and AER2). The yellow bar represents the aerosol-led warming in percentage (corresponding to the *y*-axis shown to the right). The error bar represents the standard error estimated from the spatial distribution.

average aerosol effect is estimated to be ∼0.26°C, which is ∼32% of the overall warming.

One crucial aspect that needs to be mentioned here is the significant difference in change in SST between methods 1 and 2. In method 1, the effect of CFR is minimized, but the presence of water vapor (though only data less than the 20th percentile is used) appears to dampen the aerosol impact on SST. Also, in method 2, it is found that the regression coefficients for TWV were overall positive, indicating a warming effect. Such warming due to TWV is not surprising as past studies have suggested that irradiance in the long wave (LW) spectrum increases with increasing water vapor and subsequent changes to downwelling radiation (Obregón et al., 2015). Pandey and Vinoj (2020) showed that humidity increased by 10–15% over the Northern BoB during the lockdown. Such an increase in water vapor content may induce warming [as indicated by the positive regression coefficient from method 2 (not shown)], thus reducing the overall aerosol effect. Stanhill (2011) also demonstrated a more significant sensitivity of surface temperature to LW than short wave (SW) due to water vapor. Overall, method 1 shows aerosol-induced warming of ∼10%, whereas method 2, which minimizes both the effect of CFR and TWV, shows amplified aerosol-induced warming of ∼30%.

Some Limitations of the Study

There are a few limitations in the current study. The aerosol-induced warming of ∼10–30% is expected to be a lower bound as only the direct effect under clear sky conditions is studied. The aerosols also alter radiation balance indirectly by modifying cloud properties such as effective cloud droplet radius and thus cloud albedo and are not addressed in this article. Our preliminary analysis also indicates a decline in cloud fraction during this period (not shown). In addition, another related study by Bhowmick et al. (2020) showed that warm-core eddies over this region might have also led to the increased overall SST during the lockdown. This also points to the possibility of high sensitivity to aerosols (compared to Rajeev et al., 2008) over these warm-core eddies as their interaction with water mass around them is minimal. Thus, it may be said that the aerosol effect on SST, in reality, maybe higher if their impact through cloud modifications is considered. However, quantifying these effects is beyond the scope of this work and hence not attempted.

CONCLUSION

This study explored the impact of COVID-19 lockdown during April 2020, the resultant decline in aerosol loading, and its effect on SST over the BoB using satellite observations. Our study reveals that the lockdown-induced decrease in the AOD over the Bay of Bengal was ∼30% (corresponding AOD of 0.05–0.1). Simultaneously, the SSTs over the whole basin increased by ∼+0.83°C (up to 1.5°C in certain pockets). Spatially, the decline in aerosol loading matched well with the areas showing a substantial increase in SSTs (especially over North and North-West of BoB). The analysis indicates a rise in SST of the order of +0.26°C (∼32%) attributed to aerosols' effect. The SSTs of regions closer to the coast and the North Central part of BoB were the most affected by changes in aerosol loading. Thus, our study shows that reduced aerosols due to the recent COVID-19 lockdowns have increased the SST partially in the BoB with implications to regional weather.

DATA AVAILABILITY STATEMENT

All dataset presented in this study are available in the public domain downloadable from https://giovanni.gsfc.nasa.gov/giovanni/. Any further inquiries can be directed to the corresponding author.

AUTHOR CONTRIBUTIONS

VV, DS, and KL conceived the idea. TS carried out all the analyses and prepared the plots. VV, TS, and DS wrote the manuscript with inputs from all co-authors. All authors contributed equally in discussions.

ACKNOWLEDGMENTS

The authors would like to thank the NASA Giovanni archive for providing all the datasets used in this study. TS would like to thank IIT Bhubaneswar for providing the necessary infrastructure to carry out this work as part of an internship at the institute. TS would also like to thank the Infosys Foundation for providing the funds required to continue his studies and the Ministry of Science and Technology, DST, Government for financial assistance through the INSPIRE scholarship.

REFERENCES

Acharya, P., Barik, G., Gayen, B. K., Bar, S., Maiti, A., Sarkar, A., et al. (2020). Revisiting the levels of Aerosol Optical Depth in South-Southeast Asia, Europe and USA amid the COVID-19 pandemic using satellite observations. *Environ. Res.* 193:110514. doi: 10.1016/j.envres.2020.110514

Akhil, V. P., Durand, F., Lengaigne, M., Vialard, J., Keerthi, M. G., Gopalakrishna, V. V., et al. (2014). A modeling study of the processes of surface salinity seasonal cycle in the Bay of Bengal. *J. Geophys. Res.-Oceans* 119, 3926–3947. doi: 10.1002/2013JC009632

Anderson, J. C., Wang, J., Zeng, J., Leptoukh, G., Petrenko, M., Ichoku, C., et al. (2013). Long-term statistical assessment of Aqua-MODIS aerosol optical depth over coastal regions: bias characteristics and uncertainty sources. *Tellus B* 65:20805. doi: 10.3402/tellusb.v65i0.20805

Andreae, M. O., and Rosenfeld, D. (2008). Aerosol–cloud–precipitation interactions. *Sci. Rev.* 89, 13–41.

Andreae, M. O., Jones, C. D., and Cox, P. M. (2005). Strong present-day aerosol cooling implies a hot future. *Nature* 435, 1187–1190. doi: 10.1038/nature03671

Baldasano, J. M. (2020). COVID-19 lockdown effects on air quality by NO_2 in the cities of Barcelona and Madrid (Spain) Sci. *Total Environ.* 741:140353. doi: 10.1016/j.scitotenv.2020.140353

Bauwens, M., Compernolle, S., Stavrakou, T., Müller, J. F., van Gent, J., Eskes, H., et al. (2020). Impact of coronavirus outbreak on NO2 pollution assessed using TROPOMI and OMI observations. *Geophys. Res. Lett.* 47:e2020GL087978. doi: 10.1029/2020GL087978

Bhowmick, S. A., Agarwal, N., Sharma, R., Sundar Venkatesan, R., Anoopa Prasad, C., and Navaneeth, K. N. (2020). Cyclone Amphan: oceanic conditions pre- and post-cyclone using in situ and satellite observations. *Curr. Sci.* 119, 1510–1151. doi: 10.18520/cs/v119/i9/1510

Boucher, O., Randall, D., Artaxo, P., Bretherton, C., Feingold, G., Forster, P., et al. (2013). "Clouds and aerosols," in *Climate change 2013: The physical science basis, contribution of working group I to the fifth assessment report of the intergovernmental panel on climate change*, ed. T. F. Stocker (Cambridge, UK: Cambridge University Press), 571–658.

Buckley, J. M., Mingels, B., and Tandon, A. (2020). The impact of lateral advection on SST and SSS in the northern Bay of Bengal during 2015. *Deep Sea Res. Part II* 172:104653. doi: 10.1016/j.dsr2.2019.104653

Buheji, M., da Costa, Cunha, K., Beka, G., MavriĆ, B., Leandro, et al. (2020). The extent of COVID-19 pandemic socio-economic impact on global poverty. a global integrative multidisciplinary review. *Am. J. Econ.* 2020, 213–224. doi: 10.5923/j.economics.20201004.02

Chahine, M. T., Pagano, T. S., Aumann, H. H., Atlas, R., Barnet, C., Blaisdell, J., et al. (2006). Zhou AIRS: improving weather forecasting and providing new data on greenhouse gases Bull. *Am. Meteorol. Soc.* 87, 911–926. doi: 10.1175/BAMS-87-7-911

Cheng, Y., Lohmann, U., Zhang, J., Luo, Y., Liu, Z., and Lesins, G. (2005). Contribution of change in sea surface temperature and aerosol loading to the decreasing precipitation trend in southern China. *J. Clim.* 18, 1381–1390. doi: 10.1175/JCLI3341.1

Collivignarelli, M. C., Abbà, A., Bertanza, G., Pedrazzani, R., Ricciardi, P., and Miino, M. C. (2020). Lockdown for CoViD-2019 in Milan: what are the effects on air quality? *Sci. Tot. Environ.* 2020:732.

Dave, P., Bhushan, M., and Venkataraman, C. (2020). Absorbing aerosol influence on temperature maxima: An observation based study over India. *Atmosph. Environ.* 223:117237. doi: 10.1016/j.atmosenv.2019.117237

Dey, S., Sarkar, R. P., and Singh. (2004). Comparison of aerosol radiative forcing over the Arabian Sea and the Bay of Bengal. *Adv. Space Res.* 33, 1104–1108. doi: 10.1016/S0273-1177(03)00737-3

Diao, C., Xu, Y., and Xie, S.-P. (2021). Anthropogenic aerosol effects on tropospheric circulation and Sea surface temperature (1980–2020): separating the role of zonally asymmetric forcings, atmos. *Chem. Phys. Discuss.* [Preprint]. doi: 10.5194/acp-2021-407

Duncan, B., and Han, W. (2009). Indian Ocean intraseasonal sea surface temperature variability during boreal summer: Madden-Julian Oscillation versus sub monthly forcing and processes. *J. Geophys. Res.-Oceans* 114:C05002. doi: 10.1029/2008JC004958

Dwyer, J. G., Norris, J. R., and Ruckstuhl, C. (2010). Do climate models reproduce observed solar dimming and brightening over China and Japan? *J. Geophys. Res. Atmosph.* 115:945. doi: 10.1029/2009JD012945

Gupta, P., Christopher, S. A., Wang, J., Gehrig, R., Lee, Y., and Kumar, N. (2006). Satellite remote sensing of particulate matter and air quality assessment over global cities. *Atmos. Environ.* 40, 5880–5892. doi: 10.1016/j.atmosenv.2006.03.016

Gupta, P., Khan, M. N., Silva, A., and Patadia, F. (2013). MODIS aerosol optical depth observations over urban areas in Pakistan: quantity and quality of the

data for air quality monitoring. *Atmos. Pollut. Res.* 4, 43–52. doi: 10.5094/APR.2013.005

Hansen, J. E., Sato, M., and Ruedy, R. (1997). Radiative forcing and climate response. *J. Geophys. Res.* 102, 6831–6864. doi: 10.1029/96jd03436

Jana, S., Gangopadhyay, A., and Chakraborty, A. (2015). Impact of seasonal river input on the Bay of Bengal simulation. *Cont. Shelf Res.* 104, 45–62. doi: 10.1016/j.csr.2015.05.001

Jethva, H., Chand, D., Torres, O., Gupta, P., Lyapustin, A., and Patadia, F. (2018). Agricultural Burning and Air Quality over Northern India: A Synergistic Analysis using NASA's A-train Satellite Data and Ground Measurements. *Aerosol. Air Qual. Res.* 18, 1756–1773. doi: 10.4209/aaqr.2017.12.0583

Jethva, H., Satheesh, S. K., and Srinivasan, J. (2007). Evaluation of MODIS C004 aerosol retrievals at Kanpur, Indo-Gangetic Basin. *J. Geophys. Res.* 112:D14216. doi: 10.1029/2006JD007929

Johnson, B. T., Shine, K. P., and Forster, P. M. (2004). The semi-direct aerosol effect: Impact of absorbing aerosols on marine stratocumulus. *Q. J. R. Meteorol. Soc.* 130, 1407–1422. doi: 10.1256/qj.03.61

Kahn, B. H., Chahine, M. T., Stephens, G. L., Mace, G. G., Marchand, R. T., Wang, Z., et al. (2008). Cloud type comparisons of AIRS, CloudSat, and CALIPSO cloud height and amount. *Atmos. Chem. Phys.* 8, 1231–1248. doi: 10.5194/acp-8-1231-2008

Kanniah, K. D., Zaman, N. A. F. K., Kaskaoutis, D. G., and Latif, M. T. (2020). COVID-19's impact on the atmospheric environment in the Southeast Asia region. *Sci. Tot. Environ.* 2020:736.

Kaufman, Y. J., and Tanré, D. (1998). Algorithm for remote sensing of tropospheric aerosol from MODIS. *Modis. Atbd Mod.* 9, 1–85.

Kedia, S., and Ramachandran, S. (2008). Features of aerosol optical depths over the Bay of Bengal and the Arabian Sea during pre-monsoon season: Variabilities and anthropogenic influence. *J. Geophys. Res.* 113:D11201. doi: 10.1029/2007JD009070

Koch, D., and Del Genio, A. D. (2010). Black carbon semi-direct effects on cloud cover: Review and synthesis. *Atmos. Chem. Phys.* 10, 7685–7696. doi: 10.5194/acp-10-7685-2010

Krishna, M. (2008). View on Bay of Bengal upwelling area on the basis of 19-years satellite sea surface temperature. *Int. J. Digital Earth* 1, 304–314. doi: 10.1080/17538940802149965

Kulshrestha, U., and Kumar, B. (2014). Air mass trajectories and long-range transport of pollutants: review of wet deposition scenario in South Asia. *Adv. Meteorol.* 2014, 1–14. doi: 10.1155/2014/596041

Kumar, A., Sudheer, A. K., and Sarin, M. M. (2008). Chemical characteristics of aerosols in MABL of Bay of Bengal and Arabian Sea during spring inter-monsoon: a comparative study. *J. Earth Syst. Sci.* 117: 325e332.

Lakshmi, N. B., Nair, V. S., and Suresh Babu, S. (2017). Vertical structure of aerosols and mineral dust over the Bay of Bengal from multisatellite observations. *J. Geophys. Res. Atmosph*. 122, 12,845–12,861. doi: 10.1002/2017JD027643

Leeuwenburgh, O., and Stammer, D. (2001). The effect of ocean currents on sea surface temperature anomalies. *J. Phys. Oceanogr.* 31, 2340–2358. doi: 10.1175/1520-0485(2001)031<2340:teooco>2.0.co;2

Levy, R. C., Mattoo, S., Munchak, L. A., Remer, L. A., Sayer, A. M., Patadia, F., et al. (2013). The Collection 6 MODIS aerosol products over land and ocean. *Atmos. Meas.Tech.* 6, 2989–3034. doi: 10.5194/amt-6-2989-2013

Li, L., Li, Q., Huang, L., Wang, Q., Zhu, A., Xu, J., et al. (2020). Air quality changes during the COVID-19 lockdown over the Yangtze River Delta Region: an insight into the impact of human activity pattern changes on air pollution variation. *Sci. Tot. Environ.* 2020:732.

Lin, I. I., Chen, J. P., Wong, G. T. F., Huang, C.-W., and Lien, C.-C. (2007). Aerosol input to the South China Sea: results from the moderate resolution imaging spectroradiometer, the quick scatterometer, and the measurements of pollution in the troposphere sensor. *Deep Sea Res. II* 54, 1589–1601. doi: 10.1016/j.dsr2.2007.05.013

Liu, Z., and Alexander, M. (2007). Atmospheric bridge, oceanic tunnel, and global climatic teleconnections. *Rev. Geophys.* 45:RG2005. doi: 10.1029/2005RG000172

Luo, B., Minnett, P. J., Zuidema, P., Nalli, N. R., and Akella, S. (2021). Saharan dust effects on North Atlantic sea-surface skin temperatures. *J. Geophys. Res.* 126:e2021JC017282. doi: 10.1029/2021JC017282

Mahato, S., Pal, S., and Ghosh, K. G. (2020). Effect of lockdown amid COVID-19 pandemic on air quality of the megacity Delhi. *India. Sci. Total Environ.* 730:139086. doi: 10.1016/j.scitotenv.2020.139086

Mandal, S., Sil, S., Pramanik, S., Arunraj, K. S., and Jena, B. K. (2019). Characteristics and evolution of a coastal mesoscale eddy in the western Bay of Bengal monitored by high-frequency radars Dyn. *Atmos. Oceans* 88:101107. doi: 10.1016/j.dynatmoce.2019.101107

Martin, A., Markhvida, M., and Hallegatte, S. (2020). Socio-Economic Impacts of COVID-19 on Household Consumption and Poverty. *Econ. Dis. CliCha* 4, 453–479. doi: 10.1007/s41885-020-00070-3

Mhawish, A., Banerjee, T., Broday, D. M., Misra, A., and Tripathi, S. N. (2017). Evaluation of MODIS Collection 6 aerosol retrieval algorithms over Indo-Gangetic Plain: implications of aerosols types and mass loading. *Rem. Sens. Environ.* 201, 297–313. doi: 10.1016/j.rse.2017.09.016

Milstein, A. B., and Blackwell, W. J. (2016). Neural network temperature and moisture retrieval algorithm validation forAIRS/AMSU and CrIS/ATMS. *J. Geophys. Res. Atmos.* 121, 1414–1430. doi: 10.1002/2015jd024008

Moorthy, K., Nair, Vijayakumar, S., Babu, Suresh, S., et al. (2009). Spatial and vertical heterogeneities in aerosol properties over oceanic regions around India: Implications for radiative forcing. *Q. J. R. Meteorol. Soc.* 135, 2131–2145. doi: 10.1002/qj.525

Moorthy, K., Suresh Babu, S., Manoj, M. R., and Satheesh, S. K. (2013). Buildup of aerosols over the Indian Region. *Geophys. Res. Lett.* 40, 1011–1014. doi: 10.1002/grl.50165

Muhammad, S., Long, X., and Salman, M. (2020). COVID-19 pandemic and environmental pollution: A blessing in disguise? *Sci. Total Environ.* 728:138820. doi: 10.1016/j.scitotenv.2020.138820

Mukherjee, T., Asutosh, A., Pandey, S. K., Yang, L., Panwar, A., Gogoi, P. P., et al. (2018). Increasing Potential for Air Pollution over Megacity New Delhi: A Study Based on 2016 Diwali Episode. *Aerosol. Air Q. Res.* 9:18. doi: 10.4209/aaqr.2017.11.0440

Nair, P. R., George, S. K., Aryasree, S., and Jacob, S. S. (2014). Chemical composition of aerosols over Bay of Bengal during pre-monsoon: Dominance of anthropogenic sources. *J. Atmos. Sol. Terr. Phys.* 109, 54–65. doi: 10.1016/j.jastp.2014.01.004

Nair, V. S., Moorthy, K. K., Babu, S. S., and Satheesh, S. K. (2009). Optical and physical properties of atmospheric aerosols over the Bay of Bengal during ICARB. *J. Atmos. Sci.* 66, 2640–2658. doi: 10.1175/2009jas3032.1

Obregón, M. A., Costa, M. J., Serrano, A., and Silva, A. M. (2015). Effect of water vapor in the SW and LW downward irradiance at the surface during a day with low aerosol load. *IOP Conf. Ser.* 28:012009. doi: 10.1088/1755-1315/28/1/012009

Otmani, A., Benchrif, A., Tahri, M., Bounakhla, M., El Bouch, M., and Krombi, M. H. (2020). Impact of COVID-19 lockdown on PM10, SO2 and NO2 concentrations in Salé City (Morocco). *Sci. Total Environ.* 735:139541. doi: 10.1016/j.scitotenv.2020.139541

Pagano, T. S., Chahine, M. T., Aumann, H. H., and Tian, B. (2006). "Climate research with the atmospheric infrared sounder," in *Proc. SPIE 6362, Remote Sensing of Clouds and the Atmosphere XI*, (Mass: Kluwer Acad), 63621K. doi: 10.1117/12.689148

Pandey, S. K., and Vinoj, V. (2020). Surprising Changes in Aerosol Loading over India amid COVID-19 Lockdown. *Aerosol. Air Qual. Res.* 21:200466. doi: 10.4209/aaqr.2020.07.0466

Pandey, S. K., Bakshi, H., and Vinoj, V. (2016). "Recent changes in dust and its impact on aerosol trends over the Indo-Gangetic Plain (IGP)," in *Proc. of SPIE, Remote Sensing of the Atmosphere, Clouds, and Precipitation VI*, (Cambridge, UK: Cambridge University Press), Vol. 14, 98761Z. doi: 10.1117/12.2223314

Pandey, S. K., Vinoj, V., Landu, K., and Babu, S. S. (2017). Declining pre-monsoon dust loading over South Asia: Signature of a changing regional climate. *Sci. Rep.* 7:16062. doi: 10.1038/s41598-017-16338-w

Parampil, S. R., Gera, A., Ravichandran, M., and Sengupta, D. (2010). Intraseasonal response of mixed layer temperature and salinity in the Bay of Bengal to heat and freshwater flux. *J. Geophys. Res.* 115:C05002. doi: 10.1029/2009JC005790

Patil, N., Venkataraman, C., Muduchuru, K., Ghosh, S., and Mondal, A. (2019). Disentangling sea-surface temperature and anthropogenic aerosol influences on recent trends in South Asian monsoon rainfall. *Clim. Dyn.* 52, 2287–2302. doi: 10.1007/s00382-018-4251-y

Platnick, S., Meyer, K. G., King, M. D., Wind, G., Amarasinghe, N., Marchant, B., et al. (2017). The MODIS cloud optical and microphysical products: Collection 6 updates and examples from Terra and Aqua. *IEEE Trans. Geosci. Remote Sens.* 55, 502–525. doi: 10.1109/TGRS.2016.2610522

Prasad, A. K., and Singh, R. P. (2009). Validation of MODIS Terra, AIRS, NCEP/DOE AMIP-II Reanalysis-2, and AERONET Sun photometer derived integrated precipitable water vapour using ground-based GPS receivers over India. *J. Geophys. Res. Atmos.* 2009:114.

Prospero, J. M. (1990). "Mineral-aerosol transport to the North Atlantic and North Pacific: The impact of African and Asia source," in *The Long-Range Atmospheric Transport of Natural and Contaminant Substances*, ed. A. H. Knap (Mass: Kluwer Acad), 59–86. doi: 10.1007/978-94-009-0503-0_4

Rajeev, K., Parameswaran, K., and Nair, S. K. (2008). Meenu Observational evidence for the radiative impact of Indonesian smoke in modulating the sea surface temperature of the equatorial Indian Ocean. *J. Geophys. Res.* 2008:113. doi: 10.1029/2007jd009611

Ramachandran, S. (2005). Aerosol radiative forcing over Bay of Bengal and Chennai: Comparison with maritime, continental, and urban aerosol models. *J. Geophys. Res.* 110:D21206. doi: 10.1029/2005JD005861

Ranjan, A. K., Patra, A. K., and Gorai, A. K. (2020). Effect of lockdown due to SARS COVID-19 on aerosol optical depth (AOD) over urban and mining regions in India. *Sci. Total Environ*. 745:141024. doi: 10.1016/j.scitotenv.2020.141024

Remer, L. A., Kaufman, Y. J., Tanre, D., and Mattoo, S. (2005). The MODIS aerosol algorithm, products and validation. *J. Atmos. Sci.* 62, 947–973. doi: 10.1175/JAS3385.1

Rupakheti, D., Kang, S., Bilal, M., Gong, J., Xia, X., and Cong, Z. (2019). Aerosol optical depth climatology over Central Asian countries based on Aqua-MODIS Collection 6.1 data: Aerosol variations and sources. *Atmos. Environ.* 207, 205–214. doi: 10.1016/j.atmosenv.2019.03.020

Sanap, S. D. (2021). Global and regional variations in aerosol loading during COVID-19 imposed lockdown. *Atmos. Environ.* 246:118132. doi: 10.1016/j.atmosenv.2020.118132

Satheesh, S. K. (2002). Radiative forcing by aerosols over Bay of Bengal region. *Geophys. Res. Lett.* 29:2083. doi: 10.1029/2002GL015334

Satheesh, S. K., Krishna Moorthy, K., and Srinivasan, J. (2006). Spatial and Temporal Heterogeneity in Aerosol Properties and Radiative Forcing over Bay of Bengal: Sources, Role of Aerosol Transport and Implications to Regional Climate. *J. Geophys. Res.* 111:D08202. doi: 10.1029/2005JD006374

Satheesh, S. K., Moorthy, K. K., and Das, I. (2001). Aerosol spectral optical depths over the Bay of Bengal. *Arabian Sea Ind. Ocean Curr. Sci.* 81, 1617–1625.

Satheesh, S. K., Vinoj, V., and Krishna Moorthy, K. (2010). Assessment of aerosol radiative impact over oceanic regions adjacent to Indian subcontinent using multi-satellite analysis. *Adv. Meteorol.* 2010:139186. doi: 10.1155/2010/139186

Schott, F. A., and McCreary, J. P. (2001). The monsoon circulation of the Indian Ocean. *Progr. Oceanogr.* 51, 1–123. doi: 10.1016/S0079-6611(01)00083-0

Schott, F. A., Dengler, M., and Schoenefeldt, R. (2002). The shallow overturning circulation of the Indian Ocean. *Progr. Oceanogr.* 53, 57–103. doi: 10.1016/S0079-6611(02)00039-3

Seo, H., Xie, S. P., Murtugudde, R., Jochum, M., and Miller, A. J. (2009). Seasonal effects of Indian Ocean freshwater forcing in a regional coupled model. *J. Climat.* 22, 6577–6596. doi: 10.1175/2009JCLI2990.1

Shinoda, T. (2005). Impact of the diurnal cycle of solar radiation on intraseasonal SST variability in the western equatorial Pacific. *J. Climate* 18, 2628–2636. doi: 10.1175/jcli3432.1

Soni, M., Verma, S., Jethava, H., Payra, S., Lamsal, L., Gupta, P., et al. (2021). Impact of COVID-19 on the air quality over china and india using long-term (2009-2020) multi-satellite data. *Aerosol. Air. Qual. Res.* 21:200295. doi: 10.4209/aaqr.2020.06.0295

Srivastava, A., Dwivedi, S., and Mishra, A. K. (2018). Investigating the role of air-sea forcing on the variability of hydrography, circulation, and mixed layer depth in the Arabian Sea and Bay of Bengal. *Oceanologia* 60, 169–186. doi: 10.1016/j.oceano.2017.10.001

Stratoulias, D., and Nuthammachot, N. (2020). Air quality development during the COVID-19 pandemic over a medium-sized urban area in Thailand. *Sci. Total Environ.* 746:141320. doi: 10.1016/j.scitotenv.2020.141320

Stanhill, G. (2011). The role of water vapor and solar radiation in determining temperature changes and trends measured at Armagh, 1881-2000. *J. Geophys. Res.* 116:D03105. doi: 10.1029/2010JD014044

Sumanth, E., Mallikarjuna, K., Stephen, Joshi, Moole, Mahesh, et al. (2004). Measurements of aerosol optical depths and black carbon over Bay of Bengal during post-monsoon season. *Geophys. Res. Lett.* 31:L16115.

Tian, B., Manning, E., Roman, J., Thrastarson, H., Fetzer, E. J., and Monarrez, R. (2020). *AIRS Version 7 Level 3 Product User Guide*.

Tiwari, S., Mishra, A. K., and Singh, A. K. (2016). Aerosol Climatology over the Bay of Bengal and Arabian Sea Inferred from Space-Borne Radiometers and Lidar Observations. *Aerosol Air Q. Res.* 16, 2855–2868. doi: 10.4209/aaqr.2015.06.0406

Twomey, S. (1977). The influence of pollution on the shortwave albedo of clouds. *J. Atmos. Sci.* 34, 1149–1152. doi: 10.1175/1520-0469(1977)034<1149:tiopot>2.0.co;2

Vinoj, V., Babu, S. S., Satheesh, S. K., Moorthy, K. K., and Kaufman, Y. J. (2004). Radiative forcing by aerosols over the Bay of Bengal region derived from shipborne, island-based, and satellite (Moderate-Resolution Imaging Spectroradiometer) observations. *J. Geophys. Res.* 109:D05203. doi: 10.1029/2003JD004329

Vinoj, V., and Pandey, S. (2016). "Towards understanding the variability of aerosol characteristics over the Indo-Gangetic Plain," in *Proc. SPIE 9882, Remote Sensing and Modeling of the Atmosphere, Oceans, and Interactions VI*, (Mass: Kluwer Acad), 988205. doi: 10.1117/12.2223315

Vinoj, V., and Satheesh, S. K. (2003). Measurements of aerosol optical depth over Arabian Sea during summer monsoon season. *Geophys. Res. Lett.* 30, 67-1–67-4. doi: 10.1029/2002GL016664

Vinoj, V., Satheesh, S. K., and Krishna Moorthy, K. (2010). Optical, radiative and source characteristics of aerosols at a remote island, Minicoy in the southern Arabian Sea. *J. Geophys. Res.* 115:D01201. doi: 10.1029/2009JD011810

Yu, H., Kaufman, Y. J., Chin, M., and Feingold, G. (2006). A review of measurement-based assessments of the aerosol direct radiative effect and forcing. *Atmos. Chem. Phys.* 6, 613–666. doi: 10.5194/acp-6-613-2006

Zhu, Q., Liu, Y., Shao, T., and Tang, Y. (2020). Transport of Asian aerosols to the Pacific Ocean. *Atmosph. Res.* 234:104735. doi: 10.1016/j.atmosres.2019.104735

Conflict of Interest: The authors declare that the research was conducted in the absence of any commercial or financial relationships that could be construed as a potential conflict of interest.

Publisher's Note: All claims expressed in this article are solely those of the authors and do not necessarily represent those of their affiliated organizations, or those of the publisher, the editors and the reviewers. Any product that may be evaluated in this article, or claim that may be made by its manufacturer, is not guaranteed or endorsed by the publisher.

frontiers in Marine Science

ORIGINAL RESEARCH
published: 24 August 2021
doi: 10.3389/fmars.2021.673989

Measuring the Impact of the COVID-19 Shutdown on Great Lakes Water Quality Using Remote Sensing

Karl R. Bosse[1], Michael J. Sayers[1], Robert A. Shuchman[1], John Lekki[2] and Roger Tokars[2]*

[1] Michigan Tech Research Institute, Michigan Tech University, Ann Arbor, MI, United States, [2] NASA Glenn Research Center, Cleveland, OH, United States

The states of Michigan and Ohio issued shutdown orders in mid-March 2020 in an attempt to slow the spread of the coronavirus (COVID-19), resulting in widespread disruption to economic and human activity. This study, which was commissioned by NASA headquarters, utilized satellite remote sensing data from the Visible Infrared Imaging Radiometer Suite sensor onboard the Suomi National Polar-orbiting Partnership satellite to investigate whether these changes in activity led to any short-term changes in water quality in the Great Lakes region by comparing 2020 data to a historic baseline. The water quality parameters examined included chlorophyll-*a* (CHL) and total suspended solids (TSS) concentrations, water clarity, and harmful algal bloom (HAB) extent. These parameters were investigated in two Great Lakes basins which experience significant anthropogenic pressure: the western basin of Lake Erie (WBLE) and Saginaw Bay in Lake Huron (SBLH). TSS concentrations in April 2020 were below the historic baseline in both basins, and largely remained low until September. SBLH also experienced elevated CHL concentrations in April which persisted through the summer. Additionally, the WBLE HAB extent was down in 2020 after an early end to the growing season. However, this investigation found that the COVID-19 shutdowns were likely not a direct driver of these short-term anomalies. Instead, recent trends in the indicators and co-occurring anomalies in hydrological and meteorological conditions (e.g., lake temperature, river discharge, and wind speed) appeared to be more responsible for the detected water quality changes. Future work will investigate whether the shutdowns have a long-term or delayed impact on Great Lakes water quality.

Keywords: coronavirus – COVID-19, water quality, Great Lakes, anomaly, remote sensing

OPEN ACCESS

Edited by:
Deepak R. Mishra, University of Georgia, United States

Reviewed by:
Junyu He, Zhejiang University, China
D. Swain, Indian Institute of Technology Bhubaneswar, India

****Correspondence:***
Karl R. Bosse
krbosse@mtu.edu

Specialty section:
This article was submitted to Global Change and the Future Ocean, a section of the journal Frontiers in Marine Science

Received: *28 February 2021*
Accepted: *19 July 2021*
Published: *24 August 2021*

Citation:
Bosse KR, Sayers MJ, Shuchman RA, Lekki J and Tokars R (2021) Measuring the Impact of the COVID-19 Shutdown on Great Lakes Water Quality Using Remote Sensing. Front. Mar. Sci. 8:673989. doi: 10.3389/fmars.2021.673989

INTRODUCTION

The coronavirus disease (COVID-19) was initially identified in January 2020 (Zhu et al., 2020). It spread slowly at first but the number of infections began to grow rapidly: from 44 confirmed cases on January 3, 2020 to 282 on January 20 (World Health Organization [WHO], 2020a) and over 9,826 confirmed cases in 20 countries by the end of January, prompting the World Health Organization (WHO) to issue a public health emergency of international concern (World Health Organization [WHO], 2020b).

The United States reported its first confirmed case of COVID-19 on January 20, 2020 (Holshue et al., 2020), and by February 7, 2021, had confirmed over 26 million infections and over 450,000

deaths due to the disease according to the WHO COVID-19 dashboard.[1] The states of Michigan and Ohio reported their first positive cases in the initial weeks of March 2020 (Pelzer and Hancock, 2020; State of Michigan, 2020a). Despite efforts to slow its spread, both states experienced a rapid increase in infections and deaths in the ensuing weeks, leading the governors of both states to issue temporary shutdown orders beginning on March 23rd in Ohio (Ohio Department of Health, 2020) and 24th in Michigan (State of Michigan, 2020b). During these shutdowns, most economic activity was shut down and people were encouraged to stay at home. Surveys conducted in two subsequent weeks surrounding the start of the Michigan shutdown (March 21–22, 2020 and March 28–29, 2020) revealed the immediate impact of the shutdowns on resident's activities. The percentage of respondents that reported staying at home all day for each of the prior 5 days increased from 19 to 47% and the percentage of respondents who went into work or a volunteer site at least once in the prior 5 days decreased from 46 to 30% (Cassidy-Bushrow et al., 2021). An analysis of mobile device data revealed that mobility decreased during the social distancing periods throughout both Michigan and Ohio (Garnier et al., 2021).

Initially intended to last just a few weeks, the shutdowns were extended several times as the disease continued to spread. Even as the shutdowns began to be lifted in the summer of 2020, many industries remained closed or opened at limited capacities (Bischoff, 2020; Hutchinson, 2020). According to US Bureau of Labor Statistics (BLS) data,[2] the shutdowns resulted in massive employment losses in the Michigan and Ohio manufacturing industries, with 28 and 14% declines from March 2020 to April, respectively. These numbers had somewhat recovered by June, but were still below the pre-pandemic levels (11 and 6%, respectively) (**Supplementary Figure 1**). Daily testing data from the Centers for Disease Control and Prevention[3] (CDC) reveal that the shutdowns helped to reduce the spread of COVID-19 until both states experienced resurgences in mid-summer (**Supplementary Figure 2**).

Shutdowns were a common approach used throughout the United States and in other nations. In addition to slowing the spread of COVID-19, there have been numerous reports of these shutdowns having a significant environmental impact. Several studies found that the declines in activity, including reduced vehicular traffic and industrial emissions, resulted in air quality improvements in parts of India, Italy, and Southeast Asia (Collivignarelli et al., 2020; Kanniah et al., 2020; Soni, 2021). Other studies identified improvements in marine and inland water quality coinciding with the periods of reduced activity. Many of these studies utilized remote sensing data in their analyses due to its ability to collect data at broad spatial and temporal scales and because it can be acquired without the potential health risks of *in situ* sampling. Multiple studies used Landsat 8 imagery to identify significant decreases in suspended particulate matter (SPM, used as an indicator of water pollution) in Indian inland waters (Aman et al., 2020; Yunus et al., 2020). These decreases were speculated to be due to reductions in industrial and tourism-related pollution as a result of the COVID-19 shutdowns. Another study utilized a selection of Sentinel-3 Ocean and Land Colour Imagery (OLCI) images and identified a reduction in chlorophyll-*a* (CHL) concentrations in the coastal waters off of India (extending over 100 km off shore in places) which was attributed to shutdown-related changes in urban and atmospheric nutrient deposition (Mishra et al., 2020). An analysis of Sentinel-2 imagery revealed improvements in water clarity in the Venice Lagoon due to the reduction in public transit and tourism-related boat traffic and a decline in wastewater discharge due to the lack of tourists (Braga et al., 2020). Finally, Cherif et al. (2020) utilized Sentinel-3-derived water temperature data to identify improved coastal water quality in Morocco as a result of COVID-19 related industrial discharge reductions. Each of these studies compared satellite-derived water quality metrics from imagery collected during the shutdown period to "normal" water quality as defined by a collection of historic images. However, these studies either used a single image from multiple years or multiple images from a single year (2019) to define the historic normal, potentially biasing their results if the images selected did not adequately represent the true normal state of the study areas.

As in the regions described above, human activity has been shown to have a large impact on water quality in the Great Lakes region, especially in regard to nutrient inputs. In response to widespread eutrophication in the lakes, the bi-national Great Lakes Water Quality Agreement (GLWQA) was signed in 1972 which resulted in significant reductions in point source nutrient inputs, largely due to improvements in wastewater treatment plants (Watson et al., 2016). These improvements in municipal wastewater treatment likely limit the impact of reductions in urban runoff which were hypothesized to cause some of the water quality improvements in India and Morocco. However, since the passage of the GLWQA, non-point source contributions of nutrients, including from agricultural runoff and residential septic systems, have become a major driver of water quality in several parts of the Great Lakes including the western basin of Lake Erie (WBLE) and Saginaw Bay in Lake Huron (SBLH) (He et al., 2014; Selzer et al., 2014; Stow et al., 2015). It has been estimated that 10–25% of Michigan's million-plus on-site wastewater treatment (or septic) systems are in some level of failure (Michigan Office of the Great Lakes [OGL], 2016; Public Sector Consultants [PSC], 2018). In the five counties surrounding SBLH, this results in annual discharges of untreated or partially treated wastewater between 0.5 and 1.26 billion gallons (Public Sector Consultants [PSC], 2018). Rao and Schwab also note the occurrence of storm sewers draining directly into the Great Lakes which can impact the nearshore nutrient levels (2007). Additionally, changes in agricultural practices in response to the GLWQA have led to increased loadings of bioavailable phosphorus in WBLE (Scavia et al., 2014), which along with climate change and the introduction of zebra and quagga mussels, has led to the resurgence of the WBLE harmful algal bloom (HAB) in recent years (Watson et al., 2016).

[1] https://covid19.who.int/region/amro/country/us

[2] https://data.bls.gov/

[3] https://data.cdc.gov/Case-Surveillance/United-States-COVID-19-Cases-and-Deaths-by-State-o/9mfq-cb36

Remote sensing has been a widely used tool for studying water quality in the Great Lakes due to their vast size and regional importance (the Laurentian Great Lakes make up over 20% of the freshwater on Earth and provide drinking water to over 35 million people; Herdendorf, 1982; Bootsma, 2018). The enhanced spatial and temporal sampling capabilities provided by remote sensing have helped further develop the link between anthropogenic forcing and water quality in the region (Michalak et al., 2013; Shuchman et al., 2017). Because of the greater optical complexity of these waters relative to the open ocean (Bukata, 2005; Sayers et al., 2019a), researchers have developed a range of empirical and semi-analytical water quality algorithms that are specifically tuned to the waters of the Great Lakes. Algorithms have been developed to study a range of parameters, including the concentrations of color producing agents (i.e., CHL, suspended sediments, and CDOM) (Binding et al., 2012; Shuchman et al., 2013), primary production (Warner and Lesht, 2015; Fahnenstiel et al., 2016), and the intensity and extent of HABs (Stumpf et al., 2012; Sayers et al., 2016).

The goal of this study is to use satellite imagery to understand whether the widespread disruptions caused by the COVID-19 pandemic had an observable impact on Great Lakes water quality. Due to the GLWQA-driven improvements to the municipal water treatment systems, it is unlikely that the shutdown-driven decrease in industrial activity would have a notable impact on the nutrient loads to the study areas. However, there are other ways in which nutrient loading could be impacted by the shutdowns. The transition to working at home and ceasing of most urban activity will shift some of the wastewater treatment loads from the highly effective municipal treatment plants to at-home septic systems which are more likely to release un-treated wastewater into the environment. Additionally, potential changes to the agricultural calendar, including the timing of plantings or fertilizer applications, could impact the nutrient loads. Because *in situ* sampling was heavily restricted due to the pandemic, this study used remote sensing to investigate the presence of any short-term water quality anomalies in the Great Lakes region that may be due to the COVID-19 shutdowns. For this analysis, short-term anomalies are defined as anomalies that become apparent in the weeks to months following the shutdowns. The analysis focused on water quality parameters which had been observed to be impacted elsewhere, including the concentrations of CHL and total suspended solids (TSS) and photic zone depth (PZD) was used as an indicator of water clarity. These parameters were investigated in WBLE and SBLH, two basins with an extensive history of anthropogenic impact. The HAB extent in WBLE was also investigated due to its regional importance and dependence on nutrient loading during the spring (Stumpf et al., 2012; Sayers et al., 2016, 2019b).

MATERIALS AND METHODS

Study Areas

Two basins within the Laurentian Great Lakes region (WBLE and SBLH) were analyzed for impacts related to activity changes due to the COVID-19 pandemic (**Figure 1**).

The western basin of Lake Erie and SBLH were selected as they are two of the more eutrophic basins within the Great Lakes, Both have extended histories of anthropogenic impacts (Makarewicz and Bertram, 1991; Dolan, 1993; Stow et al., 2014) and HABs (Fahnenstiel et al., 2008; Bridgeman et al., 2013; Sayers et al., 2016, 2019b; Wynne et al., 2021). Much of the anthropogenic impact is driven by nutrient-rich runoff from heavily farmed watersheds and the nearby population centers (Michalak et al., 2013; Selzer et al., 2014). There are notable differences between the two regions as well, with the SBLH watershed having 60% lower population density than the WBLE watershed (**Table 1**). The land use within the watersheds differs as well, with SBLH having less agriculture and urban area (27 and 62% less than WBLE, respectively) and 3.6 times the forested area (**Table 1**). The SBLH coastline also consists of an extensive wetlands system which serves as a highly effective nutrient sink (Wynne et al., 2021). Due to the greater agricultural area and less forested area and wetlands within the watershed, WBLE experiences greater nutrient loads than SBLH (Wynne et al., 2021).

Satellite Data Acquisition and Pre-processing

The water quality metrics used for this study were derived from remote sensing imagery. The National Oceanic and Atmospheric Administration's (NOAA) Visible Infrared Imaging Radiometer Suite (VIIRS) sensor onboard the Suomi National Polar-orbiting Partnership (SNPP) satellite was the source of imagery for this analysis, providing daily revisits at a 750-m resolution dating back to January 2012. Despite its coarse resolution, the VIIRS sensor has been used to study water quality in the Great Lakes due to its high temporal resolution (Binding et al., 2020; Son and Wang, 2020) which is necessary due to the frequent cloud cover in the region (Ackerman et al., 2013) and highly variable nature of the water conditions in the more eutrophic basins (Sayers et al., 2019a).

For each region, all intersecting imagery from March through December was acquired through the National Aeronautics and Space Administration (NASA) Ocean Biology Processing Group (OBPG) OceanColor Web data portal.[4] In total, over 4,300 images were processed for each of the two study regions. Data was acquired at Level 1, with no atmospheric corrections having been applied, along with the corresponding geo-location files. Using the Level 1 and geo-location data, the VIIRS images were subset to the regions of interest and processed to Level 2 using OBPG's L2gen module, applying a fixed model pair atmospheric correction. Atmospheric correction has been a key concern in freshwater remote sensing (Binding et al., 2020), particularly in the blue spectral bands (Budd and Warrington, 2004; Shuchman et al., 2013; Binding et al., 2019). Shuchman et al. evaluated eight different atmospheric correction techniques by comparing satellite-retrieved reflectance to *in situ* reflectance collected in a range of Great Lakes water types including sediment-dominant and chlorophyll-dominant waters (2013). The fixed model pair approach tested in their analysis performed well in each setting and produced the most accurate reflectance in intense HAB

[4]https://oceancolor.gsfc.nasa.gov/

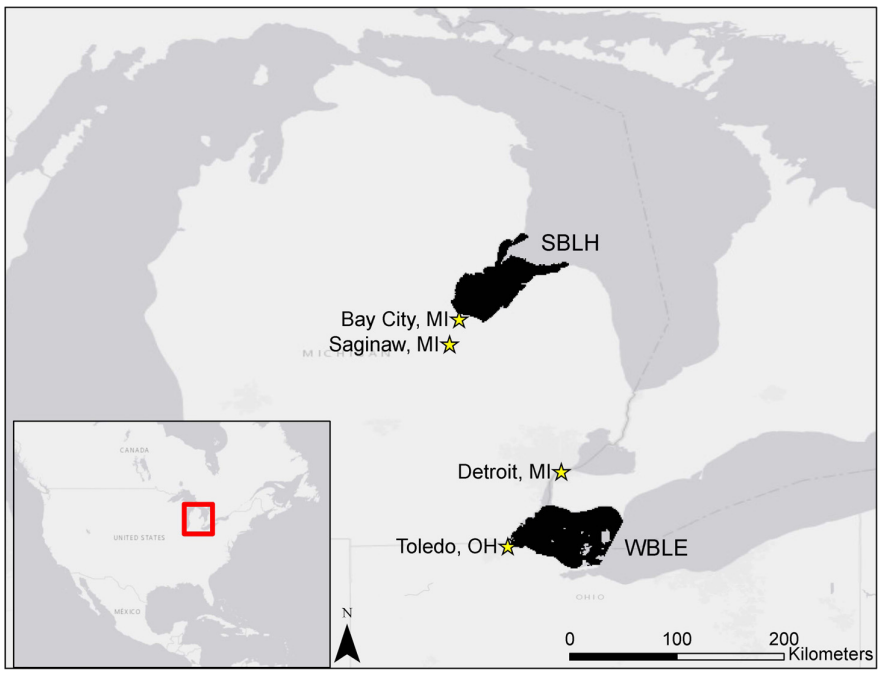

FIGURE 1 | Regions studied for impacts related to the coronavirus (COVID-19) pandemic. The western basin of Lake Erie (WBLE) and Saginaw Bay in Lake Huron (SBLH) are heavily impacted by anthropogenic factors. The major population centers around each basin are also shown, including Toledo, Ohio and Detroit, Michigan (WBLE); and Bay City, Michigan and Saginaw, Michigan (SBLH).

scenarios, where other correction techniques interpreted the elevated near infrared reflectance associated with near-surface HABs as atmospheric contamination (Shuchman et al., 2013; Sayers et al., 2016).

Derivation and Validation of Water Quality Metrics

The Color Producing Agents Algorithm (CPA-A; Shuchman et al., 2013) was used to estimate concentrations of CHL and TSS as well as CDOM absorption at 443 nm from the satellite-derived remote sensing reflectance at the following bands: 443, 486, 551, and 671 nm. This algorithm uses lake-specific parameterizations based on the range of observed inherent optical properties (IOPs) and has been shown to produce reliable results (Shuchman et al., 2013; Fahnenstiel et al., 2016), including root mean square error (RMSE) values ranging from 0.13 mg/m^3 in Lake Huron to 2.18 mg/m^3 in Lake Erie (Shuchman et al., 2013). PZD, defined as the depth where 1% of surface light remains, was used as an indicator of water clarity and was calculated from the CPA-A results as described in Fahnenstiel et al. (2016). Briefly, bulk absorption and backscatter are derived from the CPA-A retrievals and used to estimate the light attenuation coefficient at 490 nm (Kd_{490}) using methods proposed by Lee et al. (2005). Kd_{PAR} was derived empirically from Kd_{490} following methods from Saulquin et al. (2013). The inverse of Kd_{PAR} is defined as one optical depth, and the PZD is calculated as 4.605 optical depths (Lee et al., 2007).

TABLE 1 | Average population density and landcover within the two basin's watersheds.

Basin	Average Population Density (people/km^2)	Percent Landcover (%)		
		Agriculture	Forest	Urban
WBLE	169.4	79.9	6.8	8.2
SBLH	66.7	58.7	31.3	3.1

Population data comes from the United States American Community Survey (US Census Bureau, 2016) and the Canadian Census (Statistics Canada, 2019). Population density was calculated as the total population within each watershed divided by the watershed area. Landcover data came from the Climate Change Initiative (European Space Agency [ESA], 2018), with landcover groupings based on the International Panel on Climate Change (IPCC) classes (European Space Agency [ESA], 2017.

Harmful algal bloom extents in WBLE were derived from the CHL measurements. Using surface water measurements of CHL and phycocyanin pigment (PC, which can be used as an indicator of HAB presence), Sayers et al., found that minimal PC was observed at CHL concentrations below 18 mg/m^3 (2016). Above that threshold, the PC increased linearly with the CHL concentration, indicating that increased CHL is associated with HAB presence (Sayers et al., 2016). This threshold has been used to map WBLE HAB extents in multiple studies (Sayers et al., 2016, 2019b; Manning et al., 2019) with results comparing well to *in situ* surveys (87% mapping accuracy, Sayers et al., 2016). During the HABs growing season, defined as lasting from July through October (Bridgeman et al., 2013; Wynne and Stumpf, 2015), HAB extents were calculated by first converting CHL concentration maps to binary maps using the 18 mg/m^3 threshold, with each

pixel indicating HAB presence or absence. The HAB extent was then calculated as the count of pixels classified as a HAB multiplied by the pixel size.

While the water quality algorithms used in this analysis were specifically calibrated for the Great Lakes, significant changes in water quality due to the COVID-19 shutdowns could render these prior calibrations obsolete and add uncertainty to the 2020 retrievals. Due to COVID-19 restrictions, there is limited *in situ* data available from early 2020 in order to validate the derived water quality metrics. However, near-weekly water quality sampling in WBLE and SBLH started in June and July 2020, respectively, and continued through the start of October. Sampling was conducted by scientists from the Cooperative Institute for Great Lakes Research (CIGLR) and NOAA's Great Lakes Ecological Research Laboratory (GLERL). This data, which included extracted CHL concentrations and Secchi disk depths, were acquired from the NOAA-GLERL website[5] and used to assess the performance of the remote sensing algorithms in light of the potential water quality changes. Summary statistics for these observations are reported in **Table 2**. These *in situ* metrics were compared to same-day derived products, averaged over a 3 × 3 grid surrounding the sampling location. Because both the *in situ* and remotely sensed CHL retrievals have associated uncertainty, the relationship between the two variables was assessed using type II linear regression with the *lmodel2* package in R (Legendre, 2018). While Secchi disk depth and PZD are fundamentally different metrics, both are indicators of water clarity and have been shown to be related (Lee et al., 2018). For this analysis, the correlation between remote sensing-derived PZD and *in situ* Secchi disk depth was used to assess the general accuracy of the remote sensing product and its ability to track changes in water clarity.

Assessment of Water Quality Change

For each of the remote sensing-derived metrics, data from 2020 was compared to a historical baseline in order to assess change. The immediate impacts of the shutdowns were evaluated by comparing data from April 2020 to April data from prior years. April was chosen because both the Michigan and Ohio shutdowns were in place for the duration of the month and this also coincided with when the social distancing mobility decreases were peaking (Garnier et al., 2021). The metrics were also evaluated in 10-day windows from March 1 through the end of the year to assess whether any water quality changes identified during April were present prior to the shutdowns or continued as the shutdowns began to be lifted.

Two filters were applied to the remote sensing-derived data before generating the 10-day and monthly composites. First, any pixels where the CPA-A optimization failed to retrieve a valid CHL or TSS value were eliminated. Second, any CHL value where the corresponding TSS concentration was greater than 5 mg/L was removed since the heavy sediment signature can overwhelm any impact of varying CHL concentrations on the spectral signature. The 5 mg/L threshold was determined through a validation using *in situ* CHL and TSS concentrations from the CIGLR routine water quality monitoring dataset (Cooperative Institute for Great Lakes Research et al., 2019). CPA-A derived CHL estimates were compared to *in situ* CHL measurements and grouped by the corresponding TSS concentrations in 1 mg/L bins. The RMSE was then calculated within each bin, revealing a distinct shift at the 5 mg/L TSS level. The mean RMSE for TSS bins below the threshold was 6.1 mg/L compared to an RMSE of 29.8 mg/L when TSS exceeded the threshold.

Composite maps were generated in the same way for both 10-day windows and monthly data. For each year in the study period (2012–2020), composite maps were generated by calculating the mean of all images from that year within the given date range. To assess the historical significance of the observed post-shutdown water quality, the basin-wide median values from 2012 to 2019 were compared to those from April 2020 using a Wilcoxon signed-rank test (Wilcoxon, 1945) with an alpha value of 0.05 used to determine significance. Historic baseline composite maps were generated by calculating the mean of all 2012–2019 images within the given date range. Anomaly maps were then calculated for each analysis period by comparing the 2020 composite to the historic baseline composite. For each pixel in the study region, the anomaly was derived as the percent change from the baseline to the 2020 metric value (calculated as the difference between the 2020 and baseline values divided by the baseline value, and multiplied by 100). A positive anomaly indicated that the 2020 metric value was elevated relative to the historic baseline. For CHL and TSS, this represented increased concentrations, and a positive PZD anomaly indicated clearer water. In order for a 10-day window to be included in the time series, the 2020 composite map needed to have valid data in at least 50% of the pixels for that region. This requirement was put in place in order to avoid seemingly anomalous data points caused by sparse data coverage.

Harmful algal bloom extents in WBLE were generated from each of the 10-day CHL composite maps during the HABs growing season. For each 10-day window, the mean and standard deviation of HAB extent from past years were calculated to determine the historic baseline. The HAB extent anomaly was then calculated as the percent difference between the 2020 HAB extent and the baseline HAB extent.

Ancillary Indicators

In addition to the primary water quality indicators (CHL, TSS, PZD, and WBLE HAB extent), other metrics were investigated as potential drivers of water quality change. These included lake surface temperature (LST), which is known to impact CHL production and HAB growth (Behrenfeld and Falkowski, 1997;

[5]https://www.glerl.noaa.gov/res/HABs_and_Hypoxia/habsMon.html

TABLE 2 | Summary statistics for the *in situ* chlorophyll-*a* (CHL) and Secchi disk depth measurements collected in western basin of Lake Erie (WBLE) and Saginaw Bay in Lake Huron (SBLH) during the 2020 field season.

	WBLE (*N* = 113)		SBLH (*N* = 20)	
	Mean	**Range**	**Mean**	**Range**
CHL (mg/m^3)	20.7	0.8–96.4	9.9	2.6–22.0
Secchi disk depth (m)	1.3	0.2–4	1.5	1–2

Paerl and Huisman, 2008; Fahnenstiel et al., 2016). 2012–2020 LST data from the VIIRS sensor onboard the SNPP satellite was downloaded from the OBPG OceanColor Web at Level 2. The *SST_triple* product, using the default atmospheric correction (Minnett et al., 2014), was used to generate the composites and anomalies. Non-remote sensing-derived explanatory indicators included river discharge and wind speed which have been shown to impact sediment loading and HAB growth (Rao and Schwab, 2007; Stumpf et al., 2012; Sayers et al., 2016; Niu et al., 2018). Mean daily discharge data was acquired from the United States Geological Survey (USGS) National Water Information System (NWIS) using gages on the Maumee River (WBLE, gage 04193500), Detroit River (WBLE, gage 04165710), and Saginaw River (SBLH, gage 04157005). Hourly wind speeds were downloaded from buoys in NOAA's National Data Buoy Center (NDBC) network (WBLE: THL01; SBLH: SBLM4). Baseline (2012–2019) and 2020 metrics, as well as anomalies (10-day and April) were calculated for each of the explanatory indicators using the same methods as for the water quality indicators. Finally, agricultural planting data were acquired from the United States Department of Agriculture (USDA) National Agricultural Statistics Service (NASS) 2015–2020 Historical Crop Progress reports.[6] From this data, 2020 planting progress was evaluated against the prior 5-year average for three different crops (oats, corn, and soybeans) to determine if the shutdowns impacted agricultural activity.

RESULTS

Of the 134 surface water measurements collected in WBLE and SBLH in 2020, there were only 20 with valid same-day remote sensing estimates (15 in WBLE, 5 in SBLH) (**Figure 2**). The *in situ* CHL concentrations within these 20 matchups ranged from 1.7 to 31.3 mg/m^3. The Type II linear regression revealed strong agreement between the measured and estimated concentrations (R^2 = 0.66, $p < 0.01$). Similarly, there was a strong positive correlation between the *in situ* Secchi disk depth and the remotely sensed PZD (Spearman's rho = 0.69, $p < 0.01$) indicating that the PZD metric used in this analysis was adequately capturing changes in water clarity.

The annual time series of basin-wide median April indicator values (calculated from the annual April composite maps) were used to assess how water quality immediately after the shutdown began compared to prior years and whether the 2020 values were a continuation of a trend that preceded the COVID-19 pandemic (**Figure 3**). Using these plotted values, a statistical comparison was made between the 2020 observations and those from prior years in the study record. The basin-wide 2020 metric value was found to be significantly different from the historic record for all three metrics in SBLH and CHL in WBLE (Wilcoxon signed-rank test statistics and corresponding *p*-values reported in **Table 3**). Of all the metrics investigated, only SBLH CHL (**Figure 3B**) had a 2020 value falling more than two standard deviations away from the 2012–2019 mean, though this metric also appears to be in the midst of a multi-year increasing trend that pre-dates the pandemic. The 2020 TSS indicators for both basins fell within the two standard deviation window but were also at the low-end of the recent historic range after experiencing a steady decline in the past 3–4 years (**Figures 3C,D**), with the inverse being true for PZD (**Figures 3E,F**).

Mapping the anomaly data revealed spatial variability across each study basin (**Figure 4**). The majority of WBLE CHL concentrations (**Figure 4A**) were near or below the historic baseline except near the mouth of the Maumee River where the anomalies were largely positive. The SBLH CHL anomaly map (**Figure 4D**) showed widespread positive anomalies, with no clear spatial trend relative to the Saginaw River. Rather, positive anomalies were observed in most pixels except for the center of the bay, which rarely experiences significant phytoplankton accumulation due to the bay's circulation patterns (Wynne et al., 2021). TSS anomalies in both WBLE and SBLH were widely negative with a few exceptions, including near the mouths of the Maumee and Saginaw Rivers (**Figures 4B,E**). The PZD anomalies in both regions were mostly positive, indicating increased water clarity in April 2020 (**Figures 4C,F**). Median basin-wide April anomaly values for each primary indicator are displayed in **Table 4**.

Much of the spatial variability observed in **Figure 4** appeared to be related to proximity to the major river mouths. Plotting the April 2020 water quality anomalies against this distance reveals several distinct relationships (**Figure 5**). As seen in **Figure 4**, the SBLH TSS anomaly is highest within 5 km of the Saginaw River mouth where it is approximately equal to the historic baseline, but is highly negative outside of this area (**Figure 5F**). This trend is reversed for the SBLH PZD anomalies (**Figure 5I**). The trends in WBLE are slightly more complex due to the presence of two major rivers flowing into the basin. The CHL and TSS anomalies are most positive within 5–10 km of the Maumee River mouth (**Figures 5A,D**). However, both indicators experience a strong negative anomaly just outside of that range, with concentrations moving toward the historic baseline as distance increases. The trends relative to the Detroit River are more clear, with the strongest negative anomalies occurring near the river mouth and gradually increasing with distance (**Figures 5B,E**).

The water quality trends observed in April were generally also present throughout the year, as seen in the 10-day anomaly time series (**Figure 6**). These plots begin with the 10-day window starting on day 61 (March 1 in leap years; March 2 otherwise). The boxplots (**Figures 6C,F,I**) show the range of median anomaly values across the valid windows (a window was considered valid if the percent of pixels with data exceeded 50%). WBLE and SBLH had similar seasonal anomaly trends for both TSS and PZD. The TSS anomalies (**Figures 6D,E**) were consistently negative in both basins until early September aside from two outlier events in late-May and early-June. Conversely, the PZD time series (**Figures 6G,H**) revealed consistently positive anomalies aside from a few isolated events. Slight differences between the two regions were revealed in the CHL anomaly time series (**Figures 6A,B**). While the CHL anomaly in SBLH was almost uniformly positive from March through August,

[6]https://www.nass.usda.gov/Statistics_by_State/Ohio/Publications/Crop_Progress_&_Condition/index.php

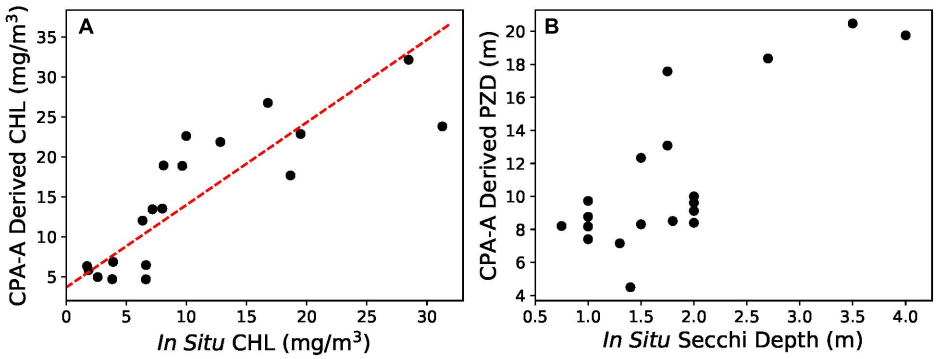

FIGURE 2 | Comparisons between remote sensing estimates and *in situ* measurements in 2020. Panel **(A)** shows a comparison between remotely sensed and *in situ* chlorophyll-*a* (CHL), with the type II regression best fit line displayed in red ($y = 3.67 + 1.03 \times x$; $R^2 = 0.66$; $p < 0.01$). Panel **(B)** shows the comparison between remotely sensed photic zone depth (PZD) and *in situ* Secchi disk depth.

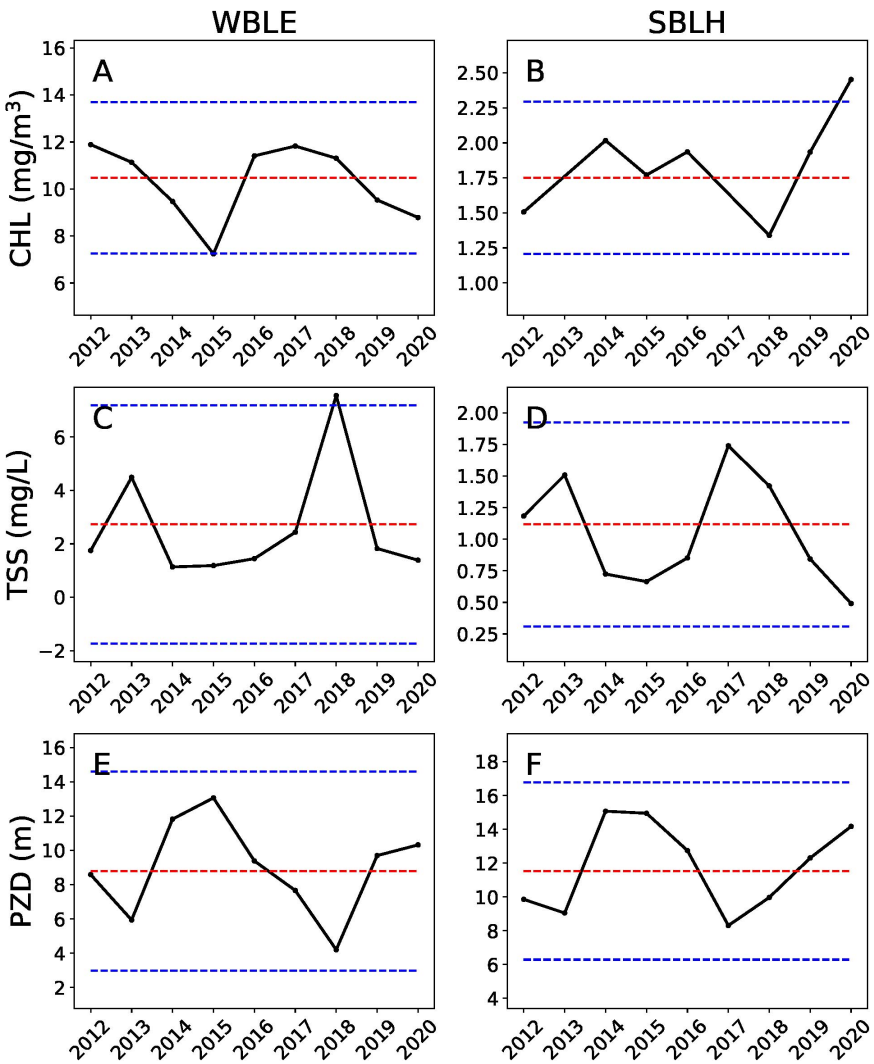

FIGURE 3 | Median April indicator values plotted over the sensor data record (2012–2020). Years in which less than 50% of the regional data pixels have data are excluded. The 2012–2019 mean is shown as the dashed red line, with the dashed blue lines representing the 2012–2019 mean plus/minus two times the 2012–2019 standard deviation. **(A,C,E)** The CHL, TSS, and PZD indicator time series for WBLE. **(B,D,F)** The CHL, TSS, and PZD indicator time series for SBLH.

TABLE 3 | Wilcoxon signed-rank test statistics (W) and *p*-values (in parentheses) for the analyses comparing basin-wide median metric values from April 2012–2019 to 2020 values.

Basin	CHL	TSS	PZD
WBLE	**3 (0.036)**	5 (0.069)	9 (0.208)
SBLH	**0 (0.028)**	**0 (0.012)**	**3 (0.036)**

Significant results, assessed against an alpha value of 0.05, are marked in bold.

the CHL anomaly in WBLE fluctuated around zero until mid-August, before experiencing a brief extreme positive anomaly in late-August (+79%). Both basins experienced prolonged periods of lower anomalies in September and October, though WBLE anomalies were up to 62% below the historic baseline and near zero in SBLH. As seen in the CHL anomaly boxplots (**Figure 6C**), SBLH had higher anomalies on average than WBLE (14.7 and −6.3%, respectively), and also experienced a much tighter range of anomalies (from −6% in June to +56% in November) while WBLE experienced anomalies ranging from −62 to +86%.

The seasonal progression of the WBLE HAB extent anomaly (**Figure 7**) was nearly identical to that of the WBLE CHL anomaly. Through July and the first few weeks of August, the 2020 HAB was slightly below the baseline extent, but within the normal range of variability. However, by mid-August, the extent began increasing rapidly, peaking in the first week of September 122% above the historic mean and several weeks earlier than the typical peak. The following week saw a rapid decline in extent, with a near total absence (mean anomaly of −86%) through the rest of the HAB season.

Seasonal and April anomalies were also assessed for three of the explanatory indicators. River discharge observed the most drastic anomalies, with the Maumee and Saginaw Rivers having April 2020 flow rates 46 and 52% below the 2012–2019 baseline, respectively, and the Detroit River with an above-average flow rate (+21%) (**Table 5**). Less extreme negative anomalies were also observed for the LST (−8 and −6% in WBLE and SBLH, respectively) and wind speed (−10 and −2%) metrics.

The seasonal anomaly trends for the explanatory indicators revealed similar results between WBLE and SBLH (**Figure 8**). LST in both basins (**Figures 8A,B**) was above average through most of March followed by negative anomalies from mid-April into June and again from September through mid-October. Each basin also experienced prolonged positive anomalies from mid-June through August. These anomalies were relatively small compared to those from the primary water quality indicators, with both regions showing a mean absolute anomaly across all valid windows of less than 10%.

The Detroit River (**Figure 8C**) had a consistently positive discharge anomaly (ranging from 15 to 30% above the historic baseline), but both the Maumee River (**Figure 8C**) and Saginaw River (**Figure 8D**) generally observed negative or near-zero discharge anomalies from April through September aside from a few extreme positive anomalies in mid-May. The wind speed time series (**Figures 8E,F**) showed no consistent anomalies throughout the season, fluctuating back and forth around the baseline. The largest observed anomaly was in WBLE at the start of September, when 2020 wind speeds were more than 40% higher than the historic baseline. This extreme wind event, along with the negative LST anomaly that started in September, likely contributed to the rapid decline in WBLE HAB extent.

The agricultural planting progress data was also analyzed to determine if the pandemic shutdowns had any impact on when oats, corn, or soybeans were planted. Some discrepancies were observed between the 2020 and 2015–2019 baseline, though these depended on the crop (**Supplementary Figure 3**). Throughout the data record, oats were the earliest crops to be planted. In 2020, despite the pandemic-driven shutdowns, planting progress for the oats was generally at least 25% ahead of the historic average through the first week of May. Corn and soybean plantings began at the end of April. The planting progress for corn was behind the baseline for several weeks but caught up by mid-May. Meanwhile 2020 soybean planting progress was ahead of the historic schedule throughout the season.

DISCUSSION

This study highlights the importance of remote sensing for environmental monitoring. In a typical year in the Great Lakes, NOAA-GLERL and CIGLR conduct routine vessel and buoy-based water quality sampling in WBLE and SBLH (see text footnote 5). Due to the health and safety concerns surrounding the COVID-19 pandemic, both vessel-based sampling and buoy deployment were delayed and limited in capacity. Satellite-based remote sensing makes it possible to investigate water quality without the health concerns of *in situ* sampling, and it provides data at a broader spatial and temporal scale than is possible with boat- and buoy-based measurements. The extensive remote sensing historical data record also allows for the assessment of anomalies over broad spatial regions. Without this data, we would not have been able to assess how the COVID-19 shutdowns impacted Great Lakes water quality.

Extending beyond the Great Lakes region, polar-orbiting satellites like the one used in this analysis collect data on a global scale, allowing for coordinated analyses across the United States and internationally. NASA, in collaboration with the European Space Agency (ESA) and Japan Aerospace Exploration Agency (JAXA), assembled research teams from across the world to assess how the pandemic has impacted a range of environmental and societal indicators. Results of this collaboration, including the data presented in this article, are available on NASA's COVID-19 dashboard.[7]

This investigation identified statistically significant short-term anomalies in several Great Lakes water quality metrics in the weeks and months following the start of the COVID-19 shutdowns, yet these anomalies cannot be directly attributed to the shutdowns as an examination of meteorological and hydrological variables has provided other plausible explanations for the observed changes Both WBLE and SBLH experienced large declines in TSS levels relative to the historic baseline in April 2020 as peak social distancing was occurring. However,

[7]https://earthdata.nasa.gov/covid19/

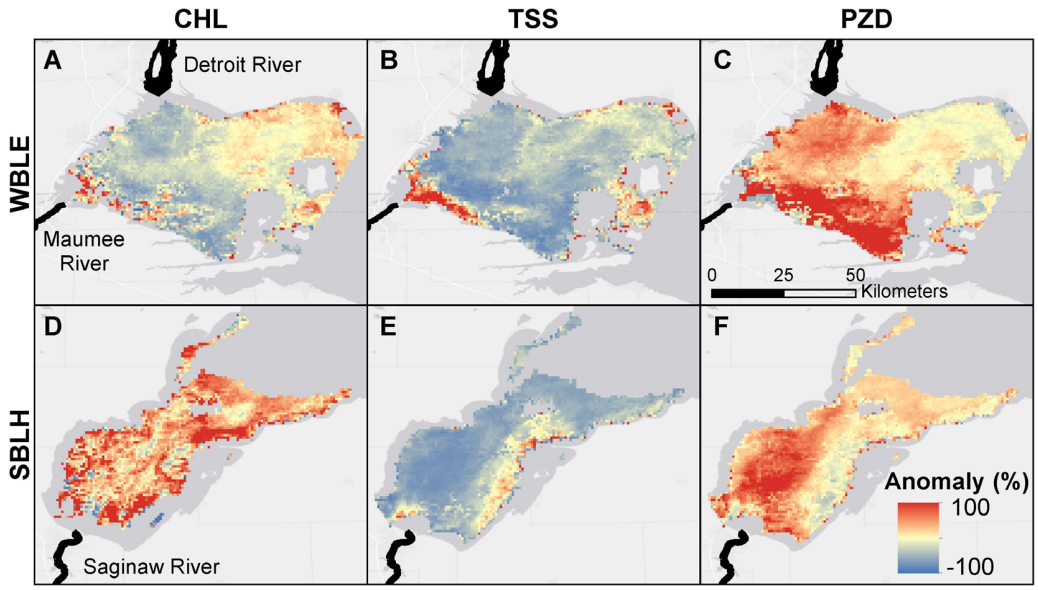

FIGURE 4 | April anomaly maps for CHL, total suspended solids (TSS), and PZD in the two study basins. All maps are scaled from blue (large negative anomaly) to red (large positive anomaly). The locations of each basin's major rivers (Maumee and Detroit Rivers in WBLE; Saginaw River in SBLH) and where they enter the basins are displayed in black. **(A–C)** The WBLE April anomaly maps for CHL, TSS, and PZD, respectively. **(D–F)** The SBLH April anomaly maps for CHL, TSS, and PZD, respectively.

co-occurring anomalies in the ancillary indicators could help explain this observation more than the changes in human activity. Both regions also experienced below average wind speed and river discharge rates in April 2020. The Detroit River was the exception, with above average discharge rates in April 2020. However, the Detroit River contributes very little sediment to WBLE, providing over 90% of the discharge but less than 6% of the sediment input, while the Maumee River provides 3% of the discharge and 45% of the sediment load (Niu et al., 2018). Because river discharge has a key role in nearshore sediment loading (Rao and Schwab, 2007) and high turbidity events in the offshore waters in WBLE are driven primarily by wind-driven resuspension (Niu et al., 2018) it is likely that natural factors (i.e., reduced wind speed and discharge) were driving the TSS reductions more than any COVID-19 impacts.

Investigating the TSS anomalies spatially revealed that despite the decreased discharge, increased TSS levels were observed in the 5–10 km nearest to the urban-adjacent Maumee and Saginaw River mouths and more negative anomalies were observed with increased distance. It is these nearshore areas that are most likely to be impacted by anthropogenic impacts such as urban or agricultural runoff (Rao and Schwab, 2007; Niu et al., 2018). However, there are plausible natural explanations for these trends as well. The reduced river discharge likely resulted in a greater concentration of the sediment nearer to the river mouths, unable to propel it further outward into the basins. This is particularly likely in WBLE, where the elevated sediment-poor Detroit River flow would further limit the extent of the diminished sediment-rich Maumee River plume (Jiang et al., 2015).

Saginaw Bay in Lake Huron also experienced a statistically significant CHL anomaly in April, with an increase of over 40% relative to the historic baseline. If this CHL increase were related to the pandemic, it would likely be due to an anomalously large influx of non-urban nutrients. It is unlikely that an increase in agricultural nutrient inputs would lead to positive anomalies basin-wide, particularly due to the greatly diminished Saginaw River discharge rates. And although the increased usage of residential septic systems during the shutdowns may have resulted in increased nutrient inputs along the SBLH coastline, this impact would most likely be observed in the very nearshore waters which are not visible with the coarse resolution satellite used in this analysis. As with TSS, there are several potential explanations for the CHL anomaly aside from the COVID-19 shutdowns. The time series of April CHL concentrations in SBLH (**Figure 3B**) indicated that the basin-wide median was stable from 2012 to 2018, but the last 2 years have seen a large increase, perhaps indicating an ongoing trend un-related to COVID-19. The decreased TSS concentrations may also be contributing to the increased CHL. Suspended sediment concentrations have been shown to be highly correlated with Kd_{PAR} (Millie et al., 2003), which is likely driving the significantly increased water clarity throughout the basin (**Figure 4H**). Other research in the Great Lakes has shown that increases in water clarity can cause increased phytoplankton production (Bierman and Dolan, 1981; Lohrenz et al., 2004; Jiang et al., 2015). WBLE also had

TABLE 4 | Median basin-wide April anomaly values for each region and indicator.

Median anomaly (%)	CHL	TSS	PZD
WBLE	−18.9	−42.3	25.3
SBLH	40.4	−54.3	23.9

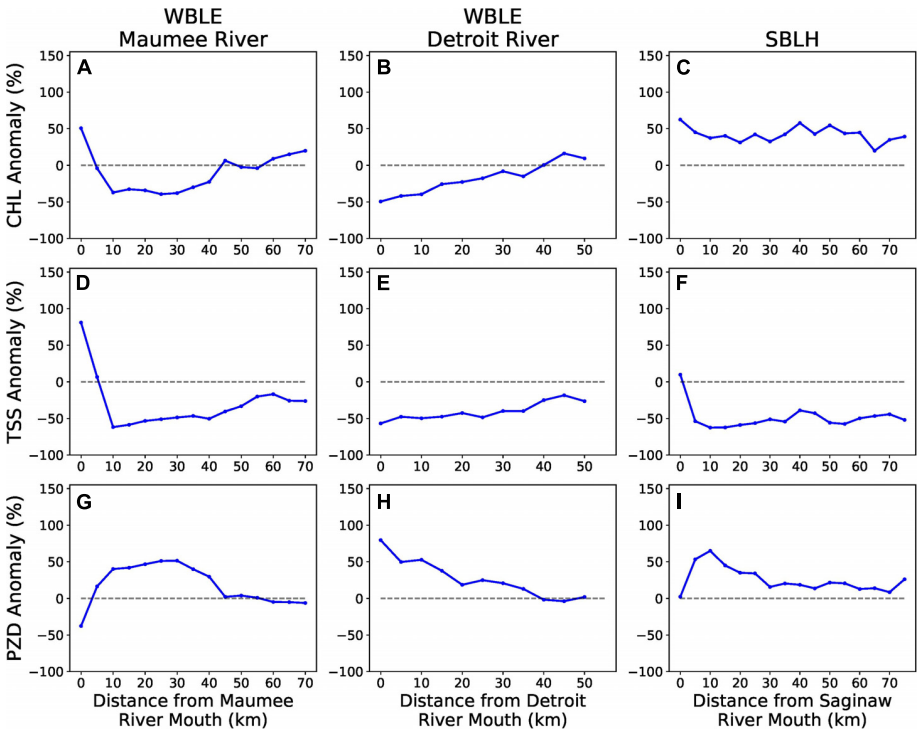

FIGURE 5 | Median April anomaly value is plotted based on distance from the nearest major river mouth (Maumee and Detroit Rivers for WBLE; Saginaw River for SBLH). The distances are binned in 5-km increments. **(A,D,G)** The average CHL, TSS, and PZD anomalies in WBLE based on distance from the Maumee River. **(B,E,H)** The average CHL, TSS, and PZD anomalies in WBLE based on distance from the Detroit River. **(C,F,I)** The average CHL, TSS, and PZD anomalies in SBLH based on distance from the Saginaw River.

a statistically significant CHL anomaly in April 2020. However, unlike SBLH, WBLE had a negative basin-wide CHL anomaly, but this varied considerably with distance from the Maumee River mouth. The 5 km nearest to the river mouth experienced a positive anomaly, while negative anomalies were observed from 5 to 45 km. Despite the increased water clarity similar to SBLH (**Figure 4C**), the decreased CHL is likely due to a nutrient limitation caused by the combination of increased nutrient-poor Detroit River discharge and decreased Maumee River discharge (Jiang et al., 2015). The stronger Detroit River plume would force the nutrient-rich Maumee River waters along the coastlines, consistent with the observed locations of increased CHL concentrations.

If the anomalies observed in April 2020 were caused by the pandemic-driven shift in activity, then it would be expected that they would dissipate in the weeks prior to and after the peak social distancing period. Instead, the trends that were observed in April tended to also be true in March and persisted further into the year. This was also generally true for the ancillary indicators which provided alternative explanations for the anomalies. WBLE and SBLH each observed negative TSS anomalies in over 80% of all qualifying 10-day windows from March 1 until the start of September. Deviations from this trend were also well explained by the ancillary indicators. Both basins observed an elevated TSS event in late May and early June, coinciding with large discharge anomalies due to an extreme storm event in late May which led to a 500-year flood event in mid-Michigan (French, 2020). Another positive TSS anomaly occurred in the first week of September, coinciding with the largest positive wind anomaly in each basin which we would expect to cause significant sediment resuspension (Niu et al., 2018).

2020 also resulted in an anomalously low HAB extent in WBLE, with a reduced severity relative to what was forecasted based on the observed levels of springtime discharge (National Oceanic and Atmospheric Administration [NOAA], 2020). While a negative anomaly was observed in a majority of windows, there was an extreme positive anomaly in late August before the bloom suddenly dissipated. Like the other observed anomalies, this trend seems to be well explained by variables not directly related to the COVID-19 shutdown. The upward trend in HAB extent coincided with a prolonged positive LST anomaly from June 29 through August 27, and the rapid bloom decline occurred simultaneously to the start of a negative LST anomaly which lasted from September 7 through the end of the typical HAB season. This decline also coincided with the aforementioned positive wind anomaly during the first weeks of September. Heavy winds force vertical mixing of the blooms which can reduce the amount of bloom visible to the satellite sensors and also limits the formation of highly concentrated surface scums until the winds calm (Wynne et al., 2010; Bosse et al., 2019; Sayers et al., 2019b). Elevated September winds also resulted in early ends to the HAB season in 2018 and 2019

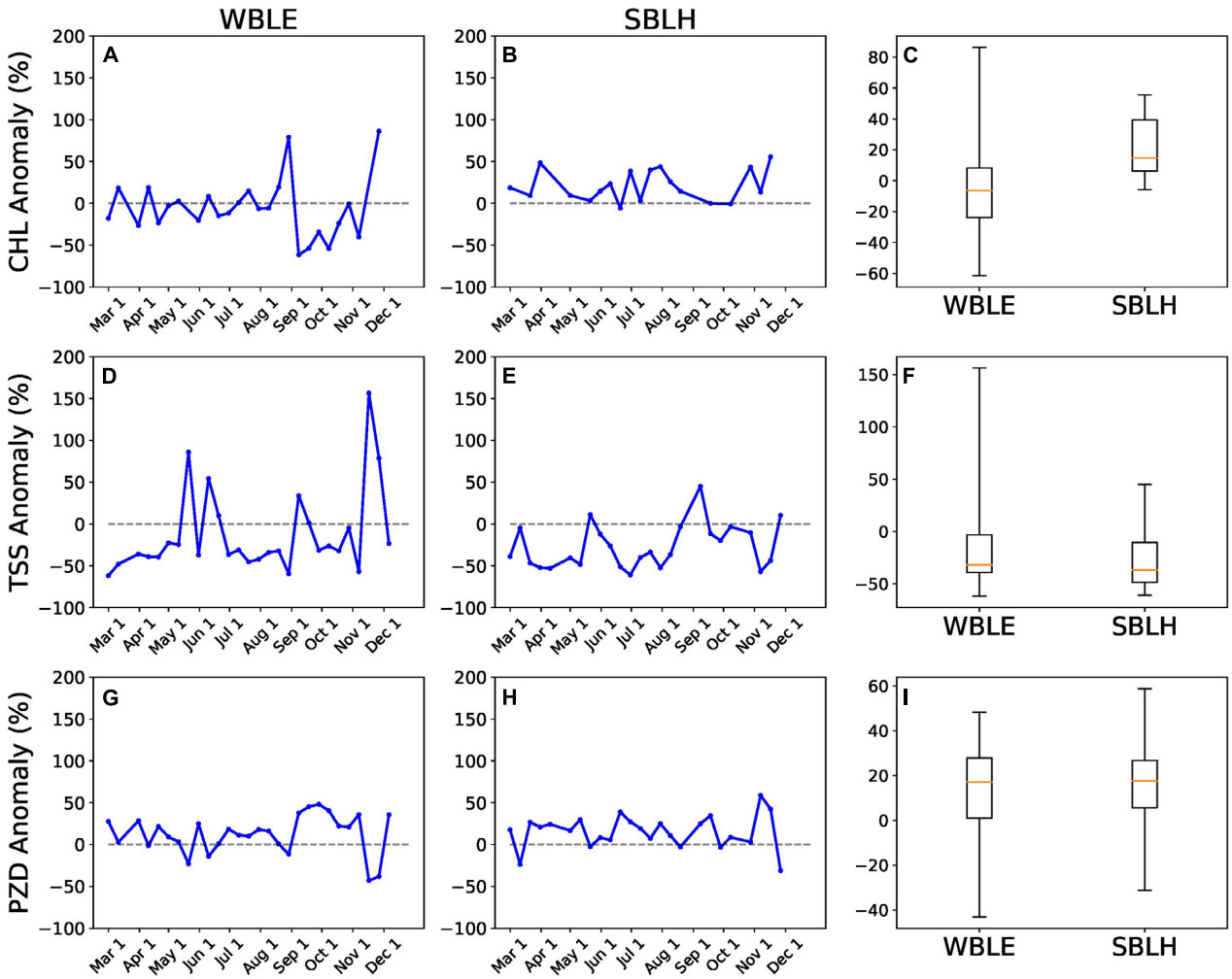

FIGURE 6 | Median basin-wide anomalies for the 10-day windows starting from March 1 to December 26. Windows in which less than 50% of the regional data pixels have data are excluded. **(A,D,G)** The CHL, TSS, and PZD anomaly time series for WBLE. **(B,E,H)** The CHL, TSS, and PZD anomaly time series for SBLH. **(C,F,I)** The distribution of CHL, TSS, and PZD anomalies in both basins from March through December.

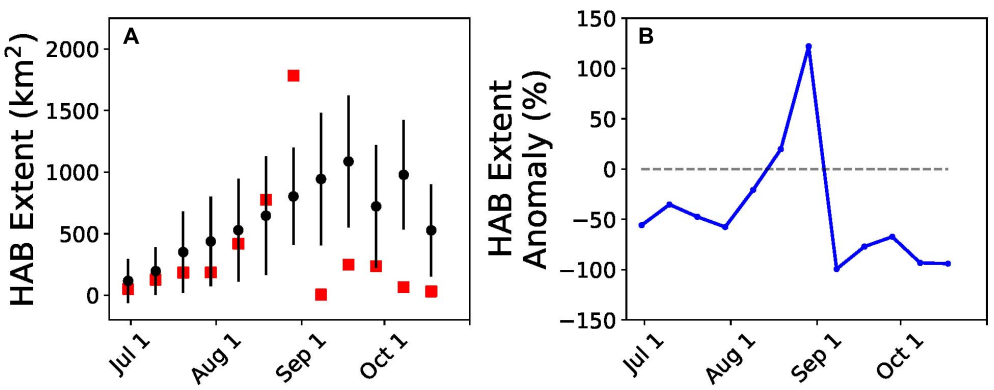

FIGURE 7 | Panel **(A)** shows median WBLE harmful algal bloom (HAB) extent for the 10-day windows starting from June 30 to October 17. The red squares represent the 2020 extents and the black dots represent the mean of prior years' (2012–2019) extents. The vertical black lines represent the standard deviations of the prior years' extents. Panel **(B)** shows the anomaly time series for the HAB extent.

TABLE 5 | Median April anomaly values for the explanatory indicators.

Median anomaly (%)	LST	River Discharge	Wind Speed
WBLE	-8.4	-46.3 (21.2)	–10.2
SBLH	-5.5	-51.5	–1.8

For WBLE discharge, Maumee River discharge is listed first and Detroit River discharge is in parentheses.

(National Oceanic and Atmospheric Administration [NOAA], 2020). Prior years had seen HABs continue through October, often peaking in September (Bridgeman et al., 2013; Wynne and Stumpf, 2015; Sayers et al., 2019b).

Several other studies in Europe and the United States also found that observed environmental changes during the shutdown periods were just as well explained by long-term trends, meteorological factors, or other confounding factors (Ordóñez et al., 2020; Tobías et al., 2020; Zangari et al., 2020). In complex ecosystems like the Great Lakes, the water quality indicators that we examined are driven by a combination of natural factors (e.g., river discharge, LST, and wind speed, etc.) in addition to the anthropogenic drivers. This can result in significant spatial and temporal variability on yearly and even weekly time scales (Sayers et al., 2019a). Because of the observed variability in each of the ancillary factors studied, it is difficult to assign responsibility for any of the anomalies to changes in human behavior.

In addition to these ancillary variables, there are several other reasons why the shutdowns may not have resulted in observable water quality changes. For one, the regions being studied in this analysis are much larger than some of the other areas where changes were observed. Three studies looked at waters within approximately 3 km of shore (Aman et al., 2020; Braga et al., 2020; Yunus et al., 2020) and another went out to approximately 10 km (Cherif et al., 2020). These more targeted areas were also directly in the vicinity of key anthropogenic influences, including large cities and wastewater treatment plants. In contrast, the WBLE and SBLH study regions were an order of magnitude larger (approximately 3,200 and 2,700 km^2, respectively). The waters studied in this analysis only extended to approximately 20 km offshore, but pixels on the eastern edges of SBLH and WBLE were up to 60–70 km away from what we would expect to be the primary drivers of change (major metropolitan areas and large river mouths). Additionally, the coarse resolution satellite used in this analysis limited the retrievals in nearshore waters where the anthropogenic influence would be magnified. VIIRS was used rather than higher resolution sensors such as the Landsat sensors or Sentinel-2 because the higher temporal resolution (1 day as compared to 5–16 days) is needed in the Great Lakes due to the frequent cloud cover, particularly in spring (Ackerman et al., 2013; Wynne et al., 2013). Sentinel-3 provides improved spatial resolution over VIIRS (300 vs 750 m) with a near-daily revisit, but this sensor has a limited historical record (launched in 2016) and the CPA-A has not yet been adequately calibrated or validated for this sensor.

Finally, the anthropogenic influence in WBLE and SBLH differs from that seen in some of the other regions where anomalies were identified. Several studies identified reduced industrial pollution and wastewater discharge as the drivers of water quality improvement (Aman et al., 2020; Cherif et al., 2020; Yunus et al., 2020) and boat traffic reductions in the normally busy Venetian Lagoon were cited as a primary cause of the observed water clarity increases (Braga et al., 2020). While motorized boat traffic was suspended in April as part of Michigan's COVID-19 response (State of Michigan, 2020c), their impact on basin-wide water quality is likely negligible due to their reduced density relative to the Venice case. The changes in industrial pollution and wastewater discharge are also less relevant in the Great Lakes region due to the stringent controls placed on these systems as part of the GLWQA. This study hypothesized that the major drivers of change would be a transition from the highly effective municipal wastewater treatment systems to on-site septic systems and changes in the agricultural calendar. The heavier usage of septic systems may have resulted in increased nutrient loads to the basin, but this impact would likely be spread out across the basins (as opposed to the larger wastewater treatment plants which would have a single outflow point) and concentrated in the nearshore waters that were not resolvable in this analysis. And even though slight changes were observed in the agricultural planting calendar, the declaration of farmers as essential workers limited the impact of the shutdowns on this source of nutrient loading.

This analysis did not identify any water quality changes clearly attributable to the COVID-19 shutdowns, but it is possible that there were changes that were subtler than could be picked up by our algorithm. The CPA-A is parameterized on a per-lake basis using a generalized set of IOPs meant to capture the observed range of optical conditions in each lake. Sayers et al. (2019a) found issues with this approach in WBLE, as large shifts in the phytoplankton community can result in changes to the specific IOPs. The CPA-A should be able to effectively capture shutdown-driven changes in the magnitude of the color producing agents. However, if the changes in human activity resulted in significant shifts in the phytoplankton community, the optical properties could shift outside the range of our historical observations, introducing additional uncertainty into our results. While we do not have any *in situ* data from spring 2020 to validate our retrievals, comparisons against *in situ* data from mid-summer through early-fall 2020 generate confidence in the late-season CHL and PZD estimates.

Additionally, by focusing on short-term, immediate impacts of the shutdowns, this analysis ignores the contribution of legacy drivers of water quality. Prior research has shown that legacy nutrients in the soil within the watershed can contribute up to 49% of the annual total phosphorus load from the Maumee River (Kast et al., 2021) and phosphorus loadings from prior years also play a significant role in determining the size of phytoplankton blooms in WBLE (Ho and Michalak, 2017). This implies that the impacts of behavior changes due to the COVID-19 shutdowns may be muted by past activity and also that they could have impacts on water quality in the coming years. These water quality indicators, in particular the HAB extent in WBLE, should continue to be studied in subsequent years to assess whether there are any potential long-term or delayed impacts of the shutdowns.

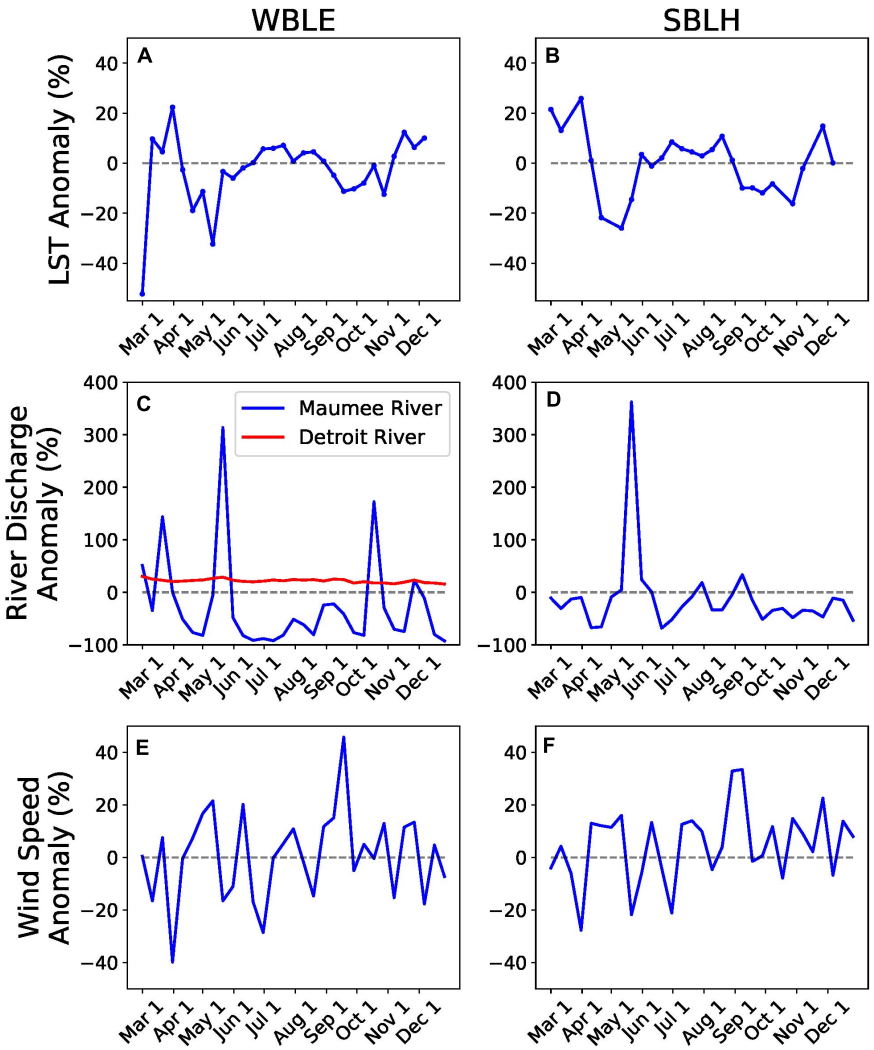

FIGURE 8 | Median 10-day anomalies for the explanatory indicators, including lake surface temperature **(A,B)**, river discharge **(C,D)**, and wind speed **(E,F)**.

CONCLUSION

The Visible Infrared Imaging Radiometer Suite satellite imagery from 2020 was compared to imagery from 2012 to 2019 to assess whether water quality in the Great Lakes' eutrophic basins was impacted by the COVID-19 pandemic shutdowns. Indicator values in April 2020, when social distancing was at its peak, revealed significant changes in both SBLH (increased CHL, decreased TSS, increased PZD) and WBLE (decreased CHL). However, these shifts continued through the year even as shutdown restrictions eased. Comparisons to trends in other indicators (e.g., wind speed and river discharge) led to the conclusion that the observed water quality changes were more likely related to natural variability rather than being a result of the shutdowns. Future research will address some of the limitations of this analysis that may have masked some potential impacts related to the change in human activity. These include the addition of higher resolution sensors to assess nearshore water quality where significant impacts may be expected and the inclusion of data past 2020 to determine if the behavioral changes had any delayed or long-term impacts.

While this study found that there was likely no relationship between the COVID-19-induced shutdowns and short-term Great Lakes water quality, it has shown the utility of using the lengthy remote sensing data record to identify water quality anomalies. This approach has been used extensively in marine systems for identifying anomalies in sea surface temperature (Stock et al., 2015), phytoplankton blooms (Wang et al., 2021), sediment/turbidity (Dogliotti et al., 2016), and HAB presence (Stumpf et al., 2003; Tomlinson et al., 2009). However, there has been limited application of the method for water quality monitoring in the Great Lakes. Going forward, utilizing this approach as imagery becomes available will allow for the identification of water quality anomalies in near real time. This can provide a better understanding

of the historical significance of any given sediment plume or phytoplankton bloom and guide *in situ* sampling efforts. It can also be expanded to the broader Great Lakes region, generating a more complete understanding of the current regional water quality conditions.

DATA AVAILABILITY STATEMENT

The raw data supporting the conclusions of this article will be made available by the authors, without undue reservation.

AUTHOR CONTRIBUTIONS

KB acquired, processed, and analyzed the data, and wrote the first draft of the manuscript. All authors contributed to the conception and design of the study, manuscript revision, read, and approved the submitted version.

FUNDING

This study was funded by NASA under contract # 80NSSC20P2097.

ACKNOWLEDGMENTS

We would like to thank Carol Tolbert and Leah Nakley for shepherding the project, Zane Almquist and Quelyn Bekkering for assistance with data acquisition and processing, and Laura Lorenzoni for inviting our team to be a part of the NASA COVID-19 dashboard.

SUPPLEMENTARY MATERIAL

The Supplementary Material for this article can be found online at: https://www.frontiersin.org/articles/10.3389/fmars.2021.673989/full#supplementary-material

REFERENCES

Ackerman, S. A., Heidinger, A., Foster, M. J., and Maddux, B. (2013). Satellite regional cloud climatology over the Great Lakes. *Remote Sens.* 5, 6223–6240. doi: 10.3390/rs5126223

Aman, M. A., Salman, M. S., and Yunus, A. P. (2020). COVID-19 and its impact on environment: improved pollution levels during the lockdown period–A case from Ahmedabad, India. *Remote Sens. Appl.* 20:100382. doi: 10.1016/j.rsase.2020.100382

Behrenfeld, M. J., and Falkowski, P. G. (1997). Photosynthetic rates derived from satellite-based chlorophyll concentration. *Limnol. Oceanogr.* 42, 1–20. doi: 10.4319/lo.1997.42.1.0001

Bierman, V. J. Jr., and Dolan, D. M. (1981). Modeling of phytoplankton-nutrient dynamics in Saginaw Bay, Lake Huron. *J. Great Lakes Res.* 7, 409–439. doi: 10.1016/S0380-1330(81)72069-0

Binding, C. E., Greenberg, T. A., and Bukata, R. P. (2012). An analysis of MODIS-derived algal and mineral turbidity in Lake Erie. *J. Great Lakes Res.* 38, 107–116. doi: 10.1016/j.jglr.2011.12.003

Binding, C. E., Stumpf, R. P., Shuchman, R. A., and Sayers, M. J. (2020). "Advances in Remote Sensing of Great Lakes Algal Blooms," in *Contaminants of the Great Lakes*, eds J. Crossman and C. Weisener (Cham: Springer), 217–232. doi: 10.1007/698_2020_589

Binding, C. E., Zastepa, A., and Zeng, C. (2019). The impact of phytoplankton community composition on optical properties and satellite observations of the 2017 western Lake Erie algal bloom. *J. Great Lakes Res.* 45, 573–586. doi: 10.1016/j.jglr.2018.11.015

Bischoff, L. (2020). *Coronavirus timeline: a look at the orders changing life in Ohio. Dayton Daily News*. Available online at: https://www.daytondailynews.com/news/local/timeline-coronavirus-prompts-orders-changing-everyday-life-ohio/gpnVSADPxZxMltlDVyqKEP/ (Accessed February 9, 2021)

Bootsma, H. A. (2018). Oceans, lakes, and inland seas: a virtual issue on the large lakes of the world. *Limnol. Oceanogr. Bull.* 27, 87–88. doi: 10.1002/lob.10230

Bosse, K. R., Sayers, M. J., Shuchman, R. A., Fahnenstiel, G. L., Ruberg, S. A., Fanslow, D. L., et al. (2019). Spatial-temporal variability of in situ cyanobacteria vertical structure in Western Lake Erie: implications for remote sensing observations. *J. Great Lakes Res.* 45, 480–489. doi: 10.1016/j.jglr.2019.02.003

Braga, F., Scarpa, G. M., Brando, V. E., Manfè, G., and Zaggia, L. (2020). COVID-19 lockdown measures reveal human impact on water transparency in the Venice Lagoon. *Sci. Total Environ.* 736:139612. doi: 10.1016/j.scitotenv.2020.139612

Bridgeman, T. B., Chaffin, J. D., and Filbrun, J. E. (2013). A novel method for tracking western Lake Erie Microcystis blooms, 2002–2011. *J. Great Lakes Res.* 39, 83–89. doi: 10.1016/j.jglr.2012.11.004

Budd, J. W., and Warrington, D. S. (2004). Satellite-based sediment and chlorophyll a estimates for Lake Superior. *J. Great Lakes Res.* 30, 459–466. doi: 10.1016/S0380-1330(04)70406-2

Bukata, R. P. (2005). *Satellite monitoring of inland and coastal water quality: retrospection, introspection, future directions*. Boca Raton: CRC Press.

Cassidy-Bushrow, A. E., Baseer, M., Kippen, K., Levin, A. M., Li, J., Loveless, I., et al. (2021). Social distancing during the COVID-19 pandemic: quantifying the practice in Michigan–a "hotspot state" early in the pandemic–using a volunteer-based online survey. *BMC Public Health* 21:245. doi: 10.1186/s12889-021-10287-w

U. S. Census Bureau, (2016). *American Community Survey, 2016 ACS 5-Year Estimates, Table B01003*. Available online at: https://data.census.gov/cedsci/ (Accessed December 10, 2020).

Cherif, E. K., Vodopivec, M., Mejjad, N., Esteves da Silva, J. C., Simonovič, S., and Boulaassal, H. (2020). COVID-19 pandemic consequences on coastal water quality using WST Sentinel-3 Data: case of Tangier, Morocco. *Water* 12:2638. doi: 10.3390/w12092638

Collivignarelli, M. C., Abbà, A., Bertanza, G., Pedrazzani, R., Ricciardi, P., and Miino, M. C. (2020). Lockdown for CoViD-2019 in Milan: what are the effects on air quality?. *Sci. Total Environ.* 732:139280. doi: 10.1016/j.scitotenv.2020.139280

Cooperative Institute for Great Lakes Research [CIGLR], University of Michigan and NOAA Great Lakes Environmental Research Laboratory. (2019). *Physical, chemical, and biological water quality monitoring data to support detection of Harmful Algal Blooms (HABs) in western Lake Erie, collected by the Great Lakes Environmental Research Laboratory and the Cooperative Institute for Great Lakes Research since 2012*. Maryland: NOAA National Centers for Environmental Information. Dataset. doi: 10.25921/11da-3x54

Dogliotti, A. I., Ruddick, K., and Guerrero, R. (2016). Seasonal and inter-annual turbidity variability in the Río de la Plata from 15 years of MODIS: El Niño dilution effect. *Estuar. Coast. Shelf Sci.* 182, 27–39. doi: 10.1016/j.ecss.2016.09.013

Dolan, D. M. (1993). Point source loadings of phosphorus to Lake Erie: 1986–1990. *J. Great Lakes Res.* 19, 212–223. doi: 10.1016/S0380-1330(93)71212-5

European Space Agency [ESA]. (2018). *Land Cover CCI Version 2.1.1*. Available online at: https://cds.climate.copernicus.eu/cdsapp#!/dataset/satellite-land-cover (Accessed December 10, 2020).

European Space Agency [ESA]. (2017). *Land Cover CCI Product User Guide Version 2. Tech. Rep*. Available online at: maps.elie.ucl.ac.be/CCI/viewer/download/ESACCI-LC-Ph2-PUGv2_2.0.pdf (Accessed December 10, 2020).

Fahnenstiel, G. L., Millie, D. F., Dyble, J., Litaker, R. W., Tester, P. A., McCormick, M. J., et al. (2008). Microcystin concentrations and cell quotas in Saginaw Bay, Lake Huron. *Aquat. Ecosyst. Health Manag.* 11, 190–195. doi: 10.1080/14634980802092757

Fahnenstiel, G. L., Sayers, M. J., Shuchman, R. A., Yousef, F., and Pothoven, S. A. (2016). Lake-wide phytoplankton production and abundance in the Upper Great Lakes: 2010–2013. *J. Great Lakes Res.* 42, 619–629. doi: 10.1016/j.jglr.2016.02.004

French, C. (2020). *How a spring rainstorm became a 500-year flood event in mid-Michigan. MLive*. Available online at: https://www.mlive.com/news/saginaw-bay-city/2020/05/how-a-spring-rainstorm-became-a-500-year-flood-event-in-mid-michigan.html (Accessed January 15, 2021)

Garnier, R., Benetka, J. R., Kraemer, J., and Bansal, S. (2021). Socioeconomic Disparities in Social Distancing During the COVID-19 Pandemic in the United States: observational Study. *J. Med. Int. Res.* 23:e24591. doi: 10.2196/24591

He, C., Zhang, L., DeMarchi, C., and Croley, T. E. II (2014). Estimating point and non-point source nutrient loads in the Saginaw Bay watersheds. *J. Great Lakes Res.* 40, 11–17. doi: 10.1016/j.jglr.2014.01.013

Herdendorf, C. E. (1982). Large lakes of the world. *J. Great Lakes Res.* 8, 379–412. doi: 10.1016/S0380-1330(82)71982-3

Ho, J. C., and Michalak, A. M. (2017). Phytoplankton blooms in Lake Erie impacted by both long-term and springtime phosphorus loading. *J. Great Lakes Res.* 43, 221–228. doi: 10.1016/j.jglr.2017.04.001

Holshue, M. L., DeBolt, C., Lindquist, S., Lofy, K. H., Wiesman, J., Bruce, H., et al. (2020). First case of 2019 novel coronavirus in the United States. *N. Engl. J. Med.* 382, 929–936. doi: 10.1056/NEJMoa2001191

Hutchinson, D. (2020). *Michigan stay-at-home order timeline: 70 days, 4 extensions, ever-changing restrictions. Click On Detroit*. Available online at: https://www.clickondetroit.com/news/local/2020/06/02/michigan-stay-at-home-order-timeline-70-days-4-extensions-ever-changing-restrictions/ (Accessed February 9, 2021)

Jiang, L., Xia, M., Ludsin, S. A., Rutherford, E. S., Mason, D. M., Jarrin, J. M., et al. (2015). Biophysical modeling assessment of the drivers for plankton dynamics in dreissenid-colonized western Lake Erie. *Ecol. Model.* 308, 18–33. doi: 10.1016/j.ecolmodel.2015.04.004

Kanniah, K. D., Zaman, N. A. F. K., Kaskaoutis, D. G., and Latif, M. T. (2020). COVID-19's impact on the atmospheric environment in the Southeast Asia region. *Sci. Total Environ.* 736:139658. doi: 10.1016/j.scitotenv.2020.139658

Kast, J. B., Apostel, A. M., Kalcic, M. M., Muenich, R. L., Dagnew, A., Long, C. M., et al. (2021). Source contribution to phosphorus loads from the Maumee River watershed to Lake Erie. *J. Environ. Manag.* 279:111803. doi: 10.1016/j.jenvman.2020.111803

Lee, Z., Du, K., Arnone, R., Liew, S., and Penta, B. (2005). Penetration of solar radiation in the upper ocean: a numerical model for oceanic and coastal waters. *J. Geophys. Res. Oceans* 110:13. doi: 10.1029/2004JC002780

Lee, Z., Shang, S., Du, K., and Wei, J. (2018). Resolving the long-standing puzzles about the observed Secchi depth relationships. *Limnol. Oceanogr.* 63, 2321–2336. doi: 10.1002/lno.10940

Lee, Z., Weidemann, A., Kindle, J., Arnone, R., Carder, K. L., and Davis, C. (2007). Euphotic zone depth: its derivation and implication to ocean-color remote sensing. *J. Geophys. Res. Oceans* 112:C03009. doi: 10.1029/2006JC003802

Legendre, P. (2018). *lmodel2: Model II Regression. R package version 1.7-3*.

Lohrenz, S. E., Fahnenstiel, G. L., Millie, D. F., Schofield, O. M., Johengen, T., and Bergmann, T. (2004). Spring phytoplankton photosynthesis, growth, and primary production and relationships to a recurrent coastal sediment plume and river inputs in southeastern Lake Michigan. *J. Geophys. Res. Oceans* 109:C10S14. doi: 10.1029/2004JC002383

Makarewicz, J. C., and Bertram, P. (1991). Evidence for the restoration of the Lake Erie ecosystem. *Bioscience* 41, 216–223. doi: 10.2307/1311411

Manning, N. F., Wang, Y. C., Long, C. M., Bertani, I., Sayers, M. J., Bosse, K. R., et al. (2019). Extending the forecast model: predicting western Lake Erie harmful algal blooms at multiple spatial scales. *J Great Lakes Res.* 45, 587–595. doi: 10.1016/j.jglr.2019.03.004

Michalak, A. M., Anderson, E. J., Beletsky, D., Boland, S., Bosch, N. S., Bridgeman, T. B., et al. (2013). Record-setting algal bloom in Lake Erie caused by agricultural and meteorological trends consistent with expected future conditions. *Proc. Natl. Acad. Sci. U. S. A.* 110, 6448–6452. doi: 10.1073/pnas.1216006110

Michigan Office of the Great Lakes [OGL] (2016). *Sustaining Michigan's Water Heritage: A Strategy for the Next Generation*. Available online at: https://www.michigan.gov/documents/deq/deq-ogl-waterstrategy_538161_7.pdf (Accessed March 14, 2021)

Millie, D. F., Fahnenstiel, G. L., Lohrenz, S. E., Carrick, H. J., Johengen, T. H., and Schofield, O. M. (2003). Physical-biological coupling in southern Lake Michigan: influence of episodic sediment resuspension on phytoplankton. *Aquat. Ecol.* 37, 393–408. doi: 10.1023/B:AECO.0000007046.48955.70

Minnett, P. J., Evans, R. H., Podestá, G. P., and Kilpatrick, K. A. (2014). "Sea-surface temperature from Suomi-NPP VIIRS: Algorithm development and uncertainty estimation," in *Proceedings of SPIE - - The International Society for Optical Engineering*, Vol. 9111, (Bellingham, WA: SPIE), 91110C. doi: 10.1117/12.2053184

Mishra, D. R., Kumar, A., Muduli, P. R., Equeenuddin, S., Rastogi, G., Acharyya, T., et al. (2020). Decline in Phytoplankton Biomass along Indian Coastal Waters due to COVID-19 Lockdown. *Remote Sens.* 12:2584. doi: 10.3390/rs12162584

National Oceanic and Atmospheric Administration [NOAA]. (2020). *NOAA Western Lake Erie Harmful Algal Bloom Seasonal Assessment*. Available online at: https://cdn.coastalscience.noaa.gov/hab-data/bulletins/lake-erie/2020/finalAssessment_2020-09.pdf (Accessed January 30, 2021).

Niu, Q., Xia, M., Ludsin, S. A., Chu, P. Y., Mason, D. M., and Rutherford, E. S. (2018). High-turbidity events in Western Lake Erie during ice-free cycles: contributions of river-loaded vs. resuspended sediments. *Limnol. Oceanogr.* 63, 2545–2562. doi: 10.1002/lno.10959

Ohio Department of Health. (2020). *Director's Stay At Home Order [Press release]*. Available online at: https://coronavirus.ohio.gov/static/publicorders/DirectorsOrderStayAtHome.pdf (Accessed February 9, 2021).

Ordóñez, C., Garrido-Perez, J. M., and García-Herrera, R. (2020). Early spring near-surface ozone in Europe during the COVID-19 shutdown: meteorological effects outweigh emission changes. *Sci. Total Environ.* 747:141322. doi: 10.1016/j.scitotenv.2020.141322

Paerl, H. W., and Huisman, J. (2008). Blooms like it hot. *Science* 320, 57–58. doi: 10.1126/science.1155398

Pelzer, J., and Hancock, L. (2020). *Three Ohioans, All From Cuyahoga County, Have Coronavirus, Gov. Mike DeWine says. cleveland.com*. Available online at: https://www.cleveland.com/healthfit/2020/03/three-ohioans-have-coronavirus-gov-mike-dewine-says.html (accessed August 12, 2021).

Public Sector Consultants [PSC]. (2018). *An assessment of failing septic systems in the Saginaw Bay region. Lansing (MI): Public Sector Consultants*. Available online at: https://publicsectorconsultants.com/an-assessment-of-failing-septic-systems-in-the-saginaw-bay-region/ (Accessed March 14, 2021).

Rao, Y. R., and Schwab, D. J. (2007). Transport and mixing between the coastal and offshore waters in the Great Lakes: a review. *J. Great Lakes Res.* 33, 202–218.

Saulquin, B., Hamdi, A., Gohin, F., Populus, J., Mangin, A., and d'Andon, O. F. (2013). Estimation of the diffuse attenuation coefficient KdPAR using MERIS and application to seabed habitat mapping. *Remote Sens. Environ.* 128, 224–233. doi: 10.1016/j.rse.2012.10.002

Sayers, M., Fahnenstiel, G. L., Shuchman, R. A., and Whitley, M. (2016). Cyanobacteria blooms in three eutrophic basins of the Great Lakes: a comparative analysis using satellite remote sensing. *Int. J. Remote Sens.* 37, 4148–4171. doi: 10.1080/01431161.2016.1207265

Sayers, M. J., Bosse, K. R., Shuchman, R. A., Ruberg, S. A., Fahnenstiel, G. L., Leshkevich, G. A., et al. (2019a). Spatial and temporal variability of inherent and apparent optical properties in western Lake Erie: implications for water quality remote sensing. *J. Great Lakes Res.* 45, 490–507. doi: 10.1016/j.jglr.2019.03.011

Sayers, M. J., Grimm, A. G., Shuchman, R. A., Bosse, K. R., Fahnenstiel, G. L., Ruberg, S. A., et al. (2019b). Satellite monitoring of harmful algal blooms in the Western Basin of Lake Erie: a 20-year time-series. *J. Great Lakes Res.* 45, 508–521. doi: 10.1016/j.jglr.2019.01.005

Scavia, D., Allan, J. D., Arend, K. K., Bartell, S., Beletsky, D., Bosch, N. S., et al. (2014). Assessing and addressing the re-eutrophication of Lake Erie: central basin hypoxia. *J. Great Lakes Res.* 40, 226–246. doi: 10.1016/j.jglr.2014.02.004

Selzer, M. D., Joldersma, B., and Beard, J. (2014). A reflection on restoration progress in the Saginaw Bay watershed. *J. Great Lakes Res.* 40, 192–200. doi: 10.1016/j.jglr.2013.11.008

Shuchman, R. A., Bosse, K. R., Sayers, M. J., Fahnenstiel, G. L., and Leshkevich, G. (2017). Satellite Observed Water Quality Changes In The Laurentian Great Lakes Due To Invasive Species, Anthropogenic Forcing, And Climate Change. *Int. Arch. Photogramm. Remote Sens. Spatial Inf. Sci.* XLII-3, 189–195. doi: 10.5194/isprs-archives-XLII-3-W2-189-2017

Shuchman, R. A., Leshkevich, G., Sayers, M. J., Johengen, T. H., Brooks, C. N., and Pozdnyakov, D. (2013). An algorithm to retrieve chlorophyll, dissolved organic carbon, and suspended minerals from Great Lakes satellite data. *J. Great Lakes Res.* 39, 14–33. doi: 10.1016/j.jglr.2013.06.017

Son, S., and Wang, M. (2020). Water quality properties derived from VIIRS measurements in the Great Lakes. *Remote Sens.* 12:1605. doi: 10.3390/rs12101605

Soni, P. (2021). Effects of COVID-19 lockdown phases in India: an atmospheric perspective. *Environ. Dev. Sustain.* 1–12. doi: 10.1007/s10668-020-01156-4 [Online ahead of print]

State of Michigan. (2020a). *Michigan announces first presumptive positive cases of COVID-19 [Press release]*. Available online at: https://www.michigan.gov/coronavirus/0,9753,7-406-98158-521365--,00.html (Accessed February 9, 2021)

State of Michigan. (2020b). *Governor Whitmer Signs "Stay Home, Stay Safe" Executive Order [Press release]*. Available online at: https://www.michigan.gov/whitmer/0,9309,7-387-90499_90640-522625--,00.html (Accessed February 9, 2021)

State of Michigan. (2020c). *Governor Whitmer Extends, Expands "Stay Home, Stay Safe" Executive Order to Save Lives [Press release]*. Available online at: https://www.michigan.gov/whitmer/0,9309,7-387-90499_90640-525173--,00.html (Accessed April 10, 2021)

Statistics Canada (2019). *Census Profile for Census Subdivisions in Ontario, 2016 Census, Catalogue no. 98-401-X2016066*. Available online at: https://www12.statcan.gc.ca/census-recensement/2016/dp-pd/index-eng.cfm (Accessed December 10, 2020).

Stock, C. A., Pegion, K., Vecchi, G. A., Alexander, M. A., Tommasi, D., Bond, N. A., et al. (2015). Seasonal sea surface temperature anomaly prediction for coastal ecosystems. *Prog. Oceanogr.* 137, 219–236. doi: 10.1016/j.pocean.2015.06.007

Stow, C. A., Cha, Y., Johnson, L. T., Confesor, R., and Richards, R. P. (2015). Long-term and seasonal trend decomposition of Maumee River nutrient inputs to western Lake Erie. *Environ. Sci. Technol.* 49, 3392–3400. doi: 10.1021/es5062648

Stow, C. A., Dyble, J., Kashian, D. R., Johengen, T. H., Winslow, K. P., Peacor, S. D., et al. (2014). Phosphorus targets and eutrophication objectives in Saginaw Bay: a 35 year assessment. *J. Great Lakes Res.* 40, 4–10. doi: 10.1016/j.jglr.2013.10.003

Stumpf, R. P., Culver, M. E., Tester, P. A., Tomlinson, M. C., Kirkpatrick, G. J., Pederson, B., et al. (2003). Monitoring Karenia brevis blooms in the Gulf of Mexico using satellite ocean color imagery and other data. *Harmful Algae* 2, 147–160. doi: 10.1016/S1568-9883(02)00083-5

Stumpf, R. P., Wynne, T. T., Baker, D. B., and Fahnenstiel, G. L. (2012). Interannual variability of cyanobacterial blooms in Lake Erie. *PLoS One* 7:e42444. doi: 10.1371/journal.pone.0042444

Tobías, A., Carnerero, C., Reche, C., Massagué, J., Via, M., Minguillón, M. C., et al. (2020). Changes in air quality during the lockdown in Barcelona (Spain) one month into the SARS-CoV-2 epidemic. *Sci. Total Environ.* 726:138540. doi: 10.1016/j.scitotenv.2020.138540

Tomlinson, M. C., Wynne, T. T., and Stumpf, R. P. (2009). An evaluation of remote sensing techniques for enhanced detection of the toxic dinoflagellate, Karenia brevis. *Remote Sens. Environ.* 113, 598–609. doi: 10.1016/j.rse.2008.11.003

Wang, M., Jiang, L., Mikelsons, K., and Liu, X. (2021). Satellite-derived global chlorophyll-a anomaly products. *Int. J. Appl. Earth Obs. Geoinf.* 97:102288. doi: 10.1016/j.jag.2020.102288

Warner, D. M., and Lesht, B. M. (2015). Relative importance of phosphorus, invasive mussels and climate for patterns in chlorophyll a and primary production in Lakes Michigan and Huron. *Freshw. Biol.* 60, 1029–1043. doi: 10.1111/fwb.12569

Watson, S. B., Miller, C., Arhonditsis, G., Boyer, G. L., Carmichael, W., Charlton, M. N., et al. (2016). The re-eutrophication of Lake Erie: harmful algal blooms and hypoxia. *Harmful Algae* 56, 44–66. doi: 10.1016/j.hal.2016.04.010

Wilcoxon, F. (1945). Individual Comparisons by Ranking Methods. *Biometrics Bull.* 1, 80–83. doi: 10.2307/3001968

World Health Organization [WHO]. (2020a). *Coronavirus disease 2019 (COVID-19): Situation report, 1*. Available online at: https://www.who.int/docs/default-source/coronaviruse/situation-reports/20200121-sitrep-1-2019-ncov.pdf?sfvrsn=20a99c10_4 (Accessed February 9, 2021)

World Health Organization [WHO]. (2020b). *Coronavirus disease 2019 (COVID-19): Situation report, 11*. Available online at: https://www.who.int/docs/default-source/coronaviruse/situation-reports/20200131-sitrep-11-ncov.pdf?sfvrsn=de7c0f7_4 (Accessed February 9, 2021)

Wynne, T. T., and Stumpf, R. P. (2015). Spatial and temporal patterns in the seasonal distribution of toxic cyanobacteria in western Lake Erie from 2002–2014. *Toxins* 7, 1649–1663. doi: 10.3390/toxins7051649

Wynne, T. T., Stumpf, R. P., and Briggs, T. O. (2013). Comparing MODIS and MERIS spectral shapes for cyanobacterial bloom detection. *Int. J. Remote Sens.* 34, 6668–6678. doi: 10.1080/01431161.2013.804228

Wynne, T. T., Stumpf, R. P., Litaker, R. W., and Hood, R. R. (2021). Cyanobacterial bloom phenology in Saginaw Bay from MODIS and a comparative look with western Lake Erie. *Harmful Algae* 103:101999. doi: 10.1016/j.hal.2021.101999

Wynne, T. T., Stumpf, R. P., Tomlinson, M. C., and Dyble, J. (2010). Characterizing a cyanobacterial bloom in western Lake Erie using satellite imagery and meteorological data. *Limnol. Oceanogr.* 55, 2025–2036. doi: 10.4319/lo.2010.55.5.2025

Yunus, A. P., Masago, Y., and Hijioka, Y. (2020). COVID-19 and surface water quality: improved lake water quality during the lockdown. *Sci. Total Environ.* 731:139012. doi: 10.1016/j.scitotenv.2020.139012

Zangari, S., Hill, D. T., Charette, A. T., and Mirowsky, J. E. (2020). Air quality changes in New York City during the COVID-19 pandemic. *Sci. Total Environ.* 742:140496. doi: 10.1016/j.scitotenv.2020.140496

Zhu, N., Zhang, D., Wang, W., Li, X., Yang, B., Song, J., et al. (2020). A novel coronavirus from patients with pneumonia in China, 2019. *N. Engl. J. Med.* 382, 727–733. doi: 10.1056/NEJMoa2001017

Conflict of Interest: The authors declare that the research was conducted in the absence of any commercial or financial relationships that could be construed as a potential conflict of interest.

Publisher's Note: All claims expressed in this article are solely those of the authors and do not necessarily represent those of their affiliated organizations, or those of the publisher, the editors and the reviewers. Any product that may be evaluated in this article, or claim that may be made by its manufacturer, is not guaranteed or endorsed by the publisher.

frontiers in Marine Science

ORIGINAL RESEARCH
published: 30 August 2021
doi: 10.3389/fmars.2021.669415

Long-Term Trends and Impact of SARS-CoV-2 COVID-19 Lockdown on the Primary Productivity of the North Indian Ocean

N. Sunanda[1], J. Kuttippurath[1], R. Peter[1], Kunal Chakraborty[2] and A. Chakraborty[1]*

[1] CORAL, Indian Institute of Technology Kharagpur, Kharagpur, India, [2] Indian National Centre for Ocean Information Services, Ministry of Earth Sciences, Hyderabad, India

OPEN ACCESS

Edited by:
Domenico D'Alelio, University of Naples Federico II, Italy

Reviewed by:
Qingyou He, South China Sea Institute of Oceanology, China
Simona Saviano, University of Naples Parthenope, Italy

****Correspondence:***
J. Kuttippurath
jayan@coral.iitkgp.ac.in

Specialty section:
This article was submitted to Global Change and the Future Ocean, a section of the journal Frontiers in Marine Science

Received: *18 February 2021*
Accepted: *29 July 2021*
Published: *30 August 2021*

Citation:
Sunanda N, Kuttippurath J, Peter R, Chakraborty K and Chakraborty A (2021) Long-Term Trends and Impact of SARS-CoV-2 COVID-19 Lockdown on the Primary Productivity of the North Indian Ocean. Front. Mar. Sci. 8:669415. doi: 10.3389/fmars.2021.669415

COrona VIrus Disease (COVID) 2019 pandemic forced most countries to go into complete lockdown and India went on complete lockdown from 24th March 2020 to 8th June 2020. To understand the possible implications of lockdown, we analyze the long-term distribution of Net Primary Productivity (NPP) in the North Indian Ocean (NIO) and the factors that influence NPP directly and indirectly, for the period 2003–2019 and 2020 separately. There exists a seasonal cycle in the relationship between Aerosol Optical Depth (AOD), Chlorophyll-a (Chl-a) and NPP in agreement with the seasonal transport of aerosols and dust into these oceanic regions. In Arabian Sea (AS), the highest Chl-a (0.58 mg/m^3), NPP (696.57 mg/C/m^2/day) and AOD (0.39) are observed in June, July, August, and September (JJAS). Similarly, maximum Chl-a (0.48 mg/m^3) and NPP (486.39 mg/C/m^2/day) are found in JJAS and AOD (0.27) in March, April, and May (MAM) in Bay of Bengal. The interannual variability of Chl-a and NPP with wind speed and Sea Surface Temperature (SST) is also examined, where the former has a positive and the latter has a negative feedback to NPP. The interannual variability of NPP reveals a decreasing trend in NPP, which is interlinked with the increasing trend in SST and AOD. The analysis of wind, SST, Chl-a, and AOD for the pre-lockdown, lockdown, and post lockdown periods of 2020 is employed to understand the impact of COVID-19 lockdown on NPP. The assessment shows the reduction in AOD, decreased wind speeds, increased SST and reduced NPP during the lockdown period as compared to the pre-lockdown, post-lockdown and climatology. This analysis is expected to help to understand the impact of aerosols on the ocean biogeochemistry, nutrient cycles in the ocean biogeochemical models, and to study the effects of climate change on ocean ecosystems.

Keywords: North Indian Ocean, primary productivity, chlorophyll-a, COVID-19 lockdown, climate change

HIGHLIGHTS

- Assessment of NPP changes in the North Indian Ocean in view of COVID-19 lockdown.
- NPP exhibits negative anomaly in Arabian Sea (AS) and Bay of Bengal (BoB) in 2020.
- SST anomalies are positive in northern AS and BoB during the lockdown.
- AOD anomalies are negative during the lockdown period due to lesser emissions.

INTRODUCTION

About half of the global net oceanic primary productivity (NPP) is contributed by the phytoplankton (Field et al., 1998; Käse and Geuer, 2018). Compared to the terrestrial NPP, the biomass of primary production is about 500 times smaller because the phytoplankton is invariably utilized by the marine food chain (Webb, 2019). The major environmental drivers of oceanic NPP are light, nutrients and temperature. These are, in turn, altered by the changes in associated oceanic and atmospheric processes, and are sensitive to the changes and variability of climate (Field et al., 1998; Chavez et al., 2011). A few of the Essential Climate Variables (ECVs) identified by the Global Climate Observation System (GCOS, 2011) are surface winds, phytoplankton, SST, and aerosols, which are either directly or indirectly connected to the amount of regional and global oceanic NPP.

It has been observed that the average rise in earth surface temperature is about 1.5°C in the past century (IPCC, 2018) and aerosols, the tiny suspended particles in the atmosphere, have also a significant role in this warming or modification of global surface temperatures. The aerosols have been influencing the earth radiation budget in several different ways, and have been studied widely in the past (e.g., Wielicki et al., 1998; Satheesh et al., 2006). To understand the response of oceans to climate change, it is crucial to study the changes in ECVs individually as well as their inter-relationships, feedback between them and their connection to NPP. Previous studies show a positive (Martin et al., 1994; Jickells et al., 2005; Patra et al., 2007; Banerjee and Prasanna Kumar, 2014), negative (Mallet et al., 2009; Paytan et al., 2009; Jordi et al., 2012) and even no correlation between aerosols and oceanic NPP at different world oceanic regions (Cropp et al., 2005; Gallisai et al., 2014).

The intense upwelling during the summer monsoon and convection during the winter monsoon enhances primary productivity in the Arabian Sea (Banerjee and Prasanna Kumar, 2014). The injection of nutrient rich water into the euphotic zone makes Arabian Sea (AS) highly productive, which is unlikely in Bay of Bengal (BoB) due to high stratification there (Prasanna Kumar et al., 2002). Although not highly productive like AS, BoB is subjected to high new production and more structured in removing atmospheric CO_2 on longer time scales (Kumar et al., 2004). Even when there is the availability of nutrients, increased riverine flux reduces the light penetration to depths and thereby restricts NPP in the summer and fall inter-monsoon months (Prasanna Kumar et al., 2010). The dependency of productivity on insolation is a major factor in the tropical oceans. The wind stirring is also a key factor for primary production in the Indian Ocean (Beaufort et al., 1997). Seasonal changes in the productivity related to nutrient and phytoplankton abundance are crucial for predicting Hilsa habitat and their migratory patterns in the deltaic regions and shelf of BoB (Hossain et al., 2020). The study of NPP in northeast (NE) BoB for the past 26,000 years reveals that the NPP is controlled by nutrient contents and their distribution within the upper water column (Zhou et al., 2020).

Despite being located in similar geographical locations, AS and BoB exhibit different physical and biological characteristics (Prasanna Kumar et al., 2002; Shenoi et al., 2002; Chakraborty et al., 2020). It is primarily due to the southwest monsoon winds where the AS encounters strong upwelling when rapid surface cooling occurs because of entrainment pushed by the strong winds (Findlater, 1969). Nevertheless, the excess precipitation over evaporation and extensive river runoff (Subramanian, 1993) make BoB strongly stratified. These differences are held to be responsible for the physical, chemical, and biological differences between the basins (Kumar et al., 1995).

Several studies have accounted for the distribution of aerosol (Li and Ramanathan, 2002) and their possible connection with Chl-a abundance (Vinayachandran et al., 2004). The sea surface cooling is responsible for injecting nutrients to the surface in the winter monsoon in the northeastern AS, which helps them sustain the primary productivity even after the monsoon (Madhupratap et al., 1996). The connection between phytoplankton bloom and dust deposition over Central AS was analyzed by Banerjee and Prasanna Kumar (2014) and found that blooms cannot be fully described by injection of nutrients by processes such as advection and mixing in the upper ocean. Shafeeque et al. (2017) compared the seasonal cycles of phytoplankton with SST, Aerosol Optical Depth (AOD), and winds off Somalia. The productivity in the high-nutrient low chlorophyll (HNLC) regions of oceans is directly affected by the iron supply (Jickells et al., 2005). Henceforth, altering nutrient types and amounts may change phytoplankton species and their composition and growth rate, and the resultant NPP (Howarth, 1988; Moore et al., 2013). Although the relationship between anthropogenic aerosols on the carbon cycle and climate change is not well understood, it is estimated that nutrient intake due to atmospheric deposition is increasing the CO_2 uptake (Mahowald et al., 2017).

Satellite data are excellent tools for examining global changes in atmospheric pollution, aerosols and primary productivity. The shortwave infrared (SWIR) bands facilitate vigorous atmospheric corrections in coastal turbid waters (Wang et al., 2009), whereas the band around 685 nm is more advantageous for the detection of phytoplankton fluorescence (Gower et al., 1999; Hu et al., 2005). Here, we examine the primary productivity in BoB and AS, and its drivers for the period 2003–2020. We investigate the Chlorophyll-a (Chl-a) variability in different seasons with respect to surface winds, Sea Surface Temperature (SST) and AOD in these oceanic basins. We estimate the NPP using the surface Chl-a, SST, Photosynthetically Active Radiation (PAR), and length of the day (Behrenfeld and Falkowski, 1997). On top of this, we

assess the impact of lockdown, due to the spread of Severe Acute Respiratory Syndrome (SARS) COrona VIrus Disease (COVID) 2019, on AOD and NPP. The long-term analysis of NPP and its drivers will be used to assess the lock-down situation and its impact on NPP.

MATERIALS AND METHODS

Data

We have used the Modern-Era Retrospective analysis for Research and Applications (MERRA-2) Aerosol Optical Depth for the period January 2003–December 2020. These data have a spatial resolution of 0.625° × 0.5° (Global Modeling and Assimilation Office (GMAO), 2015). The satellite-based bias-corrected and merged Ocean Color Climate Change Initiative (OC-CCI) version 4.2 data are taken for the Chl-a measurements (Sathyendranath et al., 2020). The OC-CCI data consist of [MEdium Resolution Imaging Spectrometer–MERIS: 2002–2012, MODIS on Aqua: 2002–to date, and Sea-viewing Wide Field-of-view Sensor (SeaWiFS): 1997–2010] satellite measurements on a 4 × 4 km resolution for the period 1997–2020. The daily surface winds (at 10 m) and SST were taken from the European Centre for Medium Range Weather Forecast's (ECMWF) Reanalyses, ERA5 data of 25 × 25 km resolution for the period from 2003 to 2020 (Hersbach et al., 2020). The NPP calculation is carried out using monthly data of Photosynthetically Active Radiation (Goddard Space Flight Center (NASA) et al., 2018), SST (Werdell et al., 2013) from MODIS–Aqua for the period from 2003 to 2020 at 4 km resolution. We started our analysis from the year 2003 because MODIS-Aqua data are continuous from that year onward. Further details of the datasets are provided in **Table 1**.

Methods

The analysis has been carried out for the period 2003–2019, but we have also considered the year 2020 to examine the impact of COVID-19 lockdown on primary productivity. We have divided the year 2020 into three periods: pre-lockdown (1 January–24 March), lockdown (25 March–7 June), and post-lockdown (8 June–30 June). We have analyzed SST, winds, AOD and Chl-a for these periods. We have also analyzed the temporal variability of Chl-a, AOD and NPP separately for the year 2020 and for the period 2003–2019, and made a comparison between both analyses to assess the effect of lockdown on NPP. The NPP is calculated using the equation,

$$NPP = Chl - a \times pb_{opt} \times daylength \times \left[\frac{0.66125 \times par}{(par + 4.1)}\right] \times z_{eu}$$

where Chl-a is Chlorophyll concentration in mg/m^3, pb_{opt} is the maximum carbon fixation rate within a water column (mgC/mgChl/hr), day length is the number of hours of daylight at the given location and NPP is milligrams of carbon fixed per day unit volume, par is the Photosynthetically Active Radiation (PAR) and z_{eu} is the euphotic depth.

Further details about the NPP calculations are provided in Behrenfeld and Falkowski (1997). We have also made a seasonal analysis of Chl-a, AOD, SST overlaid with winds and NPP from 2003 to 2019 to understand the variability of these variables over the North Indian Ocean (NIO). The seasons are divided according to the classification of the India Meteorological Department. They are: Winter monsoon: January and February (JF), Pre-monsoon: March, April and May (MAM), Monsoon: June, July, August and September (JJAS) and Post-monsoon: October, November and December (OND).

Our analysis is mainly divided into two parts: one is the spatial analysis over the whole NIO region and temporal analysis over selected regions. First, we made a climatology using monthly data from the year 2003 to 2019. To examine the impact of COVID-19, we have made use of daily data because we are focusing on three periods and compared them with the monthly climatology. We have done the analysis for the same period, i.e., pre-lockdown, lockdown and post-lockdown for the year 2018 for comparison. We calculated the anomaly of these periods from the climatology of 17 years (2003–2019) and repeated the same for 2018. We have also chosen three concentric regions in the BoB, which are described in **Supplementary Table 1**. These areas are depicted in **Figure 1**.

The wind stress (WS) is calculated using,

$$\tau = \rho_{air} * Cd * |U|^2$$

where,

ρ_{air} = 1.225 kg/m3, Cd = 0.0013, and U is the magnitude of wind.

We have analyzed the pixel-wise spatial trend of SST, WS, AOD, Chl-a, and NPP from 2003 to 2019. We have computed the spatial trend to analyze the patterns with respect to recent years. We select two regions in BoB and AS, which represent the positive/negative spatial trend of NPP to depict the interannual variability of Chl-a, SST, WS, AOD, and NPP. This interannual variability is represented as a box plot that has two parts; different quartiles and two whiskers.

RESULTS

Chl-a, AOD, and SST and Their Relationship With NPP

When we consider the effects of atmospheric deposition on the phytoplankton abundance, it is also necessary to assess the impact of global land surface and oceanic warming. **Figure 1** shows the monthly SST climatology overlaid by 10 m wind vectors. The tropical Indian Ocean SST has a major role in the climate and its regional variability (Chowdary et al., 2015; Kuttippurath et al., 2021a) and its variability in global scales (Schott et al., 2009). The monthly analysis of SST shows a primary peak in May and a secondary peak in November, and the seasonal reversal of winds associated with the SW (southwest) and NE monsoons (Webster et al., 1998). The observed annual cycle in AS shows two modes of SST seasonality with the primary peak during April–May and the secondary peak in October (Vinayachandran and Shetye, 1991;

TABLE 1 | Details of datasets used in this study.

Sl. No.	Variable	Dataset	Temporal coverage	Spatial resolution
1	SST	ERA5	2003–2020	25 km × 25 km
2	Chl-a	OC-CCI	2003–2020	4 km × 4 km
3	AOD	MERRA-2	2003–2020	0.625 × 0.5°
4	SST (for NPP calculation)	MODIS-Aqua	2003–2020	4 km × 4 km
5	PAR (for NPP calculation)	MODIS-Aqua	2003–2020	4 km × 4 km

Murtugudde and Busalacchi, 1999; Fathrio et al., 2017). During April–May, prior to the onset of Indian summer monsoon, AS is one of the warmest regions in the tropical oceans (Joseph et al., 2006). The seasonal SST cycle is very prominent in BoB, with maxima in May and October (Rahaman et al., 2020). The three concentric box regions are chosen for further discussion (Prakash et al., 2012).

Figure 2 shows the seasonal variation of AOD, Chl-a, NPP and WS over NIO. Surrounded by several deserts, AS is characterized by higher AOD which peaks in JJAS. The concentration of AOD again increases in OND, and the minimum aerosol loading is observed in JF. In BoB, the highest concentration of AOD is observed in MAM in the northern Bay and lowest in OND. In southern BoB, AOD concentrations remain about 0.25 – 0.3 across all the seasons. There are two peaks in AS, one in MAM and the other in JJAS (Kuttippurath and Raj, 2021). However, our analyses reveal the highest concentration of AOD in JJAS although small regions depict an aerosol concentration of 0.4–0.5 in the south eastern AS during MAM. The first peak is due to continental air mass carried to sea by prevailing north-easterly winds (e.g., Ramachandran and Jayaraman, 2002). The second peak is the result of transport of land-originated aerosols from northern Africa and Gulf regions (e.g., Patra et al., 2005). The highest average AOD in AS is about 0.39 in JJAS and lowest in JF of about 0.203. In BoB, the highest AOD is about 0.27 in MAM and lowest in OND of about 0.2. The basin-averaged values in different seasons are listed in **Supplementary Table 2**. The source of aerosols over BoB is mostly from the Indian Subcontinent (e.g., Moorthy et al., 2003). It is also necessary to understand that the aerosols from the northern Africa and Gulf regions are naturally formed desert dust or sand (Prospero et al., 2002). In contrast, those produced in the Indian subcontinent are mostly anthropogenic and composed mainly of black carbon (soot) and fly ash originated due to the fossil fuel combustion and biomass burning (Ramanathan et al., 2001; Prospero et al., 2002).

The AS shows higher concentrations of Chl-a than those over BoB in all months and the smallest difference is observed during MAM, as shown in **Figure 2**. The northeastern AS has the highest concentrations throughout the year with the least seasonal variability, whereas contrasting characteristics are exhibited by the southern AS with significant seasonal changes. The northwest AS shows high Chl-a concentration during JJAS. The northern AS depicts higher concentration of Chl-a in JF, whereas over the rest of AS, the Chl-a remains marginally small. During the pre-monsoon season, the southern regions exhibit relatively smaller concentrations of Chl-a. With the advent of monsoon in JJAS, the southern AS show higher amounts of Chl-a, particularly in the SW and some parts of SE regions. The seasonality of Chl-a in the southern regions is prominent, but the northern AS remains nearly similar in all months. In BoB, the Chl-a concentration shows 0.2–0.4 mg/m^3 smaller than that in AS throughout the year. The northern BoB shows small seasonal variability compared to that of the southern BoB. However, BoB shows the highest concentration of Chl-a in JJAS followed by OND, JF and the smallest in MAM. There is an increase in Chl-a in JJAS near Sri Lankan coast, associated to the upwelling along the southwest coast of India and transport by the monsoonal currents (Vinayachandran et al., 2004; Chakraborty et al., 2018). The southwest BoB shows a higher concentration of Chl-a than that of the southeast BoB with increasing its concentration from OND to JF. The magnitude of Chl-a in AS is higher in NW, and then it gradually decreases with NE, SW, and SE regions (Patra et al., 2007). The highest average Chl-a concentration is about 0.58 mg/m^3 in AS and 0.48 mg/m^3 in BoB.

The biological activity of AS is influenced by intense seasonal activity of the atmospheric circulation resulting in strong upwelling along the west coast and series of entrainments forced by winds in the central AS (McCreary et al., 2009). The NPP has a spatial pattern similar to that of Chl-a. The NW region of AS shows high NPP close to 1000 mgCm^2/day during JF, while the NPP is significantly smaller during MAM, coinciding with the smaller Chl-a there. It is also important to note that the primary peak of SST in AS occurs in MAM, which may be one of the reasons for the smaller primary productivity over AS in this period. The NW and SW regions of AS exhibit high productivity during JJAS. The upward Ekman pumping and coastal upwelling drive the increased productivity in the western coastal AS (Anderson and Prell, 1992; Anderson et al., 1992). Therefore, productivity in the central and northern AS also increases during the SW monsoon (Keen et al., 1997; Prasanna Kumar et al., 2001; Caley et al., 2011). The mixing and WS in the upper layers, as well as the Ekman pumping generated by the positive WS curl, lead to the advection of nutrients to the surface layers to enhance NPP in these regions (Lee et al., 2000; Prasanna Kumar et al., 2001; Wiggert et al., 2005). The Chl-a and WS exhibit a positive relationship and prominent seasonal cycle in AS and BoB with a peak WS of 0.11 and 0.08 in JJAS. The changes in the WS and its curl can condition the biological productivity, and as such, there is no straight connection between boreal summer productivity and summer monsoon intensity (Le Mézo et al., 2017). NPP show comparatively smaller values in BoB except near Sri Lanka in JJAS.

The spatial variability of SST, WS, AOD, Chl-a, and NPP reveals varying trends over different NIO regions (**Figure 3**). In

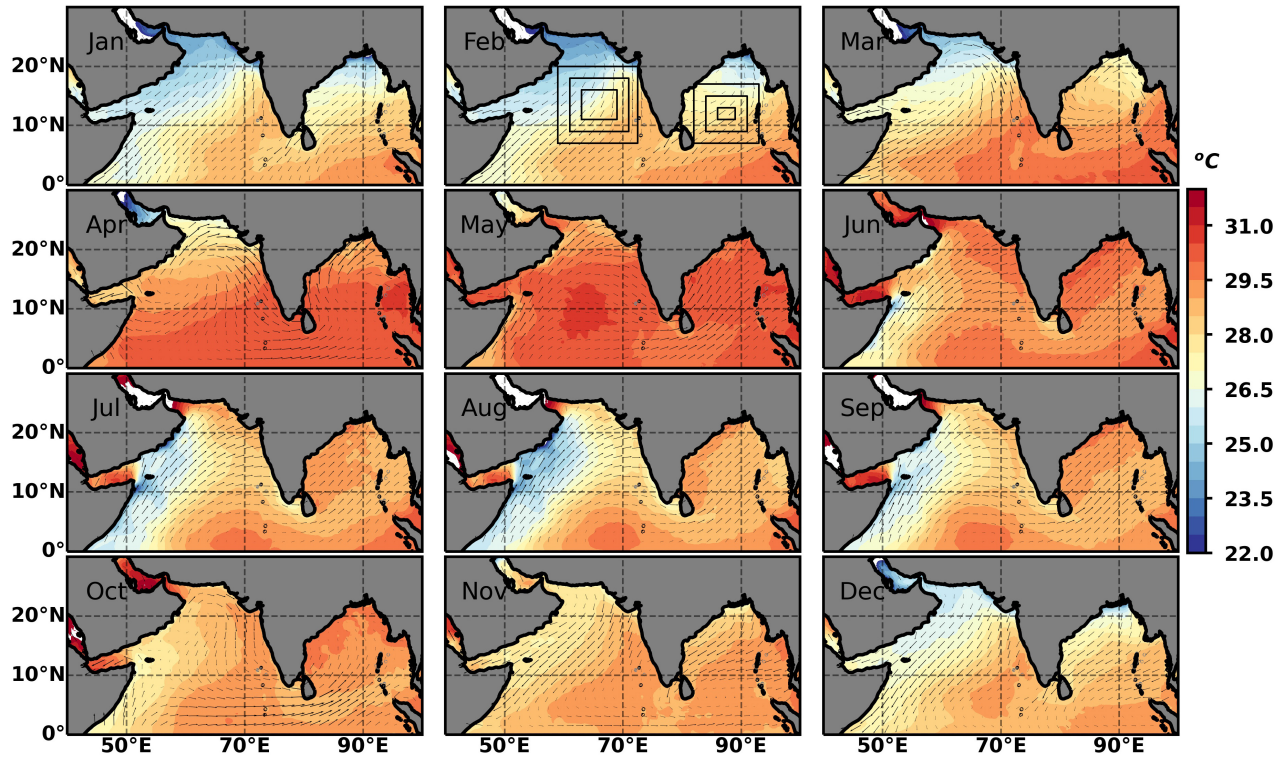

FIGURE 1 | Monthly Climatology of Sea Surface Temperature (SST) overlaid with wind vectors from 2003 to 2019 over the North Indian Ocean. The concentric boxes (**Supplementary Table 1**) are also marked in the figure.

AS, there is a significant increasing trend of AOD in the northern and southern regions particularly in the central and western parts. The western BoB also shows a significant increasing trend whereas an insignificant decreasing trend in the southern BoB. Even though the southern parts of AS and BoB show a noticeable warming trend in SST, the northern parts show an insignificant decreasing trend. The Chl-a shows a decreasing trend in the regions where SST shows an increasing trend. A similar variability is also observed for NPP. Nevertheless, the rising trend of NPP for the regions with suppressed warming highlights the role of physical processes in controlling the phytoplankton dynamics. There is a decelerating trend of NPP and Chl-a in the AS, except for some small regions in the northeastern coast of AS, but an increasing trend in Chl-a and NPP in the southern BoB. It highlights the recent warming and the change in stratification causing the enhancement of the phytoplankton and NPP in recent years. Over the past few decades, there has been an increase in the Chl-a concentration in the coastal waters around the world (Goes et al., 2005; Gregg et al., 2005) and in the oceanic heat content (Levitus et al., 2000). The nutrients exhibit a decreasing trend in the western and an increasing trend in the southeast Indian Ocean, where the warming is not prominent. In this context, the atmospheric deposition is more critical for triggering NPP (Patra et al., 2007). The changing monsoonal circulation and winds (Roxy et al., 2015) also affect the phytoplankton dynamics because it affects the upwelling mechanism (Goes et al., 2005). Even though the values of NPP and Chl-a show small values in BoB compared to that in AS, an accelerating trend in NPP and Chl-a is observed in BoB.

The Interannual Variability of NPP

Interannual Variability

We have considered three concentric box regions in AS and BoB to understand the interannual variability of Chl-a, AOD and NPP (presented in **Supplementary Figures 1**, **2**). The Chl-a is more abundant in AS compared to BoB, whereas AOD shows similar values over AS and BoB. The seasonal cycle of Chl-a is more prominent and well developed in AS than in BoB. The increasing/decreasing abundances in Chl-a is also linked to El-Niño Southern Oscillation (ENSO), Indian Ocean Dipole (IOD) episodes and linked to the passage of cyclones (Kuttippurath et al., 2021b), but we do not focus on those events here, as those are beyond the scope of this study. Instead, we concentrate on the interannual variability of Chl-a and AOD over AS and BoB. **Supplementary Figures 1**, **2** depict the dominance of seasonality over the interannual changes. Since the increase in Chl-a is significantly smaller, it is compelling to note that the Chl-a concentration in BoB is increasing in recent decade relative to the previous decades. In contrast, AS exhibits a reduction in magnitude of Chl-a compared to the earlier years. As the trend of AOD is increasing in both the basins, it is noteworthy that the atmospheric deposition plays a major role in modifying the Chl-a concentration over the NIO with negative correlation of −0.61

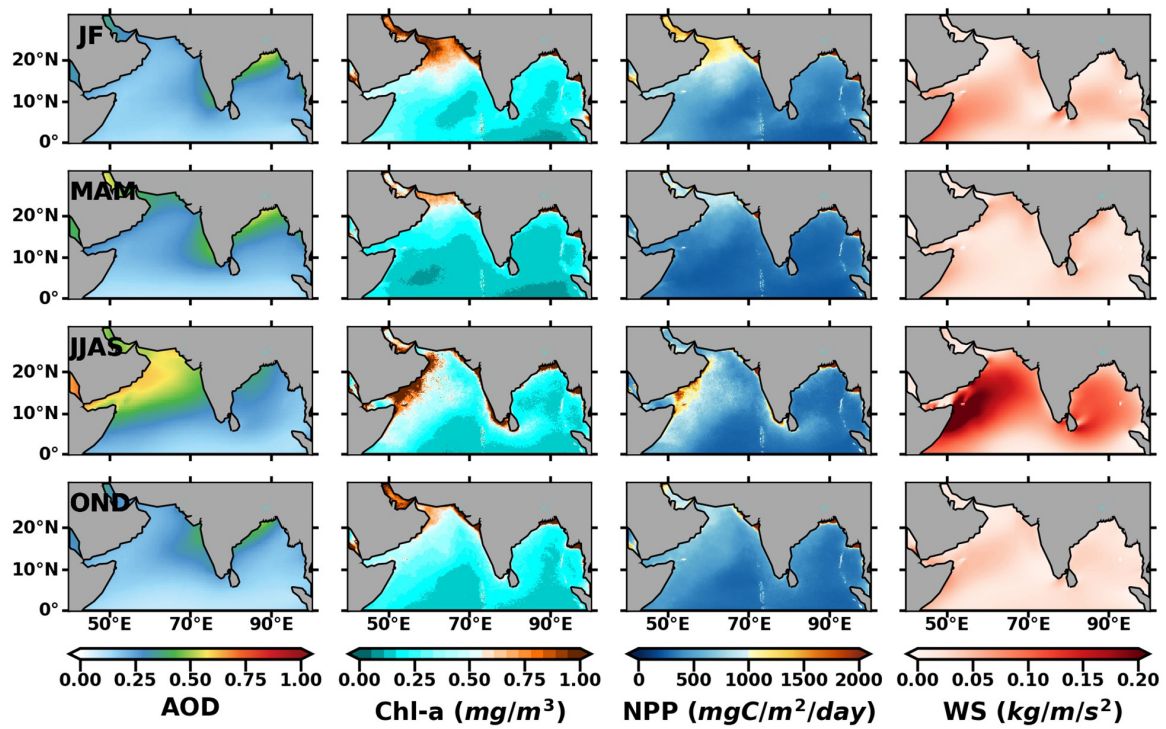

FIGURE 2 | Seasonal Climatology of Aerosol Optical Depth (AOD), Chlorophyll-a (Chl-a), Net Primary Productivity (NPP) and wind stress (WS) for different seasons January and February (JF), March, April, and May (MAM), June, July, August and September (JJAS), and October, November and December (OND) from 2003 to 2019.

in AS and −0.52 in BoB, respectively; consistent with previous studies (e.g., Patra et al., 2007).

Supplementary Figures 3, **4** show the interannual variability of Chl-a and SST in the concentric box like regions in AS and BoB. As discussed earlier, the warming of oceans is associated with lower Chl-a, whereas insignificant warming regions exhibit enhanced Chl-a. Therefore, we have also examined the interannual variability of Chl-a and WS over AS and BoB (**Supplementary Figures 5**, **6**). The analyses reveal that SST has negative and WS has a positive feedback on Chl-a abundance with a dominant seasonal cycle. The analyses show that SST and Chl-a have negative feedback, but WS and Chl-a have positive feedback with distinct seasonal cycles. It is evident from the analysis that the phytoplankton concentration is influenced by the combined effects of these physical processes. As observed in the case of Chl-a and AOD, the seasonal cycle is predominant in AS than the annual cycle in SST and WS. Some of the previous studies also suggest atmospheric deposition as a reason for increasing phytoplankton biomass along the eastern coast of India during the winter monsoon (e.g., Yadav et al., 2016) and it could be one of the factors for increasing Chl-a and NPP in BoB in recent years, such as 2018 and 2019.

Statistical Analysis on Interannual Variability of NPP

In addition to the analysis using the concentric box regions, we have also used a box plot to depict the interannual variability of Chl-a, NPP, SST, and WS. We have considered four regions (AS1, AS2, BB1, and BB2) based on positive/negative spatial trends of NPP (**Figure 3**) in AS and BoB, respectively, and these regions are marked in **Figure 3**.

The box plots and annual mean (black line) of AS1 and BB1 along with 95 % confidence intervals of basin average (AS and BoB) are presented in **Figure 4**. The year-wise distribution is represented using different boxes with the median in the middle, and whiskers of the corresponding boxes represent the maximum and minimum excluding outliers. The analyses reveal the overall decrease in NPP and Chl-a. The large dispersions are exhibited more over AS (larger box regions) than that in BoB (smaller box regions). From 2003 to 2014, the median values decreased and reached up to 0.25 mg/m^3 in 2014. The median value increased in 2015 and is about 0.5 mg/m^3, and further decreases until 2019. NPP exhibits a similar pattern as for Chl-a. The median values are below 750 mg/C/m^2/day in AS1 and below 500 mg/C/m^2/day in BB1. Nevertheless, it is shown that the long-term trends in both basins show a decrease in Chl-a and NPP. The Chl-a are generally positively skewed (mean values greater than median) although they exhibit noticeable variability in distribution in AS1. They are positively skewed in 2003 and 2004, and remain symmetric (equal distribution) up to 2008. Furthermore, they are positively skewed up to 2016 and negatively skewed (mean less than median) in 2017, but are again positively skewed in 2018 and 2019. Similar distribution is depicted in the case of NPP. The Chl-a and NPP values are much smaller in BB1 although it exhibits an upward skewness. The distribution of SST exhibits negative skewness in

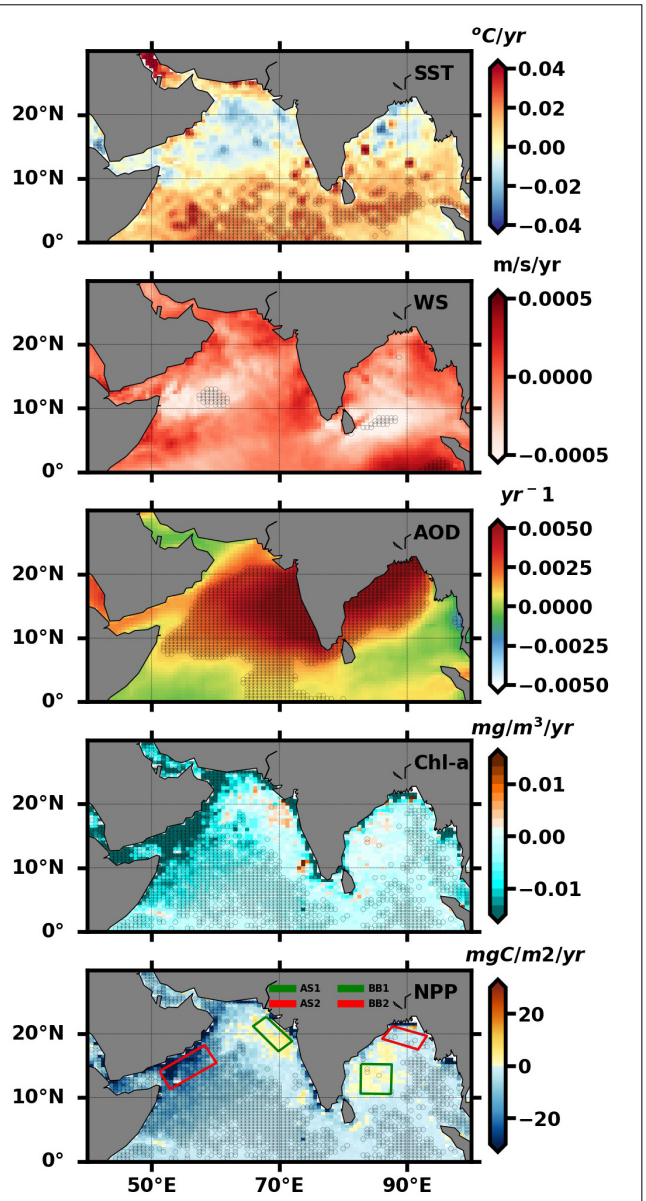

FIGURE 3 | Trends in Sea Surface Temperature (SST), wind stress (WS), Aerosol Optical Depth (AOD), Chlorophyll-a (Chl-a), and Net Primary Productivity (NPP) as computed from the data from 2003 to 2019 in NIO. The boxes AS1, AS2, BB1, and BB2 are represented here.

AS1 and BB1. The variability of WS is prominent in BB1 and is positively skewed in AS1 and BB1. There are outliers in WS that indicate tendency toward maximum extremes, as shown in AS1 and BB1. AOD also exhibits positive skewness with outliers tending toward maximum extremes.

The distribution of Chl-a, SST, WS, AOD, and NPP in AS2 and BB2 are shown in **Supplementary Figure 7**. The Chl-a, NPP, WS, AOD, and SST exhibit upward skewness in AS2. The SST depicts a downward skewness in BB2, whereas Chl-a, AOD, WS and NPP show small variability in BB1. Both basins show comparable changing patterns of the previously mentioned variables. The annual mean of Chl- a shows a similar pattern until 2007 where there is a sudden decline in 2007, but increases in 2008. There was an abrupt decline with very small Chl-a (0.25 mg/m^3) values in 2014, but increased thereafter. The NPP distribution also reveals decline as observed in Chl-a. The mean Chl-a and NPP values in AS1 are about 0.38 mg/m^3 and 564.4 mg/C/m^2/day in AS1. The dip observed in 2007 is complemented with a rise in SST with respect to 2006. There was a drop in SST in 2008. The abrupt drop in SST was observed in 2012 and it further increased in 2015. The mean SST in AS1 is about 27.94°C and about 28.91°C in BB1. WS shows very small changes when compared to other variables. The mean AOD concentrations in AS1 and BB1 are about 0.35 and 0.26, respectively.

We have calculated the correlation of Chl-a with respect to SST, NPP, and WS. The correlation and lag/lead between the variables are estimated at 95 % confidence level. The phase relationships between the variables can help identify the underlying causes (Shafeeque et al., 2017) and therefore, we have used the phase relationships to find the correlation between the variables. The Chl-a is positively correlated with WS and NPP with correlations of 0.90 and 0.98 in AS1 and 0.66 and 0.97 in BB1. The Chl-a is negatively correlated with AOD and SST with correlations −0.66 and −0.83 in AS1 and −0.69 and −0.75 in BB1. All the correlations are statistically significant. The correlation values along with lag/lead information are presented in **Supplementary Table 3**.

Impact of COVID-19 Lockdown on NPP

The worldwide spread of contagious disease caused by SARS-CoV-2 compelled governments to declare countrywide lockdown. The immediate consequence of the lockdown was that there were considerable changes in the anthropogenic inputs to the atmosphere (Kumar, 2020; Singh and Chauhan, 2020). Although there are studies on the impact of lockdown on atmospheric pollution and air quality, no study is performed yet to examine the impact of lockdown on oceanic processes. To understand the impact of lockdown on the oceanic Chl-a and NPP, we analyzed the data for three periods: pre-lockdown, lockdown, and post-lockdown. **Figure 5A** shows the variability of SST overlaid with 10 m surface wind vectors for these periods and the corresponding anomaly (**Figure 5B**) for the year 2020 from the 17-year climatology (2003–2019). The analysis shows a warming (positive anomaly) in the lockdown period throughout the northern BoB and AS, although no significant change is observed in the southern BoB and AS. This might be probably due to the increased oceanic heat content in the northern AS and BoB (Gnanaseelan et al., 2017; Cheng et al., 2021). It is challenging to hold lockdown responsible for this warming as the ocean responds a little later than the atmosphere and it is already known that NIO is warming at alarming rates. In spite of lockdown and lower emissions due to COVID-19, the upper ocean warms up to 2,000 m (Cheng et al., 2021), making 2020 one of the hottest years. However, the SST anomaly over the lockdown period reveals a warming episode over the northern regions of AS and BoB, while the wind anomalies do not show any significant change over the period.

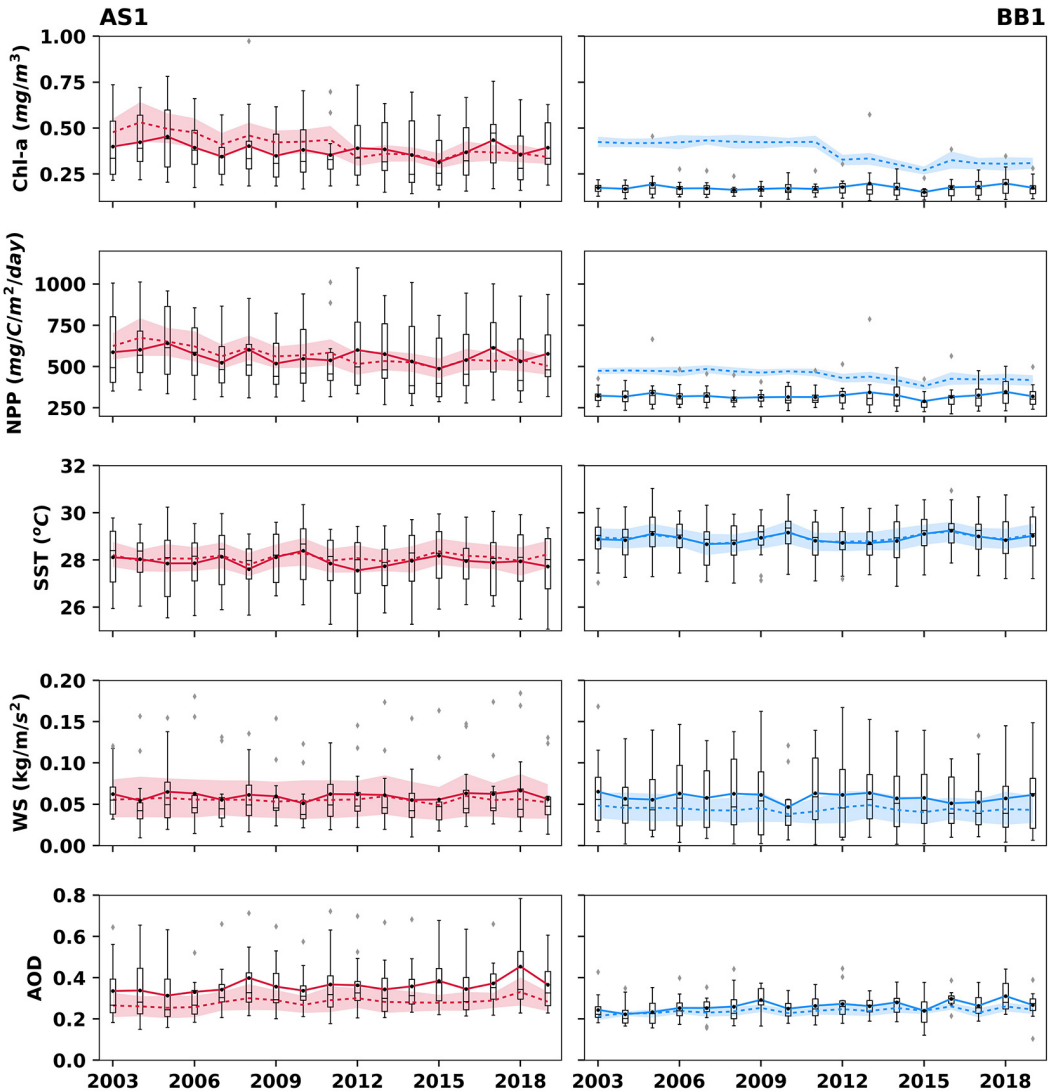

FIGURE 4 | Box analysis of Chlorophyll-a (Chl-a), Net Primary Productivity (NPP), Sea Surface Temperature (SST), Wind Stress (WS) and Aerosol Optical Depth (AOD) over AS1 and BB1 (see text for details). The Red and Blue solid lines are the yearly box averages. The dotted lines represent the basin averages and the shaded regions show the standard error at 95% confidence interval.

Most Indian states and metropolitan cities exhibited negative AOD anomalies during the lockdown period compared to the pre-lockdown period as reported in Singh and Chauhan (2020), and the reasons might be restrictions in movement, lesser emissions due to shutdown/limited working of industries and reduction in human activities due to complete shutdown leading to lesser concentration of aerosols. Our analysis (**Figures 5C,D**) also shows a higher AOD in the pre-lockdown period, further dips in the lockdown period. There are negative anomalies of AOD during the lockdown period. During the post-lockdown period, the anomalies are positive. The effect of aerosols is such that it helps in backscattering which leads to cooling in the atmosphere whereas strong aerosols absorb radiation which facilitates warming. The reduction of aerosols in turn leading to reduction of backscattering might be the reason for warming during the lockdown period. **Figures 5E,F** represent the Chl-a for the periods and the corresponding anomaly. During the lockdown period, a positive anomaly was observed in the eastern AS. The anomaly was negative in the western and northern AS, which coincides with the warming there. The BoB does not exhibit any significant changes in the Chl-a. The statistical significance of anomalies is calculated using the student *t*-test. The significance of anomalies is provided in **Supplementary Table 4**.

To ensure that the changes are related to or can be related to impacts of COVID-19 lockdown, we made a similar analysis for the year 2018 over the same dates such as pre-lockdown, lockdown, and post-lockdown and are shown in **Supplementary Figure 8**. The anomalous warming observed in 2020 is not replicated in 2018 in the lockdown period. However, AOD shows

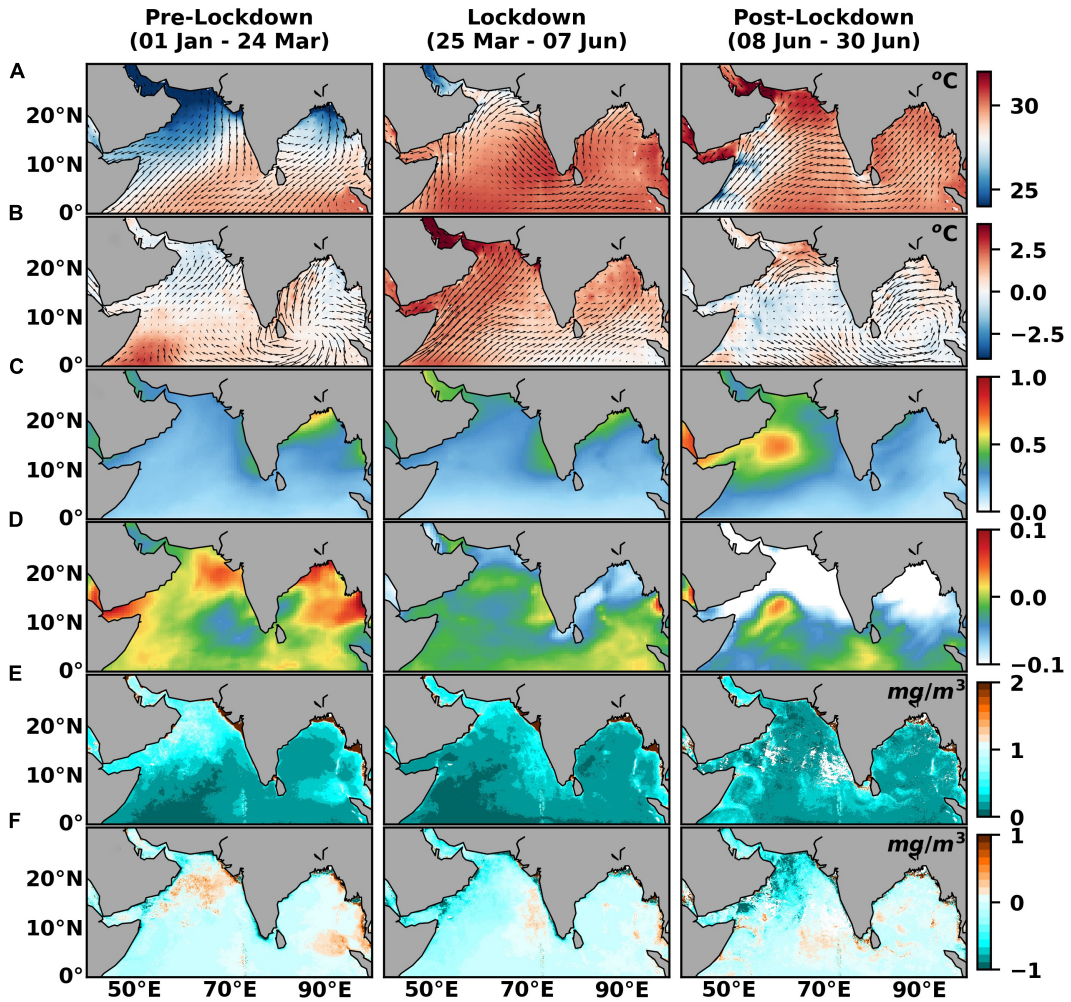

FIGURE 5 | The Sea Surface Temperature (SST), Aerosol Optical Depth (AOD) and Chlorophyll-a (Chl-a) for pre-lockdown, lockdown, and post-lockdown period and their anomalies from climatology (2003–2019) **(A)** SST, **(B)** SST anomaly, **(C)** AOD, **(D)** AOD anomaly, **(E)** Chl-a, and **(F)** Chl-a anomaly.

a positive anomaly in AS and BoB in contrast to the negative anomaly observed in 2020 in the lockdown period. Although it is difficult to confirm that these effects are only due to the lockdown, the negative anomaly of AOD in 2020 might be due to the reduced anthropogenic activities during the lockdown period. The Chl-a distribution does not show reasonable changes in comparison to 2020.

To make a comprehensive assessment, we look into the temporal variability of AOD, Chl-a, and NPP in 2020. To understand the difference more efficiently, we compared it with climatology (**Figure 6**). AOD values remain well below the climatology in all the three boxes in AS during the lockdown period in comparison to pre and post-lockdown periods. The seasonal peaks during MAM and JJAS in 2020 are below the climatology which could be attributed to the imposed lockdown. However, the Chl-a values do not exhibit much changes during the lockdown period and further increases in the post-lockdown period. The peaks are observed in August and September. The Chl-a is maximum during JJAS, and therefore, these changes may not be directly related to post-lockdown. AOD is higher in the post-lockdown period in Box 1 in BoB, whereas in Box 2 and Box 3, it is lower than the climatological mean.

The temporal analysis of NPP (**Figure 6**) shows that NPP is very small in the lockdown period in AS, whereas there is a sharp decline in NPP during the lockdown period in Boxes 2 and 3 in BoB. However, this decline was not observed for Chl-a (**Figure 6**). The NPP depends on PAR, SST and the length of the day, and might be one of these factors during the lockdown might have contributed to the smaller NPP in MAM. We have not analyzed each of these factors separately, instead we analyzed the available data to examine the impact of COVID-19 lockdown on NPP. We observe that SST is higher during the period when the NPP is smaller (**Supplementary Figure 9**).

Similarly, we also made the monthly analysis over the concentric boxes over the same period but for the year 2018, to examine whether the changes are associated with COVID-19 lockdown (**Supplementary Figure 10**). The peaks of AOD generally present in MAM and JJAS are less than the climatology

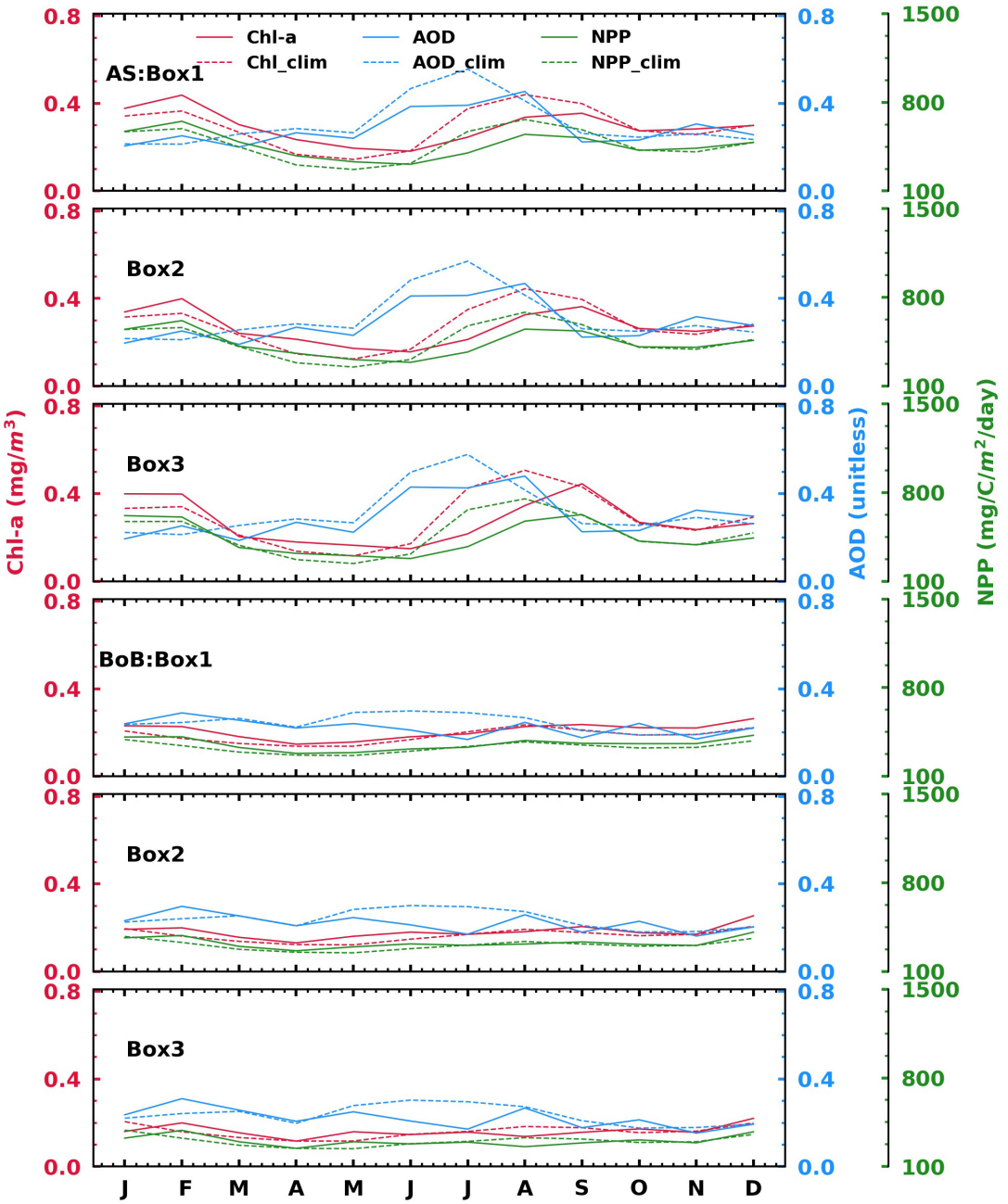

FIGURE 6 | The temporal variation of Aerosol Optical Depth (AOD), Chlorophyll-a (Chl-a), and Net Primary Productivity (NPP) for 2020.

in 2020, but it exceeds the climatology in 2018. Chl-a values are higher than climatology in 2018, whereas they are lesser than climatology in 2020. The negative anomaly of Chl-a and AOD with respect to the climatological mean, however, is not significant during the lockdown period. The analyses suggest that the lockdown can be one of the reasons for the lesser AOD and less Chl-a in both basins.

The monthly analysis of NPP and AOD in concentric boxes for the same period in 2018, is carried out to check whether these changes are associated with the lockdown. The results are presented in **Supplementary Figure 11**. It shows lower values of NPP than the climatology during the lockdown period of 2020, but the same feature was not observed in 2018 and they are higher than the climatology. This again indicates the impact of COVID-19 lockdown on the open ocean primary production. The increase in productivity in the monsoon months observed in 2018 is also not observed in 2020, which might also be connected to the COVID-19 lockdown.

CONCLUSION

We use satellite and reanalysis data for 17 years across all seasons to examine the interannual variability of NPP and the impact of lockdown on NPP. One of the major reasons for choosing OC-CCI Chl-a data is the improved coverage, particularly during the monsoon periods. The main aim of the study is the estimation of variability of primary productivity in NIO and examine them in the context of COVID-19 lockdown. We find that Chl-a has positive correlation with NPP and wind, but a negative correlation with SST with a time lag, consistent with known seasonal changes in winds and SST.

We analyze the response of NIO to the lockdown implemented in connection with COVID-19 pandemic. Our analysis suggests that AOD shows an increasing trend over AS and BoB, while Chl-a and NPP show a decreasing trend in AS, particularly in the southern AS where an increasing trend in SST is observed; implying the reduction in oceanic productivity with global ocean warming. In BoB, the central regions show an increasing trend of Chl-a and NPP, which is also evident in the interannual variability of Chl-a, AOD, and NPP. The seasonal cycle of all variables is more prominent in AS than that in BoB. Although Chl-a throughout AS shows higher values than that in BoB, there is a small increase in Chl-a over BoB compared to the previous years. Our study also shows an increase in AOD over both basins, and the increasing trend of NPP coincides with a decreasing trend in SST in the same region. The NPP is very small during the lockdown period in 2020, which is also complemented by an increase in SST during the lockdown period. AOD is relatively lower during the lockdown period, which may be due to the effect of lockdown. The decrease in AOD in the lockdown period in 2020 is not observed in 2018. Although it is difficult to confirm, the analyzed results suggest that the changes in AOD, SST and NPP in 2020 are very likely due to the lockdown. Analyses of ship or onboard measurements may strengthen our conclusions, yet the initial analyses do exhibit changes related to lockdown such as the increase in aerosols, and SST, and thus reduction in NPP. Henceforth, our analyses provide new insights into the impact of the changes in atmospheric input on the oceanic primary productivity.

DATA AVAILABILITY STATEMENT

The original contributions presented in the study are included in the article/**Supplementary Material**, further inquiries can be directed to the corresponding author.

AUTHOR CONTRIBUTIONS

JK conceived the idea and supervised the research. NS did the analyses and drew the figures. JK and NS wrote the first draft which was subsequently modified by inputs from JK, RP, KC, and AC. All authors contributed to the article and approved the submitted version.

ACKNOWLEDGMENTS

The authors would like to thank Head CORAL, the Director of Indian Institute of Technology Kharagpur (IIT Kgp), Sponsored Research and Industrial Consultancy of IIT Kgp, and Indian National Centre for Ocean Information Services, Ministry of Earth Sciences, Hyderabad (INCOIS, O-MASCOT project). The authors would also like to thank Ocean Color Climate Change Initiative (OC-CCI) for providing us with the daily chlorophyll-a data, NASA Ocean Color and European Centre for Medium-Range Weather Forecast (ECMWF) for the various data sets used in this study. This is INCOIS contribution number 431.

SUPPLEMENTARY MATERIAL

The Supplementary Material for this article can be found online at: https://www.frontiersin.org/articles/10.3389/fmars.2021.669415/full#supplementary-material

REFERENCES

Anderson, D. M., and Prell, W. L. (1992). The structure of the southwest monsoon winds over the Arabian Sea during the late Quaternary: observations, simulations, and marine geologic evidence. *J. Geophys. Res. Ocean* 97, 15481–15487. doi: 10.1029/92jc01428

Anderson, D. M., Brock, J. C., and Prell, W. L. (1992). Physical upwelling processes, upper ocean environment and the sediment record of the southwest monsoon. *Geol. Soc. London Spec. Publ.* 64, 121–129. doi: 10.1144/gsl.sp.1992.064.01.08

Banerjee, P., and Prasanna Kumar, S. (2014). Dust-induced episodic phytoplankton blooms in the Arabian Sea during winter monsoon. *J. Geophys. Res. Ocean* 119, 7123–7138. doi: 10.1002/2014jc010304

Beaufort, L., Lancelot, Y., Camberlin, P., Cayre, O., Vincent, E., Bassinot, F., et al. (1997). Insolation cycles as a major control of equatorial Indian Ocean primary production. *Science* 278, 1451–1454. doi: 10.1126/science.278.5342.1451

Behrenfeld, M. J., and Falkowski, P. G. (1997). Photosynthetic rates derived from satellite-based chlorophyll concentration. *Limnol. Oceanogr.* 42, 1–20. doi: 10.4319/lo.1997.42.1.0001

Caley, T., Malaizé, B., Zaragosi, S., Rossignol, L., Bourget, J., Eynaud, F., et al. (2011). New Arabian Sea records help decipher orbital timing of Indo-Asian monsoon. *Earth Planet. Sci. Lett.* 308, 433–444. doi: 10.1016/j.epsl.2011.06.019

Chakraborty, K., Lotliker, A. A., Gupta, G. V. M., Narayanan Nampoothiri, S. V., Paul, A., Ghosh, J., et al. (2020). Assessment of an ocean-ecosystem model in simulating the Indian coastal marine ecosystem dynamics. *J. Oper. Oceanogr* 2020, 1–19. doi: 10.1080/1755876x.2020.1843298

Chakraborty, K., Valsala, V., Gupta, G. V. M., and Sarma, V. (2018). Dominant biological control over upwelling on pCO2 in sea east of Sri Lanka. *J. Geophys. Res. Biogeosci.* 123, 3250–3261. doi: 10.1029/2018jg004446

Chavez, F. P., Messié, M., and Pennington, J. T. (2011). Marine Primary Production in Relation to Climate Variability and Change. *Ann. Rev. Mar. Sci.* 3, 227–260. doi: 10.1146/annurev.marine.010908.163917

Cheng, L., Abraham, J., Trenberth, K. E., Fasullo, J., Boyer, T., Locarnini, R., et al. (2021). Upper ocean temperatures hit record high in 2020. *Adv. Atmos. Sci.* 38, 523–530. doi: 10.1007/s00376-021-0447-x

Chowdary, J. S., Parekh, A., Ojha, S., and Gnanaseelan, C. (2015). Role of upper ocean processes in the seasonal SST evolution over tropical Indian Ocean in

climate forecasting system. *Clim. Dyn.* 45, 2387–2405. doi: 10.1007/s00382-015-2478-4

Cropp, R. A., Gabric, A. J., McTainsh, G. H., Braddock, R. D., and Tindale, N. (2005). Coupling between ocean biota and atmospheric aerosols: dust, dimethylsulphide, or artifact?. *Global Biogeochem. Cycles* 19:GB4002.

Fathrio, I., Iizuka, S., Manda, A., Kodama, Y.-M., Ishida, S., Moteki, Q., et al. (2017). Assessment of western Indian Ocean SST bias of CMIP5 models. *J. Geophys. Res. Ocean* 122, 3123–3140. doi: 10.1002/2016jc012443

Field, C. B., Behrenfeld, M. J., Randerson, J. T., and Falkowski, P. (1998). Primary production of the biosphere: integrating terrestrial and oceanic components. *Science* 281, 237–240. doi: 10.1126/science.281.5374.237

Findlater, J. (1969). A major low-level air current near the Indian Ocean during the northern summer. *Q. J. R. Meteorol. Soc.* 95, 362–380. doi: 10.1002/qj.49709540409

Gallisai, R., Peters, F., Volpe, G., Basart, S., and Baldasano, J. M. (2014). Saharan dust deposition may affect phytoplankton growth in the Mediterranean Sea at ecological time scales. *PLoS One* 9:e110762. doi: 10.1371/journal.pone.0110762

GCOS (2011). Systematic Observation Requirements from Satellite-Based Data Products for Climate 2011 Update. Supplemental Details to the Satellite-Based Component of the "Implementation Plan for the Global Observing System for Climate in Support of the UNFCCC. *GCOS Rep.* 154, 138.

Global Modeling and Assimilation Office (GMAO) (2015). *MERRA-2 instM_2d_gas_Nx: 2d,Monthly mean,Instantaneous,Single-Level,Assimilation,Aerosol Optical Depth Analysis V5.12.4*. Greenbelt: Goddard Earth Sciences Data and Information Services Center.

Gnanaseelan, C., Roxy, M. K., and Deshpande, A. (2017). "Variability and trends of sea surface temperature and circulation in the Indian Ocean," in *Observed climate variability and change over the Indian Region*, eds M. Rajeevan and S. Nayak (Singapore: Springer), 165–179. doi: 10.1007/978-981-10-2531-0_10

Goddard Space Flight Center (NASA), Ocean Ecology Laboratory, Ocean Biology Processing Group, and Moderate-resolution Imaging Spectroradiometer (MODIS). (2018). *Aqua Photosynthetically Available Radiation Data; 2018 Reprocessing*. Greenbelt: NASA Goddard Space Flight Center, doi: 10.5067/AQUA/MODIS/L3M/PAR/2018 Accessed on 06/25/2021. .

Goes, J. I., Thoppil, P. G., do, R., Gomes, H., and Fasullo, J. T. (2005). Warming of the Eurasian landmass is making the Arabian Sea more productive. *Science* 308, 545–547. doi: 10.1126/science.1106610

Gower, J. F. R., Doerffer, R., and Borstad, G. A. (1999). Interpretation of the 685 nm peak in water-leaving radiance spectra in terms of fluorescence, absorption and scattering, and its observation by MERIS. *Int. J. Remote Sens.* 20, 1771–1786. doi: 10.1080/014311699212470

Gregg, W. W., Casey, N. W., and McClain, C. R. (2005). Recent trends in global ocean chlorophyll. *Geophys. Res. Lett.* 32:L03606.

Hersbach, H., Bell, B., Berrisford, P., Hirahara, S., Horányi, A., Muñoz-Sabater, J., et al. (2020). The ERA5 global reanalysis. *Q. J. R. Meteorol. Soc.* 146, 1999–2049.

Hossain, M. S., Sarker, S., Sharifuzzaman, S. M., and Chowdhury, S. R. (2020). Primary productivity connects hilsa fishery in the Bay of Bengal. *Sci. Rep.* 10:5659.

Howarth, R. W. (1988). Nutrient limitation of net primary production in marine ecosystems. *Annu. Rev. Ecol. Syst.* 19, 89–110. doi: 10.1146/annurev.es.19.110188.000513

Hu, C., Muller-Karger, F. E., Taylor, C. J., Carder, K. L., Kelble, C., Johns, E., et al. (2005). Red tide detection and tracing using MODIS fluorescence data: a regional example in SW Florida coastal waters. *Remote Sens. Environ.* 97, 311–321. doi: 10.1016/j.rse.2005.05.013

IPCC (2018). " Global Warming of 1.5°C. An IPCC Special Report on the impacts of global warming of 1.5 C above pre-industrial levels and related global greenhouse gas emission pathways," in *The Context of Strengthening the Global Response to the Threat of Climate Change, Sustainable Development, and Efforts to Eradicate Poverty*, eds V. Masson-Delmotte, P. Zhai, H.-O. Portner, D. Roberts, and J. Skea (Geneva: World Meteorological Organization), 32.

Jickells, T. D., An, Z. S., Andersen, K. K., Baker, A. R., Bergametti, C., Brooks, N., et al. (2005). Global iron connections between desert dust, ocean biogeochemistry, and climate. *Science* 308, 67–71. doi: 10.1126/science.1105959

Jordi, A., Basterretxea, G., Tovar-Sánchez, A., Alastuey, A., and Querol, X. (2012). Copper aerosols inhibit phytoplankton growth in the Mediterranean Sea. *Proc. Natl. Acad. Sci. U. S. A.* 109, 21246–21249. doi: 10.1073/pnas.1207567110

Joseph, P. V., Sooraj, K. P., and Rajan, C. K. (2006). The summer monsoon onset process over South Asia and an objective method for the date of monsoon onset over Kerala. *Int. J. Climatol.* 26, 1871–1893. doi: 10.1002/joc.1340

Käse, L., and Geuer, J. K. (2018). "Phytoplankton responses to marine climate change–an introduction," in *YOUMARES 8–Oceans Across Boundaries: Learning from each other*, eds S. Jungblut, V. Liebich, and M. Bode (Cham: Springer), 55–71. doi: 10.1007/978-3-319-93284-2_5

Keen, T. R., Kindle, J. C., and Young, D. K. (1997). The interaction of southwest monsoon upwelling, advection and primary production in the northwest Arabian Sea. *J. Mar. Syst.* 13, 61–82. doi: 10.1016/s0924-7963(97)00003-1

Kumar, M. D., Naqvi, S. W. A., Jayakumar, D. A., George, M. D., Narvekar, P. V., and de Sousa, S. N. (1995). Carbon dioxide and nitrous oxide in the North Indian Ocean. *Curr. Sci.* 69, 672–678.

Kumar, S. (2020). Effect of meteorological parameters on spread of COVID-19 in India and air quality during lockdown. *Sci. Total Environ.* 745:141021. doi: 10.1016/j.scitotenv.2020.141021

Kumar, S., Ramesh, R., Sardesai, S., and Sheshshayee, M. S. (2004). High new production in the Bay of Bengal: possible causes and implications. *Geophys. Res. Lett.* 31:L18304.

Kuttippurath, J., Murasingh, S., Stott, P. A., Sarojini, B. B., Jha, M. K., Kumar, P., et al. (2021a). Observed rainfall changes in the past century (1901–2019) over the wettest place on Earth. *Environ. Res. Lett.* 16:24018.

Kuttippurath, J., Sunanda, N., Martin, M. V., and Chakraborty, K. (2021b). Tropical storms trigger phytoplankton blooms in the deserts of north Indian Ocean. npj Clim. *Atmos. Sci.* 4:11. doi: 10.1038/s41612-021-00166-x

Kuttippurath, J., and Raj, S. (2021). Two decades of aerosol observations by AATSR, MISR, MODIS and MERRA-2 over India and Indian Ocean. *Remote Sens. Environ.* 257:112363. doi: 10.1016/j.rse.2021.112363

Le Mézo, P., Beaufort, L., Bopp, L., Braconnot, P., and Kageyama, M. (2017). From monsoon to marine productivity in the Arabian Sea: insights from glacial and interglacial climates. *Clim. Past* 13, 759–778. doi: 10.5194/cp-13-759-2017

Lee, C. M., Jones, B. H., Brink, K. H., and Fischer, A. S. (2000). The upper-ocean response to monsoonal forcing in the Arabian Sea: seasonal and spatial variability. *Deep Sea Res. II Top. Stud. Oceanogr.* 47, 1177–1226. doi: 10.1016/s0967-0645(99)00141-1

Levitus, S., Antonov, J. I., Boyer, T. P., and Stephens, C. (2000). Warming of the world ocean. *Science* 287, 2225–2229. doi: 10.1126/science.287.5461.2225

Li, F., and Ramanathan, V. (2002). Winter to summer monsoon variation of aerosol optical depth over the tropical Indian Ocean. *J. Geophys. Res. Atmos.* 107, AAC2–1–AAC2–13.

Madhupratap, M., Kumar, S. P., Bhattathiri, P. M. A., Kumar, M. D., Raghukumar, S., Nair, K. K. C., et al. (1996). Mechanism of the biological response to winter cooling in the northeastern Arabian Sea. *Nature* 384, 549–552. doi: 10.1038/384549a0

Mahowald, N. M., Scanza, R., Brahney, J., Goodale, C. L., Hess, P. G., Moore, J. K., et al. (2017). Aerosol deposition impacts on land and ocean carbon cycles. *Curr. Clim. ChangE. Rep.* 3, 16–31. doi: 10.1007/s40641-017-0056-z

Mallet, M., Chami, M., Gentili, B., Sempéré, R., and Dubuisson, P. (2009). Impact of sea-surface dust radiative forcing on the oceanic primary production: a 1D modeling approach applied to the West African coastal waters. *Geophys. Res. Lett.* 36:L15828.

Martin, J. H., Coale, K. H., Johnson, K. S., Fitzwater, S. E., Gordon, R. M., Tanner, S. J., et al. (1994). Testing the iron hypothesis in ecosystems of the equatorial Pacific Ocean. *Nature* 371, 123–129.

McCreary, J. P., Murtugudde, R., Vialard, J., Vinayachandran, P. N., Wiggert, J. D., Hood, R. R., et al. (2009). Biophysical processes in the Indian Ocean. *Indian Ocean Biogeochem. Process. Ecol. Var.* 185, 9–32. doi: 10.1029/2008gm000768

Moore, C. M., Mills, M. M., Arrigo, K. R., Berman-Frank, I., Bopp, L., Boyd, P. W., et al. (2013). Processes and patterns of oceanic nutrient limitation. *Nat. Geosci.* 6, 701–710.

Moorthy, K. K., Babu, S. S., and Satheesh, S. K. (2003). Aerosol spectral optical depths over the Bay of Bengal: role of transport. *Geophys. Res. Lett.* 30:1249.

Murtugudde, R., and Busalacchi, A. J. (1999). Interannual variability of the dynamics and thermodynamics of the tropical Indian Ocean. *J. Clim.* 12, 2300–2326. doi: 10.1175/1520-0442(1999)012<2300:ivotda>2.0.co;2

Patra, P. K., Behera, S. K., Herman, J. R., Maksyutov, S., Akimoto, H., and Yamagata, T. (2005). The Indian summer monsoon rainfall: interplay of coupled dynamics,

radiation and cloud microphysics. *Atmos. Chem. Phys*. 5, 2181–2188. doi: 10.5194/acp-5-2181-2005

Patra, P. K., Kumar, M. D., Mahowald, N., and Sarma, V. (2007). Atmospheric deposition and surface stratification as controls of contrasting chlorophyll abundance in the North Indian Ocean. *J. Geophys. Res. Ocean* 112:C05029.

Paytan, A., Mackey, K. R. M., Chen, Y., Lima, I. D., Doney, S. C., Mahowald, N., et al. (2009). Toxicity of atmospheric aerosols on marine phytoplankton. *Proc. Natl. Acad. Sci. U. S. A*. 106, 4601–4605. doi: 10.1073/pnas.0811486106

Prakash, P., Prakash, S., Rahaman, H., Ravichandran, M., and Nayak, S. (2012). Is the trend in chlorophyll-a in the Arabian Sea decreasing?. *Geophys. Res. Lett.* 39:L23605.

Prasanna Kumar, S., Muraleedharan, P. M., Prasad, T. G., Gauns, M., Ramaiah, N., De Souza, S. N., et al. (2002). Why is the Bay of Bengal less productive during summer monsoon compared to the Arabian Sea?. *Geophys. Res. Lett.* 29, 88–81. doi: 10.1029/2002GL016013

Prasanna Kumar, S., Ramaiah, N., Gauns, M., Sarma, V., Muraleedharan, P. M., Raghukumar, S., et al. (2001). Physical forcing of biological productivity in the Northern Arabian Sea during the Northeast Monsoon. *Deep Sea Res. II Top. Stud. Oceanogr.* 48, 1115–1126. doi: 10.1016/s0967-0645(00)00133-8

Prasanna Kumar, S., Roshin, R. P., Narvekar, J., Kumar, D., and Vivekanandan, E. (2010). What drives the increased phytoplankton biomass in the Arabian Sea?. *Curr. Sci.* 99, 101–106.

Prospero, J. M., Ginoux, P., Torres, O., Nicholson, S. E., and Gill, T. E. (2002). Environmental characterization of global sources of atmospheric soil dust identified with the Nimbus 7 Total Ozone Mapping Spectrometer (TOMS) absorbing aerosol product. *Rev. Geophys.* 40, 1–31.

Rahaman, H., Srinivasu, U., Panickal, S., Durgadoo, J. V., Griffies, S. M., Ravichandran, M., et al. (2020). An assessment of the Indian Ocean mean state and seasonal cycle in a suite of interannual CORE-II simulations. *Ocean Model.* 145:101503. doi: 10.1016/j.ocemod.2019.101503

Ramachandran, S., and Jayaraman, A. (2002). Premonsoon aerosol mass loadings and size distributions over the Arabian Sea and the tropical Indian Ocean. *J. Geophys. Res. Atmos.* 107, AAC 1–1-AAC 1–21.

Ramanathan, V., Crutzen, P. J., Lelieveld, J., Mitra, A. P., Althausen, D., Anderson, J., et al. (2001). Indian Ocean Experiment: an integrated analysis of the climate forcing and effects of the great Indo-Asian haze. *J. Geophys. Res. Atmos.* 106, 28371–28398. doi: 10.1029/2001JD900133

Roxy, M. K., Ritika, K., Terray, P., Murtugudde, R., Ashok, K., and Goswami, B. N. (2015). Drying of Indian subcontinent by rapid Indian Ocean warming and a weakening land-sea thermal gradient. *Nat. Commun.* 6:7423.

Satheesh, S. K., Moorthy, K. K., Kaufman, Y. J., and Takemura, T. (2006). Aerosol optical depth, physical properties and radiative forcing over the Arabian Sea. *Meteorol. Atmos. Phys.* 91, 45–62. doi: 10.1007/s00703-004-0097-4

Sathyendranath, S., Jackson, T., Brockmann, C., Brotas, V., Calton, B., Chuprin, A., et al. (2020). *Global Chlorophyll-a Data Product s Gridded on a Sinusoidal Projection, Version 4.2*. Chilton: Centre for Environmental Data Analysis.

Schott, F. A., Xie, S.-P., and McCreary, J. P. Jr. (2009). Indian Ocean circulation and climate variability. *Rev. Geophys.* 47:RG1002.

Shafeeque, M., Sathyendranath, S., George, G., Balchand, A. N., and Platt, T. (2017). Comparison of seasonal cycles of phytoplankton chlorophyll, aerosols, winds and sea-surface temperature off Somalia. *Front. Mar. Sci.* 4:386. doi: 10.3389/fmars.2017.00386

Shenoi, S. S. C., Shankar, D., and Shetye, S. R. (2002). Differences in heat budgets of the near-surface Arabian Sea and Bay of Bengal: implications for the summer monsoon. *J. Geophys. Res. Ocean* 107, 1–5.

Singh, R. P., and Chauhan, A. (2020). Impact of lockdown on air quality in India during COVID-19 pandemic. *Air Qual. Atmos. Health* 13, 921–928. doi: 10.1007/s11869-020-00863-1

Subramanian, V. (1993). Sediment load of Indian rivers. *Curr. Sci.* 64, 928–930.

Vinayachandran, P. N., and Shetye, S. R. (1991). The warm pool in the Indian Ocean. *Proc. Indian Acad. Sci. Planet. Sci.* 100, 165–175.

Vinayachandran, P. N., Chauhan, P., Mohan, M., Nayak, S. (2004). Biological response of the sea around Sri Lanka to summer monsoon. *Geophys. Res. Lett.* 31:L01302. doi: 10.1029/2003GL018533

Wang, M., Son, S., and Shi, W. (2009). Evaluation of MODIS SWIR and NIR-SWIR atmospheric correction algorithms using SeaBASS data. *Remote Sens. Environ.* 113, 635–644. doi: 10.1016/j.rse.2008.11.005

Webb, P. (2019). *Introduction to oceanography*. Bristol: Roger Williams University.

Webster, P. J., Magana, V. O., Palmer, T. N., Shukla, J., Tomas, R. A., Yanai, M. U., et al. (1998). Monsoons: processes, predictability, and the prospects for prediction. *J. Geophys. Res. Ocean* 103, 14451–14510. doi: 10.1029/97jc02719

Werdell, P. J., Franz, B. A., Bailey, S. W., Feldman, G. C., Boss, E., Brando, V. E., et al. (2013). Generalized ocean color inversion model for retrieving marine inherent optical properties. *Appl. Opt.* 52, 2019–2037. doi: 10.1364/ao.52.002019

Wielicki, B. A., Barkstrom, B. R., Baum, B. A., Charlock, T. P., Green, R. N., Kratz, D. P., et al. (1998). Clouds and the Earth's Radiant Energy System (CERES): algorithm overview. *IEEE Trans. Geosci. Remote Sens.* 36, 1127–1141.

Wiggert, J. D., Hood, R. R., Banse, K., and Kindle, J. C. (2005). Monsoon-driven biogeochemical processes in the Arabian Sea. *Prog. Oceanogr.* 65, 176–213. doi: 10.1016/j.pocean.2005.03.008

Yadav, K., Sarma, V., Rao, D. B., and Kumar, M. D. (2016). Influence of atmospheric dry deposition of inorganic nutrients on phytoplankton biomass in the coastal Bay of Bengal. *Mar. Chem.* 187, 25–34. doi: 10.1016/j.marchem.2016.10.004

Zhou, X., Duchamp-Alphonse, S., Kageyama, M., Bassinot, F., Beaufort, L., and Colin, C. (2020). "Primary productivity dynamics in the northeastern Bay of Bengal over the last 26,000 years," in *EGU General Assembly Conference Abstracts, 10253*. Munich: European Geosciences Union.

Conflict of Interest: The authors declare that the research was conducted in the absence of any commercial or financial relationships that could be construed as a potential conflict of interest.

Publisher's Note: All claims expressed in this article are solely those of the authors and do not necessarily represent those of their affiliated organizations, or those of the publisher, the editors and the reviewers. Any product that may be evaluated in this article, or claim that may be made by its manufacturer, is not guaranteed or endorsed by the publisher.

frontiers in Marine Science

ORIGINAL RESEARCH
published: 17 November 2021
doi: 10.3389/fmars.2021.718909

Sustenance of Indian Moored Buoy Network During COVID-19 Pandemic – A Saga of Perseverance

R. Venkatesan, K. Jossia Joseph, C. Anoopa Prasad, M. Kalyani, M. Arul Muthiah, S. Ramasundaram, P. Murugesh, K. Thirumurugan, R. Sundar, B. Kesavakumar, G. Vengatesan, K. Ramesh, M. V. Martin, K. N. Navaneeth, P. Senthilkumar, Biswajit Haldar, Abhishek Tandon, R. Sridharan, S. Sundar Jesuraj, C. Muthukumar, N. Sundaravadivelu and M. Saravanan*

Ocean Observation Systems, National Institute of Ocean Technology, Ministry of Earth Sciences, Government of India, Chennai, India

OPEN ACCESS

Edited by:
Stefano Vignudelli, National Research Council (CNR), Italy

Reviewed by:
Germo Väli, Tallinn University of Technology, Estonia
Rashmi Sharma, Indian Space Research Organization, India

***Correspondence:**
K. Jossia Joseph
jossia@gmail.com

Specialty section:
This article was submitted to Global Change and the Future Ocean, a section of the journal Frontiers in Marine Science

Received: *01 June 2021*
Accepted: *30 September 2021*
Published: *17 November 2021*

Citation:
Venkatesan R, Joseph KJ, Prasad CA, Kalyani M, Muthiah MA, Ramasundaram S, Murugesh P, Thirumurugan K, Sundar R, Kesavakumar B, Vengatesan G, Ramesh K, Martin MV, Navaneeth KN, Senthilkumar P, Haldar B, Tandon A, Sridharan R, Jesuraj SS, Muthukumar C, Sundaravadivelu N and Saravanan M (2021) Sustenance of Indian Moored Buoy Network During COVID-19 Pandemic – A Saga of Perseverance. Front. Mar. Sci. 8:718909. doi: 10.3389/fmars.2021.718909

The moored buoy network in the Indian Ocean revolutionized the observational programs with systematic time-series measurement of *in situ* data sets from remote marine locations. The real-time meteorological and oceanographic data sets significantly improved the weather forecast and warning services particularly during extreme events since its inception in 1997. The sustenance of the network requires persistent efforts to overcome the multitude of challenges such as vandalism, biofouling, rough weather, corrosion, ship time availability, and telemetry issues, among others. Besides these, the COVID-19 pandemic constrained the normal functioning of activities, mainly by delaying the maintenance of the network that resulted in losing a few expensive buoy system components and precious data sets. However, the improvements in the buoy system, in-house developed data acquisition system, and efforts in ensuring the quality of measurements together with "best practice methods" enabled 73% of the buoy network to be functional even when the cruises were reduced to 33% during the COVID-19 lockdown in 2020. The moored buoys equipped with an Indian buoy data acquisition system triggered high-frequency transmission during the Super cyclone Amphan in May 2020, which greatly helped the cyclone early warning services during the COVID-19 pandemic. The COVID-19 lockdown points toward the reliability and enhanced utility of moored buoy observations particularly when other modes of measurements are limited and necessitates more such platforms to better predict the weather systems. The present study analyzed the enhancement of the buoy program and improvisation of the buoy system that extended the life beyond the stipulated duration and enabled the high-frequency data transmission during cyclones amid the COVID-19 lockdown. The recommendations to better manage the remote platforms specifically in the event of a pandemic based on the operational experience of more than two decades were also presented.

Keywords: moored buoy, ocean observation, marine sensor, cyclone, COVID-19, North Indian Ocean

INTRODUCTION

The unprecedented spread of COVID-19 has taken the world by storm with significant socio-economic impact besides a large number of casualties and severe disruption of daily life. The Covid pandemic revealed that the world is ill-equipped to make real-time measurements of economic activity and its immediate consequences. The pandemic demonstrated the urgent need for improved data, models and analysis to understand and correct those deficiencies (Diffenbaugh et al., 2020). The immediate impact of the pandemic associated lockdown is also reported with some positive changes such as an abrupt 8.8% decrease in global CO_2 emissions in the first half of 2020 compared to the same period in 2019 (Liu et al., 2020), decrease in NO_2 in seven cities in India during the 2020 lockdown period (Vadrevu et al., 2020), and substantial reduction in pollutant concentrations in the industrial cities of Western India (Nigam et al., 2021). Similarly, the significant reduction in marine traffic (March et al., 2021) across the globe during the COVID-19 lockdown resulted in a substantial reduction in marine noise (Thomson and Barclay, 2020). The consequences of the COVID-19 situation are likely to persist for a longer duration with a significant impact on the socio-economic and scientific realm across the globe. Adapting to the COVID-19 situation necessitates better assessment, which is severely impaired by the inoperative measurement systems specifically the remote ocean platforms.

As the nations struggled to control the spread of the COVID-19 pandemic, the impact on the environment particularly the marine environment is less addressed. Perhaps one of those strongly affected by the pandemic are the ocean observation systems such as moored buoys, drifting buoys, Argo floats, and radars, to name a few. Even though these systems are robust and capable of operating autonomously for years, regular deployment and refurbishment are required for the upkeep of the resilient network (Heslop et al., 2020). Sustained ocean observations are necessary to meet the growing demand for weather and climate services whereas pandemic-associated slowdown in maintenance activities have adversely affected the data return (Viglione, 2020). The decline in the data flow can adversely affect the reliability of the weather forecast particularly during extreme events with potentially devastating consequences such as the propagation of the possible errors caused by the gap in the measurements. The survey conducted by the Global Ocean Observation System (GOOS) in April 2020 on the immediate impact of COVID-19 on ocean observations indicate a possible impact on 30–50% of the moorings, pausing a threat of losing the crucial data sets and even the equipment (Heslop et al., 2020). Prioritizing the maintenance activities under essential service is suggested considering the importance of ocean observations in weather services and long-term climate change.

The Indian Ocean plays a vital role in better understanding the global climate and is significantly inter-connected and impacted by the El-Niño and La-Niña phenomena. Two decades ago, the Indian Ocean was significantly under-sampled compared to other tropical oceans. The available information was mostly based on numerical models, ship-based observations, and few specific scientific experiments such as the International Indian Ocean Experiment (IIOE), Arabian Sea Monsoon Experiment (ARMEX), and Bay of Bengal Monsoon Experiment (BOBMEX), among others. The inception of the moored buoy program by the National Institute of Ocean Technology (NIOT) under the aegis of the Ministry of Earth Sciences (erstwhile Department of Ocean Development) in August 1997, earmarked a new era of systematic collection of meteorological and oceanographic parameters in the North Indian Ocean. This network is operational now, for more than two decades, transmitting uninterrupted meteorological and oceanographic observations in real-time at selected strategic locations despite innumerable challenges (Venkatesan et al., 2016). The long term moored buoy measurements of surface meteorological as well as subsurface oceanic parameters provided many new insights into the ocean dynamics of the North Indian Ocean such as the barrier layer dynamics in the Bay of Bengal (BoB), characteristics of warm pool in the Arabian Sea (AS), significant monsoon intraseasonal oscillations in BoB and complex air-sea flux exchange, to name a few. The predictive capability of cyclone track and intensity is significantly improved with the incorporation of the crucial upper ocean measurements such as temperature profile, salinity profile, and Tropical Cyclone Heat Potential (TCHP) in real-time during the passage of cyclones (Venkatesan et al., 2014, 2020; Navaneeth et al., 2019). The moored buoys captured the signals of more than 30 low-pressure systems and withstood the fury of intense cyclones such as Phailin in October 2013, Ockhi in December 2017, and Amphan in May 2020 showing the success of the engineering design as well as transmitted uninterrupted high-frequency data as per the rapid mode algorithm implemented by NIOT.

The maintenance activities and data services of the moored buoy network in the Indian Seas are also impacted by pandemic restrictions. However, the experience in maintaining the moored buoy network over two decades by overcoming various challenges helped to disseminate the critical real-time met-ocean observations amid the COVID-19 pandemic. The challenges faced in general and particularly during the lockdown in 2020 never deterred the program from providing its services to the end-users, particularly during extreme events. The present study detailed the evolution of moored buoy network, the impact of pandemic restrictions on data return, enhanced support during cyclones amid the COVID-19 lockdown during the year 2020, and the specific challenges during the pandemic. The recommendations for better maintenance of a remote platform based on the operational experience for more than two decades specifically during the pandemic were also presented.

ESTABLISHMENT AND ENHANCEMENT OF THE MOORED BUOY NETWORK IN THE INDIAN OCEAN

The "Indian moored buoy network," the first of its kind in the Indian Seas, was established with the primary objective of supporting the cyclone and tsunami early warning services in the North Indian Ocean. The present buoy network (**Figure 1**) includes 12 Ocean Moored buoy Network for the Northern Indian Ocean (OMNI) buoys with profile measurements (seven

in the BoB and five in the AS) in deep waters, four coastal buoys, three tsunami buoys (one in AS and two in BoB) and one CALibration and VALidation (CAL-VAL) buoy, which is specifically deployed for the validation of satellite data. In addition, Indian Arctic (IndARC) buoy has been maintained in Arctic region since July 2014.

Instrumentation

The moored buoy program was initiated with sensors to measure the meteorological and surface oceanographic parameters such as air temperature, relative humidity, wind, sea level pressure, wave, sea surface temperature, sea surface salinity, and surface current. Furthermore, additional sensors for measuring shortwave radiation, longwave radiation, precipitation, Conductivity-Temperature (CT) sensors at discrete depths (1, 5, 10, 15, 20, 30, 50, 75, 100, 200, and 500 m) for subsurface temperature and salinity measurements and Acoustic Doppler Current Profiler (ADCP) for subsurface current measurements up to 150 m were introduced to the existing buoys in 2010. The meteorological sensors are fitted on the mast at 3 m above the mean sea level as per the recommendations of the World Meteorological Organization (Jarraud, 2008) whereas the downward-looking ADCP is connected at 5 m depth in the mooring line. The measurements are carried out at specified intervals as suggested for data collection and dissemination by GOOS. The moored data buoys transmit data every 3 h, whereas the high-frequency internal data is made available after the retrieval of the mooring.

The selection of the communication method largely depends on how far the buoy is from shore and the data bandwidth required, though other factors such as timeliness, cost, and energy requirements also play a role (Venkatesan et al., 2013). The moored buoy close to shore utilizes both general packet radio service (GPRS) and satellite communication whereas the offshore platforms depend only on satellite communication. The communication with the buoy is a bi-directional link based on the Inmarsat-C satellite system, which also includes a global positioning system (GPS) receiver providing position information. The redundant position indicating facility incorporated using Argo satellite/Indian National Satellite (INSAT) telemetry helped in tracking the vandalized buoys during COVID-19 lockdown. The in-house developed coastal buoys, except sensors, with GPRS telemetry helped in extending

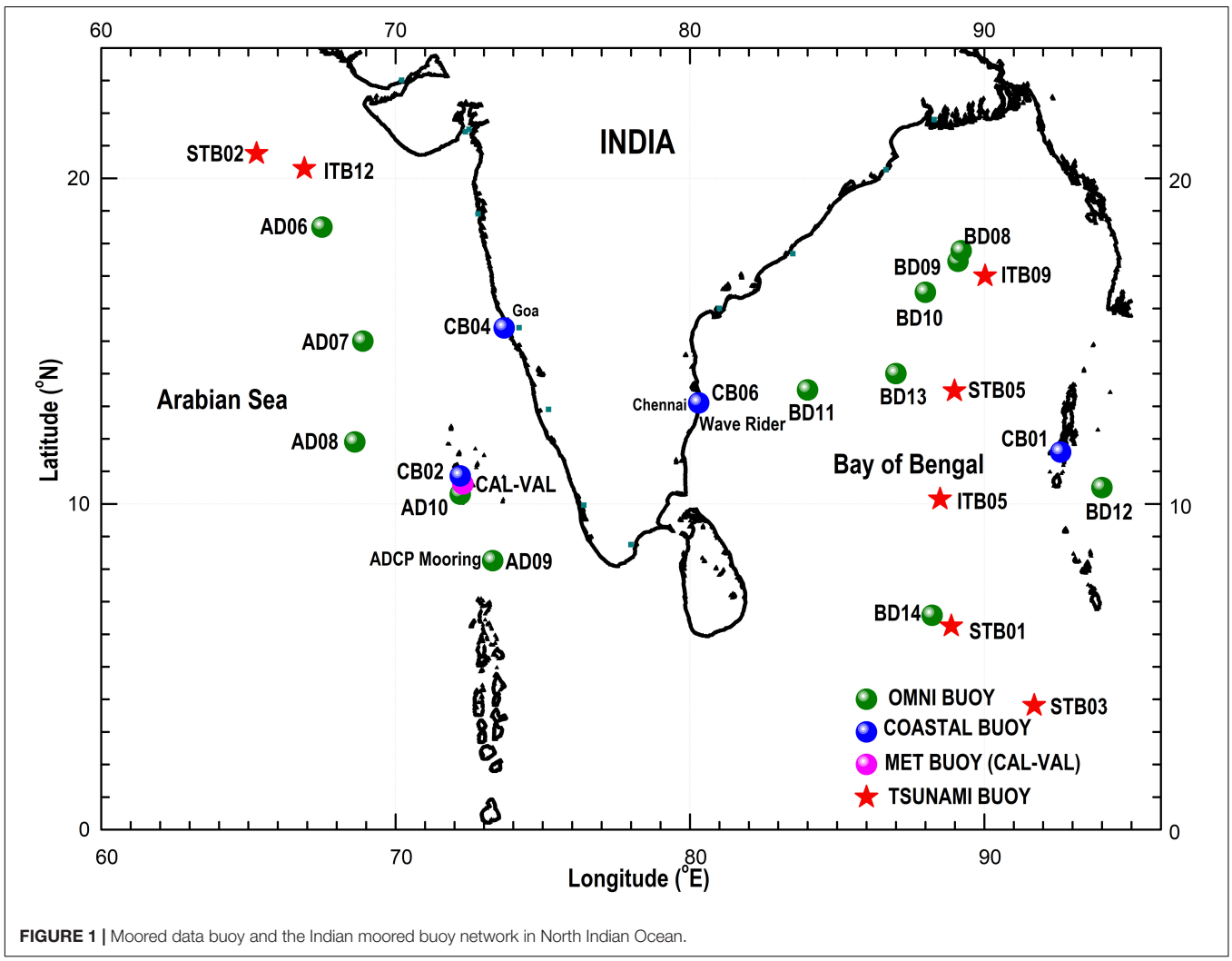

FIGURE 1 | Moored data buoy and the Indian moored buoy network in North Indian Ocean.

the period of operation, particularly during COVID-19 lockdown by significantly reducing energy consumption.

Regular calibration of sensors and data acquisition system (DAS) electronics are done at periodic intervals to ensure the quality of the data. In-house calibration facility for precipitation sensor, humidity sensor, DAS, and air pressure sensor helped in cost savings and delay in sending the sensor to original equipment manufacturer (OEM) for calibration. Apart from the efforts taken in ensuring the continuity of data, the quality of the data is ensured by comparing with other standard reference platform/systems.

Marine biofouling is a serious issue in tropical waters with hundreds of organisms that can get attached to the buoy system and mooring. Various methods of anti-fouling approaches are used in sub-surface oceanographic sensors including copper guard protection, protective sensor casing, and anti-fouling paints, to name a few (Venkatesan et al., 2017). Zinc oxide cream (Desitin) and silicone-based grease which were applied to the sensing parts of the ADCP were found to control the biological growth (Bigorre and Galbraith, 2018). The highest drift reported in the conductivity cell is reduced by installing the anti-fouling device impregnated with tributyltin oxide (TBTO) on each end of the conductivity cell in CT sensors (Sea-Bird Electronics, 2016). Efforts in reducing the biofouling along with the regular refurbishment and calibration of the sensors ensured sustained data collection, which was well paid off during the extended period of operation during the COVID-19 pandemic.

Moored Buoy Data Center

The moored buoy data center plays a vital role as a nerve center, hosting a suite of IT infrastructure facilities to receive, process, visualize, monitor, and manage the data from buoy networks around Indian Seas (**Figure 2A**). This facility is strategically important with round-the-clock support and acts as the nodal point for dissemination of real-time data to the Indian National Center for Ocean Information Services (INCOIS), Hyderabad who in turn work with the National Disaster Management Authorities for the promulgation of alerts and warnings to the countrymen. The data center established in 1997 has undergone significant improvements with customized tools to suit the requirement evolved over a period of more than two decades of operational experience. ADvanced Data REception and AnalysiS System (ADDRESS) is a customized software solution developed in-house for information sharing and process automation across organizational needs (**Figure 2B**). It facilitates the monitoring of data reception from remote ocean platforms and endurance of individual buoys systems such as buoy drift, sensor stoppage and is aimed at eliminating the practical difficulties in data visualization/analysis and maintaining inventory of equipment/items used in the buoy systems.

Advanced data reception and analysis system is incorporated with QC procedures for automatically assessing the quality of data received from buoys and presents data quality metrics to ensure the normal functioning of the sensors. The sensor malfunctioning, drift in measurements, sensor stoppage, transmission issues, and buoy drift, among others, are monitored regularly. ADDRESS also provides the deployment details along with the metadata that encompasses instrument descriptions, manufacturer details, calibration details, and detailed information on the suite of sensors attached to specific buoy systems, to name a few. The up-gradation of the data reception center in October 2018 with a suite of high-tech IT infrastructure facilities to meet the processing demands, growing storage requirements, and to enhance the data services greatly helped in the uninterrupted data reception and dissemination during the COVID-19 lockdown.

Optimized Mooring Design

The buoy system mooring in general is designed based on the depth of the deployment location, characteristics of the ocean current, wind, and wave during extreme storm events and fatigue cycles. The NIOT moored buoy system consists of a hull, instrument container, mast assembly, keel weight, and keel frame. The buoy hulls are discus shaped to have good wave following capability and also acts as a buoyancy module. A keel weight is attached at the bottom of the instrument container of the surface buoy to prevent the capsizing of the hull and a keel frame to install near-surface sensors. A water-tight instrument container made up of marine-grade aluminum alloy is used to position electronics and batteries. It is also facilitated with safety features like a vent valve for the ventilation of batteries

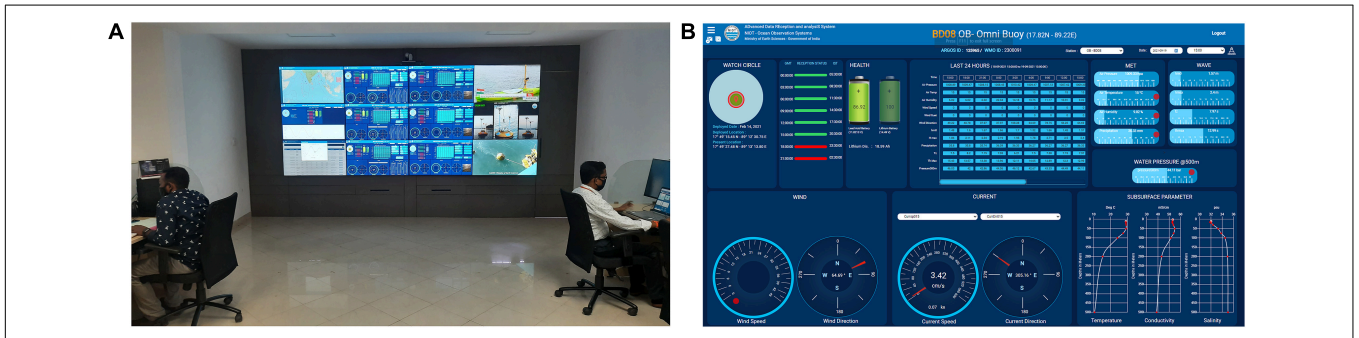

FIGURE 2 | (A) The data center being manned by limited manpower and enforcing social distancing during COVID-19 and **(B)** the dashboard of the in-house developed data management system ADDRESS.

and a pressure relief valve. The lid lock bolts are used to lock the lid over the instrument container and are designed with a central pin and a special key to dismantling the bolt as an anti-vandalism measure. The inverse catenary configuration with a mooring scope of 1.2 reduces the static as well as dynamic loading that helps to withstand the intense cyclones. Inductive cable is used in the top 500 m with CT/ Conductivity, Temperature, and Depth (CTD) sensors connected at selected depths through which data is transferred to facilitate real-time transmission. The preventive measures taken to safeguard the mooring from threats like vandalism, corrosion, biofouling, and fatigue were decisive in extending the operational period amid intense cyclones and COVID-19 lockdown.

Technology Developments

The development of the Indian DAS (IDAS) "Hrudaya" and the incorporation of an intelligent power management system (PMS) were the major developments that helped in sustaining the buoy network during the pandemic. Data acquisition, processing, storage, and transmission are the key functions of the DAS (Meindl, 1996). IDAS is meticulously designed in-house to work in marine conditions, activates the respective sensors at pre-determined intervals, and logs the received data. The raw data is processed, encrypted, and is sent through the satellite to the shore-based data reception center and stores high-frequency data (Venkatesan et al., 2018a). The reduced power processor with sleep mode provisions and multi-level watchdog timers protect the IDAS from software hang-ups and ensured higher endurance.

The development of controlled high-frequency transmission was initiated to support the weather and early warning services, particularly during cyclone passages. The algorithm incorporated in the IDAS in coastal and deep ocean buoys successfully triggered rapid mode in the vicinity of a low-pressure system and resumed normal mode after the passage of the cyclone. This enabled the real-time availability of critical met-ocean data set at higher frequency during the cyclone passages amid the COVID-19 lockdown.

The incorporation of a Hybrid charge controller has enabled NIOT buoy systems to work for a longer period of more than a year. The intelligent PMS controls the charging and discharging of the batteries, distributes the power to the connected loads, provides power system status information to the IDAS, and provides a constant voltage to the sensor irrespective of the changes in the battery voltage. The primary source of power is the lead-acid battery charged by the solar panel, and the secondary source is the primary lithium thionyl chloride battery (Linden and Thomas, 2002; Gordon and Deines, 2011). The initial power to the entire buoy system is supplied by the primary source. The PMS monitors and switches the buoy power to the secondary source when there is an outage of the primary source. The underwater sensors are self-powered with redundant power from the main power source of the buoy, which enhanced the endurance of the sensor operation.

The steady and sustained growth of the moored buoy program over the years is depicted in **Figure 3**. The program started with the deployment of the first buoy in August 1997 off Chennai in BoB, made its presence felt year after year by its strong commitment to the scientific community. The

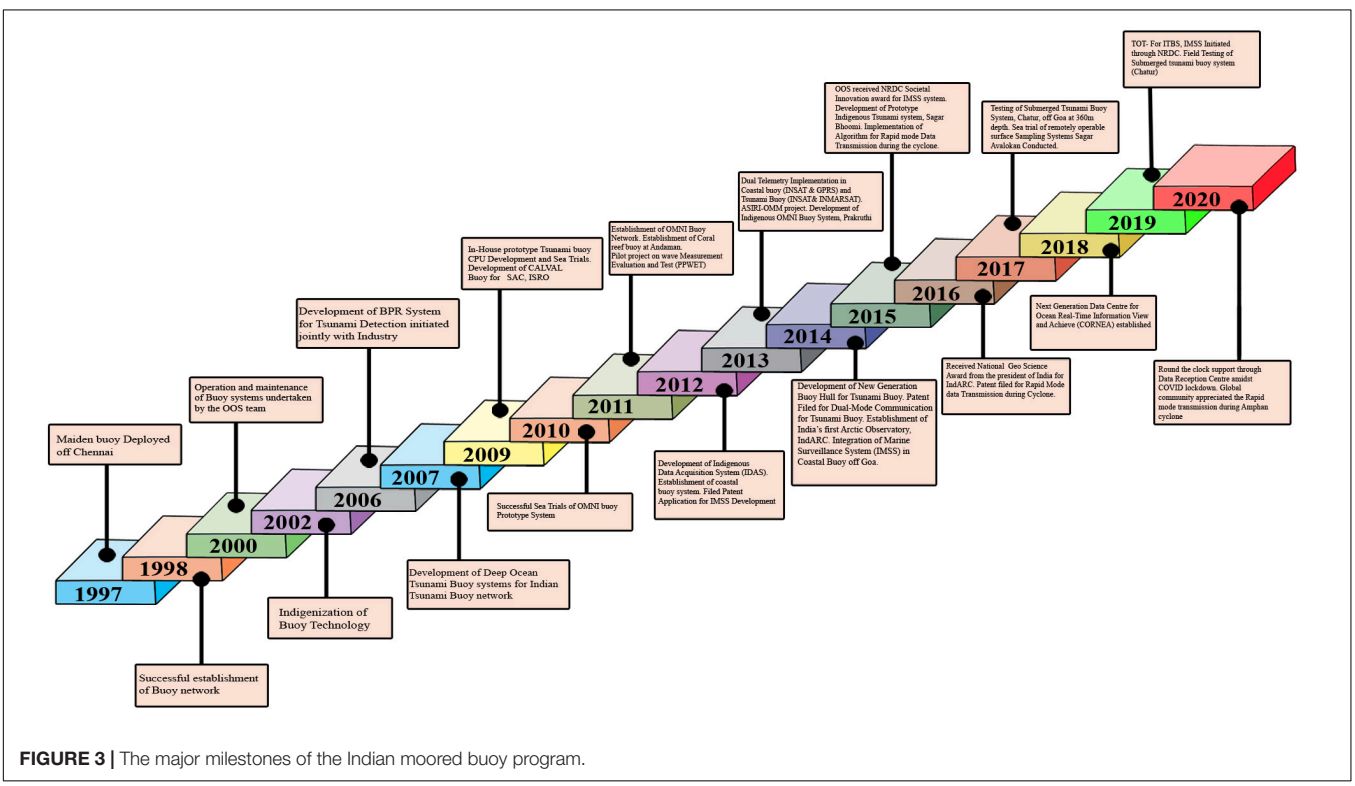

FIGURE 3 | The major milestones of the Indian moored buoy program.

network got inducted with tsunami buoys in 2004 and got revamped in 2010 with additional surface and subsurface sensors. The buoy program had advanced measurement capabilities with a multifaceted approach to new observational techniques, technology developments, state of art data reception centers, research dimensions on new scientific areas, and international collaborative projects.

MOORED BUOY PROGRAM DURING COVID-19 LOCKDOWN IN 2020

Working remotely or work from home has become a new normal due to pandemic lockdown affecting every possible realm, which brought new challenges to the moored buoy program, and the regular operations got impacted the most. Maximum efforts were put forward to ensure the continuity of data by formulating a mitigation plan by prioritizing the tasks, ensuring the 24/7 support of the data center, and by extending the operational period of buoys in the field. The data reception center continued to operate 24x7 with skeletal manpower and ensured uninterrupted real-time dissemination of buoy data to the end-users during the unprecedented and challenging times amidst lockdown. COVID-19 protocols and safety measures were strictly followed by ensuring the quarantine, social distancing, sanitization, and safety gears apart from the regular monitoring of the temperature and oxygen levels. The majority of the data reception systems were automated with minimal manual intervention and the software tool ADDRESS with automated quality control and visual representation greatly helped in uninterrupted data dissemination to end-users.

Performance and Maintenance of the Buoy Network

The sustenance of the moored buoy network has never been an easy task that required perseverance and dedicated effort as evident from the operational statistics (**Figure 4A**). The annual schedule includes four deep-sea cruises (two each in AS and BoB)

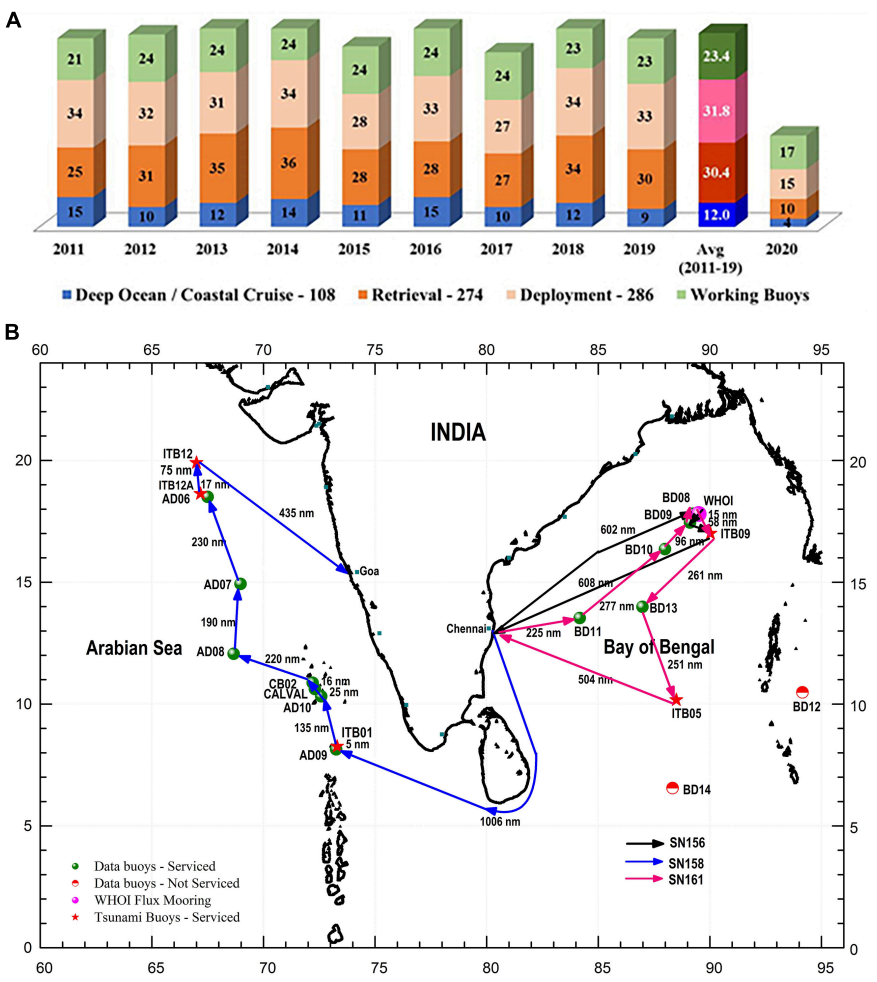

FIGURE 4 | (A) The operational statistics of the moored buoy program during the period 2011 to 2020 and **(B)** the tracks of the cruises undertaken to service the buoys during the COVID-19 pandemic.

comprising of approximately 30 days each and 3–4 coastal cruises apart from the additional cruises to deploy/retrieve the buoys that are stopped/drifted/vandalized. There were 108 cruises spanning 1,445 man-days sailing over 1,36,038 nm to carry out 286 deployments and 274 retrievals over the period from 2011 to 2019 that accounts for an approximate annual average of 12 deep ocean/coastal cruises with 32 deployments and 30 retrievals traversing 15,115 nm with 161 man-days (**Figure 4A**).

The year 2020 indicates minimum cruises and field operations due to the ongoing COVID-19 pandemic, which substantially affected the buoy maintenance operations leading to a significant reduction in the overall performance of the network. The cruises planned from March to May 2020 to service the moored buoy network in AS and BoB and all the fieldwork from March to September were canceled due to the COVID-19 lockdown, whereas the cruises which were scheduled from September to December 2020 were partially carried out.

National Institute of Ocean Technology has undertaken three cruises immediately after the relaxation in lockdown to service the buoys which have already crossed the expected period of operation, to replace the buoys which were vandalized and the ones which stopped transmission. The first cruise was undertaken onboard ORV Sagar Nidhi from 29 September to 14 October to retrieve INCOIS Flux mooring (**Figure 4B**), which was due in May 2020. The vandalized buoy BD09 (89.1°E/17.5°N) in northern BoB was also retrieved and deployed a new buoy system. The AS cruise was followed immediately (November 2 to December 3, 2020) again onboard ORV Sagar Nidhi, which carried out a total of 48 operations including eight buoy deployments, 10 retrievals, 13 CTD operations apart from the samples collected for scientific research. The BoB cruise in February 2021, was mainly focusing on the replacement of buoy systems, which have already crossed the expected period of operation due to the long gap of 14 months between the services (**Figure 4B**).

Data Return From Buoy Network During COVID-19 Pandemic

Quality data return with a minimum gap is the key target of the moored buoy program wherein the efforts are undertaken to ensure the quality as well as quantity. However, the COVID-19 pandemic has affected the ocean observation network globally as reported by GOOS with a significant reduction in data return. It is worth noting that 73% of the Indian buoy network was functional during the pandemic in 2020 even when the cruises were reduced to 33% (**Table 1**). The deployments during the corresponding period were 47%, whereas the retrievals were only 33%. The substantial reduction of cruises resulted in the loss of buoy systems as reflected in the reduction of retrievals.

The AS buoys recorded higher data return (>80%) from air temperature, air pressure, wind, and rainfall sensors even during the COVID-19 pandemic, whereas the humidity and radiation sensors recorded comparatively less data return (∼55%) owing to the sensor damage/drift over a longer period of operation

TABLE 1 | The performance of the moored buoy network during the year 2020 amid COVID-19 pandemic.

Network statistics	Average (2011–2019)	Performance during 2020
Working Buoys	23.4	17 (72.65%)
Deployments	31.8	15 (47.17%)
Retrievals	30.4	10 (32.89%)
Cruise/Field trips	12	4 (33.33%)

(**Figure 5A**). The average data return of surface meteorological parameters in BoB is significantly impacted due to the loss of buoy systems and vandalized meteorological sensors (**Figure 5B**). The impact of the COVID-19 pandemic was visible in the significant reduction (∼ 50%) of data return in BoB, compared to an average data return of 97.9% for the meteorological parameters (Venkatesan et al., 2018b) during two decades of operation. The wave data and CT profiles reported high data return in AS and BoB, which was recovered after the retrieval of the buoy system, including the ones which stopped real-time transmission. The self-powered underwater sensors, ADCP, and CT profiles with self-recording facility provided 93.3% and 80% of data return in AS, whereas the corresponding figures in BoB are 58.3% and 85.7%, respectively. The importance of independent power sources and redundant storage in increasing data return is evident from the higher data return in ADCP and CT profiles, which was recovered from the internal storage of the sensor even when the surface buoy system was lost.

Challenges

The maintenance of the moored buoy network involves the execution of a large number of cruises huge inventories of sensors and buoy systems, logistics related to re-calibration, and purchase of sensors apart from the regular monitoring, archiving, quality control, and dissemination of data sets. The availability of ship time and sensors, unsupportive weather conditions, the continuous menace due to corrosion, biofouling, piracy in AS, and vandalism, to name a few, are the major challenges in sustaining the moored buoy program. Even after extensive efforts made over several years, in particular in sensitizing fishing communities, vandalism remains a significant problem. The awareness campaigns on the application and importance of these data buoys, through direct discussions, and the distributions of multi-lingual brochures, among others, were carried out but have met with only limited success.

The cruises were carried out by following the COVID-19 protocol and guidelines (**Figure 6A**). The cruise participants were quarantined before boarding the vessel and ensured, social distancing, hygiene, whereby carrying out the buoy maintenance activities. During the pandemic, the guidelines issued by Port Health officials (PHO) and linked activities required additional days for quarantine and more funds for the related works.

The delay in service has resulted in significant loss, wherein two vandalized buoys could not be retrieved in time. The surface buoy system along with meteorological components and data logger drifted away and was lost at the BD10 (88°E/16.3°N)

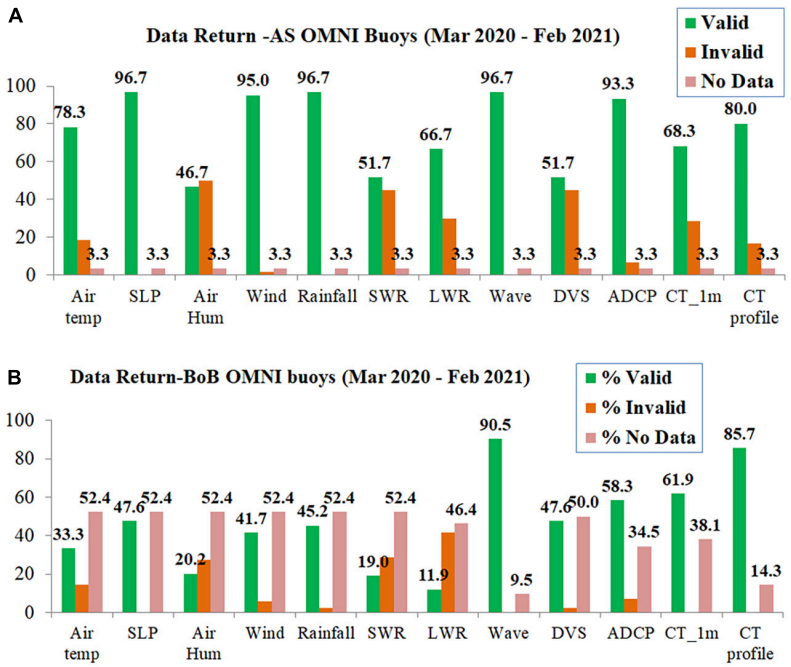

FIGURE 5 | The percentage of data return **(A)** in AS and **(B)** in BoB after the preliminary quality analysis during the period March 2020–February 2021.

location in BoB. However, the subsurface sensors were retrieved with the entangled fish net from the seabed after a comprehensive search near the anchor drop location (**Figure 6C**). The vandalized surface buoy AD06 was drifting in AS and was retrieved by the cruise team, with a damaged mast where the meteorological sensors were missing (**Figure 6B**). The subsurface sensors along with the measured data set and mooring components could not be retrieved from the AD06 location. The BD13 buoy (14N/87E) in BoB, which stopped transmitting data after the passage of the cyclone Amphan in May 2020, could not be traced even after an extensive search in the location around the last transmitted position. The program suffered significant losses in terms of money and precious data, particularly the high-frequency data set. The delay in service also caused significant issues due to the biofouling of subsurface sensors and drift in measured data. Timely service could have reduced the loss of vandalized sensors, buoy systems, and high-frequency data.

Moored Buoy Observations During the Cyclones Amid the COVID-19 Pandemic

The impact of COVID lock down on the functioning of moored buoys beyond the service period is visible in the status of the network during the passage of cyclones Amphan (May 2020), Nisarga (June 2020) and Nivar (November 2020) as shown in **Figure 7**. Substantial reduction in the number of working buoys towards the fag end of 2020 during Nivar (**Figure 7C**) is evident.

The moored buoy network except for BD10 in BoB was fully operational at the beginning of the COVID-19 lockdown in March 2020. These buoys were serviced during October-December 2019 and the regular maintenance cruises were scheduled during April–May 2020. Even though the intelligent PMS can power the buoy for more than a year, the possible drift in the sensors, specifically the biofouling in underwater conductivity

FIGURE 6 | (A) The team proceeding for the cruise, **(B)** the retrieval of the buoy system entangled with fishing net, and **(C)** the bio-fouling and net entanglement in retrieved sensors.

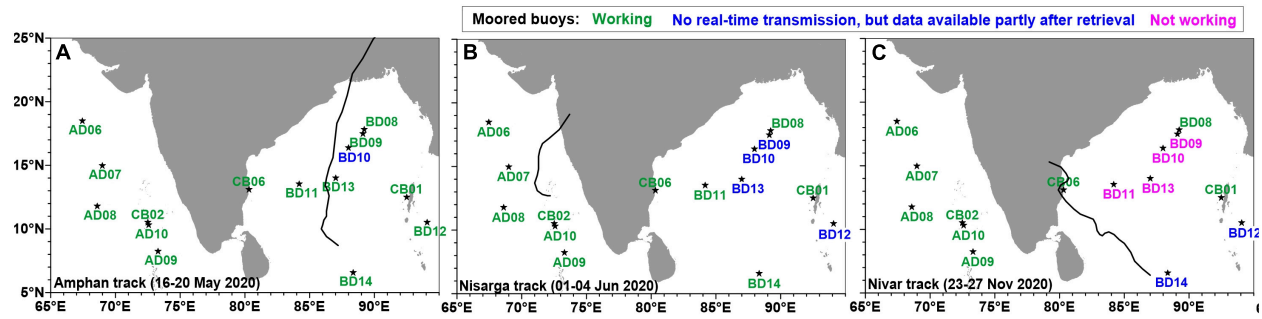

FIGURE 7 | The tracks of the cyclones **(A)** Amphan, **(B)** Nisarga, and **(C)** Nivar during the year 2020 in the north Indian Ocean along with the moored buoy network.

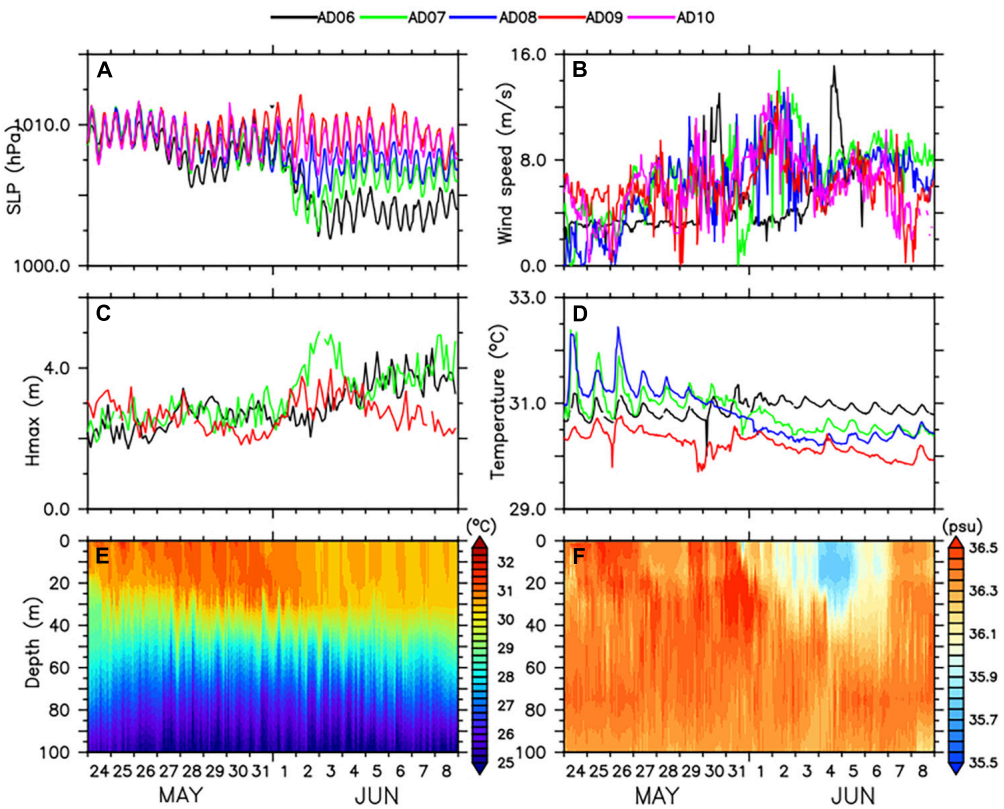

FIGURE 8 | Time series observations of **(A)** Sea level pressure, **(B)** Wind speed **(C)** Height of highest wave, **(D)** SST, **(E)** temperature profile at AD07, and **(F)** salinity profile at AD07 during the passage of Cyclone Nisarga in AS.

sensors necessitated the service at an interval of 6 months to ensure the quality data return.

The moored buoy network captured the signals of the cyclones as well as transmitted high-frequency data during the year 2020 amid COVID-19 lockdown. The cyclone season in the North Indian Ocean started with the Super cyclone Amphan in May 2020, which was the highest intensity cyclone ever recorded in BoB during the pre-monsoon season (**Figure 7A**). The severity of oceanic response was recorded in moored buoys as the significant drop in sea-level pressure (SLP), rapid increase in wind speed and wave height, and substantial drop in temperature and salinity. Some components of moored buoys BD09 (89°E/18°N) and BD13 (14°N/87°E) in the proximity of cyclone were damaged due to the extreme wind and stopped transmission on May 19 and May 24, 2020, respectively.

During the passage of the cyclone Nisarga, all the OMNI buoys in the Arabian Sea were operational (**Figure 7B**). Severe Cyclonic Storm Nisarga was the first cyclonic storm over the AS during 2020 amid the COVID-19 pandemic and ongoing restrictions in sailing. The network of five OMNI buoys in AS captured the signals of the cyclone at various stages from its genesis till the landfall (**Figure 8**). The impact of cyclone Nisarga was observed

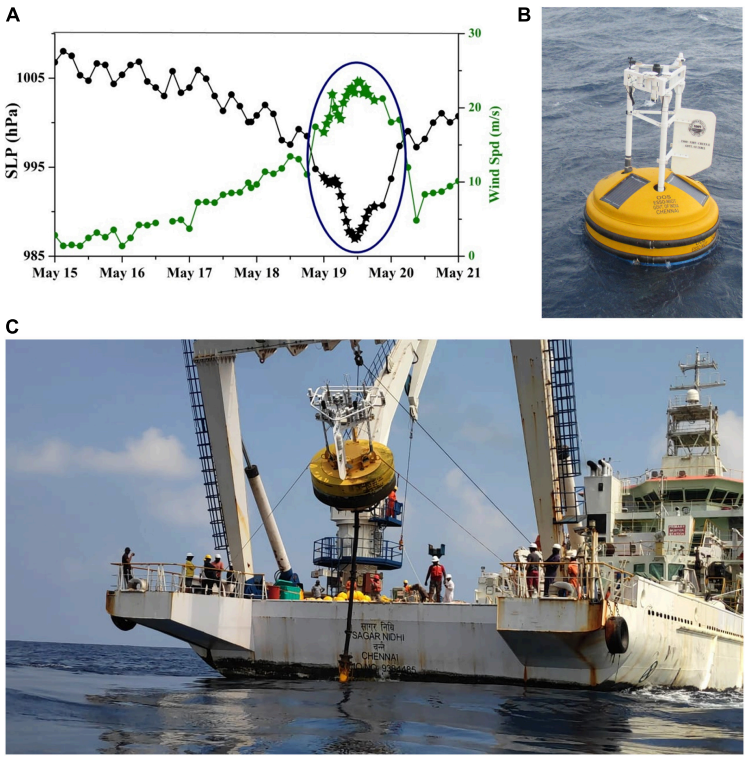

FIGURE 9 | (A) Time-series observations of air pressure and wind speed with high-frequency real-time data during cyclone AMPHAN in BoB, **(B)** the Indian buoy system with tripod mast deployed in AS, and **(C)** retrieval of the INCOIS flux mooring.

in the surface parameters of OMNI buoys particularly in AD06 (67.5°E/18.5°N) and AD07 (68.97°E/14.9°N) in the central AS.

The maximum drop in SLP at ∼1,002 hPa was observed in AD06 and AD07 (**Figure 8A**) which were at a distance of 280 and 225 nm from the cyclone track, respectively. The wind speed of 13.8 m/s was recorded in AD07 (**Figure 8B**) with a corresponding wave height of 5 m on 3 June (**Figure 8C**). Significant variability in SLP, wind speed, and temperature were observed in AD08 (68.6°E/12.0°N) whereas minor response was recorded in AD09 (73.3°E/8.1°N) and AD10 (72.6°E/10.3°N) which were located south of the cyclone genesis areas in southern AS.

Prominent diurnal oscillation in SST was observed at all buoy locations before the cyclone followed by a considerable drop at AD07 and AD08 locations after the cyclone passage (**Figure 8D**). Significant pre-cyclone diurnal warming was observed in the shallow mixed layer in which the cooling associated with cyclone passage was limited to the upper few meters for a period of 3–4 days. Substantial freshening of ∼1.2 psu was observed in the upper mixed layer during the cyclone passage. It was observed that the response to the cyclone was significant only in the upper mixed layer at AD07 (**Figures 8E,F**), which was located at a considerable distance of 225 nm on the left side of the track.

Even though the buoys in AS were fully operational, two coastal buoys and one OMNI buoy were only operational in BoB during the passage of the cyclones Nivar in November 2020 and Burevi in December 2020 resulting in the non-availability of real-time data from the rest of the buoys. The buoys in the AS were serviced during November 2020 whereas that of BoB was carried out in February 2021. Even though the real-time data was not available, the high-frequency data sets were recovered from the buoys after the retrieval of the buoy system.

Achievements

The efforts to upkeep the moored buoy network operational during the COVID-19 pandemic also resulted in achieving a few significant tasks such as the deployment of indigenous tripod buoy system, OceanSITES mooring in AS, and BoB, and Rapid Transmission during cyclones, among others. The development and implementation of rapid mode transmission in moored buoys was a major achievement, which greatly helped the early warning services with the high-frequency transmission during many cyclones since its incorporation in 2016, including the cyclones in 2020 amid the COVID-19 pandemic (**Figure 9A**). The moored buoys incorporated with IDAS such as BD09 during Cyclone Amphan in May 2020, CAL-VAL buoy (72.3°E/10.6°N) during the cyclone Nisarga in June 2020, and CB06 (80.3°E/13.1°N) during the cyclone Nivar in November 2020 triggered high-frequency transmission, among which the rapid transmission in BD09 during the Super Cyclone Amphan was widely appreciated. The OMNI buoy BD09 triggered high-frequency data transmission on 19 May 2020 as the Amphan cyclone approached the buoy. The buoy transmitted data at 1-h interval, while the normal transmission was at every 3 h. BD09 recorded minimum air pressure of 988 hPa on May 12

at 12:00 p.m. (**Figure 9**), while transmitting at rapid mode and continued for 17 h by providing 11 additional real-time data sets. The CAL-VAL buoy (72.3°E/10.6°N) and CB06 (80.3E/13.1N) buoy were incorporated with a refined algorithm and provided high-frequency transmission at an interval of 30 min during the cyclone Nisarga in June 2020 and Nivar in November 2020, respectively. The rapid mode algorithm enabled the buoy system to provide the critical met-ocean data sets to stakeholders with higher frequency in real-time, during the devastating cyclones amid the COVID-19 pandemic.

The buoy system design was updated with a target to extend the endurance and accommodate redundant sensors. The cylindrical-shaped buoy hull with more reserve buoyancy and tripod mast helps to accommodate more sensors and ensures ease of maintenance. The enlarged instrument container with a protective hood and more space for batteries can extend the endurance for 2 years. The wind vane aligns the buoy and anemometer in the direction of wind whereas the existing buoy aligns the buoy with the surface current. Orienting buoy and anemometer in the direction of wind ensure that measured wind data is not obstructed by other components on the sensor arm. The wind vane has an area of 0.57 m^2 and it experiences 35.6 kg of wind load at 30 m/s for the alignment. The mooring part for this buoy system remains the same as the existing buoy system. This updated buoy system was successfully deployed at AD08 location at a depth of 4,300 m during the AS cruise in November 2020 (**Figure 9B**).

The existing OceanSITES mooring at AD07 location in AS is retrieved and redeployed a new buoy system during the AS cruise in November 2020. The OceanSITES location in BoB was established at BD11 (13.6°N/ 84.1°E) and deployment of hydrophone for acoustic applications was carried out during the cruise in February 2021. The retrieval of the Flux mooring in BoB (**Figure 9C**), the maintenance of the tsunami buoys in AS and BoB, and extensive sample collection for the studies on microplastics in the marine environment was also successfully carried out during the COVID-19 pandemic.

RECOMMENDATIONS

The OMNI buoy network has proven its mettle in serving the society during COVID-19 pandemic. The pandemic served as a learning experience and helped in identifying the gaps as well as the strengths in sustaining the network. The refinement of the buoy system along with the efforts in extending the deployment period tremendously helped during the pandemic. The recommendation for the better management of remote platforms based on the experience in managing the OMNI network for more than two decades specifically during the COVID-19 pandemic are listed below:

(a) **Self-Sustainable Data Center:** The shore-based data center plays a vital role in any remote data acquisition network being the hub between remote platforms and the end-users. Ideally, these centers should be designed for automated data reception, quality control, data dissemination, and data archival with minimum human intervention. The necessity for manual intervention will be challenging during a pandemic or similar extreme events. The critical weather services and early warning applications requiring real-time data from these platforms should also be well connected. State of the art, fully dedicated hardware, software, network, and power backup facility with redundancy is essential to support during any casualties. It is proposed to locate an independent and easily accessible facility well protected from the possible impacts of natural disasters such as floods, cyclones, tsunami, and earthquakes, among others. The well-equipped data reception center with customized, fully automated data reception and dissemination facility enabled the uninterrupted real-time dissemination of OMNI buoy data during the COVID-19 pandemic.

(b) **Customized Data Acquisition System:** Data acquisition system that caters to the key functions of data acquisition, processing, storage, and transmission plays a decisive role in the successful operation of moored data buoys. Customization of the DAS to suit the operational efficacy and user requirement has a substantial impact on the endurance and data return of the remote platforms. The IDAS with hybrid charge controller, redundant telemetry, and rapid data transmission facilitated the real-time transmission for an extended period.

(c) **Intelligent Power Management System:** The power source of the remote platforms should be capable enough to deliver an uninterrupted supply beyond the normal working period when the regular servicing is delayed due to unanticipated issues. Reduced power processor with sleep mode provisions along with hybrid charge controller, considerably enhanced the endurance of the OMNI buoy system and made it operational for more than a year during the COVID-19 Pandemic.

(d) **Enhancement of Sensors:** Ocean observation platforms need to be strengthened with smart sensors with independent power sources and self-recording facilities that can operate for a longer duration. This will avoid the loss of data due to snapped connection with the buoy CPU, which had been reported on many occasions including the COVID-19 pandemic. Redundant sensors are suggested to ensure continuity and to assess the quality/drift of the data over a longer period. It is recommended to focus on the refinement of sensors that can self-calibrate at the field. This will avoid spurious data when the working period extends beyond the expected time.

(e) **Local Calibration Facility:** Regular calibration, ideally after each retrieval of sensors is required to ensure the quality and reliability of the measurements. The absence of a local calibration facility leads to a long waiting period for the calibration of the sensors at overseas facilities, particularly for conductivity and temperature sensors which are prone to biofouling. The in-house facility at NIOT to calibrate air humidity, air temperature, air pressure, and precipitation sensors has greatly helped in executing the maintenance cruises during the Pandemic.

(f) **Optimized Telemetry:** Real-time transmission of data sets from remote platforms is an important feature that supports weather services. Two-way communications with the buoy system will sort out a lot of issues. Dual telemetry is recommended to overcome the issues associated with satellite communication. Additional GPRS-based communication is suggested for coastal moorings and redundant satellite communication for offshore platforms. Apart from this, an additional position indicating facility using Argo was found to be critical in providing the location information during buoy stoppage and drifting, particularly in vandalized buoys.

(g) **Robust Mooring System:** The mooring components selected should be capable of working for a longer period withstanding the dynamic loads and mooring motions, in order to hold the system in the deployed location. The major loss of buoy system and components were attributed to vandalism during the pandemic period that necessitates strengthening the anti-vandalism measures.

(h) **Best Practice Methods:** The endurance and performance of remote platforms in the harsh marine environment can be optimally maximized by following the best-practice methods without compromising the quality of the system. The quality of measurement is ensured in NIOT-OMNI buoys by following the best-practice methods (Venkatesan et al., 2018a) evolved over the years of services in maintaining the moored buoy network in the Indian Seas.

(i) **Rapid Data Transmission:** The remote ocean observation platforms are in general configured to acquire data at a higher frequency, i.e., at 1 min, which is stored internally and transmit at a lower frequency, i.e., at 3 h. The high-frequency data is available after the retrieval of the buoy system, which varies between 6 months to more than a year. Vandalism or delay in maintenance may lead to the loss of the buoy system or the sensors, which in turn results in the total loss of the critical high-frequency data as reported during the COVID-19 pandemic. The rapid data transmission during cyclones in NIOT buoys was a boon to the end-users amid the pandemic associated data loss. An extension of the algorithm to trigger high-frequency transmission at periodic intervals or event-based can save the critical data sets.

(j) **Open Data Policy:** The COVID-19 pandemic has significantly affected the data return from remote ocean platforms that can significantly affect the weather services and climate studies. The pandemic point toward the necessity to share the available data sets to meet the growing need of weather and climate studies. The OMNI-RAMA data portal, wherein the moored buoy data from OMNI as well as RAMA buoys are made available for the public is a major milestone toward open data policy. It is highly recommended to follow the open data policy in all remote platforms, which can fuel scientific research across the globe.

(k) **International Co-operation:** The pandemic has severely affected the field trips and cruises to service the remote platforms owing to limited resources, travel restrictions, fund cuts, and safety measures, which necessitates sharing the facilities with national and international organizations. The existing memorandum of understanding (MoU) between the Ministry of Earth Sciences (MoES)-India and National Oceanic and Atmospheric Administration/ Pacific Marine Environmental Laboratory (NOAA/PMEL), United States has eased out the many obstacles in maintaining the RAMA network and serves as a good example of resource sharing. The support extended by the Indian Navy and Coast Guard have greatly contributed to maintaining the buoy network particularly during the buoy stoppage/drifting/vandalism.

SUMMARY

Sustaining the observational program and ensuring high-quality data with minimal data gap amidst the multitude of challenges require enormous vision and teamwork. Apart from the regular challenges such as vandalism, biofouling, rough weather, and limited ship time availability, the COVID-19 lockdown has added the risk of delay in servicing the buoys in remote marine environments. The recent increase in the frequency and intensity of cyclones in AS and BoB, demands enhanced observational capability and improved collaborations across the globe. The present-day moored buoy system is the result of incessant research and technological developments over two decades. Continuous improvements in various aspects such as buoy system components, state-of-the-art data reception facility, reliability checks, and best practice methods, along with the untiring efforts of the team were rewarded by providing continuous data during the devastating cyclones during COVID-19 lockdown, where the other modes of measurement were interrupted.

Adapting to the present COVID-19 situation particularly the field operation is necessary to ensure the continuity of measurements. The expected impacts of the pandemic in the coming years, necessitate collective efforts and better collaboration among the scientific and user community across the political boundaries to achieve a resilient system. The COVID-19 lockdown has proved the increasingly significant role of remote observational platforms, which necessitates integrated efforts to evolve revised observational requirements to realize a sustainable ocean observation network.

DATA AVAILABILITY STATEMENT

The raw data supporting the conclusion of this article will be made available by the authors, without undue reservation.

AUTHOR CONTRIBUTIONS

RV and KJJ conceived the manuscript, provided the guidance to co-authors, and coordinated the author contributions. CAP and MK contributed to preparing the activities during the COVID-19 pandemic, reviewed and edited the manuscript. MAM, BK,

BH, GV, KR, and AT contributed to the technology developments and field operations/cruises. PM, KT, and PS contributed to the mooring design, cruise details, and challenges. SRS, RSu, MK, MVM, KN, and CAP carried out the data processing and analysis. RSr, SJ, CM, NS, and MS supported in data collection. All the authors contributed to the article and approved the submitted version.

FUNDING

This study was funded by the Ministry of Earth Sciences (MoES), Government of India.

ACKNOWLEDGMENTS

The authors would like to thank the Ministry of Earth Sciences (MoES), Government of India, for funding the moored buoy program. The authors would like to thank the director, NIOT for providing the facilities and encouragement in carrying out this study. The authors would like to thank and appreciate the efforts put forward by the officers in MoES as well as at NIOT and other MoES institutions who were instrumental in the establishment and sustenance of the moored buoy network in the Indian Seas. The authors would also like to thank the staff of the Vessel Management Cell of the NIOT and crew of the research vessels for their support in maintaining the moored buoy network.

REFERENCES

Bigorre, S. P., and Galbraith, N. R. (2018). "Sensor performance and data quality control," in *Observing the Oceans in Real Time*, eds R. Venkatesan, A. Tandon, E. D'Asaro, and M. Atmanand (Berlin: Springer), 243–261.

Diffenbaugh, N. S., Field, C. B., Appel, E. A., Azevedo, I. L., Baldocchi, D. D., Burke, M., et al. (2020). The COVID-19 lockdowns: a window into the Earth System. *Nat. Rev. Earth Environ.* 1, 470–481.

Gordon, L., and Deines, K. (2011). Lithium battery packs for long term ocean deployments, Tadiran's pulse plus technology triples deployment durations. *Mar. Technol. Soc.* 39, 1–6.

Heslop, E., Fischer, A., Tanhua, T., Legler, D., Belbeoch, M., Kramp, M., et al. (2020). *Covid-19's Impact on the Ocean Observing System and Our Ability to Forecast Weather and Predict Climate Change*. Available online at: https://www.goosocean.org/index.php?option=com_oe&task=viewDocumentRecord&docID=26920 (accessed May 03, 2021).

Jarraud, M. (2008). *Guide to Meteorological Instruments and Methods of Observation (WMO-No. 8)*. Geneva: World Meteorological Organisation.

Linden, D., and Thomas, B. R. (2002). *Handbook of Batteries*. NewYork, NY: McGraw Hill.

Liu, Z., Ciais, P., Deng, Z., Lei, R., Davis, S. J., Feng, S., et al. (2020). Near-real-time monitoring of global CO 2 emissions reveals the effects of the COVID-19 pandemic. *Nat. Commun.* 11:5172.

March, D., Metcalfe, K., Tintoré, J., and Godley, B. J. (2021). Tracking the global reduction of marine traffic during the COVID-19 pandemic. *Nat. Commun.* 12:2415.

Meindl, A. (1996). *Guide to Moored Buoys and Other Ocean Data Acquisition Systems*. Geneva: WMO & IOC.

Navaneeth, K. N., Martin, M. V., Joseph, K. J., and Venkatesan, R. (2019). Contrasting the upper ocean response to two intense cyclones in the Bay of Bengal. *Deep Sea Res. Part I: Oceanographic Res. Papers* 147, 65–78. doi: 10.1016/j.dsr.2019.03.010

Nigam, R., Pandya, K., Luis, A. J., Sengupta, R., and Kotha, M. (2021). Positive effects of COVID-19 lockdown on air quality of industrial cities (Ankleshwar and Vapi) of Western India. *Sci. Rep.* 11:4285. doi: 10.1038/s41598-021-83393-9

Sea-Bird Electronics (2016). *Anti-foulant Device*. Bellevue, DC: Sea-Bird Electronics.

Thomson, D. J., and Barclay, D. R. (2020). Real-time observations of the impact of COVID-19 on underwater noise. *J. Acoust. Soc. Am.* 147, 3390–3396. doi: 10.1121/10.0001271

Vadrevu, K. P., Eaturu, A., Biswas, S., Lasko, K., Sahu, S., Garg, J., et al. (2020). Spatial and temporal variations of air pollution over 41 cities of India during the COVID-19 lockdown period. *Sci. Rep.* 10:16574. doi: 10.1038/s41598-020-72271-5

Venkatesan, R., Lix, J. K., Phanindra Reddy, A., Arul Muthiah, M., and Atmanand, M. A. (2016). Two decades of operating the Indian moored buoy network: significance and impact. *J. Operational Oceanography* 9, 45–54. doi: 10.1080/1755876X.2016.1182792

Venkatesan, R., Mathew, S., Vimala, J., Latha, G., Muthiah, M. A., Ramasundaram, S., et al. (2014). Signatures of very severe cyclonic storm Phailin in met–ocean parameters observed by moored buoy network in the Bay of Bengal. *Curr. Sci.* 107, 589–595.

Venkatesan, R., Ramesh, K., Kishor, A., Vedachalam, N., and Atmanand, M. A. (2018a). Best practices for the ocean moored observatories. *Front. Mar. Sci.* 5:469. doi: 10.3389/fmars.2018.00469

Venkatesan, R., Sannasiraj, S., Ramanamurthy, M., Senthilkumar, P., and Dhinesh, G. (2018b). Development and performance validation of a cylindrical buoy for deep-ocean tsunami monitoring. *IEEE J. Oceanic Eng.* 44, 415–423.

Venkatesan, R., Senthilkumar, P., Vedachalam, N., and Murugesh, P. (2017). Biofouling and its effects in sensor mounted moored observatory system in Northern Indian Ocean. *Int. Biodeterioration Biodegradation* 116, 198–204.

Venkatesan, R., Shamji, V. R., Latha, G., Mathew, S., Rao, R., Muthiah, A., et al. (2013). In situ ocean subsurface time-series measurements from OMNI buoy network in the Bay of Bengal. *Curr. Sci.* 104, 1166–1177.

Venkatesan, R., Vedachalam, N., Vengatesan, G., Weller, R. A., Tandon, A., and Atmanand, M. A. (2020). Fuel for cyclones: quantification of ocean-atmosphere energy exchange during tropical cyclones in the Bay of Bengal using indian ocean moored observatories. *Mar. Technol. Soc. J.* 54, 81–92.

Viglione, G. (2020). How COVID_19 could ruin weather forecasts and climate records. *Nature* 580, 440–442. doi: 10.1038/d41586-020-00924-6

Conflict of Interest: The authors declare that the research was conducted in the absence of any commercial or financial relationships that could be construed as a potential conflict of interest.

Publisher's Note: All claims expressed in this article are solely those of the authors and do not necessarily represent those of their affiliated organizations, or those of the publisher, the editors and the reviewers. Any product that may be evaluated in this article, or claim that may be made by its manufacturer, is not guaranteed or endorsed by the publisher.

frontiers in Marine Science

ORIGINAL RESEARCH
published: 02 December 2021
doi: 10.3389/fmars.2021.722401

An Evaluation of the Impact of Pandemic Driven Lockdown on the Phytoplankton Biomass Over the North Indian Ocean Using Observations and Model

*Vivek Seelanki and Vimlesh Pant**

Centre for Atmospheric Sciences, Indian Institute of Technology Delhi, New Delhi, India

The unprecedented nationwide lockdown due to the 'coronavirus disease 2019' (COVID-19) affected humans and the environment in different ways. It provided an opportunity to examine the effect of reduced transportation and other anthropogenic activities on the environment. In the current study, the impact of lockdown on chlorophyll-a (Chl-a) concentration, an index of primary productivity, over the northern Indian Ocean (IO), is investigated using the observations and a physical-biogeochemical model. The statistics of model validation against observations shows a correlation coefficient of 0.85 (0.89), index of agreement as 0.90 (0.91). Root mean square error of 0.45°C (0.50°C) for sea surface temperature over the Bay of Bengal (BoB) (Arabian Sea, AS) is observed. The model results are analyzed to understand the upper-oceanic physical and biological processes during the lockdown. A comparison of the observed and model-simulated data during the lockdown period (March–June, 2020) and pre-pandemic period (March–June, 2019) shows significant differences in the physical (temperature and salinity) and biogeochemical (Chl-a concentration, nutrient concentration, and dissolved oxygen) parameters over the western AS, western BoB, and regions of Sri Lanka. During the pandemic, the reduced anthropogenic activities lead to a decrease in Chl-a concentration in the coastal regions of western AS and BoB. The enhanced aerosol/dust transport due to stronger westerly winds enhanced phytoplankton biomass in the western Arabian Sea (WAS) in May–June of the pandemic period.

Keywords: COVID-19, lockdown, chlorophyll, ocean temperature, primary productivity

OPEN ACCESS

Edited by:
Deepak R. Mishra, University of Georgia, United States

Reviewed by:
Samiran Mandal, Indian Institute of Technology Bombay, India
Aneesh Anandrao Lotliker, Indian National Centre for Ocean Information Services, India

***Correspondence:**
Vimlesh Pant
vimlesh@cas.iitd.ac.in

Specialty section:
This article was submitted to Coastal Ocean Processes, a section of the journal Frontiers in Marine Science

Received: *08 June 2021*
Accepted: *03 November 2021*
Published: *02 December 2021*

Citation:
Seelanki V and Pant V (2021) An Evaluation of the Impact of Pandemic Driven Lockdown on the Phytoplankton Biomass Over the North Indian Ocean Using Observations and Model. Front. Mar. Sci. 8:722401. doi: 10.3389/fmars.2021.722401

INTRODUCTION

Severe acute respiratory syndrome coronavirus 2 (SARS-CoV-2), officially named coronavirus disease 2019 (COVID-19), is a global pandemic that started in late 2019. This pandemic affected almost all the countries and territories around the world. The WHO declared the COVID-19 outbreak a global health emergency in January 2020. As of August 31, 2021, worldwide, 218,213,889

confirmed cases of COVID-19 are being reported. Out of these cases, 18,595,281 are active cases, and 4,528,115 deaths have been reported due to COVID-19 (Worldometers.info, 2020). Considering the seriousness of the disease, the government of India implemented a nationwide lockdown in four phases starting from March 25, 2020. In the first phase of the lockdown (March 25 to April 14, 2020), strict restrictions were imposed on physical gatherings for the cultural, religious, political, academic, sports, and academic events. Most industrial operations, construction works, and markets were shut down, and only emergency or essential services were allowed in the first phase of lockdown. The subsequent three phases of lockdown in India were imposed as phase 2: April 15 to May 3, 2020; phase 3: May 4–17, 2020; and phase 4: May 18–31, 2020. The restrictions on the industrial and agricultural activities were mostly lifted after the first phase. After that, to restart the Indian economy, two unlock phases were announced (unlock 1: June 1–30, 2020; unlock 2: July 1–31, 2020), which allowed the opening of markets and physical gathering in a phased manner.

In addition, the countries adjoining the western Arabian Sea (WAS) had lockdown restrictions. Most of the countries around the WAS imposed the pandemic restrictions from the mid-March 2020 by closing the borders, schools, physical gatherings, and international travel. Oman implemented a lockdown from April 10–22, 2020, which was extended further until May 29, 2020. Yemen imposed partial restrictions in May–June 2020. In Somalia, the authorities responded with drastic measures after the first confirmed COVID-19 case on March 16, 2020. They decided to close the borders, schools, limiting travel, and prohibiting most group functions. Due to the imposed restrictions during the lockdown in various countries, there was a significant reduction in the air pollution level in the living environment (Chimurkar et al., 2020).

Oceans play a crucial role in the global climate system. Life on the Earth in terms of productivity is directly influenced by ocean characteristics (Morel and Antoine, 1994). The changes in ocean surface properties affect the life on Earth as oceans produce more than 50–80% of the oxygen on the Earth (NOAA, 2020). Several studies are conducted to study the effect of COVID-19 on air and water quality (Chimurkar et al., 2020; Navinya et al., 2020; Madineni et al., 2021; Pandey and Vinoj, 2021). But the impact of lockdown on the upper-oceanic physical and biogeochemical parameters is not explored. The pandemic has also affected oceanic *in situ* measurements as several research cruises were postponed. It affected the data collection and maintenance of existing observational instruments in the ocean.

Due to COVID-19, the governments have imposed restrictions on several industrial and human activities. The consequences of such lockdowns have been remarkable as the pollution levels have dropped significantly. For instance, the emissions of greenhouse gases, nitrogen dioxide, black carbon have decreased drastically (Zambrano-Monserrate et al., 2020). It has been reported that the lockdown due to pandemics has improved the coastal ocean water and atmospheric air quality (Chauhan and Singh, 2020; Paital, 2020). A significant reduction in CO_2 concentration is noticed due to the imposed pandemic and reduced human activities (Le Quéré et al., 2020). The primary productivity is an estimation of oceans plant biomass and, the Chl-a concentration represents the phytoplankton distribution (Morin et al., 1999). Many parameters influence ocean productivity, such as ocean temperature, nutrients, and carbon cycle (Behrenfeld et al., 2006; Gerecht et al., 2014).

Before the COVID-19 pandemic, in recent decades, a significant increase in the sea surface temperature (SST) is apparent in the global ocean directly influencing the ocean (Yeh et al., 2009; Knutson et al., 2010). However, the reduction in global atmospheric CO_2 concentration by about 7% during the pandemic (Le Quéré et al., 2020) has influenced the air-sea flux of carbon and ocean biogeochemistry. The impact of lockdown on the marine ecosystem could be associated with several factors, such as the changes in SST, aerosol optical depth (AOD), dust mass concentration at the sea surface, and nitrogen dioxide. The WAS receives a large influx of dust particles through westerly winds from the desert regions (Clemens, 1998; Patra et al., 2005; Ramaswamy et al., 2017), which makes it worth investigating the influences of the lockdown-induced factors, particulate matter/aerosols, and dust loading on the Chl-a concentration in the Arabian Sea (AS).

Aerosol particles, both natural and anthropogenic, span over a wide range of sizes from a few nanometers to hundreds of micrometers. These aerosols can be produced locally or be transported long distances (thousands of kilometers) by winds. Depending on their generating source characteristics and long-range transport pathway in the atmosphere, these particles possess different chemical compositions. The gravitational settling, scavenging, and wet removal are the major sinks for aerosols. Once settled over the ocean surface, these particles add their constituents to the seawater and alter the mixing ratio of various dissolved gases and nutrients in the upper ocean (few tens of meters). These aerosol particles are known to be an important source of macronutrients, e.g., nitrogen (N), and phosphate (P), and micronutrients. The most prominent micronutrient is iron (Fe). Other micronutrients, such as zinc and cobalt, are also essential for the biological processes. The macronutrients and micronutrients are essential building blocks for the phytoplankton growth (Duce and Tindale, 1991; Mahowald et al., 2005; Meskhidze et al., 2005; Gallisai et al., 2014). The mechanical disruption of the sea surface by winds lead to the formation of sea-spray and sea-salt aerosols (O'Dowd et al., 1997; Satheesh et al., 2006; Mulcahy et al., 2008; Pant et al., 2008; Glantz et al., 2009; Meskhidze and Nenes, 2010). Such sea-salt aerosols remain suspended in the atmosphere, undergo a transformation during long-range transport, and a large fraction of it settles back to the ocean surface. The emissions from industry, transport, and power plants, etc., contribute to the concentration and characteristics of marine aerosols. Globally, the anthropogenic emissions are largely reduced during the pandemic driven lockdown. This reduction in aerosol concentration is expected to influence the biogeochemistry of the upper ocean, particularly near the coastal regions. Further, the decline in NO_2 emissions reduced nitrogen concentration, particularly in the coastal regions (Mishra et al., 2020).

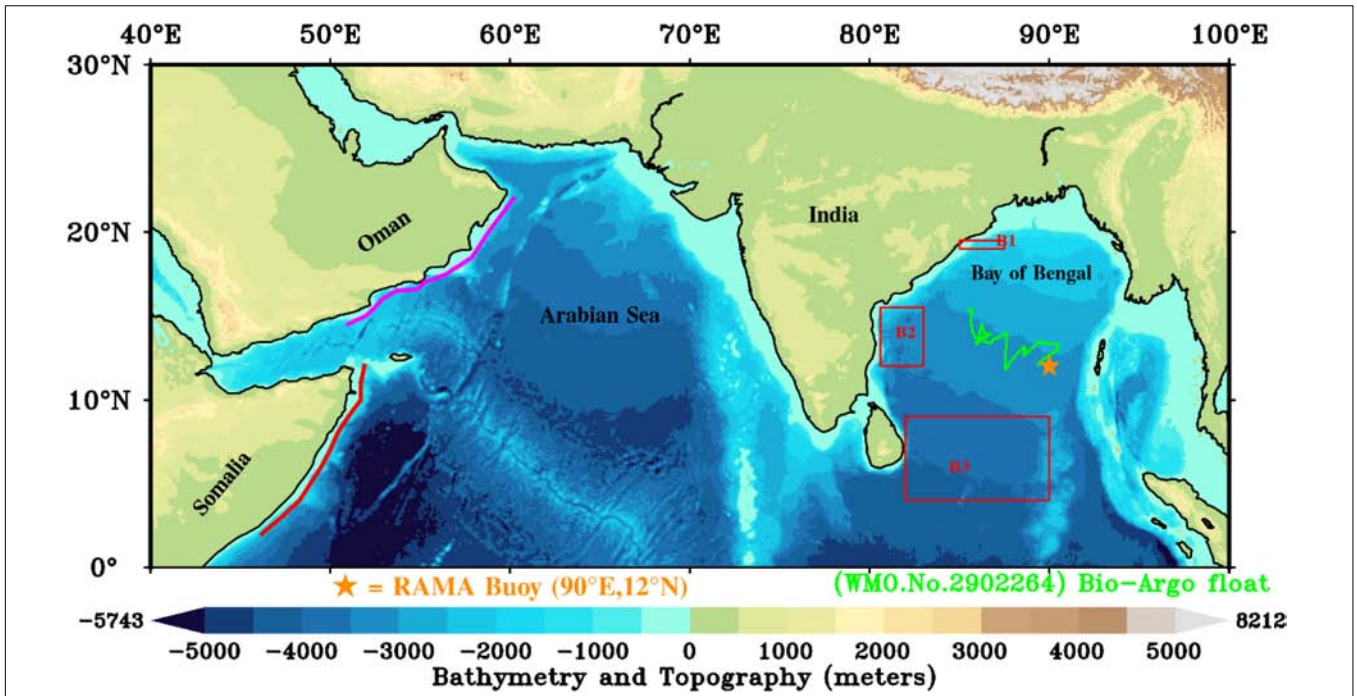

FIGURE 1 | The study domain of the North Indian Ocean (NIO) with the bathymetry and topography in shades (in meters). The continuous contour lines off the Somalia and Oman coasts and red boxes (B1, B2, and B3) in the Bay of Bengal (BoB) show the regions of vertical profile analysis. The location of the Research Moored Array for African–Asian–Australian Monsoon Analysis and Prediction (RAMA) buoy is marked with a star and the trajectory of Bio-Argo float is shown with a green curve.

TABLE 1 | Summary of datasets used in the study.

Variable	Dataset	Spatial resolution	Temporal resolution	Source
Chl-a concentration	OC-CCI	4 km × 4 km	2019–2020	https://www.oceancolour.Org
SST	AMSR2	0.25° × 0.25°	2019–2020	https://las.incois.gov.in/las
AOD	MODIS-Aqua	1° × 1°	2019–2020	https://giovanni.gsfc.nasa.gov/giovanni/
NO_2	OMI	0.25° × 0.25°	2019–2020	https://giovanni.gsfc.nasa.gov/giovanni/
DUSMASS	MERRA-2	0.5°×0.625°	2019–2020	https://gmao.gsfc.nasa.gov/reanalysis/MERRA-2
SSSMASS	MERRA-2	0.5°×0.625°	2019–2020	https://gmao.gsfc.nasa.gov/reanalysis/MERRA-2
Winds	ERA5	25 km × 25 km	2019–2020	https://cds.climate.copernicus.eu/

Typically, the AS and the Bay of Bengal (BoB) receive up to 20 and 10 g m^{-2} $year^{-1}$ mineral dust from the adjacent land regions, respectively, with a peak deposition during the June, July, August (JJA) period (Patra et al., 2007). The dust bearing northwesterly winds prevail close to the sea surface around 45°E but rise to 3 km around 70°E (Clemens, 1998) with a gradient of about 0.1 km $degree^{-1}$ longitude. Jin et al. (2018) reported that tons of dust aerosols emitted from the Arabian Peninsula (AP) and its surrounding areas are transported to the AS by the strong northwesterly "Shamal" winds during boreal summer. From the absorbing aerosol index (AAI) distribution and tracer transport modeling, Patra et al. (2005) concluded that a large amount of aerosols is transported to the AS from northern Africa and the Gulf region during JJA months, and a major fraction of these aerosols are deposited on the AS surface. Over the AP and the northwestern AS, more than 50% of the AOD is contributed by mineral dust (Jin et al., 2018).

Jickells et al. (2005) emphasized the significance of atmospheric inputs of nutrients and micro-nutrients to the surface ocean. Patra et al. (2005) ascribed northern Africa and the Gulf as the source regions of aerosols found over the AS during the southwest monsoon. This observation is consistent with

TABLE 2 | The correlation coefficient (CC) and root mean square error (RMSE) for model-simulated parameters against *in situ* measurements (shown in **Figure 4**).

Parameter	Comparison	CC	RMSE
Temperature	RAMA vs Model	0.81	0.52
Salinity	RAMA vs Model	0.63	0.4
Temperature	Bio-Argo vs Model	0.91	0.57
Salinity	Bio-Argo vs Model	0.59	0.45
Chlorophyll-a concentration	Bio-Argo vs Model	0.49	0.09
Dissolved oxygen	Bio-Argo vs Model	0.71	3.44

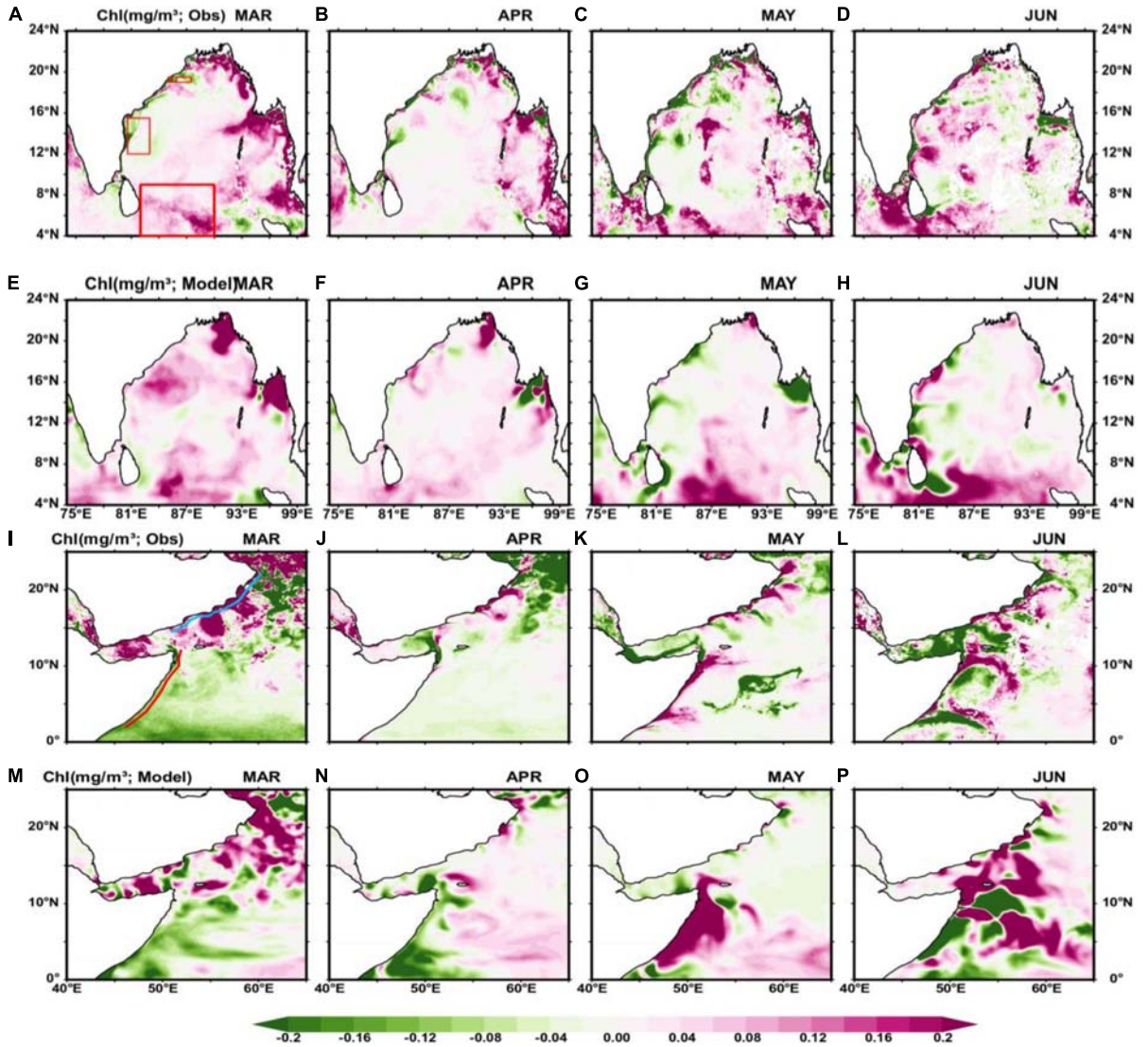

FIGURE 2 | Chlorophyll-a (Chl-a) concentration difference (milligram per cubic meter) from pandemic period (March–June of 2020) to pre-pandemic period (March–June of 2019) from the observations (rows 1 and 3) and model simulations (rows 2 and 4) over the BoB (rows 1 and 2) and western Arabian Sea (WAS) (rows 3 and 4). The red rectangular boxes [in panel **(A)**] are chosen for the vertical profile analysis, and the red (sky blue) continuous line [in panel **(I)**] represents the 1,000 m isobath section in Somalia (Oman) coast used to study the vertical profiles.

the higher sinking fluxes of lithogenic and dolomite materials in the AS, derived from the Arabian region and transported by north-westerly winds during the southwest monsoon (Nair, 2006). These mineral dust aerosols deposited on the AS surface are found to be rich in nutrients and micro-nutrients (Measures and Vink, 1999; Tindale and Pease, 1999; Rengarajan and Sarin, 2004). Measures and Vink (1999) have shown that the supply of Fe through aeolian dust is a requirement for biological production in the nutrient-rich upwelled water in the WAS, and more prominently in the water that advects offshore.

In the current study, an ocean bio-physical model together with the available observations is used to understand the impact of lockdown on phytoplankton biomass (Chl-a concentration) over the north Indian Ocean (NIO), particularly in the coastal regions. The model data are useful in the absence of *in situ* and satellite observations. The temperature, Chl-a concentration data are available from the satellites but, there are large gaps owing to the presence of clouds. Most of the earlier studies based on the satellite measurements of ocean color provided the spatiotemporal evolution of Chl-a concentration over large oceanic areas (Jayaram et al., 2018; Mandal et al., 2021). However, ocean color monitors (primarily visible and infrared band) on satellites are incapable of observing through clouds and below the ocean surface. The *in situ* measurements from autonomous profiling or ship-based observations (e.g., Thushara et al., 2019) can provide high-quality information on the subsurface physical and biogeochemical variables but these observations have limited spatial coverage and, often, sampling location changes from

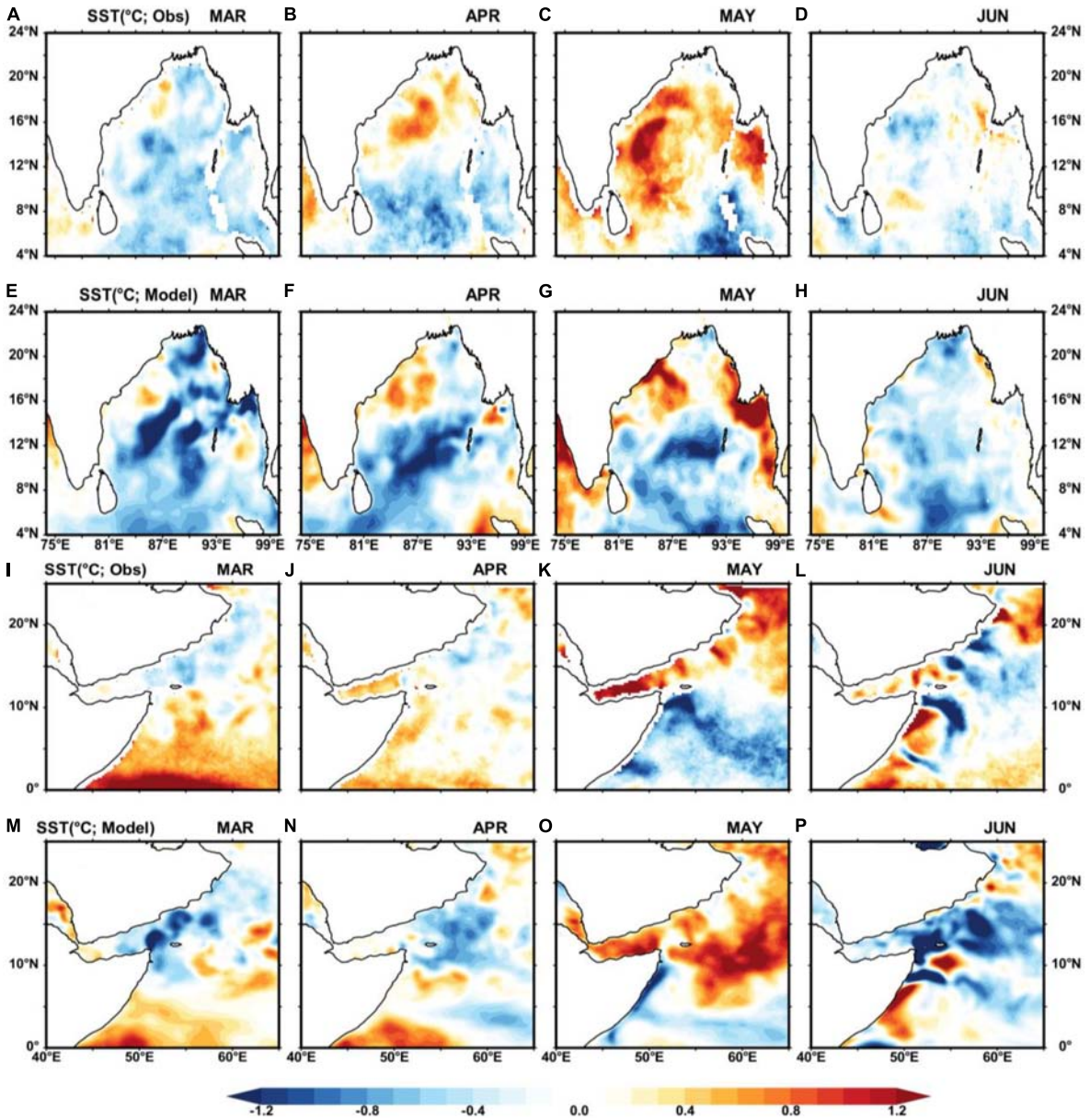

FIGURE 3 | Sea surface temperature (SST) difference (degree centigrade) from pandemic period (March–June of 2020) to pre-pandemic period (March–June of 2019) from the observations (rows 1 and 3) and model simulations (rows 2 and 4) over the BoB (rows 1 and 2) and WAS (rows 3 and 4).

one profile to another. Further, several ocean expeditions and observational cruises were postponed due to the pandemic, which affected the data collection and maintenance of existing *in situ* data platforms. To overcome these limitations of satellite and *in situ* data, the bio-physical model is used to study the evolution of subsurface features. The objectives of the current study are to assess the changes in upper-ocean physical and biogeochemical parameters during COVID-19 driven lockdown period with respect to the pre-pandemic period and to examine the causative atmospheric and oceanic processes leading to the observed differences. The Chl-a concentration simulated by the eco-system model and observed from *in situ* and remote sensing methods is analyzed to infer the impact on the biogeochemistry during the pandemic lockdown compared with the non-pandemic period.

DATA AND MODEL DESCRIPTION

In situ Data

The ocean temperature and salinity profiles are derived using *in situ* observations from the moored buoy array program, consisting of the Research Moored Array for African–Asian–Australian Monsoon Analysis and Prediction (RAMA) buoy (at 90°E, 12°N) (McPhaden et al., 2009). The

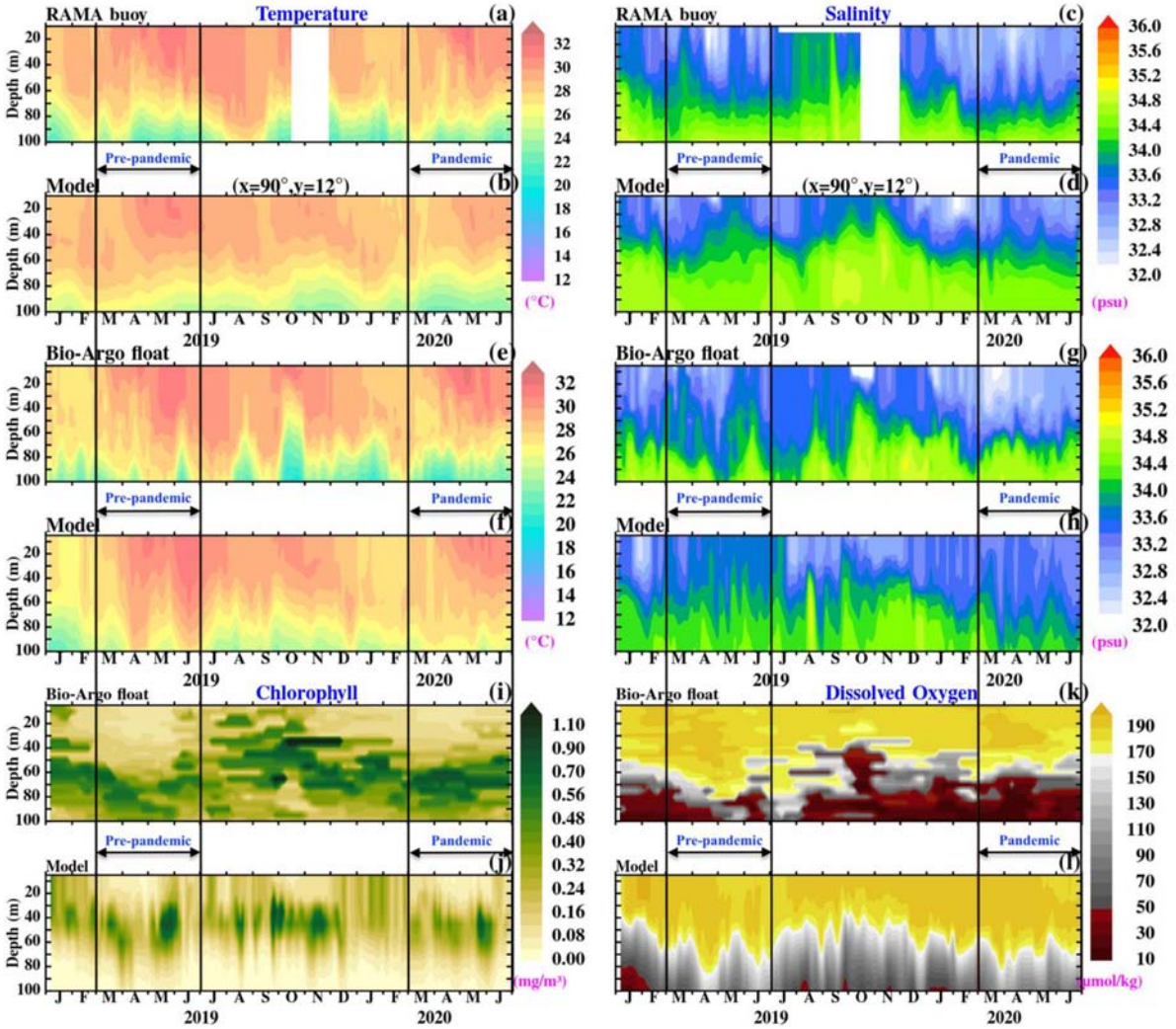

FIGURE 4 | Time-depth section of temperature and salinity from RAMA buoy location at 90°E, 12°N **(A,C)** in the BoB compared with model-simulated temperature and salinity over the same location **(B,D)**. The observed temperature, salinity, Chl-a concentration, and dissolved Oxygen **(E,G,I,K)** from the Bio-Argo float (WMO ID. 2902264) in the central BoB compared with the model-simulated parameters along the trajectory of float **(F,H,J,L)**.

RAMA buoys were deployed for the improved description, understanding, and prediction of the African, Asian, and Australian monsoon systems. This high resolution near real-time data of moored RAMA buoy obtained from the Tropical Atmosphere Ocean Project Office of the National Oceanic and Atmospheric Administration–Pacific Marine Environmental Laboratory http://www.pmel.noaa.gov/tao. The buoy gauges represent the open-ocean conditions and are not affected by the neighboring land orography and surface heating (Bowman et al., 2003; Bowman, 2005; McPhaden et al., 2009). Additionally, the Bio-Argo float (WMO ID: 2902264) deployed in the central BoB (CBoB) (83.85°E, 13.4°N) is used[1] for validation and analysis. This Bio-Argo float provides measurement/estimate of temperature, salinity, Chl-a concentration, dissolved oxygen with respect to depth in the ocean. This profiling float was equipped with a temperature, conductivity, and depth sensor of Seabird (SBE41CP), dissolved oxygen sensor (Aanderra Optode 4330), and chlorophyll fluorescence sensor (WET Labs FLBB). These floats are used in the Indian ARGO project managed by the Indian National Centre for Ocean Information Services (INCOIS) and were manufactured by Sea-Bird Electronics. In the present study, *in situ* observations from RAMA and Bio-Argo in the upper 100 m of the water column are used for the duration from January 1, 2019 to June 30, 2020. The Bio-Argo float trajectory and location of RAMA buoy used in this study are shown on the map in **Figure 1**.

Satellite Data

The Chl-a concentration data were obtained from the European Space Agency Ocean Color-Climate Change Initiative project

[1]http://www.coriolis.eu.org/

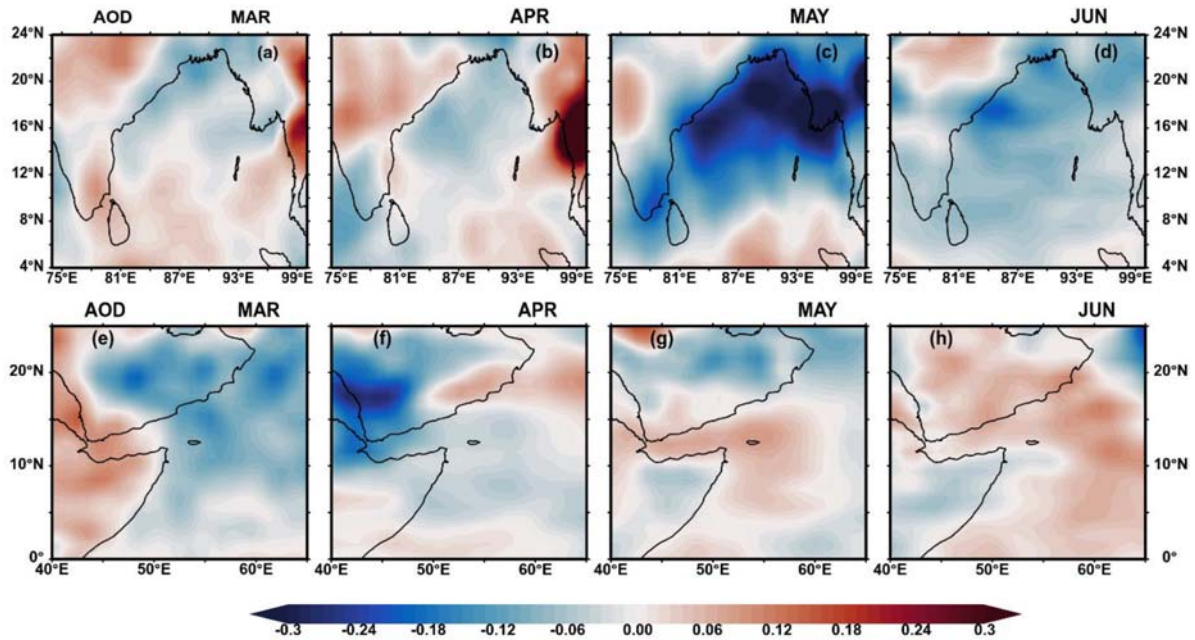

FIGURE 5 | Difference (pandemic – pre-pandemic) in aerosol optical depth over the BoB **(A–D)** and WAS **(E–H)**.

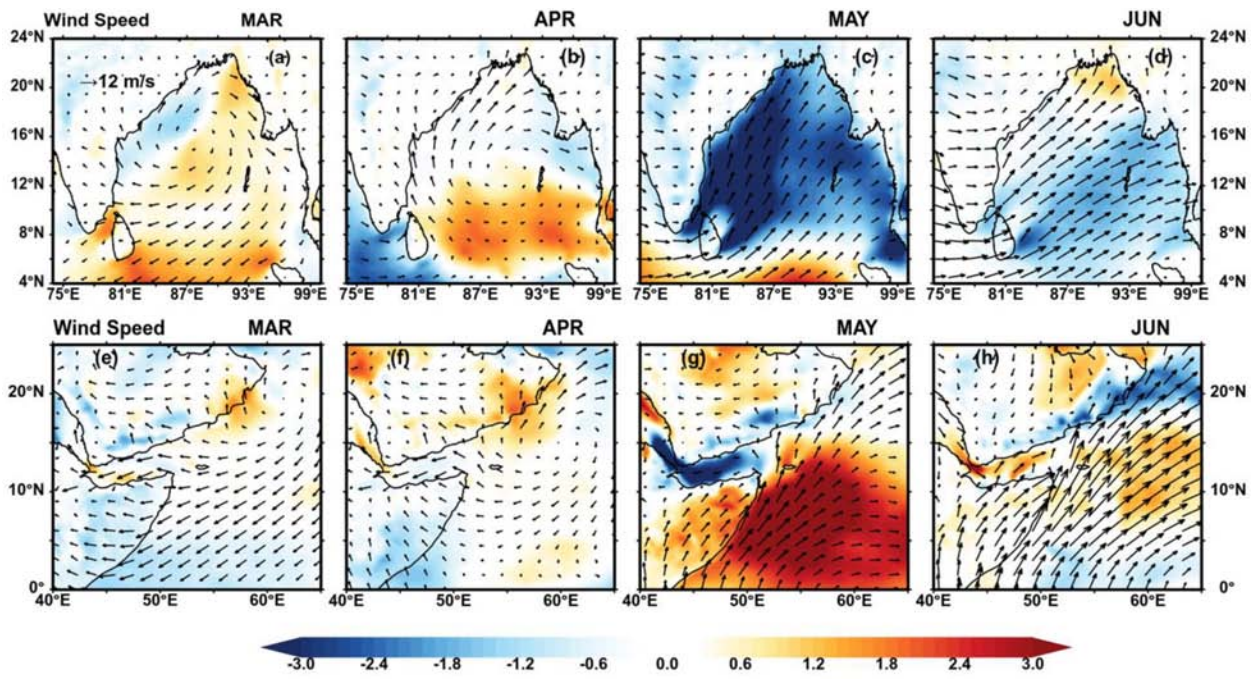

FIGURE 6 | Difference of wind speed (shaded, in meter per second) over the BoB **(A–D)** and WAS **(E–H)** for the year 2020 to 2019 (i.e., pandemic – pre-pandemic period) overlaid with climatological mean (2013 to 2020) wind vectors for respective months derived from ERA5 reanalysis data.

(ESA-OC-CCI).[2] The Chl-a concentration daily data were downloaded for the COVID-19 pandemic (March–June 2020) and pre-pandemic (March–June 2019) periods. Version 5.0 of this dataset is produced using the processing chain software developed by ESA-OC-CCI. This dataset contains global daily composites of merged sensor products: SeaWiFS, MERIS, MODIS Aqua, VIIRS, and OLCI. This dataset provides global ocean surface Chl-a concentration from the different satellite

[2]https://www.oceancolour.org

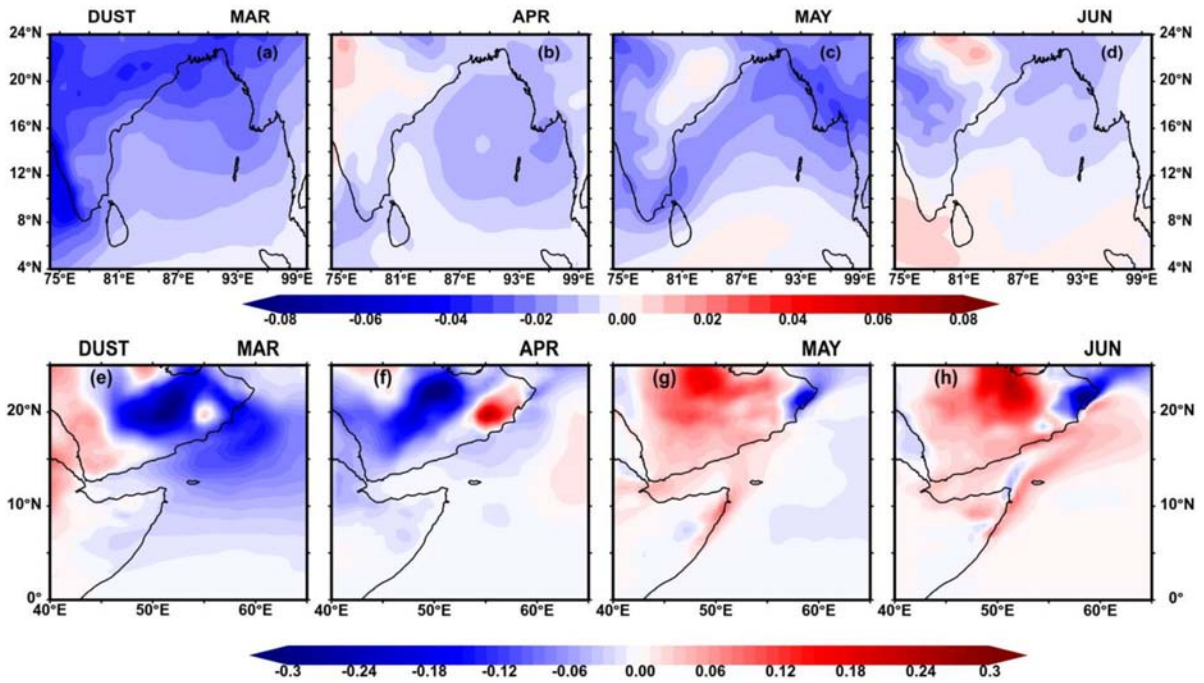

FIGURE 7 | Difference (pandemic – pre-pandemic) in dust mass concentration ($\times 10^{-6}$ kg m^{-3}) over the BoB **(A–D)** and WAS **(E–H)**.

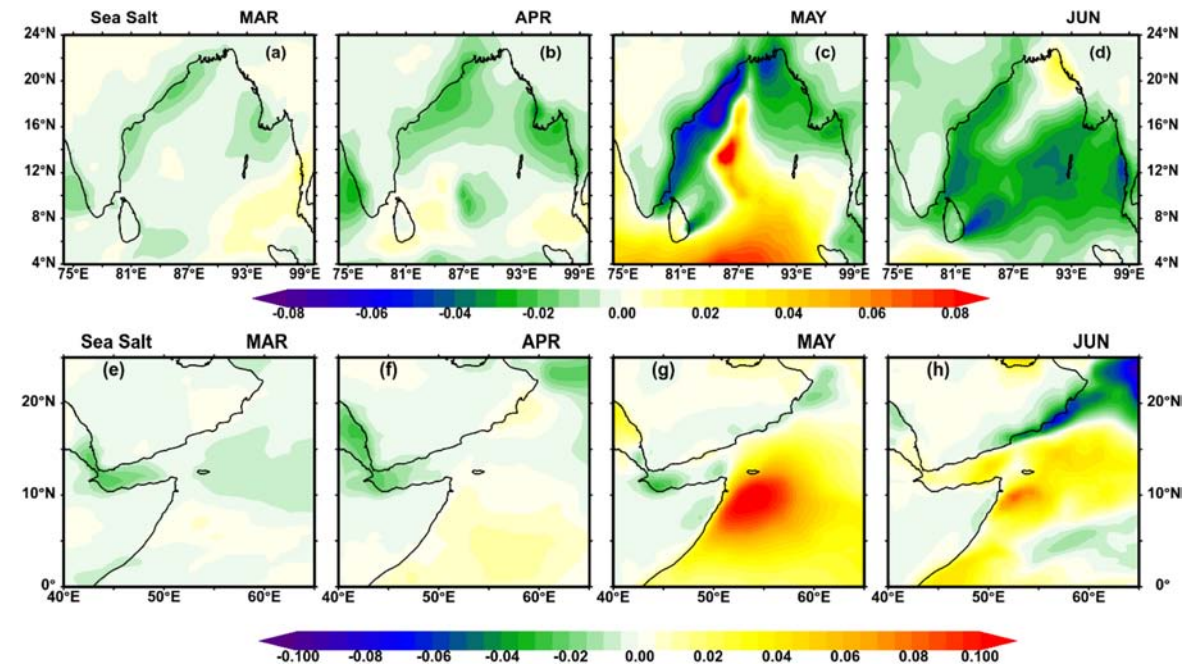

FIGURE 8 | Difference (pandemic – pre-pandemic) in sea salt concentration ($\times 10^{-6}$ kg m^{-3}) over the BoB **(A–D)** and WAS **(E–H)**.

sensors with 4 km horizontal and daily temporal resolution. The SST data were obtained from Advanced Microwave Scanning Radiometer (AMSR2)[3] for the same period. The 3-day composite blended SST of AMSR2 has a spatial resolution of 0.25° × 0.25°. The daily surface winds at 10 m were taken from the European Centre for Medium Range Weather Forecast's (ECMWF) reanalysis, ERA5 data of 25 km × 25 km resolution for the period from 2019 to 2020. For the atmospheric aerosol

[3]https://las.incois.gov.in/las

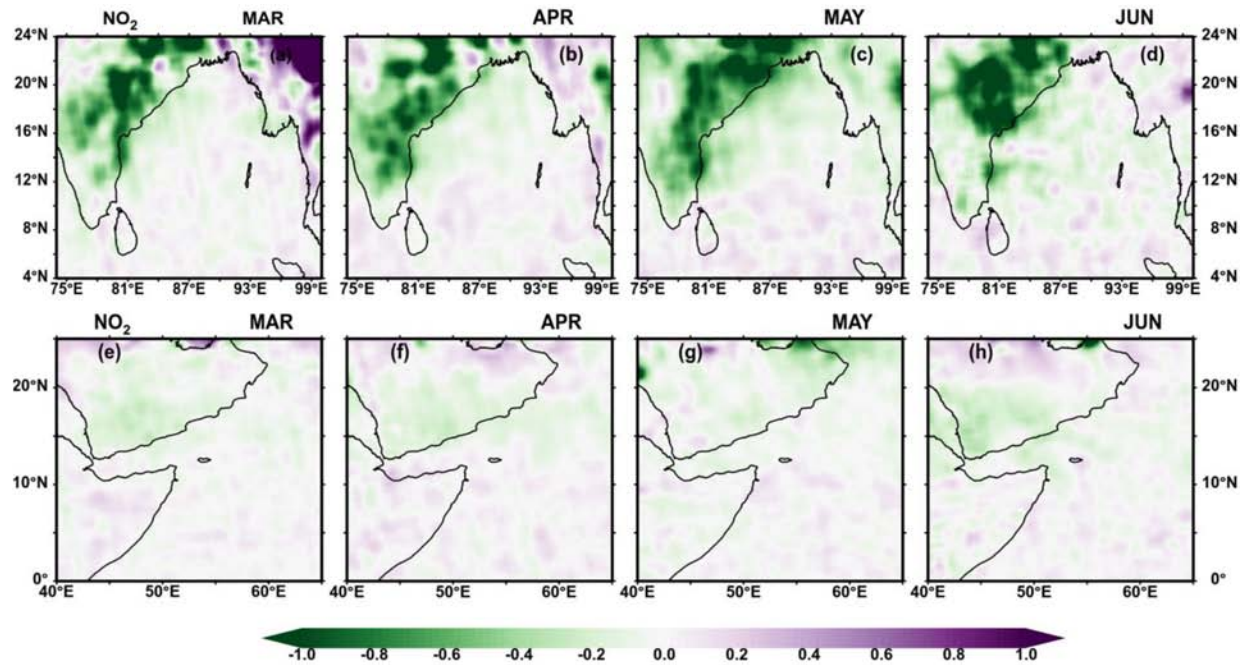

FIGURE 9 | Difference (pandemic – pre-pandemic) in NO_2 concentration ($\times 10^{15}$ mole cm^{-2}) over the BoB **(A–D)** and WAS **(E–H)**.

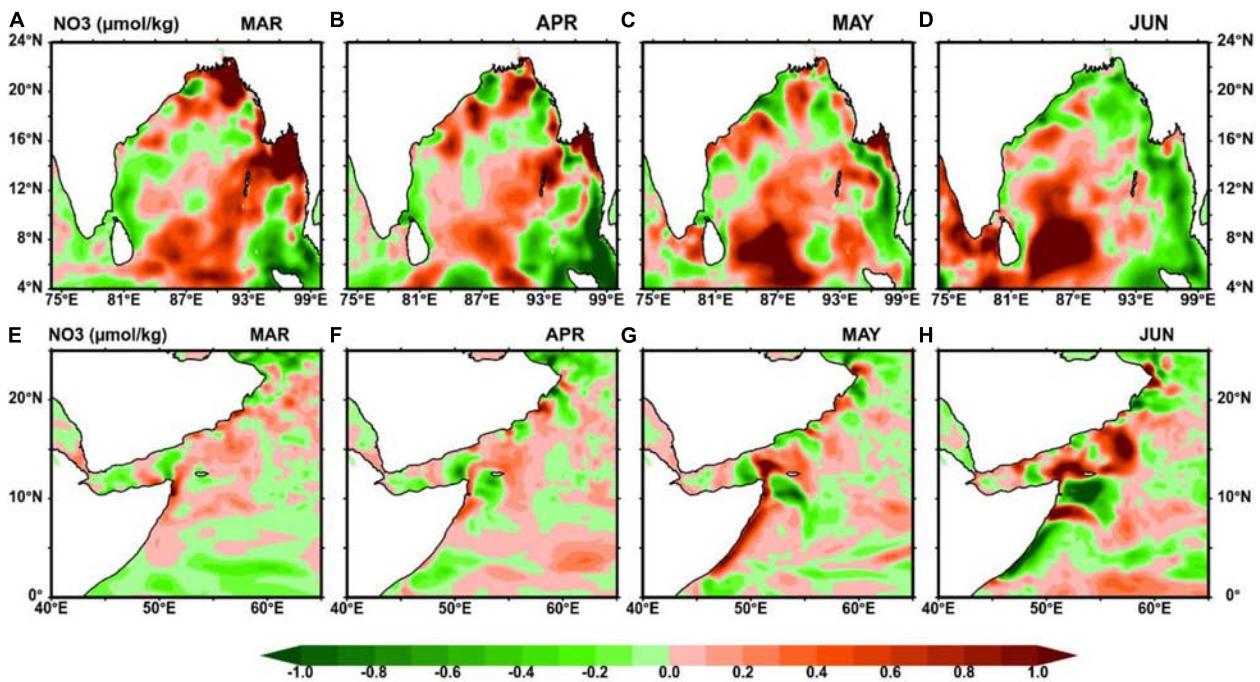

FIGURE 10 | Difference (pandemic – pre-pandemic) in model-simulated Nitrate (NO_3) concentration (micromol per kilogram) averaged from surface to 75 m depth over the BoB **(A–D)** and WAS **(E–H)**.

loading, the Moderate Resolution Imaging Spectro-radiometer Aqua (MODIS Aqua) derived AOD is utilized. The AOD data are from the level 3 of MOD08_D3_v6.1 with 1° spatial resolution. The combined dark target and deep blue AOD at 550 nm are used. Nitrogen dioxide (NO_2) data are obtained from the ozone monitoring instrument (OMI) within tropospheric column of 30% cloud screened level 3 product (OMNO2d.v003) with 0.25° × 0.25° horizontal

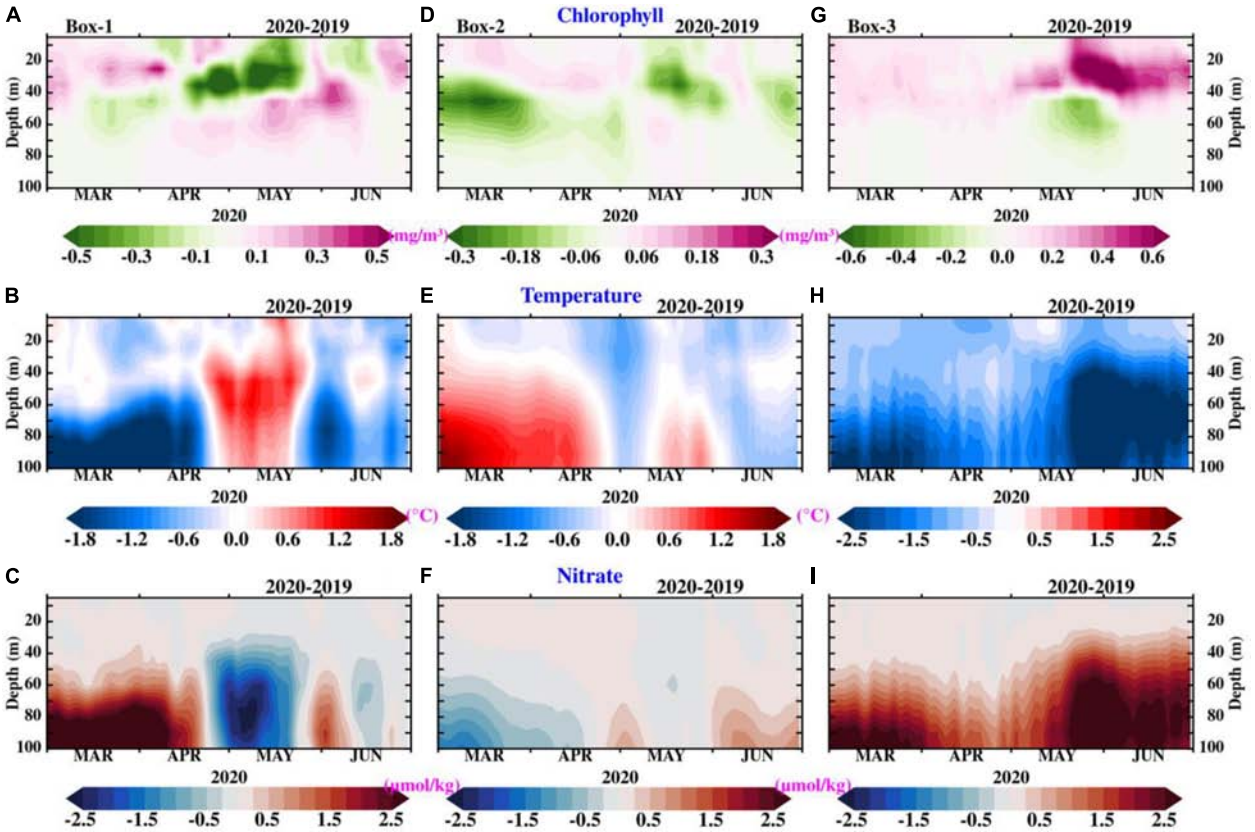

FIGURE 11 | Time-depth section of the difference of pandemic to the pre-pandemic period (the year 2020 – 2019) of model-simulated Chl-a concentration, temperature, and nitrate in the BoB averaged over **(A–C)** Box1 (85°E-87.5°E, 19°N-19.5°N), **(D–F)** Box2 (80.6°E-83°E, 12°N-15.5°N), and **(G–I)** Box3 (82°E-90°E, 4°N-9°N) regions. Box1, Box2, and Box3 are marked in **Figure 1**.

resolution. These datasets are downloaded from the NASA website https://giovanni.gsfc.nasa.gov/giovanni/. Dust surface mass concentration (DUSMASS) and sea salt surface mass concentration (SSSMASS) are downloaded from https://gmao.gsfc.nasa.gov/reanalysis/MERRA-2 of Modern-Era Retrospective Analysis for Research and Applications, version 2 (MERRA-2) with a resolution of 0.5° × 0.625°. A summary of datasets that are used and their resolution and sources are provided in **Table 1**.

Model

The coupled physical-biogeochemical model has been set-up over the Indian Ocean (IO) basin (30°N-30°S and 30°E-120°E) (Seelanki et al., 2021) with a 1/4° horizontal grid resolution and 40 vertical sigma layers using a Regional Ocean Modelling System (ROMS) version 3.7 (Haidvogel et al., 2008). Many studies (Jana et al., 2015; Chakraborty et al., 2018; Nigam et al., 2018; Sandeep and Pant, 2018; Dandapat et al., 2020) used the ROMS model to understand the processes and temporal and spatial variability over the NIO (such as, AS and BoB) region. The bathymetry in the model domain is adopted from the 2-min Gridded Global Relief Data (ETOPO2) (Smith and Sandwell, 1997). The model initial conditions of temperature and salinity are derived from the World Ocean Atlas (WOA13) based on the Levitus data (Levitus, 1983). The daily climatological surface forcing of precipitation data used from tropical rainfall measuring mission (TRMM),[4] surface winds adopted from QuikScat scatterometer,[5] and other meteorological parameters (air temperature, specific humidity, sea level pressure, and net longwave, shortwave radiation) obtained from the National Centre for Environmental Prediction (NCEP) reanalysis data (Kalnay et al., 1996). River discharges from major rivers draining into the BoB (i.e., Ganga, Brahmaputra, Mahanadi, Irrawaddy, Krishna, and Godavari) are incorporated in the model using point-source method with the monthly climatological runoff (Fekete and Vörösmarty, 2007). The physical ROMS model was started from a state of rest and spun-up for 10 years using daily climatological forcing for the period 2000–2008. After the physical model stabilized, the ecosystem model (Bio-fennel) was coupled with the physical model and the coupled model run was executed for another 10 years with same daily climatological forcing. The 10th-year output of coupled biophysical simulation used as the initial condition for the interannual simulations. Further details of this model configuration are described in Seelanki et al. (2021). The simulations with actual observed surface forcing were performed

[4]http://daac.gsfc.nasa.gov/precipitation
[5]https://las.incois.gov.in/las

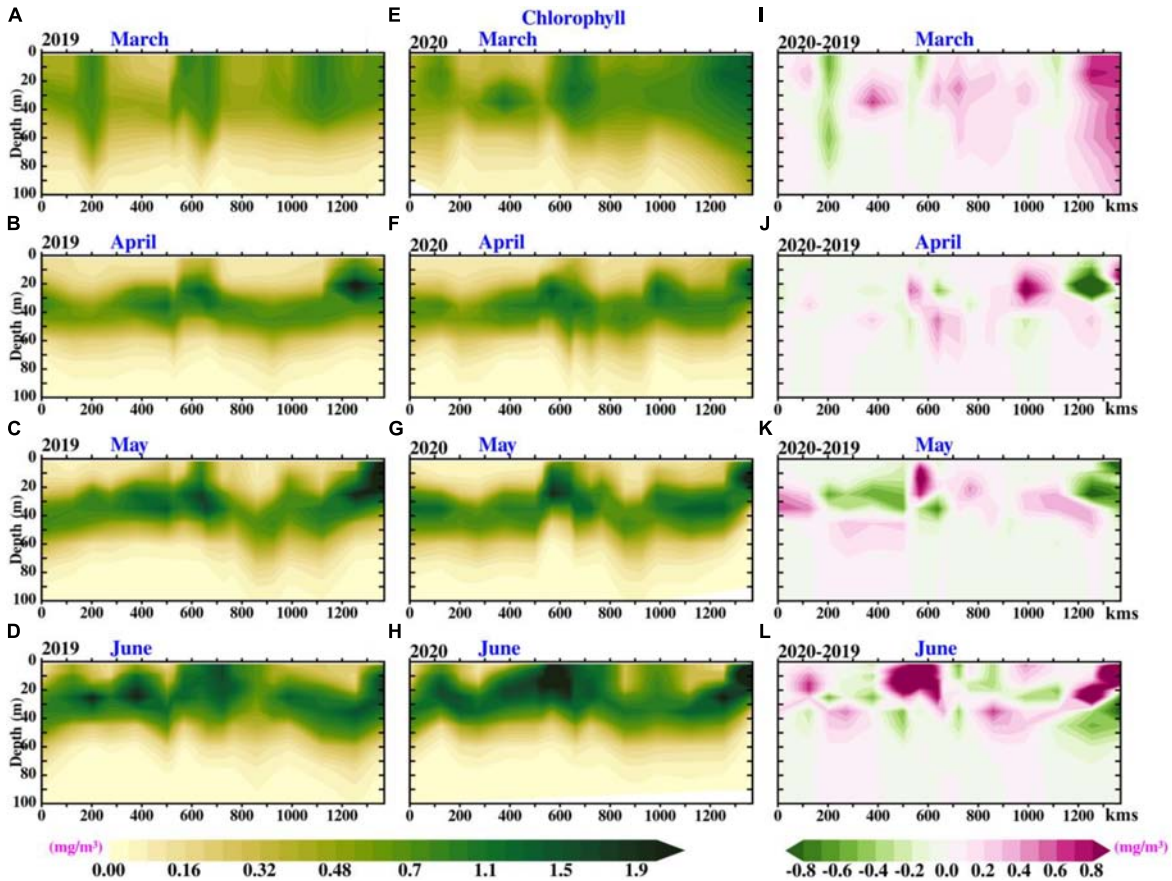

FIGURE 12 | Evolution of model-simulated Chl-a concentration along the 1,000 m isobath off Oman coast (as shown in **Figure 1**): **(A–D)** during the pre-pandemic period (March–June, 2019), **(E–H)** pandemic period (March–June, 2020), and **(I–L)** Chl-a concentration difference (pandemic–pre-pandemic period).

with QuikScat daily winds from January 1, 2000 to December 31, 2008 and then used ASCAT winds up to September 31, 2020, precipitation data from TRMM, air temperature, specific humidity, sea level pressure, and net longwave, shortwave radiation data from NCEP reanalysis (Kalnay et al., 1996).

The Bio-Fennel is a biogeochemical component (Fennel et al., 2006, 2008, 2011) of the ROMS model. The biogeochemical variables of nitrogen and oxygen were taken from WOA13 for model initialization and boundary conditions. In view of the lack of spatial information over the IO, the rest of the biogeochemical variables are initially set to a small homogenous value of 0.1 mmol N m^{-3}.

RESULTS AND DISCUSSION

Model Validation and Impact of Lockdown on Surface Chl-a Concentration

The capability of the model in reproducing the physical and biogeochemical features over the NIO is analyzed with a special emphasis on the coastal BoB and WAS. The analysis was carried out for a period of March 1–June 30 for both 2019 and 2020. An inter-comparison of the simulations of 2 years provides a quantitative relative change in the upper-ocean properties during COVID-19 pandemic 2020 as compared with the pre-pandemic condition prevailed in 2019. The study region is selected as the NIO because the BoB experienced severe tropical cyclones during this period (Pentakota et al., 2018) whereas, over the AS, March to June usually accompanied with dust storms (Middleton, 1986; Pease et al., 1998; Léon and Legrand, 2003; Gautam et al., 2009). The period of study is chosen such that the summer monsoon (June-September) is not included to avoid the precipitation driven wash-out of aerosols in either pandemic or non-pandemic years.

In the BoB region, the model-simulated SST has a positive correlation coefficient (CC) of 0.85, index of agreement (IOA) as 0.90, and root mean square error (RMSE) of 0.45°C with respect to AMSR2 observations. The simulated surface Chl-a concentration is compared with a merged satellite product (OC-CCI). A positive CC of 0.57 and IOA = 0.50 with RMSE = 0.10 mg m^{-3} between model simulation and observation of Chl-a concentration over BoB region is observed, which indicates that the model reasonably captures the Chl-a concentration pattern.

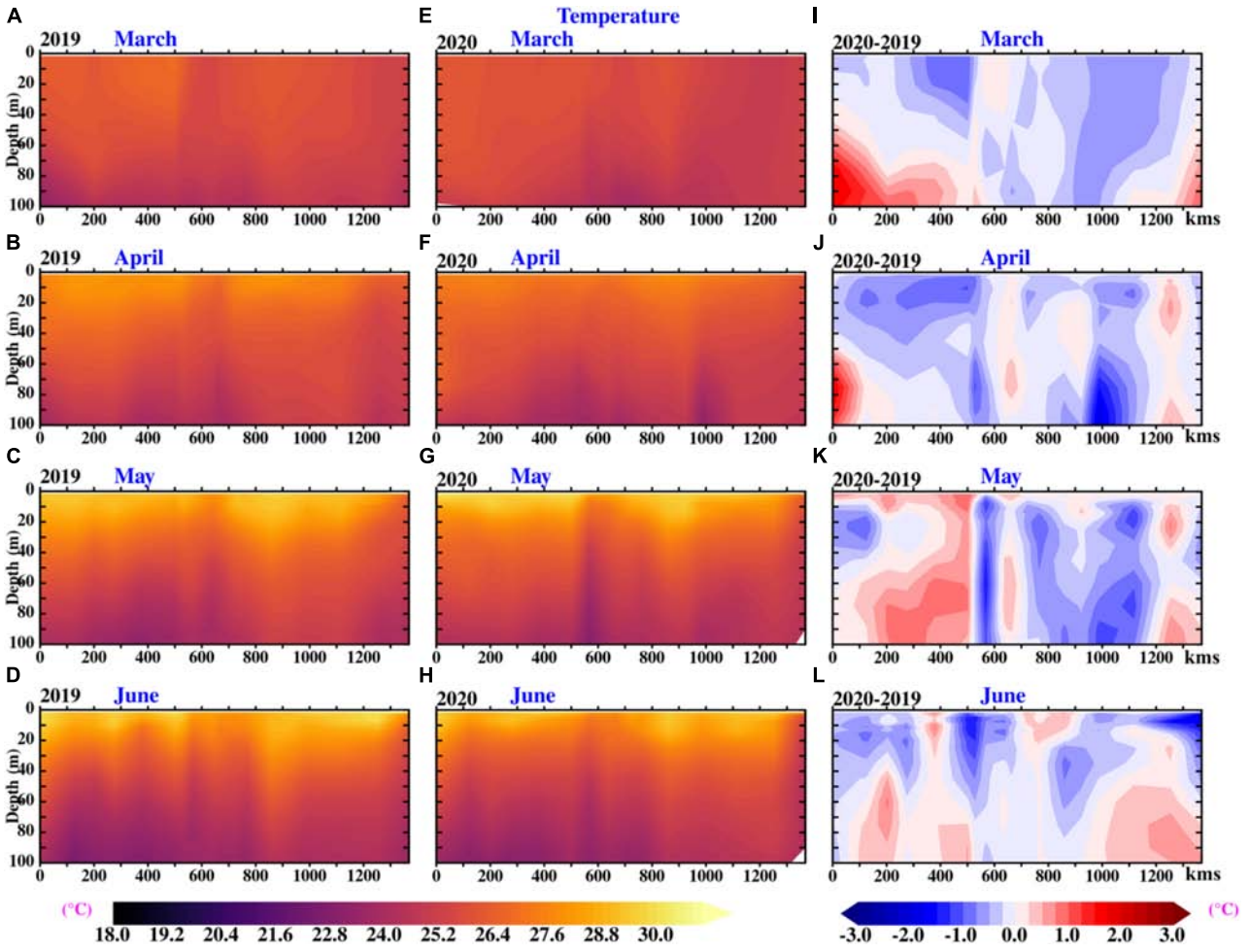

FIGURE 13 | Evolution of model-simulated temperature profile along 1,000 m isobath off Oman coast (as shown in **Figure 1**): **(A–D)** during the pre-pandemic period (March–June, 2019), **(E–H)** pandemic period (March–June, 2020), and **(I–L)** temperature difference (pandemic–pre-pandemic period).

The Chl-a concentration of 2019 (pre-pandemic) is subtracted from that of 2020 (pandemic) for the respective months over the BoB and AS (**Figure 2**). In addition, the model-simulated difference (2020 minus 2019) of surface Chl-a concentration is compared against the observed difference of Chl-a concentration for the same from OC-CCI observations. It can be inferred from the figure that the Chl-a concentration differences are reasonably well captured by the model over both the regions. In the coastal regions along the east coast of India, the Chl-a concentration found to decrease in both the model and observations during the pandemic period (2020) as compared with the non-pandemic period (2019). On the other hand, the Sri Lanka dome observes higher Chl-a concentration during the pandemic period as compared with 2019. In the CBoB, high Chl-a was observed in May during the pandemic time. This increase in Chl-a concentration is associated with the tropical cyclone Amphan in the BoB from May 16 to 21, 2020. With the wind speed of 130 Knots, it was one of the most severe cyclones in the BoB after the Odisha super cyclone. The cyclonic wind stress leads to surface Ekman mass divergence, which supports the supply of nutrients to the euphotic zone and enhances the primary productivity. The high Chl-a concentration is noticed in both the model and observations during May 2020 (**Figures 2A–H**) over the northern parts of the BoB.

Changes in the Arabian Sea

The model-simulated SST and Chl-a concentration compared well with the observations over the AS domain. The model-simulated SST has a positive CC of 0.89 with IOA = 0.91 and RMSE = 0.5∘C. Whereas the statistics for surface Chl-a concentration over the AS were found to be CC = 0.49, IOA = 0.58 with an RMSE of 0.18 mg m^{-3}. Given the complexity of simulating the coupled physical-biogeochemical processes, the statistics of Chl-a concentration against observations are reasonably good in the current study. Particularly, the phytoplankton biomass regions are well simulated. Moreover, the results presented in this study are based on the inter-comparison of the model-simulated Chl-a concentration during the pandemic-time against the non-pandemic period. The OC-CCI observations show a decrease in Chl-a concentration in the

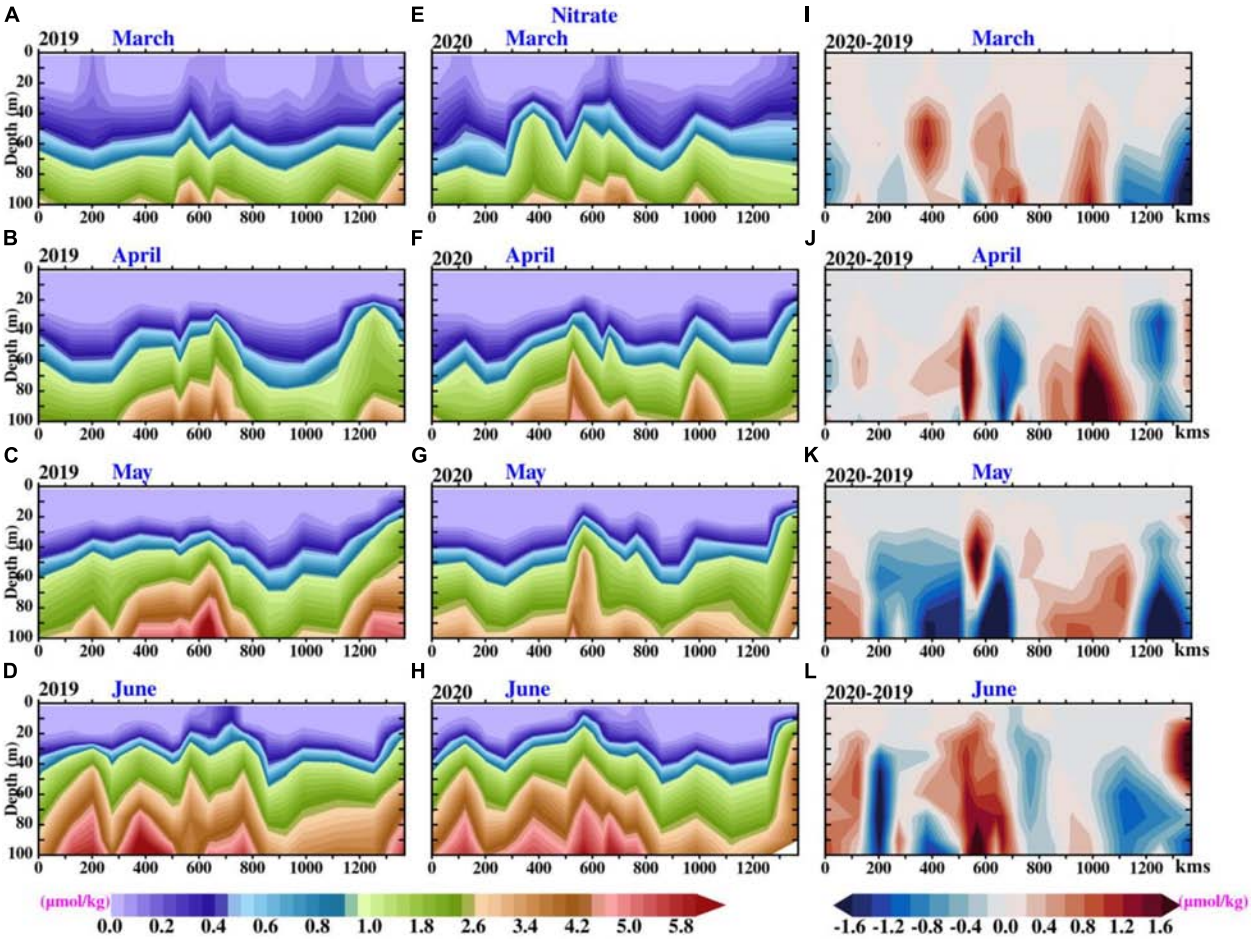

FIGURE 14 | Evolution of model-simulated nitrate profile along 1,000 m isobath off Oman coast (as shown in **Figure 1**): **(A–D)** during the pre-pandemic period (March–June, 2019), **(E–H)** pandemic period (March–June, 2020), and **(I–L)** nitrate concentration difference (pandemic – pre-pandemic period).

WAS during March–April of the pandemic period as compared with normal (2019) (**Figures 2I–P**). The model simulations also resemble this decrease in Chl-a concentration in the WAS. However, the Chl-a concentration increased in the May–June period of the pandemic. Offshore along the Oman coastline, the Chl-a bloom (i.e., the high concentration of Chl-a) persisted throughout the March–June period of the pandemic.

There is an impact of the pandemic on the SST in the NIO. The SST is found to be 0.5°C lower in the pandemic period than the non-pandemic period in both the observations and model (**Figure 3**). This reduction in SST could be due to multiple factors, such as a change in the cloud cover, changes in surface and advective heat fluxes, and changes in atmospheric CO_2 and aerosol loading during the pandemic year (Al Shehhi and Abdul Samad, 2021). These regions are found to have high rapid warming trends (Reid et al., 2009; Roxy et al., 2016). Comparing the Chl-a concentration (**Figure 2**) and SST (**Figure 3**), the SST reduction coincides with an increase in Chl-a concentration over both the regions in the NIO. This could be associated with the oceanic uptake of atmospheric CO_2 and enhancement of photosynthesis process due to the reduction in SST. Along the coastal regions of Somalia, warmer SST was observed in March–April during the pandemic year. However, with the reversal of winds, the SST reduced over WAS along Somalia coastline during May–June. This reduction in SST could be associated with the initiation of the coastal upwelling process at the Somalia coast. On the other hand, colder than normal SST (**Figures 3I–P**) observed along the Oman coast during March–April of the pandemic year, which is accompanied with high Chl-a concentration off the Oman coast (**Figures 2I–P**).

Signatures of the Pandemic Impact From *in situ* Observations

Figures 4A–D shows the time-depth vertical profiles measured from the RAMA moored buoy (90°E, 12°N) in the BoB. Additionally, the model-simulated profiles are shown for comparison. The model-simulated temperature and salinity profiles agree well with the buoy measurements (statistics of model validation is provided in **Table 2**). During the non-pandemic period, higher temperature and salinity are noticed in the upper-oceanic layers as compared with the pandemic period.

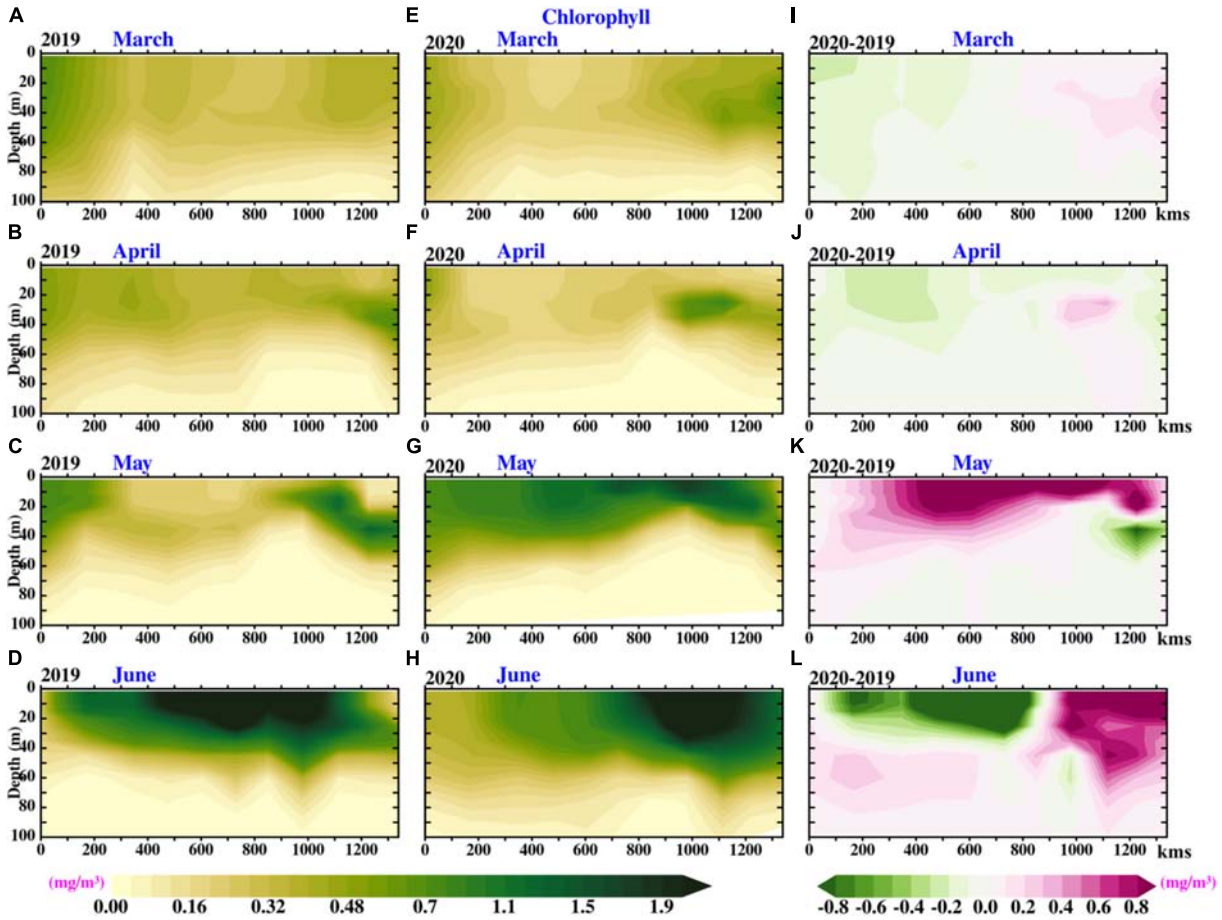

FIGURE 15 | Evolution of model-simulated Chl-a concentration along the 1,000 m isobath off Somalia coast (as shown in **Figure 1**), **(A–D)** during the pre-pandemic period (March–June 2019), **(E–H)** pandemic period (March–June, 2020), and **(I–L)** Chl-a concentration of 2019 are subtracted from 2020 with respected months (March–June).

Figures 4E–L) shows the time-depth validation of upper ocean temperature, salinity, Chl-a concentration, and dissolved oxygen are from the *in situ* measurements of a Bio-Argo float (WMO ID: 2902264) deployed in the CBoB. A comparison is made between the model simulations and the bio-Argo observations (**Figures 4F,H,J,L**). It can be seen from the figure that the model-simulated parameters along the trajectory of the Bio-Argo float are well reproduced (as shown in **Table 2** for statistics). During the pre-pandemic period, the upper ocean was warmer up to a depth of 50 m as compared with the pandemic time.

Impact of Atmospheric Aerosols/Dust and Ocean Processes

Figures 5A–D shows the difference of AOD over the BoB for the pandemic and non-pandemic periods. The AOD difference along the east coast of India shows a slight decrease during March–April of the pandemic period. Further, the effect of tropical cyclone Amphan on the aerosol loading is noticed in terms of a negative value in the difference plots. **Figures 5E–H** shows the difference (pandemic – pre-pandemic) of aerosol loading from the AP region in March–June which is associated with the stronger wind speed and dust storms in this region. Except in March, the rest of the pandemic shows a high AOD due to this wind-driven aerosol loading. These aerosols settle on the ocean surface which is favorable for the supply of nutrients in the upper ocean. This could be a reason for the observed high Chl-a concentration (**Figures 2I–P**) over this region during the pandemic period. To demonstrate the role of winds in dust transport, the difference in surface wind speed from pandemic to pre-pandemic period is shown in **Figure 6**. The wind vectors in the figure show the climatological (2013–2020) winds for the respective months over the BoB, and AS derived from ERA5 reanalyssis data. The figure shows stronger than normal westerly winds from desert regions to the AS in May of the pandemic period.

The atmospheric aerosols (dust) deposition is responsible for providing macronutrients and micronutrients to the open ocean (Fung et al., 2000; Gabric et al., 2002; Jickells et al., 2005). The phytoplankton growth is observed in heavy dust event time due to the availability of micronutrients content in the dust (Wang et al., 2012). **Figures 7A–D** shows the low dust amount deposition

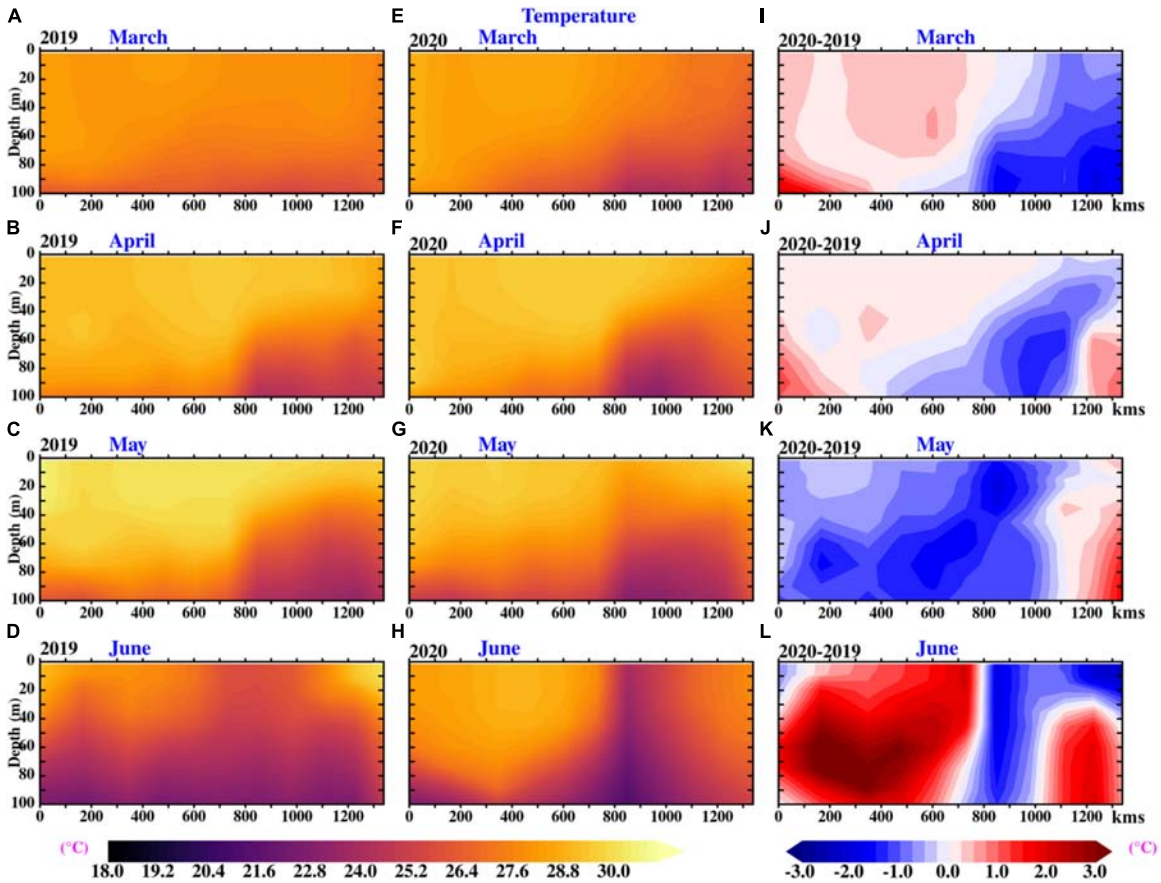

FIGURE 16 | Evolution of model-simulated temperature along the 1,000 m isobath off Somalia coast (as shown in **Figure 1**), **(A–D)** during the pre-pandemic period (March–June 2019), **(E–H)** pandemic period (March–June, 2020), and **(I–L)** difference in temperature (2020–2019) for respected months from March to June.

along the coast during March of the pandemic. This is also one of the reasons for the lack of supply of nutrients in the ocean over the WAS in March (**Figures 7E–H**). The dust deposition increased during April–June which supplied nutrients to the open ocean favoring high Chl-a concentration. The sea salt surface concentration along the east coast of India (WBoB) is shown in **Figure 8**. It shows negative values from March–June. Over the CBoB, a high concentration of sea salt is observed in May, which could be due to strong winds prevailed during the passage of cyclone Amphan. The AS also observed a high concentration of sea salt during May–June of the pandemic year (**Figures 8E,F**).

Figures 9A–D shows a decline in NO_2 concentration along the east coast of India during the pandemic which altered coastal nitrogen inputs (Mishra et al., 2020). This reduction in NO_2 is attributed to the reduced anthropogenic activities which could be a reason for the drop of Chl-a concentration in the WBoB coastal region (**Figure 2A–H**). **Figures 9E–H** shows positive values of NO_2 over the AP during the pandemic time which contributed to nitrogen input in the ocean. **Figure 10** shows model-simulated nitrate concentration averaged from 0 to 75 m. Nitrate is the primary nutrient for the growth of phytoplankton. During March–June along the east coast of India, low nitrate availability results in low Chl-a concentration (as noticed in **Figures 2A–H**). At the same time, Sri Lanka dome and CBoB have high nitrate which is conducive for the high Chl-a concentration over these regions.

Since the lockdown-driven reduced anthropogenic inputs primarily affect the coastal ocean, three analyses regions in the BoB are selected as Box1 (85°-87.5°E, 19°-19.5°N), Box-2 (80.6°-83°E, 12°-15°N), and Box3 (82°-90°E, 4°-9°N). The locations of these analyses regions are marked by red boxes in **Figure 1**. **Figure 11** shows the time-depth section of the difference of pandemic to pre-pandemic period (year 2020 minus 2019) of model-simulated Chl-a, temperature, and nitrate in the BoB averaged over Box1, Box2, and Box3 regions in the BoB. In the Box1 region (northwestern coastal BoB), warmer temperature and negative anomaly of subsurface Chl-a concentration observed during April–June of pandemic. Similarly, the Box2 region in western coastal BoB shows a decrement in Chl-a concentration during the pandemic period with respect to pre-pandemic conditions. This decrease in Chl-a concentration is attributed to the reduced anthropogenic emissions during the lockdown and, hence, a lack of micronutrients in the upper ocean. In the Box3 region (in southern BoB off Sri Lanka), Chl-a concentration was abundant at a depth of 20–50 m during pandemic. In May, a reduction in SST and increase in Chl-a

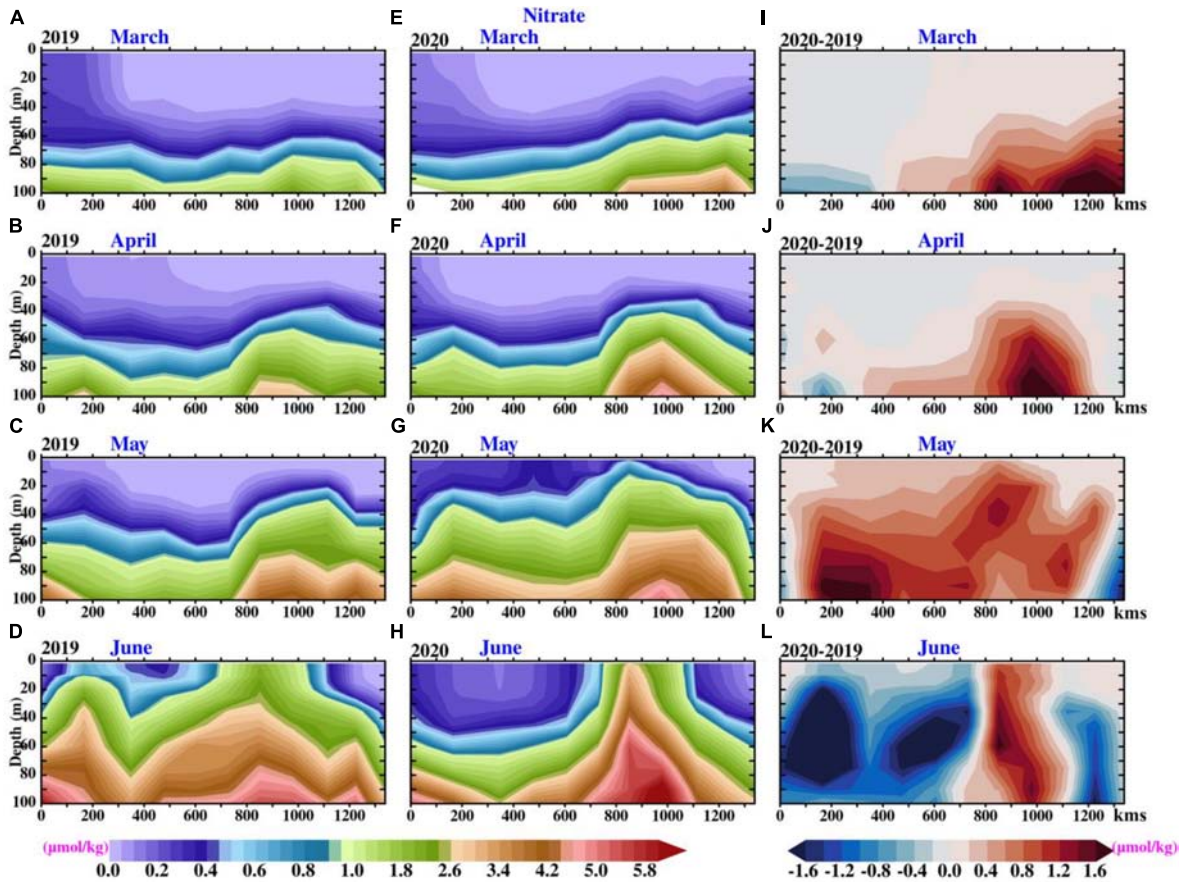

FIGURE 17 | Evolution of model-simulated nitrate along the 1,000 m isobath off Somalia coast (as shown in **Figure 1**), **(A–D)** during the pre-pandemic period (March–June 2019), **(E–H)** pandemic period (March–June, 2020), and **(I–L)** difference in nitrate concentration (2020 – 2019) for respected months from March to June.

concentration (by more than 0.5 mg m^{-3}) were observed due to Amphan cyclone-induced upwelling in the Box3 region. The Sri Lanka dome experiences upwelling by early May due to change in wind direction. A Chl-a bloom can be seen in mid-May to the end of June over the dome region in Box3.

The latitudinal sections across the Oman coast (as shown in **Figure 1** as blue contour) for the model-simulated Chl-a concentration, temperature, and nitrate are shown in **Figures 12–14**, respectively. At the northern part of the Oman coast, intense Chl-a blooms are observed in the pre-monsoon. In the northern Oman coast during March of the pandemic, the upper ocean Chl-a concentration shows a positive difference with respect to normal (**Figure 12I**), low warming (**Figure 13I**), and enough nutrient supply (**Figure 14I**). In April–May, the Oman coast experienced low productivity due to weaker winds and increase in SST. The weaker winds reduced the convective mixing leading to a reduction of nitrate concentration. During May–June, the reversal of monsoon winds triggers the mixing and at the same time, the coastal upwelling supports the supply of nutrients from the subsurface to the surface leading to Chl-a bloom.

The model-simulated Chl-a concentration, temperature, and nitrate across the latitudinal cross-sections along the Somalia coast (as shown by a red contour in **Figure 1**) are shown in **Figures 15–17**, respectively. The summer-time strong coastal upwelling in the northern part of the Somalia coast led to the intense phytoplankton bloom (high Chl-a concentration) present in the northern part of the transect (**Figure 15I**). However, the Chl-a concentration drops in the region of the Southern Gyre. This reduction in Chl-a concentration could be due to the weaker frontal system (Smith and Codispoti, 1980; Chatterjee et al., 2019). In May along the Somalia coast, high Chl-a concentration (**Figure 15K**), negative temperatures difference (**Figure 16K**), and the presence of nutrient-rich waters in the upper ocean (**Figure 17K**) were observed. Overall, during the COVID-19 pandemic, the northern part of the Somalia coast showed high productivity in the upper ocean water column due to low temperatures, high aerosol/dust deposition, and a sufficient supply of nutrients.

A schematic diagram shown in **Figure 18** summarizes various atmospheric and oceanic processes involved in the formation of phytoplankton biomass leading to a high Chl-a concentration. The wind-blown dust from the desert regions and its long-range transport, mineral dust, and other aerosols in the marine boundary layer gets deposited on the sea surface. These aerosol

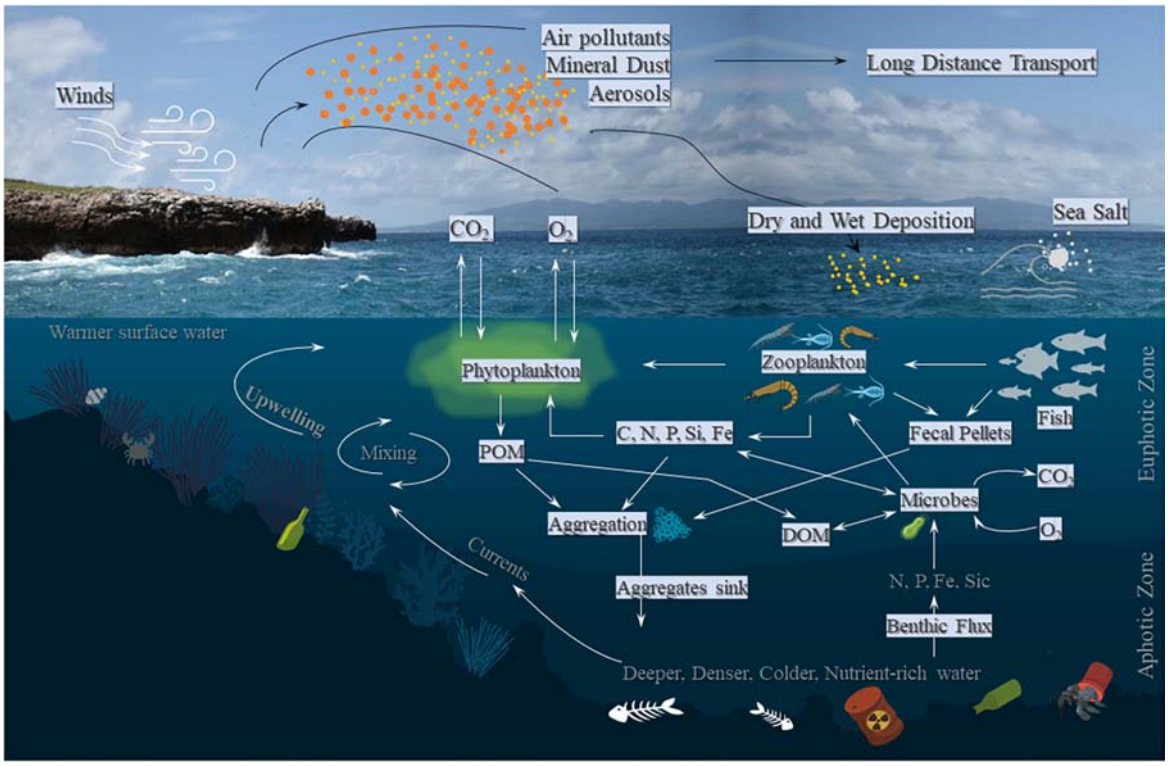

FIGURE 18 | Schematic diagram showing various physical and biogeochemical processes governing the oceanic phytoplankton biomass. The transport and deposition of aerosol and dust on the sea surface and its influence on the biogeochemical processes in the ocean are also shown.

and dust particles provide essential nutrients in the upper ocean, resulting in phytoplankton biomass. The wind-driven mixing, ocean subsurface processes (i.e., coastal upwelling), and cycling of dissolved gases and nutrients from one form to another constitute and regulate the overall primary productivity of the ocean.

CONCLUSION

An ocean physical-biological coupled model along with available satellite and *in situ* observations is used to access the impact of the lockdown due to the COVID-19 pandemic on the upper-ocean characteristics in the NIO. The differences observed in oceanic physical parameters (temperature and salinity) and biogeochemical parameters (Chl-a concentration, nutrients, dissolved oxygen, etc.) in the COVID-19 pandemic period of March–June 2020 as compared with the non-pandemic reference period of March–June 2019 are examined. The model shows a good comparison with the satellite-derived Chl-a concentration (CC = 0.57 and RMSE = 0.10 mg m^{-3} in BoB; CC = 0.49 and RMSE = 0.18 mg m^{-3} in the AS) and *in situ* measurements from a moored RAMA buoy and a bio-Argo float in the BoB (statistics shown in **Table 2**). Larger differences between the pandemic and pre-pandemic conditions are observed in the coastal regions of the north-western AS, in the Sri Lanka dome region, and along the east coast of India. In the WBoB, the Chl-a concentration decreased during March–April of the pandemic period. The coastal BoB regions along the east coast of India show a decrement in Chl-a concentration associated with the reduced anthropogenic activities during the pandemic period. Similarly, there was a decrease in Chl-a concentration in the WAS during March–April of the pandemic year, which increased thereafter when the aerosol/dust loading increased due to dust storms over this region (supported by wind anomaly and AOD analysis). The SST is found to be 0.5°C lower in the pandemic period than in the non-pandemic period. The enhanced AOD and dust deposition during May 2020 was found to enhance the ocean phytoplankton biomass through an increased supply of nutrients in the surface waters of WAS. The high Chl-a concentration (increment by > 0.5 mg m^{-3}) over the Sri Lanka dome is associated with the change in wind direction in May. During March of the pandemic year, there was a positive difference (with respect to normal year) in Chl-a concentration associated with ample supply of nutrients in the northern Oman coast. The coastal waters along northern Somalia experienced high phytoplankton biomass during the pandemic period.

DATA AVAILABILITY STATEMENT

The original contributions presented in the study are included in the article/**Supplementary Material**, further inquiries can be directed to the corresponding author.

AUTHOR CONTRIBUTIONS

VS and VP conceptualized the study, analyzed the results, and wrote the manuscript. VS performed model simulations and analysis. Both authors contributed to the article and approved the submitted version.

ACKNOWLEDGMENTS

The authors acknowledge the Ocean Color Climate Change Initiative (OC-CCI) dataset used in this study made available by the European Space Agency through the link https://www.oceancolour.org/. The dust and sea salt mass concentration data obtained from MERRA2 are acknowledged. The SST data provided by AMSR2 and AOD data derived from MODIS-Aqua are thankfully acknowledged. The High-Performance Computing (HPC) facility provided by IIT Delhi and supported by the Department of Science and Technology (DST-FIST, 2014), Govt. of India are thankfully acknowledged.

SUPPLEMENTARY MATERIAL

The Supplementary Material for this article can be found online at: https://www.frontiersin.org/articles/10.3389/fmars.2021.722401/full#supplementary-material

REFERENCES

Al Shehhi, M. R., and Abdul Samad, Y. (2021). Effects of the Covid-19 pandemic on the oceans. *Rem. Sens. Lett.* 12, 325–334. doi: 10.1080/2150704x.2021.1880658

Behrenfeld, M. J., O'Malley, R. T., Siegel, D. A., McClain, C. R., Sarmiento, J. L., Feldman, G. C., et al. (2006). Climate-driven trends in contemporary ocean productivity. *Nature* 444, 752–755. doi: 10.1038/nature05317

Bowman, K. P. (2005). Comparison of TRMM Precipitation Retrievals with Rain Gauge Data from Ocean Buoys. *J. Clim.* 18, 178–190. doi: 10.1175/jcli3259.1

Bowman, K. P., Phillips, A. B., and North, G. R. (2003). Comparison of TRMM rainfall retrievals with rain gauge data from the TAO/TRITON buoy array. *Geophys. Res. Lett.* 30:1757. doi: 10.1029/2003GL017552

Chakraborty, K., Valsala, V., Gupta, G. V. M., and Sarma, V. V. S. S. (2018). Dominant Biological Control Over Upwelling on pCO2 in Sea East of Sri Lanka. *J. Geophys. Res. Biogeosci.* 123, 3250–3261. doi: 10.1029/2018jg004446

Chatterjee, A., Kumar, B. P., Prakash, S., and Singh, P. (2019). Annihilation of the Somali upwelling system during summer monsoon. *Sci. Rep.* 9, 1–14. doi: 10.1038/s41598-019-44099-1

Chauhan, A., and Singh, R. P. (2020). Decline in PM2. 5 concentrations over major cities around the world associated with COVID-19. *Environ. Res.* 187:109634. doi: 10.1016/j.envres.2020.109634

Chimurkar, N. D., Patidar, G., and Phuleria, H. C. (2020). Changes in air quality during the COVID-19 lockdown in India. *ISEE Confer. Abstracts* 2020:648. doi: 10.1289/isee.2020.virtual.o-os-648

Clemens, C. S. (1998). Dust response to seasonal atmospheric forcing: Proxy evaluation and calibration. *Paleoceanography* 13, 471–490. doi: 10.1029/98pa02131

Dandapat, S., Gnanaseelan, C., and Parekh, A. (2020). Impact of excess and deficit river runoff on Bay of Bengal upper ocean characteristics using an ocean general circulation model. *Deep Sea Res. Part II Topical Stud. Oceanogr.* 172:104714. doi: 10.1016/j.dsr2.2019.104714

Duce, R. A., and Tindale, N. W. (1991). Atmospheric transport of iron and its deposition in the ocean. *Limnol. Oceanogr.* 36, 1715–1726. doi: 10.4319/lo.1991.36.8.1715

Fekete, B. M., and Vörösmarty, C. J. (2007). The current status of global river discharge monitoring and potential new technologies complementing traditional discharge measurements. *IAHS Publ.* 309, 129–136.

Fennel, K., Hetland, R., Feng, Y., and DiMarco, S. (2011). A coupled physical-biological model of the Northern Gulf of Mexico shelf: model description, validation and analysis of phytoplankton variability. *Biogeosciences* 8, 1881–1899. doi: 10.5194/bg-8-1881-2011

Fennel, K., Wilkin, J., Levin, J., Moisan, J., O'Reilly, J., and Haidvogel, D. (2006). Nitrogen cycling in the Middle Atlantic Bight: Results from a three−dimensional model and implications for the North Atlantic nitrogen budget. *Glob. Biogeochem. Cycles* 20:2005GB002456. doi: 10.1029/2005GB002456

Fennel, K., Wilkin, J., Previdi, M., and Najjar, R. (2008). Denitrification effects on air−sea CO2 flux in the coastal ocean: Simulations for the northwest North Atlantic. *Geophys. Res. Lett.* 35:2008GL036147. doi: 10.1029/2008GL036147

Fung, I. Y., Meyn, S. K., Tegen, I., Doney, S. C., John, J. G., and Bishop, J. K. (2000). Iron supply and demand in the upper ocean. *Glob. Biogeochem. Cycles* 14, 281–295. doi: 10.1002/(ISSN)1944-9224

Gabric, A. J., Cropp, R., Ayers, G. P., McTainsh, G., and Braddock, R. (2002). Coupling between cycles of phytoplankton biomass and aerosol optical depth as derived from SeaWiFS time series in the Subantarctic Southern Ocean. *Geophys. Res. Lett.* 29, 16–11. doi: 10.1029/2001GL013545

Gallisai, R., Peters, F., Volpe, G., Basart, S., and Baldasano, J. M. (2014). Saharan dust deposition may affect phytoplankton growth in the Mediterranean sea at ecological time scales. *PLoS One* 9:e110762. doi: 10.1371/journal.pone.0110762

Gautam, R., Liu, Z., Singh, R. P., and Hsu, N. C. (2009). Two contrasting dust−dominant periods over India observed from MODIS and CALIPSO data. *Geophys. Res. Lett.* 36:2008GL036967. doi: 10.1029/2008GL036967

Gerecht, A. C., Šupraha, L., Edvardsen, B., Probert, I., and Henderiks, J. (2014). High temperature decreases the PIC/POC ratio and increases phosphorus requirements in Coccolithus pelagicus (Haptophyta). *Biogeosciences* 11, 3531–3545. doi: 10.5194/bg-11-3531-2014

Glantz, P., Nilsson, E. D., and von Hoyningen-Huene, W. (2009). Estimating a relationship between aerosol optical thickness and surface wind speed over the ocean. *Atmos. Res.* 92, 58–68. doi: 10.1016/j.atmosres.2008.08.010

Haidvogel, D. B., Arango, H., Budgell, W. P., Cornuelle, B. D., Curchitser, E., Di Lorenzo, E., et al. (2008). Ocean forecasting in terrain-following coordinates: Formulation and skill assessment of the Regional Ocean Modeling System. *J. Computat. Phys.* 227, 3595–3624. doi: 10.1016/j.jcp.2007.06.016

Jana, S., Gangopadhyay, A., and Chakraborty, A. (2015). Impact of seasonal river input on the Bay of Bengal simulation. *Continental Shelf Res.* 104, 45–62. doi: 10.1016/j.csr.2015.05.001

Jayaram, C., Priyadarshi, N., Pavan Kumar, J., Udaya Bhaskar, T. V. S., Raju, D., and Kochuparampil, A. J. (2018). Analysis of gap-free chlorophyll-a data from MODIS in Arabian Sea, reconstructed using DINEOF. *Int. J. Rem. Sens.* 39, 7506–7522. doi: 10.1080/01431161.2018.1471540

Jickells, T. D., An, Z. S., Andersen, K. K., Baker, A. R., Bergametti, G., Brooks, N., et al. (2005). Global iron connections between desert dust, ocean biogeochemistry, and climate. *Science* 308, 67–71. doi: 10.1126/science.1105959

Jin, Q., Wei, J., Pu, B., Yang, Z., and Parajuli, S. P. (2018). High Summertime Aerosol Loadings Over the Arabian Sea and Their Transport Pathways. *J. Geophys. Res. Atmospheres* 123:2018jd028588. doi: 10.1029/2018jd028588

Kalnay, E., Kanamitsu, M., Kistler, R., Collins, W., Deaven, D., Gandin, L., et al. (1996). The NCEP/NCAR 40-year reanalysis project. *Bull. Am. Meteorol. Soc.* 77, 437–472. doi: 10.1175/1520-04771996077<0437:TNYRP<2.0.CO;2

Knutson, T. R., McBride, J. L., Chan, J., Emanuel, K., Holland, G., Landsea, C., et al. (2010). Tropical cyclones and climate change. *Nat. Geosci.* 3, 157–163. doi: 10.1175/BAMS-D-18-0189.1

Le Quéré, C., Jackson, R. B., Jones, M. W., Smith, A. J., Abernethy, S., Andrew, R. M., et al. (2020). Temporary reduction in daily global CO 2 emissions during the COVID-19 forced confinement. *Nat. Clim. Change* 10, 647–653. doi: 10.1038/s41558-020-0797-x

Léon, J. F., and Legrand, M. (2003). Mineral dust sources in the surroundings of the north Indian Ocean. *Geophys. Res. Lett.* 30:2002GL016690. doi: 10.1029/2002GL016690

Levitus, S (1983). "Climatological Atlas of the World Ocean.". *EOS Transact. Am. Geophys. Union* 64, 962–963. doi: 10.1029/EO064i049p00962-02

Madineni, V. R., Dasari, H. P., Karumuri, R., Viswanadhapalli, Y., Perumal, P., and Hoteit, I. (2021). Natural processes dominate the pollution levels during COVID-19 lockdown over India. *Sci. Rep.* 11:4. doi: 10.1038/s41598-021-94373-4

Mahowald, N. M., Baker, A. R., Bergametti, G., Brooks, N., Duce, R. A., Jickells, T. D., et al. (2005). Atmospheric global dust cycle and iron inputs to the ocean. *Glob. Biogeochem. Cycles* 19:GB4025. doi: 10.1029/2004GB002402

Mandal, S., Behera, N., Gangopadhyay, A., Susanto, R. D., and Pandey, P. C. (2021). Evidence of a chlorophyll "tongue" in the Malacca Strait from satellite observations. *J. Mar. Syst.* 223:103610. doi: 10.1016/j.jmarsys.2021.103610

McPhaden, M. J., Meyers, G., Ando, K., Masumoto, Y., Murty, V. S. N., Ravichandran, M., et al. (2009). RAMA The Research Moored Array for African–Asian–Australian Monsoon Analysis and Prediction. *Bull. Am. Meteorol. Soc.* 90, 459–480. doi: 10.1175/2008BAMS2608.1

Measures, C. I., and Vink, S. (1999). Seasonal variations in the distribution of Fe and Al in the surface waters of the Arabian Sea. *Deep Sea Res. Part II Topical Stud. Oceanogr.* 46, 1597–1622. doi: 10.1016/s0967-0645(99)00037-5

Meskhidze, N., and Nenes, A. (2010). Effects of ocean ecosystem on marine aerosol-cloud interaction. *Adv. Meteorol.* 2010:239808. doi: 10.1155/2010/239808

Meskhidze, N., Chameides, W. L., and Nenes, A. (2005). Dust and pollution: a recipe for enhanced ocean fertilization? *J. Geophys. Res. Atmos.* 110:D03301. doi: 10.1029/2004JD005082

Middleton, N. J. (1986). A geography of dust storms in South−west Asia. *J. Climatol.* 6, 183–196. doi: 10.1002/joc.3370060207

Mishra, D. R., Kumar, A., Muduli, P. R., Equeenuddin, S., Rastogi, G., Acharyya, T., et al. (2020). Decline in Phytoplankton Biomass along Indian Coastal Waters due to COVID-19 Lockdown. *Rem. Sens.* 12:2584. doi: 10.3390/RS12162584

Morel, A., and Antoine, D. (1994). Heating rate within the upper ocean in relation to its bio–optical state. *J. Physical Oceanogr.* 24, 1652–1665. doi: 10.1175/1520-04851994024<1652:HRWTUO>2.0.CO;2

Morin, A., Lamoureux, W., and Busnarda, J. (1999). Empirical models predicting primary productivity from Chlorophyll a and water temperature for stream periphyton and lake and ocean phytoplankton. *J. North Am. Benthol. Soc.* 18, 299–307. doi: 10.2307/1468446

Mulcahy, J. P., O'Dowd, C. D., Jennings, S. G., and Ceburnis, D. (2008). Significant enhancement of aerosol optical depth in marine air under high wind conditions. *Geophys. Res. Lett.* 35:L16810. doi: 10.1029/2008GL034303

Nair, T. M. B. (2006). Monsoon control on trace metal fluxes in the deep Arabian Sea. *J. Earth Syst. Sci.* 115, 461–472. doi: 10.1007/bf02702874

Navinya, C., Patidar, G., and Phuleria, H. C. (2020). Examining Effects of the COVID-19 National Lockdown on Ambient Air Quality across Urban India. *Aerosol Air Qual. Res.* 20, 1759–1771. doi: 10.4209/aaqr.2020.05.02568

Nigam, T., Pant, V., and Prakash, K. R. (2018). Impact of Indian ocean dipole on the coastal upwelling features off the southwest coast of India. *Ocean Dynam.* 68, 663–676. doi: 10.1007/s10236-018-1152-x

NOAA (2020). *How much oxygen comes from the ocean?*. Washington, D.C: NOAA.

O'Dowd, C. D., Smith, M. H., Consterdine, I. E., and Lowe, J. A. (1997). Marine aerosol, sea-salt, and the marine sulphur cycle: a short review. *Atmos. Environ.* 31, 73–80. doi: 10.1016/S1352-2310(96)00106-9

Paital, B. (2020). Nurture to nature via COVID-19, a self-regenerating environmental strategy of environment in global context. *Sci. Total Environ.* 2020:139088. doi: 10.1016/j.scitotenv.2020.139088

Pandey, S. K., and Vinoj, V. (2021). Surprising Changes in Aerosol Loading over India amid COVID-19 Lockdown. *Aerosol Air Qual. Res.* 21:200466. doi: 10.4209/aaqr.2020.07.0466

Pant, V., Deshpande, C. G., and Kamra, A. K. (2008). On the aerosol number concentration–wind speed relationship during a severe cyclonic storm over south Indian Ocean. *J. Geophys. Res.* 113:D02206. doi: 10.1029/2006JD008035

Patra, P. K., Behera, S. K., Herman, J. R., Maksyutov, S., Akimoto, H., and Yamagata, Y. (2005). The Indian summer monsoon rainfall: interplay of coupled dynamics, radiation and cloud microphysics. *Atmos. Chem. Phys.* 5, 2181–2188. doi: 10.5194/acp-5-2181-2005

Patra, P. K., Kumar, M. D., Mahowald, N., and Sarma, V. V. S. S. (2007). Atmospheric deposition and surface stratification as controls of contrasting chlorophyll abundance in the North Indian Ocean. *J. Geophys. Res.* 112:C05029. doi: 10.1029/2006JC003885

Pease, P. P., Tchakerian, V. P., and Tindale, N. W. (1998). Aerosols over the Arabian Sea: geochemistry and source areas for aeolian desert dust. *J. Arid Environ.* 39, 477–496. doi: 10.1006/jare.1997.0368

Pentakota, S., Vivek, S., and Rao, K. S. (2018). Role of Andaman Sea in the intensification of cyclones over Bay of Bengal. *Nat. Hazards* 91, 1113–1125. doi: 10.1007/s11069-018-3170-x

Ramaswamy, V., Muraleedharan, P. M., and Babu, C. P. (2017). Mid-troposphere transport of Middle-East dust over the Arabian Sea and its effect on rainwater composition and sensitive ecosystems over India. *Sci. Rep.* 7:1. doi: 10.1038/s41598-017-13652-1

Reid, P. C., Fischer, A. C., Lewis-Brown, E., Meredith, M. P., Sparrow, M., Andersson, A. J., et al. (2009). Impacts of the oceans on climate change. *Adv. Mar. Biol.* 56, 1–150. doi: 10.1016/S0065-2881(09)56001-4

Rengarajan, R., and Sarin, M. M. (2004). Atmospheric deposition fluxes of 7Be, 210Pb and chemical species to the Arabian Sea and Bay of Bengal. *Ind. J. Mar. Sci.* 33, 56–64.

Roxy, M. K., Modi, A., Murtugudde, R., Valsala, V., Panickal, S., Prasanna Kumar, S., et al. (2016). A reduction in marine primary productivity driven by rapid warming over the tropical Indian Ocean. *Geophys. Res. Lett.* 43, 826–833. doi: 10.1002/2015GL066979

Sandeep, K. K., and Pant, V. (2018). Evaluation of Interannual Simulations and Indian Ocean Dipole Events During 2000–2014 from a Basin Scale General Circulation Model. *Pure Appl. Geophys.* 175, 4579–4603. doi: 10.1007/s00024-018-1915-9

Satheesh, S. K., Srinivasan, J., and Moorthy, K. K. (2006). Contribution of sea-salt to aerosol optical depth over the Arabian Sea derived from MODIS observations. *Geophys. Res. Lett.* 33:L03809. doi: 10.1029/2005GL024856

Seelanki, V., Nigam, T., and Pant, V. (2021). Upper-ocean physical and biological features associated with Hudhud cyclone: A bio-physical modelling study. *J. Mar. Syst.* 215:103499. doi: 10.1016/j.jmarsys.2020.103499

Smith, S. L., and Codispoti, L. A. (1980). Southwest monsoon of 1979: chemical and biological response of Somali coastal waters. *Science* 209, 597–600. doi: 10.1126/science.209.4456.597

Smith, W. H., and Sandwell, D. T. (1997). Global sea floor topography from satellite altimetry and ship depth soundings. *Science* 277, 1956–1962. doi: 10.1126/science.277.5334.1956

Thushara, V., Vinayachandran, P. N. M., Matthews, A. J., Webber, B. G. M., and Queste, B. Y. (2019). Vertical distribution of chlorophyll in dynamically distinct regions of the southern Bay of Bengal. *Biogeosciences* 16, 1447–1468. doi: 10.5194/bg-16-1447-2019

Tindale, N. W., and Pease, P. P. (1999). Aerosols over the Arabian Sea: Atmospheric transport pathways and concentrations of dust and sea salt. *Deep Sea Res. Part II Topical Stud. Oceanogr.* 46, 1577–1595. doi: 10.1016/s0967-0645(99)00036-3

Wang, S. H., Hsu, N. C., Tsay, S. C., Lin, N. H., Sayer, A. M., Huang, S. J., et al. (2012). Can Asian dust trigger phytoplankton blooms in the oligotrophic northern South China Sea? *Geophys. Res. Lett.* 39:2011GL050415. doi: 10.1029/2011GL050415

Yeh, S. W., Kug, J. S., Dewitte, B., Kirtman, B., and Jin, F. F. (2009). Recent changes in El Niño and its projection under global warming. *Nature* 461, 511–515. doi: 10.1038/nature08316

Zambrano-Monserrate, M. A., Ruano, M. A., and Sanchez-Alcalde, L. (2020). Indirect effects of COVID-19 on the environment. *Sci. Total Environ.* 728:138813. doi: 10.1016/j.scitotenv.2020.138813

Conflict of Interest: The authors declare that the research was conducted in the absence of any commercial or financial relationships that could be construed as a potential conflict of interest.

Advantages of publishing in Frontiers

OPEN ACCESS
Articles are free to read for greatest visibility and readership

FAST PUBLICATION
Around 90 days from submission to decision

HIGH QUALITY PEER-REVIEW
Rigorous, collaborative, and constructive peer-review

TRANSPARENT PEER-REVIEW
Editors and reviewers acknowledged by name on published articles

Frontiers
Avenue du Tribunal-Fédéral 34
1005 Lausanne | Switzerland

Visit us: www.frontiersin.org
Contact us: frontiersin.org/about/contact

REPRODUCIBILITY OF RESEARCH
Support open data and methods to enhance research reproducibility

DIGITAL PUBLISHING
Articles designed for optimal readership across devices

FOLLOW US
@frontiersin

IMPACT METRICS
Advanced article metrics track visibility across digital media

EXTENSIVE PROMOTION
Marketing and promotion of impactful research

LOOP RESEARCH NETWORK
Our network increases your article's readership